TECHNISCHE UNIVERSITÄT DARMSTADT

GEORG SPEYER HAUS
INSTITUT FÜR TUMORBIOLOGIE
UND EXPERIMENTELLE THERAPIE

The influence of radio-immunotherapy on the tumor microenvironment of breast-to-brain metastasis and the investigation of novel adjuvant therapies

vom Fachbereich Biologie

der Technischen Universität Darmstadt

zur Erlangung des Grades

Doctor rerum naturalium (Dr.rer.nat.)

Dissertation

von Katja Anne Niesel (M.Sc.)

aus Kaiserslautern

Erstgutachterin: Prof. Dr. Beatrix Süß

Zweitgutachter: Prof. Dr. Ralf Galuske

Externe Betreuerin: Dr. Lisa Sevenich

Darmstadt 2021

Niesel, Katja Anne: The influence of radio-immunotherapy on the tumor microenvironment of breast-to-brain metastasis and the investigation of novel adjuvant therapies
Darmstadt, Technische Universität Darmstadt
Jahr der Veröffentlichung der Dissertation auf TUprints: 2021
URN: urn:nbn:de:tuda-tuprints-185778
Tag der mündlichen Prüfung: 04.05.2021

Summary

With ongoing progress in cancer research and continuously improving treatment strategies for primary tumors, the incidence of brain metastasis is steadily increasing. The treatment options for brain metastasis patients, however, are limited and only prolong survival for a short duration. With the advent of immunotherapies, the cancer field was revolutionized. Checkpoint inhibitors, which reactivate T cell responses against cancer cells, show promising results even for aggressive cancers such as advanced metastatic melanoma. The brain was regarded as an immune privileged site for a long time. However, only recently a classical lymphatic system has been revealed in the brain. Moreover, the central nervous system harbors a greater variety of immune cells than previously assumed. Therefore, immunotherapies including checkpoint inhibitors, also gain interest for the treatment of brain metastases. To date, most research in the cancer field focusses on highly immunogenic cancer entities, whereas tumors of low immunogenicity such as breast cancer are less well investigated, as they are thought to be resistant to checkpoint inhibition. The development of strategies to convert 'cold' tumors of low immunogenicity into 'hot' tumors with a pro-inflammatory tumor microenvironment is of great interest, as they potentially sensitize highly immune suppressive tumor microenvironments to immune checkpoint inhibition. One strategy, that has shown promising results for different cancer entities is the combination of checkpoint inhibition with radiotherapy. The efficacy of this combination is investigated in clinical trials, including the treatment of brain metastasis. Current research focusses mostly on melanoma and lung cancer derived brain metastasis, and only little information is available on the efficacy of radio-immunotherapy in the treatment of breast cancer brain metastasis. Therefore, the aim of this thesis was to investigate if standard of care radiotherapy can sensitize breast cancer brain metastasis to immune checkpoint inhibition. In this context, the tumor microenvironment of the murine breast cancer brain metastasis model 99LN-BrM was investigated in detail. The purpose was to obtain an overview of proportions of cells, counteracting T cell responses, versus cells that are crucial for efficient checkpoint inhibition. It was confirmed that the tumor microenvironment of 99LN-BrM is a typical 'cold' microenvironment dominated by myeloid cells. However, cell types, crucial for checkpoint blockade, such as T cells and dendritic cells were identified, too. The next step was the examination of the influence of ionizing radiation on brain homing breast cancer cells and on the immune cell composition in 99LN-BrM. It was revealed that brain homing breast cancer cells increasingly express inflammatory markers, such as TNFα and IL1β, after *in vitro* irradiation. In a preclinical trial, the treatment of 99LN-BrM mice with fractionated whole brain radiotherapy, did not lead to increased recruitment of potentially immune suppressive cell types, such as blood borne myeloid cells or regulatory T cells. Moreover, radiosensitive cell types, crucial for efficient checkpoint inhibition, such as T cells

and dendritic cells were not depleted. On the contrary, the infiltration of cytotoxic CD8+ T cells into 99LN-BrM lesion was increased by fractionated whole brain radiotherapy. To obtain a deeper understanding of the T cell compartment in 99LN-BrM, TCRβ-profiling was performed next. These data reveled, that T cells in 99LN-BrM lesions and in CNS draining lymph nodes, clonally expand, indicating prior tumor directed T cell activation. However, a negative correlation of T cell expansion with brain metastasis volume was observed. This indicates progressive inhibition of T cell responses, which was confirmed by *in vivo* T cell depletion experiments. The depletion of T cells in mice, injected with brain homing 99LN-BrM cells, did not shorten the time of brain metastasis onset. This demonstrates that T cell responses in the microenvironment of 99LN-BrM are sufficiently suppressed. A checkpoint axis, which often plays a crucial role in immune system evasion of cancer cells, is the PD-1/PD-L1 axis. By expressing PD-L1, tumor cells can inhibit PD-1 positive T cells in the tumor microenvironment. Assessment of PD-L1 expression by brain homing breast cancer cell lines showed expression on the RNA- and protein level *in vitro*. *In vivo* analysis revealed that a high proportion of T cells in 99LN-BrM express PD-1, whereas PD-L1 is expressed by tumor cells, myeloid and T cells. Furthermore, analysis of the myeloid compartment demonstrated that a high proportion of infiltrating myeloid cells is PD-L1 positive, which is not the case for brain resident microglia. In a preclinical trial, treatment of 99LN-BrM mice with anti-PD-1, whole brain radiotherapy or a combination of both exhibited superior efficacy of the radio-immunotherapy over the monotherapies. Tumor progression slowed down, which translated into significantly prolonged median survival. However, long term survival was not achieved. The flow cytometric and histological analysis of brain metastases from mice in the preclinical trial, revealed that only in the combination cohort, both the infiltration of CD4+ and CD8+ T cells was enhanced in the brain metastasis lesions. At the same time, increased infiltration of blood-borne PD-L1+ myeloid cells, especially monocyte derived macrophages, was observed. Moreover, this infiltration was most prominent in the combination treatment group and indicates a crucial role of monocyte derived macrophages in acquired resistance to radio-immunotherapy. Furthermore, the *in vitro* assessment of T cell inhibitory capacity of 99LN-BrM conditioned microglia versus monocyte derived macrophages, revealed that the latter inhibit T cells more efficiently. To develop strategies to induce long term efficacy, macrophages were targeted pharmacologically, in addition to radio-immunotherapy. One strategy included the inhibition of the chemokine receptor CXCR4, expressed by macrophages, with the CXCR4 inhibitor AMD3100. This approach aimed at inhibiting the recruitment of monocyte derived macrophages to brain metastases. The second approach was aimed at targeting all macrophages by inhibiting CSF1R, the receptor to the macrophage survival factor CSF1. *In vitro*, the components of both signaling pathways were expressed by brain homing breast cancer cell lines. However, *in vivo*, both macrophage targeting strategies did not induce long

term efficacy of radio-immunotherapy with anti-PD-1. Analysis of 99LN-BrM lesions revealed that CXCR4 inhibition failed to inhibit the recruitment of monocyte derived macrophages and even increased the infiltration of 99LN-BrM with PD-L1+ immune cells. The pharmacological inhibition of CSF1R not only led to the depletion of most macrophages in brain metastasis, including microglia, but also significantly decreased T cell infiltration, which is crucial for the efficacy of checkpoint inhibition. To induce long term efficacy in the future, a deeper understanding of myeloid immune suppressive cells in breast cancer brain metastasis is crucial. Additionally, treatment strategies, targeting the recruitment of blood borne myeloid cells specifically, while sparing other immune cells, need to be developed.

Zusammenfassung

Durch fortschreitende Entwicklungen in der Krebsforschung und Verbesserungen der Behandlungsoptionen zur Bekämpfung primärer Tumore steigt auch die Inzidenz von Hirnmetastasen. Die Therapiemöglichkeiten für Patienten mit Hirnmetastasen sind jedoch begrenzt und verlängern das Überleben nur kurzzeitig. Mit dem Aufkommen neuartiger Immuntherapien wurde das Feld der Krebsforschung revolutioniert. Checkpoint Inhibitoren, die T-Zellen gegen Krebszellen reaktivieren können, zeigen nach ersten Erkenntnissen Erfolge, sogar im Falle aggressiver Krebsarten wie fortgeschrittener Melanome und Lungenkarzinome. Das Gehirn wurde lange Zeit als immun privilegiert angesehen. Kürzlich wurde jedoch ein klassisches lymphatisches System im zentralen Nervensystem entdeckt. Außerdem ist die Vielfalt an Immunzellen größer als bisher angenommen. Aus diesem Grund, gewinnen Immuntherapien wie Checkpoint Inhibitoren an Bedeutung für die Behandlung von Patienten mit Hirnmetastasen. Der aktuelle Fokus der Forschung liegt auf hochgradig immunogenen Krebsentitäten. Tumore mit geringer Immunogenität wie Brustkrebs wurden bisher weniger intensiv erforscht, da hier von Resistenzen gegen Checkpoint Inhibitoren ausgegangen wird. Die Entwicklung von Strategien um sogenannte ‘kalte‘ Tumore mit geringer Immunogenität in ‘heiße‘ Tumore mit pro-inflammatorischem Tumormikromilieu umzuwandeln und sie somit für Checkpoint Inhibition zu sensibilisieren, ist von großem Interesse. Eine vielversprechende Strategie, die gute Ergebnisse in der Behandlung verschiedener Krebsarten zeigt, ist die Kombination von Checkpoint Inhibitoren mit Radiotherapie. Die Wirksamkeit dieser Kombination wird aktuell in klinischen Studien untersucht, auch in Bezug auf Hirnmetastasen. Dennoch liegt der Fokus auch im Falle der Kombinationstherapien hauptsächlich auf dem Melanom und Lungenkrebs, während Erkenntnisse zur Wirksamkeit von Radio-Immuntherapie gegen Brustkrebs-Hirnmetastasen sehr begrenzt sind. Aus diesem Grund war das Ziel dieser Arbeit zu untersuchen, ob Standard-Radiotherapie Brustkrebs-Hirnmetastasen für Checkpoint Inhibition sensibilisieren kann. In diesem Zusammenhang wurde das Tumormikromilieu des murinen Brustkrebs-Hirnmetastase Modells 99LN-BrM im Detail untersucht, mit dem Hintergrund, den Anteil T-Zell hemmender Zelltypen im Gegensatz zu Zellen, die essenziell für Checkpoint Inhibition sind, zu bestimmen. Es konnte bestätigt werden, dass das Tumormikromilieu von 99LN-BrM zwar ein typisch ‘kaltes‘ Milieu ist, das von myeloiden Zellen dominiert wird. Jedoch konnten auch Zelltypen, die für Checkpoint Inhibition essenziell sind, identifiziert werden. Im nächsten Schritt wurde der Einfluss von Bestrahlung auf Brustkrebszelllinien und auf die Komposition von Immunzellen in 99LN-BrM Hirnmetastasen untersucht. Es zeigte sich, dass Brustkrebszelllinien mit Hirntropismus nach *in vitro* Bestrahlung verstärkt inflammatorische Marker wie TNFα and IL1β exprimieren. Präklinischen Studien offenbarten, dass die Behandlung von 99LN-BrM Mäusen mit fraktionierter

Ganzhirnbestrahlung nicht die Rekrutierung potenziell immun suppressiver Zelltypen wie peripherer myeloider Zellen oder regulatorischer T-Zellen verstärkt. Außerdem wurden radiosensitive Zelltypen wie T-Zellen und dendritische Zellen, die ausschlaggebend für die Wirkung von Checkpoint Inhibition sind, nicht depletiert. Im Gegenteil, fraktionierte Ganzhirnbestrahlung steigerte sogar die Infiltration von zytotoxischen CD8+ T-Zellen in 99LN-BrM Läsionen. Um ein tieferes Verständnis des T-Zell Kompartiments in 99LN-BrM Läsionen zu erhalten, wurde TCRβ-Sequenzierung angewendet. Diese Analysen zeigten, dass T-Zellen in 99LN-BrM Läsionen und zervikalen Lymphknoten klonal expandieren, was ein Indikator für vorangehende T-Zellaktivierung ist. Jedoch wurde auch eine negative Korrelation von T-Zell Expansion mit Tumorvolumen beobachtet. Dies deutet auf eine fortschreitende Suppression der T-Zellantwort hin, was mit *in vivo* T-Zell Depletions-Experimenten bestätigt werden konnte. Die Depletion von T-Zellen in Mäusen denen 99LN-BrM Zellen intrakardial injiziert wurden, verringerte nicht die Zeit bis zur Entstehung der Hirnmetastasen. Dies weist auf eine effektive Suppression der T-Zellantwort in 99LN-BrM hin. Tumorzellen nutzen hierbei grundlegende Mechanismen der Regulation der T-Zellaktivität mittels Immuncheckpunkten aus. In diesem Zusammenhang spielt die PD-1/PD-L1-Achse eine zentrale Rolle. Durch die Expression von PD-L1 können Tumorzellen PD-1 positive T-Zellen im Tumormikromilieu hemmen. Die *in vitro* Analyse der PD-L1 Expression in Brustkrebszelllinien mit Hirntropismus zeigte, dass der Ligand auf RNA- und Proteinebene exprimiert wird. *In vivo* Analysen demonstrierten, dass ein hoher Anteil an T-Zellen in 99LN-BrM Läsionen PD-1 exprimieren, während PD-L1 von Tumorzellen, myeloiden Zellen und T-Zellen exprimiert wird. Die Analyse des myeloiden Kompartiments zeigte außerdem, dass ein hoher Anteil der infiltrierenden myeloiden Zellen PD-L1 positiv ist. Dies ist nicht der Fall bei den hirnresidenten Mikroglia. In einer präklinischen Studie von 99LN-BrM Mäusen mit anti-PD-1, Bestrahlung oder eine Kombination aus Beidem, zeigte die Radio-Immuntherapie erhöhte Wirksamkeit im Vergleich zu den Monotherapien. Die Tumorprogression wurde verzögert, was zu einem signifikant erhöhten medianen Überleben führte. Ein langfristiger Effekt konnte jedoch nicht erzielt werden. Durchflusszytometrie und histologische Analysen offenbarten, dass die Infiltration von CD4- als auch CD8-positiven T-Zellen, nur in der Kombinationsgruppe erhöht war. Zur selben Zeit verstärkte sich jedoch auch die Infiltration mit PD-L1 positiven peripheren myeloiden Zellen, besonders mit Knochenmarks-Makrophagen. Am ausgeprägtesten war diese Infiltration in der Kombinationsgruppe zu beobachten, was auf eine wichtige Rolle der peripheren Makrophagen in der Resistenzentwicklung gegen die angewendete Radio-Immuntherapie hindeutet. Außerdem ist die Fähigkeit von tumorkonditionierten Knochenmarks-Makrophagen, T-Zellen *in vitro* zu hemmen, größer im Vergleich zu tumorkonditionierten Mikroglia. Um Möglichkeiten zu finden Langzeiteffekte zu erzielen, wurden zusätzlich zur Radio-Immuntherapie mit anti-PD-1 Makrophagen

pharmakologisch inhibiert. Eine Strategie beinhaltete die Inhibition des CXCR4 Rezeptors, der von Makrophagen exprimiert wird, durch den CXCR4 Inhibitor AMD3100. Dieser Ansatz sollte die Rekrutierung von Knochenmarks-Makrophagen zu den Hirnmetastasen hemmen. Der zweite Ansatz umfasste die Blockade von CSF1R, der Rezeptor des Zytokins CSF1, das wichtig ist für das Überleben von Makrophagen im Allgemeinen. *In vitro* Analysen bestätigten die Expression der Komponenten beider Signalwege in Brustkrebszelllinien. In präklinischen Studien konnten beide Strategien jedoch keine Langzeitwirkung der Radio-Immuntherapie induzieren. Die Analyse der 99LN-BrM Läsionen zeigte, dass die Inhibition von CXCR4 nicht die Rekrutierung von Knochenmarks-Makrophagen aufhalten konnte. Die Infiltration von PD-L1 positiven Immunzellen wurde sogar verstärkt. Die pharmakologische Hemmung von CSF1R führte zwar zur Depletion der meisten Makrophagen in den Hirnmetastasen, Mikroglia eingeschlossen, sie führte jedoch auch zu einer signifikanten Verringerung der T-Zellinfiltration, welche essenziell für die Wirksamkeit von Checkpoint Inhibition ist. Um in der Zukunft Langzeiteffekte zu erzielen, muss ein tiefergehendes Verständnis der Rolle myeloider immunsuppressiver Zellen in Brustkrebs-Hirnmetastasen erreicht werden. Außerdem müssen Strategien entwickelt werden, die spezifisch die Rekrutierung peripherer myeloider Zellen hemmen, während andere Immunzellen verschont bleiben.

Table of Content

1. Introduction

1.1. Brain metastasis - statistics and standard of care

Brain metastases (BrM), the most frequent intracranial tumors, represent an especially dire prospect of cancer, with high mortality rate and a median survival of 1-2 month and 6 month for untreated and standard of care treated patients, respectively (Fidler, 2015). It is estimated that approximately 30% of patients with solid tumors develop BrM (Suh *et al*, 2020). The incidence of BrM is increasing even further with advanced imaging detection and treatment of primary tumors, as more patients will survive to develop metastases (Tabouret *et al*, 2012; Suh *et al*, 2020). The most common primary cancers to develop BrM are melanoma, lung and breast cancer for both genders, with breast cancer being the leading cause of BrM for female patients (Cagney *et al*, 2017; Stelzer, 2013). Triple negative breast cancer (TNBC) is the breast cancer subtype with the highest propensity to metastasize to the brain, with approximately 25-46% of patients developing BrM (Adams *et al*, 2014; Chamberlain *et al*, 2017). The standard of care for these patients is mostly local treatment, such as radiotherapy delivered as whole brain radiotherapy (WBRT) or stereotactic radiosurgery (SRS), and surgery. Systemic targeted treatments are not often used yet and not well investigated (Chamberlain *et al*, 2017). Standard treatments mostly prolong survival for a short time only, so there is a need for better understanding of BrM and a consequent development of new therapeutic strategies. One reason for a limited progress in this field is that BrM patients are often excluded from clinical trials and data available are mostly retrospective analyses. This means not only limited advance in research, but also limited access of BrM patients to new treatment opportunities. Another aspect of BrM, which makes scientific advances challenging, is the immense complexity of the brain microenvironment and the disease itself. The central nervous system (CNS) contains multiple specialized cell types, which cannot be found in other tissues. Additionally, BrM are derived from distinct primary tumor entities, therefore the disease can have different characteristics and can lead to various microenvironmental and immune responses. Having increasing proof, that checkpoint inhibition is beneficial for melanoma BrM patients for example, does not automatically allow the conclusion that this holds true for patients with less immunogenic brain tumors, such as breast cancer derived BrM. Therefore, treatments must be investigated in detail, tailored specifically to the BrM type and brain tumor microenvironment (TME).

1.2. From the primary tumor to brain metastasis

In 2000 Hanahan and Weinberg proposed six characteristics shared by all cancers, termed the hallmarks of cancer (Hanahan & Weinberg, 2000). These are **sustaining proliferative signaling**, **evading growth suppressors**, **resisting cell death**, **enabling replicative immortality**, **inducing angiogenesis** and **activating invasion and metastasis** (Fig.1.1: yellow). In 2011 these hallmarks have been revised to additionally include **deregulating cellular energetics**, **genome instability and mutation**, **tumor promoting inflammation** and **avoiding immune destruction** (Hanahan & Weinberg, 2011) (Fig.1.1: blue). The latter actually has already been proposed 7 years earlier by Dunn *et al*. as an additional hallmark of cancer (Dunn *et al*, 2004). In line with the focus of this thesis, three characteristics of cancer will be described in more detail in this chapter: **avoiding immune destruction** (section 1.2.1), **tumor promoting inflammation** (section 1.2.2) and **activating invasion and metastasis** (section 1.2.3) (Fig 1.1: green).

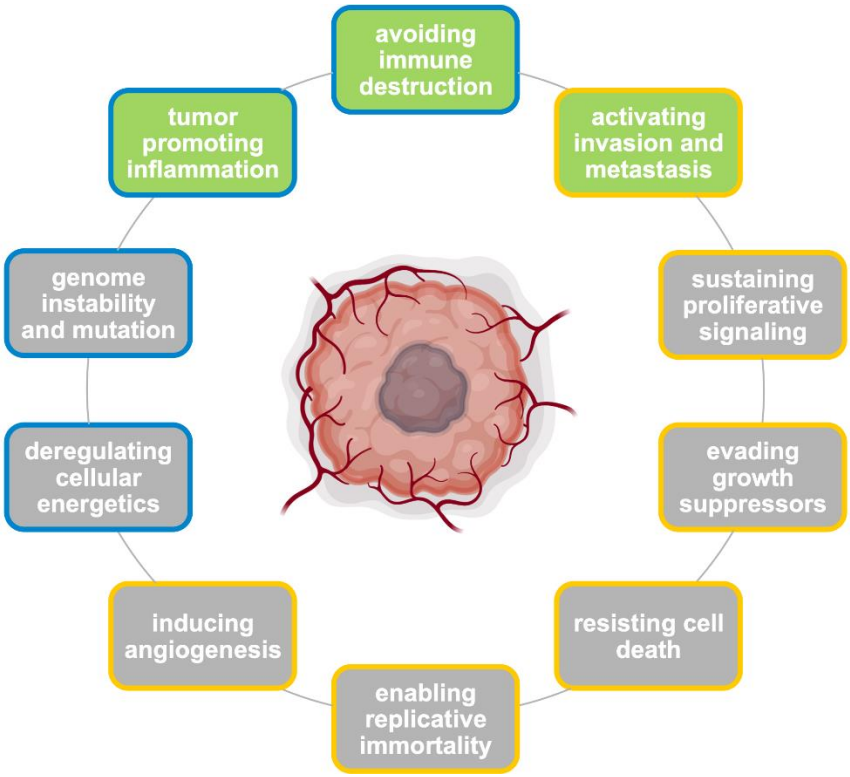

Fig. 1.1: The hallmarks of cancer. This scheme depicts hallmarks (yellow) and emerging hallmarks (blue) of cancer proposed by Hanahan and Weinberg (Hanahan & Weinberg, 2000, 2011). Green boxes highlight hallmarks of special interest for this thesis. These hallmarks will be introduced in more detail in the following sections, namely 'avoiding immune destruction', 'tumor promoting inflammation' and 'activating invasion and metastasis', with a special focus on brain metastasis.

1.2.1. Avoiding immune destruction

Already in 1909, Paul Ehrlich proposed that a host can be protected from neoplasia by the immune system (Ehrlich, 1909). Decades later, Burnet and Thomas named this the 'cancer immune surveillance hypothesis' (Burnet, 1971, 1964; Thomas, 1961), which, unfortunately, could not have been proven with the given experimental methods at the time. Nowadays, it is known that tumors consist of an extraordinarily complex tumor microenvironment, interspersed with a variety of cell types, including immune cells. It is widely accepted for most cancer types, including brain tumors, that the immune system takes part in the development and progression of tumors (Kroemer *et al*, 2015; Quail & Joyce, 2017). It can have a role in the initial protection against cancer as well as support of development and outgrowth of tumors, as depicted in the following sections. To evade the immune system, cancer cells have to undergo three phases of cancer immunoediting proposed in 2004 by Dunn *et al*., namely, Elimination, Equilibrium and Escape phase (Dunn *et al*, 2002, 2004).

In the elimination phase, immunogenic tumor cells are still recognized and eliminated by the immune system. During elimination, both, adaptive immune cells, such as CD4+ or CD8+ T lymphocytes, and innate immune cells, such as natural killer cells (NK) and Natural killer T cells (NKT cells), play a vital role in killing emerging tumors (Ostroumov *et al*, 2018; Smyth *et al*, 2001). Interferon-γ (IFNγ) secretion in response to the tumor has been shown to be a key cytokine for a sufficient immune response in this phase (Shankaran *et al*, 2001). It can act directly on tumor cells and induce apoptosis or increase the immune response via acting on immune cells.

In the second phase, the tumor reaches a state of equilibrium, which can continue for several years. In this phase, tumor growth and killing by the immune system are balanced. The high mutation rates and high heterogeneity of tumors ensures that some cancer cells survive and continue to grow under the constant selective pressure of the immune system. This pressure leads to an evolution of the tumor, leading to the emergence of cells which are less immunogenic, so it can finally break free and reach the escape phase (Dunn *et al*, 2004).

In the escape phase the tumor can grow out via different evolved mechanisms to prevent destruction by the immune system. For example, tumor antigens or major histocompatibility complex I (MHCI), which is important for presentation of these antigens, can be downregulated (Garrido & Algarra, 2001). The IFNγ sensitivity can be reduced, for example through dysfunction of IFNγ signaling in tumor cells. Other examples include secretion of immune suppressive cytokines or the recruitment of immune suppressive cells, such as macrophages and Forkhead-Box-Protein P3 positive (FoxP3+) regulatory T cells (Treg) (Dunn *et al*, 2004). Treg by their nature inhibit the proliferation and effector functions of several T cell subsets, as well as NK, NKT and B cells (Sakaguchi *et al*, 2010). Meta-analyses of human data show a negative correlation of Treg infiltration with overall survival of patients across several cancer

types, indicating that these cells help in evading the immune system (Shang *et al*, 2015). Moreover, cancer cells can express increased amounts of Indoleamine 2,3-dioxygenase, which leads to a stress response in T cells, potentially inducing a polarization to immune suppressive Treg and to the recruitment of myeloid derived suppressor cells (Holmgaard *et al*, 2015; Leibold *et al*, 2019). Another example of brain tumors avoiding immune destruction is induction of apoptosis in T cells via CD70 signaling by cancer cells (Wischhusen *et al*, 2002). Finally, ligands to immune checkpoint receptors can be expressed by tumor cells or by other cells in the TME. Binding of these ligands to checkpoint receptors, expressed by effector T cells, can inhibit T cells effectively (Pardoll, 2012). The inhibition of immune checkpoints is a major focus of this thesis and will be discussed in greater detail in section 1.4.2. In conclusion, the functions of immune cells in the TME are ambiguous. On the one hand, they are crucial for cancer cell killing and containment, on the other hand, they foster the process of cancer immunoediting, and help cancers to reach the escape phase via a multitude of mechanisms.

1.2.2. Tumor promoting inflammation

Inflammation can promote all phases of tumor development. Human data shows, that chronic inflammation can induce neoplasia. A well-known example is *Heliobacter pylori* induced gastritis which predisposes to cancer (Houghton *et al*, 2004). As described in the section before, inflammation can lead to immunoediting of cancer cells and therefore foster decrease of immunogenicity and increase of malignancy (Dunn *et al*, 2002). Leukocytes, recruited to the tumor cells, can secrete chemicals, such as reactive oxygen species (ROS) and consequently increase genetic instability of cancer cells (Weinberg *et al*, 2019) which heightens the possibility that they reach replicative immortality.

Beyond these initial steps, chronic inflammation plays a prominent role in both the escape phase and in established cancer. Immune cells recruited to the tumor can have a dual role where they not only elicit anti-tumor functions, but very often develop tumor promoting functions in the ‘Darwinian microenvironment’ of growing cancer (Balkwill & Mantovani, 2001; Balkwill *et al*, 2005). Key cell types involved in establishing tumor promoting inflammation and an immune suppressive microenvironment are myeloid cells, such as macrophages. However, lymphocytes, such as Treg, have been found to play a role, too (Balkwill *et al*, 2005; Facciabene *et al*, 2012; Quail & Joyce, 2017). Immune cells are recruited to lesions and polarized to elicit tumor promoting functions in response to various cytokines and chemokines secreted by cancer cells, such as transforming growth factor β (TGFβ) and C-C chemokine receptor type 2 (CCR2) (Flavell *et al*, 2010; Mollica Poeta *et al*, 2019). Tumor promoting inflammation has been described as an ‘enabling’ characteristic by Hanahan and Weinberg, meaning that it can enable or promote other hallmarks of cancer (Hanahan & Weinberg, 2011). For example, leukocytes, recruited during inflammation, such as tumor associated

macrophages (TAM), can help cancer cells evade the immune system, as described previously. They can also facilitate angiogenesis, the growth of new vessels, essential for nutrient and oxygen supply to the tumor (Balkwill *et al*, 2005; Mantovani & Locati, 2016). Moreover, tumor associated leukocytes can secrete growth factors and therefore enable continued growth of tumor or provide factors which protect cancer cells from programmed cell death (apoptosis) (Aras & Zaidi, 2017; Kaler *et al*, 2010). Furthermore, they are able to facilitate invasion and metastasis of cancer cells via secreting proteases to digest the extracellular matrix (ECM) of tumors, or in the case of BrM, process junctional adhesion molecules, to foster transmigration through the blood-brain-barrier (BBB) (Kessenbrock *et al*, 2010; Sevenich *et al*, 2014). The role of immune cells in the invasion-metastasis cascade will be the focus of the next section. The role of the individual immune cell types in the brain tumor microenvironment will be described in section 1.3.

1.2.3. The metastatic cascade

At first detection of cancer, many patients already have micro- or macrometastases. Indeed, over 90% of solid cancer patients die as the consequence of metastatic spread (Jiang *et al*, 2015). Already in 1889 it has been realized that certain cancers (seed) are prone to metastasize to specific secondary tissues (soil). The phenomenon was named the 'seed and soil' theory (Paget, 1889). For example, cancer types such as breast, lung cancer or melanoma, are more prone to form BrM than others (Stelzer, 2013). In order to reach the secondary tissue, cancer cells must survive the metastatic cascade, a process, consisting of a number of complex steps, for which the cells have to constantly adapt. These steps include dissemination and migration from the primary tumor, intravasation into the adjacent blood vessels, survival in the blood stream, arrest followed by extravasation, and finally colonization in the secondary tissue, for example the brain. Timewise, metastasis does not always occur after full establishment of the primary tumor (late dissemination model) and can also develop in parallel (early dissemination model) (Klein, 2008) (Fig. 1.2).

Cancers with an epithelial origin, including breast cancer, are typically held in place by an array of junction proteins. Downregulation or disruption of these proteins leads to increased capacity of tumor cells to disseminate from the tumor bulk and to invade adjacent tissue (Jiang *et al*, 2015). Well-known examples, important for cell-cell adhesion, are proteins from the Claudin-family or E-cadherin. E-cadherin is often lost or downregulated by cancer cells, which increases the potential of metastatic dissemination (Cavallaro & Christofori, 2004; Onder *et al*, 2008).

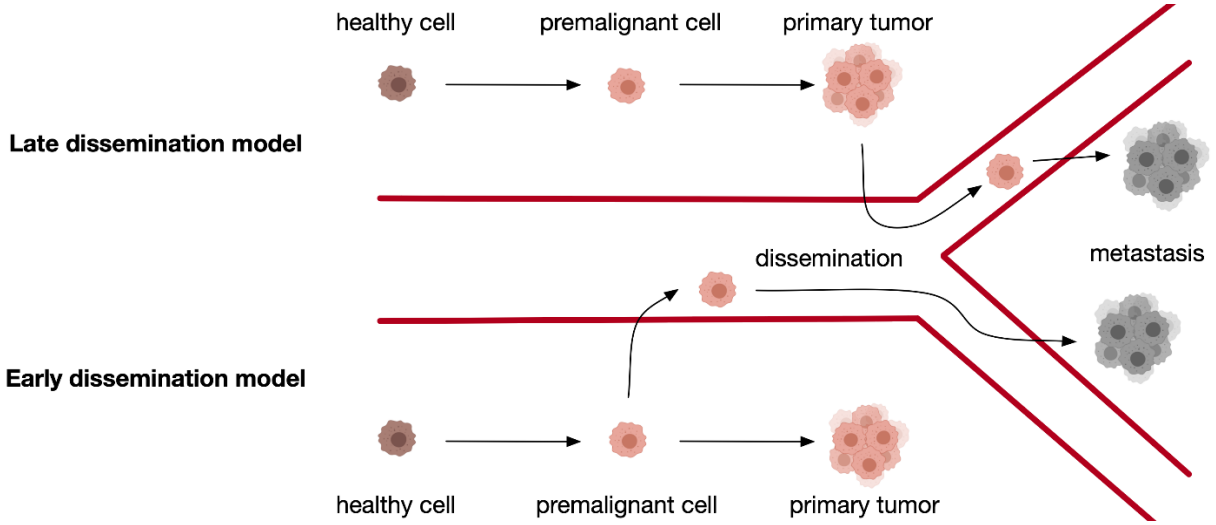

Fig. 1.2: Models of dissemination of metastasizing cells from the primary tumor. Scheme representing the two theories of dissemination. The model of late dissemination depicts a scenario where the metastasizing cell leaves the tumor after the process of immunoediting. Metastasizing cells will be genetically similar to the primary tumor. This is not the case for the early dissemination model. In this model the metastasizing cell disseminates from the premalignant cell before completion of immunoediting and establishment of the primary tumor. The consequence is that metastasis and primary tumor will evolve very differently and will be genetically more distinct than in the late dissemination model, which complicates treatment of patients further (Klein, 2008).

The complex role of E-cadherin loss is not fully elucidated. However, it has been shown to play a role in other mechanisms of metastasis development. One of these is its role in epithelial-mesenchymal transition (EMT), the dedifferentiation of epithelial cells to more mesenchymal phenotypes. This process allows cancer cells to be more motile, migrate and invade adjacent tissue and cell layers till they finally reach the circulation. Loss of E-cadherin by cancer cells leads to upregulation of a multitude of proteins which foster EMT, such as Twist (Onder *et al*, 2008). As described before for the primary tumor, cells in the TME, including immune cells, support metastatic cells on their way through tissues and physically restrictive environments, such as the ECM. Macrophages have been shown to closely interact with tumor cells during this process via a Colony stimulating factor 1 (CSF1) - Epidermal growth factor (EGF) paracrine loop, which increases the motility of cancer cells (Wyckoff *et al*, 2004). The route of cancer spread, most relevant for BrM, is over the blood circulation. Perivascular macrophages have been shown to directly interact with tumor cells at vessels and foster their intravasation into the vessel lumen (Wyckoff *et al*, 2007). Once in the circulation, cancer cells must survive in the blood stream. Major challenges here are mechanical stress, such as shear forces, or the risk of immune recognition (Strilic & Offermanns, 2017). As mentioned previously, immunoediting leads to less immunogenic tumor cells, which also helps to avoid the immune system in the blood via, for example, MHCI downregulation (Dunn *et al*, 2004). Another mechanism for tumor cells to survive in the blood stream, is to attach to circulating cells, such as platelets.

These can cover cancer cells and therefore shield them from immune detection, as well as protect them from shear forces (Gay & Felding-Habermann, 2011). Nevertheless, most metastatic cells will not survive in the blood stream and only a very small percentage actually grow out to metastases, a phenomenon called 'metastatic inefficiency' (Strilic & Offermanns, 2017; Wong *et al*, 2001). Surviving cancer cells need to arrest at the target tissue, whilst being in the blood flow. This mostly happens in microvessels, often at branching points, where cancer cells or cancer cell aggregates get physically stuck (Weiss, 1992). This has also been confirmed for BrM through real-time microscopy in different mouse models (Kienast *et al*, 2010). If the cancer cells survive this pressure on the cell body, the extravasation into parenchyma must follow quickly. In the case of BrM, this means crossing the highly restrictive BBB, which will be described in the next section. Once the cells have passed this barrier, they must colonize the extremely specialized microenvironment of the brain parenchyma, which will be the focus of section 1.3.

1.2.4. Crossing the Blood Brain Barrier

The brain parenchyma can be a sanctuary site for metastatic tumor cells, mostly due to the BBB. It restricts the entry of most drugs and agents, used for the treatment of the primary tumor or extracranial metastases. It is formed by endothelial cells, rigidly connected by tight junctions, enveloped by a specialized basal lamina, interspersed with pericytes and ensheathed by a layer of astrocyte endfeet, the so-called glia limitans. Together with microglia and neurons which are physically interacting with the BBB, these cell types form the neurovascular unit (NVU) (Arvanitis *et al*, 2020). CNS homeostasis is dependent on proper NVU function, which means not only strictly controlling the influx of molecules and cells, but also active efflux of xenobiotics and toxins through specialized transporters. Within the brain tumor, the BBB is called 'blood tumor barrier' (BTB) as it changes and is disrupted during tumor progression and therefore is partially leaky. Nevertheless, it remains functional enough to decrease drug penetration heterogeneously, thus hindering effective treatment (Arvanitis *et al*, 2020).

To be able to extravasate into the brain parenchyma, metastatic cancer cells must acquire strategies to cross the BBB. Kienast et al. demonstrated that extravasation occurs at small holes in the vascular wall and that a strict perivascular position is necessary. To survive in the brain parenchyma and form BrM, extravasated cancer cells need access to nutrients and oxygen. Therefore, they stay close to vessels and either continue growing along existing vessels (co-option) or induce sprouting of new vessels (angiogenic growth) (Kienast *et al*, 2010). In 2009, a BrM gene signature for breast cancer was identified. Together with Cyclooxygenase 2 (COX2) and EGF receptor (EGFR), ST6GALNAC5 has been identified. Noteworthy, the expression of this gene is typically restricted to the brain. However, when expressed by cancer cells it increased the BBB transmigration. The authors hypothesized that

this is facilitated by increased adhesion of the cancer cells to brain endothelial cells (Bos *et al*, 2009). Additionally, it has been demonstrated that at this step of metastasis, tumor cells rely on the help of stromal cell types. In experimental BrM, Cathepsin S fostered BBB transmigration via cleavage of junctional adhesion molecule B (JAM-B), an adhesion protein which is part of tight junctions. This protein was not only expressed by the cancer cells, but also by adjacent stromal cells. Only by inhibiting the expression of Cathepsin S by both, the tumor and stroma cells, was it possible to abrogate its supportive function in BrM. This indicates that stromal cells support metastatic cells during brain colonization via Cathepsin S (Sevenich *et al*, 2014). It has been shown, that in TNBC derived BrM Angiopoietin 2 (Ang-2) secretion by endothelial cells in the brain microvasculature impairs tight junctions and increases the permeability of the BBB, thus helping tumor cell colonization. Moreover, expression of COX-2 by human brain endothelial cells induced matrix metalloproteinase-2 (MMP-2) expression by the same cells, which in turn mediated the transmigration of breast cancer cells through the BBB (Lee *et al*, 2011). Furthermore, microglia, the main immune cells of the brain, can actively assist tumor cells to invade the brain tissue in a Wnt-dependent manner (Pukrop *et al*, 2010). Similarly, astrocytes can help tumor cell invasion into the brain via expression of Sphingosin-1-phosphat-Rezeptor 3 (S1P3), which leads to secretion of Interleukin 6 (IL6) and CC-Chemokin-Ligand-2 (CCL2), followed by loosening of endothelial cell adhesions in the BBB (Gril *et al*, 2018). In conclusion, cancer cells require the support of different stromal cell types to cross the strictly controlled BBB. After crossing the BBB, they need to survive and adapt to the specialized brain microenvironment described in the following sections.

1.3. The brain microenvironment and immune surveillance in the CNS

The brain is a highly specialized and complex microenvironment which must be protected at all times to prevent neuronal damage. Every small change in CNS homeostasis can lead to fatal neurodegeneration. In order to keep this critical balance, everything entering or leaving the brain parenchyma is strictly controlled. As described before, the BBB enables this tight control. However, neuronal damage can easily be induced through inflammation. Therefore, the immune surveillance of the CNS is equally heavily regulated. Microglia, the brain resident macrophages, are the main immune cell type in the brain parenchyma. For a long time, it was believed that the brain is an immune privileged organ, with lack of peripheral immune surveillance through blood borne immune cells, owing to the BBB and insufficient lymphatic drainage (Head & Griffin, 1985; Korn & Kallies, 2017). This was mostly due to early animal experiments, showing that tumor grafts, implanted into the brain parenchyma, were not rejected, leading to the conclusion that the brain is completely cut off of systemic immunity

(Murphy & Sturm, 1923). However, this paradigm has changed recently, as it is recognized, that while CNS immunity is highly controlled, the CNS is not completely devoid of blood-borne immune cells. Several macrophage populations patrol the linings of the CNS, such as dural boarder associated, perivascular and choroid plexus macrophages (Mrdjen *et al*, 2018). Moreover, even dendritic cells capable of presenting antigen, as well as CD4+ and CD8+ T cells have been identified in the meninges and choroid plexus (D'Agostino *et al*, 2012; Korin *et al*, 2017; Mrdjen *et al*, 2018; Russo & McGavern, 2015). This is in concordance with the transplantation experiments from 1923, which showed that tissue transplanted into the brain parenchyma was rejected when it touched border regions or the ventricles (Murphy & Sturm, 1923). Furthermore, it has been demonstrated that afferent antigen sampling from the CNS takes place and that CNS-derived antigen can induce priming of naïve T cells (Harris *et al*, 2014). In 2015, classical lymphatic vessels were identified in the meninges for the first time. These vessels can drain antigen into the deep cervical lymph nodes (Aspelund *et al*, 2015; Louveau *et al*, 2015; Raper *et al*, 2016). Recently, this vessel network has been investigated in more detail in the scenario of experimental brain tumors (glioma and melanoma BrM). It has been revealed that the dorsal meningeal lymphatic vessels are the main vessels draining antigen from the brain in case of brain tumors (Hu *et al*, 2020). However, these mouse models, unlike human BrM, do not have an extracranial tumor. Lorger *et al*. showed that an extracranial tumor is necessary to induce CD8+ T cell trafficking to the brain (Taggart *et al*, 2018). Song *et al*. confirmed that the drainage from tumors, restricted to the brain parenchyma, is insufficient to lead to proper T cell priming of naïve T cells in the cervical lymph nodes. In this case vascular endothelial growth factor C (VEGF-C), a pro lymphatic factor, was enough to induce T cell priming of naïve T cells in the cervical lymph nodes (Song *et al*, 2020). To simplify, it has been demonstrated, that the brain has a classical lymphatic system which drains antigen, and therefore is connected to systemic immunity, but in the case of brain tumors, the drainage might be too weak, to induce a proper adaptive immune response. If this holds true, or is an artefact of intracranial mouse models, must be further investigated. It is known, however, that the brain tumor microenvironment can harbor a multitude of brain resident and recruited cell types (Quail & Joyce, 2017). Functions of these cell types in brain tumors will be summarized in the following sections and are depicted in Figure 1.3.

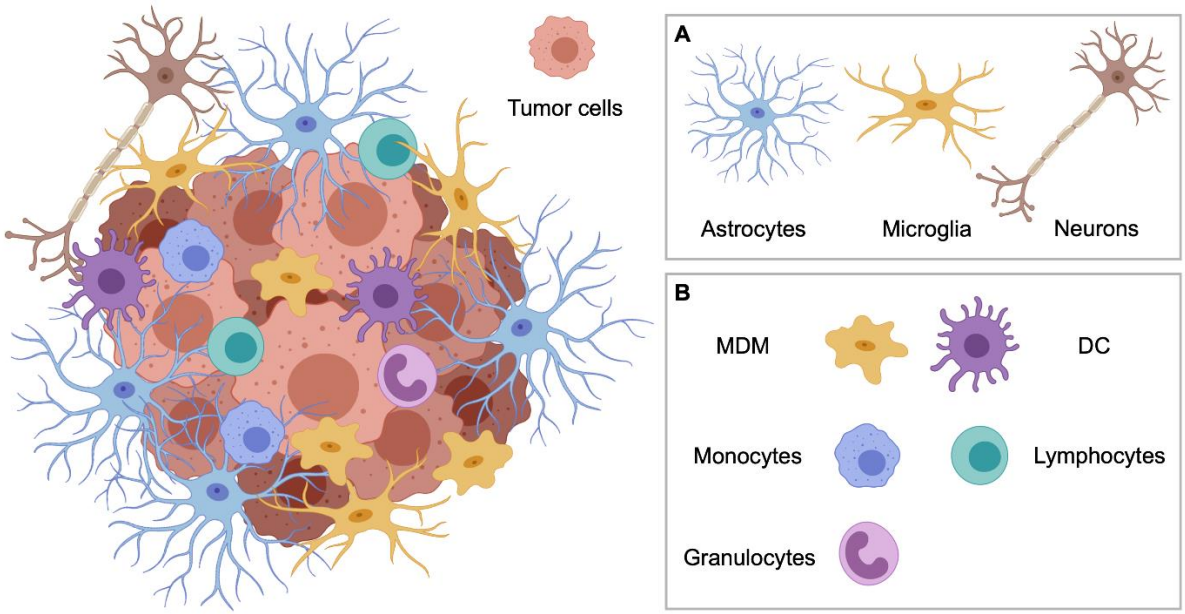

Fig. 1.3: The microenvironment of brain tumors. Depicted are crucial cell types identified in the tumor microenvironment of brain tumors. (A) Includes Neurons and neuroglia, which are resident to the steady state brain parenchyma. They are described in section 1.3.1. (B) Includes cell types potentially recruited to the brain parenchyma under disease conditions such as BrM. Functions of these cell types are described in section 1.3.2.

1.3.1. Brain resident cells and their role in brain metastasis

Neurons & Neuroglia

Neurons are responsible for cell-to-cell signal transmission and are the most crucial cell type in the CNS. Through chronic inflammation induced by BrM, neuroinflammation, followed by neurodegeneration is induced (Schulz *et al*, 2019). Furthermore, neurons can be damaged by deformation and physical pressure on the cell body, caused by a growing brain tumor in the confined space of the scull (Seano *et al*, 2019). Additionally, different standard treatments, such as chemotherapy or radiotherapy, can lead to neuronal loss and severe side effects. For a long time, research has mainly focused on how to prevent this fatal neurodegeneration, when treating brain tumors. Nowadays, more effort is placed onto elucidating how tumor cells can adapt to the specific environment of the brain, and whether neurons can facilitate this adaptation and BrM progression. In 2014 Neman et al. demonstrated, that human breast derived BrM cells can acquire a GABAergic phenotype, similar to that of neurons, which enables these cancer cells to use gamma-aminobutyric acid (GABA) as an energy source in the brain (Neman *et al*, 2014). In 2019 it has been proven that neurons can directly interact with glioma cells through the formation of synapses and provide glutamatergic input. This interaction has been shown to promote tumor progression (Venkataramani *et al*, 2019; Venkatesh *et al*, 2019). In the same year, Zeng et al. demonstrated that the direct interaction via pseudo-synapses is also facilitating the colonization of breast cancer derived BrM cells (Zeng *et al*, 2019).

Neurons are outnumbered by non-neuronal cells that populate the brain, the so-called neuroglia. In the CNS, these comprise oligodendrocytes, ependymal cells, astrocytes and microglia. Most research in the brain tumor field focuses on the role of astrocytes and microglia, which delineate brain tumors from the stroma via gliosis formation. The role of microglia will be described in the next section. Astrocytes are the most abundant cell type in the brain. They are extremely heterogenous and have a complex array of functions, e.g. they participate in the formation of the BBB, supply neurons with nutrients, play a role in damage repair through scar formation, and participate in synapse formation (Marina *et al*, 2018; Anderson *et al*, 2016; Allen & Eroglu, 2017). It has been demonstrated that astrocytes can actively help cancer cells to transmigrate through the BBB. Furthermore, it has been revealed that they can facilitate BrM progression via activating peroxisome proliferator-activated receptor γ (PPARγ) on brain metastatic cancer cells, for example. This receptor has been shown to be expressed highly in human BrM samples and is important for uptake of fatty acids. Increased activation of this receptor through astrocytes led to increased proliferation of BrM cells and inhibiting it *in vivo* led to prolonged survival (Zou *et al*, 2019). Another example is the expression of TGFβ2 by astrocytes, which leads to Angiopoietin-like 4 (ANGPTL4) expression by TNBC cells and increases their potential to form BrM (Gong *et al*, 2019). Moreover, astrocytes protect the brain parenchyma from infiltration by T cells via Fas Ligand (FasL), which induces apoptosis of T cells (Bechmann *et al*, 2002). This mechanism could potentially further increase immune suppression in the TME of BrM. Astrocytes can however also elicit anti-tumor functions, e.g. plasmin expressed by the reactive stroma can convert membrane bound astrocytic FasL, so it serves as a death signal for extravasated tumor cells in the brain parenchyma (Valiente *et al*, 2014).

CNS resident immune cells

Recently, higher variability of immune cell populations than initially expected has been discovered in the CNS. The majority are compartment specific macrophage populations, such as perivascular macrophages, choroid plexus macrophages, meningeal macrophages and microglia. However, also monocytes, neutrophils, NK cells, dendritic cells (DC), B cells and T cells can be identified in nonparenchymal regions of the CNS (Hove *et al*, 2019; Korin *et al*, 2017). Microglia are the major immune cell type in the CNS and the only macrophage population in the homeostatic brain parenchyma. They are phagocytic cells, responsible for immune surveillance and host defense, clearance of debris, but also play a role in synaptic pruning and brain homeostasis (Low & Ginhoux, 2018; Schulz *et al*, 2019). In contrast to blood borne myeloid cells, microglia are derived from primitive hematopoietic progenitors of the yolk sac. They populate the brain during early embryogenesis. Unlike blood borne macrophages, microglia are exceptionally long lived and have a high self-renewing potential. Therefore, under

homeostatic conditions, the microglia pool in the brain parenchyma is not replaced or sustained by blood borne monocytes, but by self-renewing local microglia cluster (Ginhoux *et al*, 2010; Bruttger *et al*, 2015). Under pathological conditions such as brain tumors, immune cells from the periphery, including blood borne monocyte derived macrophages (MDM), can infiltrate the brain parenchyma. It has been shown that up to 30% of the total tumor mass in BrM can consist of tumor associated macrophages. If these are microglia or MDM was not distinguished (Sevenich *et al*, 2014). MDM from the periphery morphologically resemble microglia when infiltrating the brain and BrM. However, microglia have a distinct expression profile and functional signatures in the naïve as well as brain tumor bearing brain (O *et al*, 2014; Bowman *et al*, 2016). These signatures led to the discovery of stable markers, such as CD49d, to distinguish MDM from microglia in the brain, without having to revert to transplantation or parabiosis experiments in mice (Bowman *et al*, 2016). This discovery is quite recent and, therefore, elucidating the explicit role of microglia in BrM and other brain tumors is just at the beginning. Moreover, it is not clear if the functions of tumor associated microglia and recruited macrophages are redundant and if the case, to which extend. However, high throughput single cell profiling via transcriptional sequencing and mass cytometry identified disease-associated microglia (DAM), which share a similar signature in mouse models of neuroinflammatory and neurodegenerative diseases such as experimental autoimmune encephalomyelitis (EAE; multiple sclerosis mouse model) and Alzheimer's disease. This signature is distinct from other myeloid subsets and might represent a universal disease-associated microglia signature (Keren-Shaul *et al*, 2017; Deczkowska *et al*, 2018; Mrdjen *et al*, 2018). Furthermore, transcriptomic analysis of BrM associated myeloid cells revealed an inflammatory signature in tumor associated microglia, intriguingly similar to the proposed DAM signature, and distinct from myeloid cells, recruited from the periphery (Schulz *et al*, 2020). These results support the suggestion that brain-resident microglia have distinct functional properties in BrM from myeloid cells, infiltrating from the periphery, such as MDM. As the differentially expressed genes indicate an inflammatory phenotype, this allows the hypothesis that brain-resident microglia are not completely polarized to a pro-tumor phenotype, but rather maintain anti-tumor functions. On the other hand, Pukrop et al. demonstrated, that microglia can facilitate BrM via actively helping extravasation and colonization of breast cancer cells into brain tissue in a Wnt-dependent manner (Pukrop *et al*, 2010). To sum it up, insights on microglia functions in BrM development and progression are too scares yet to predict their role in BrM progression. Especially in the context of the advent of immunotherapies, it is important to obtain a better understanding of the role of brain-resident microglia in opposition to infiltrating MDM. In the next section the role of immune cells, which potentially infiltrate BrM from the periphery, will be described in greater detail.

1.3.2. Brain infiltrating immune cells and their role in brain metastasis

Myeloid cells

Tumors can attract a variety of bone marrow derived immune cells. In the tumor microenvironment, these can increase immune suppression and support tumor growth, instead of fulfilling their protective role and targeting the tumor. Additionally, brain tumors, such as glioma and BrM, remodel the BBB, making it more penetrable for immune cells from the periphery. These cells include myeloid cells, such as granulocytes, inflammatory monocytes and monocyte derived macrophages (Pyonteck *et al*, 2013; Schulz *et al*, 2019, 2020).

To date, little is known about the impact of neutrophils on BrM progression. Existing data suggests pro tumor functions and indicates that neutrophils are predictors of poor survival for BrM patients. A study in 2016 demonstrated, that Non-small-cell lung carcinoma (NSCLC) patients with high neutrophil to lymphocyte ratio (NLR) in peripheral blood are more prone to developing BrM (Koh *et al*, 2016). High NLR has also been shown to be a predictor of worse survival after SRS or resection of BrM (Chowdhary *et al*, 2018; Mitsuya *et al*, 2017). Moreover, neutrophils have been implicated to participate in the generation of a premetastatic niche in the brain for metastasizing cancer cells in a breast cancer mouse model (Liu *et al*, 2013). Interestingly, in 2020 it has been demonstrated, that BrM cells in several mouse models recruit Arginase 1 (Arg1) and Programmed cell death 1 ligand 1 (PD-L1) positive immune suppressive neutrophils, which foster BrM outgrowth. By blocking the recruitment of these neutrophils, BrM development could be hampered (Zhang *et al*, 2020).

However, a stronger focus is currently put on the role of MDM in cancer progression, including BrM. As mentioned before, they are not derived from yolk sac progenitors, but from bone marrow derived monocytes, which differentiate to macrophages in tissues they are recruited to (Ginhoux *et al*, 2010). Before the development of lineage tracing models, radiosensitive MDM were distinguished from radioresistant microglia via whole body radiotherapy, followed by bone marrow transplantation in experimental brain tumors. However, radiotherapy can induce, or increase the infiltration of MDM, possibly skewing the quantification of these cells (Bowman *et al*, 2016; Schulz *et al*, 2020). Therefore, only the application of lineage tracing models and the discovery of stable MDM markers in the brain, such as CD49d, allowed proper quantification of MDM in brain tumors (Bowman *et al*, 2016). In experimental glioma and lung cancer derived BrM, MDM can constitute more than 35% and 20% of TAM, respectively (Bowman *et al*, 2016; Schulz *et al*, 2020). A high macrophage infiltration in tumors is often correlated to worse patient prognosis (Bingle *et al*, 2002; Mahmoud *et al*, 2012; Aras & Zaidi, 2017) and strategies targeting TAM are being tested in clinical trials (Cassetta & Pollard, 2018). Moreover, the targeting of TAM demonstrated success in preclinical trials of glioma (Stafford *et al*, 2016; Pyonteck *et al*, 2013). Nevertheless, the effects of macrophage targeting in brain metastases are only transient (Klemm *et al*, 2021, manuscript in revision). One of the reasons

for that might be the high plasticity of macrophages. Therefore, targeting the entire macrophage population might be counterproductive. In response to different stimuli such as cytokines or damage associated patterns, phenotypes can range from classically activated pro-inflammatory to alternatively activated immune suppressive. Historically, these extremes are called M1 and M2 polarization, even though researchers agree that this classification is too superficial for the diversity and plasticity of macrophages. Nonetheless, macrophages with a polarization resembling the M2 classification are thought to be tumor-promoting, whereas classical inflammatory M1 macrophages are thought to have anti-tumor functions (Mantovani *et al*, 2004). It is conceivable, that microglia, which often express pro inflammatory genes, might be important for tumor rejection and recovery, instead of promoting tumor growth. Therefore, it is essential to have a differential look on distinct macrophage subsets. As mentioned before, transcriptome sequencing has revealed distinct functional profiles for tumor associated MDM and microglia in brain tumors, including BrM (Bowman *et al*, 2016; Schulz *et al*, 2020). Whereas microglia expressed transcriptional profiles connected to housekeeping functions, such as synaptic pruning, and to host defense mechanisms, MDM expressed transcripts related to wound healing, antigen presentation and immune suppression, leading to the hypothesis that they have pro tumor functions (Schulz *et al*, 2020). The pro-tumor functions of macrophages are diverse and can include facilitation of vasculogenesis and angiogenesis, supply of growth factors, acceleration of therapy resistance and suppression of local and systemic immunity (Brown *et al*, 2017; Kioi *et al*, 2010; Mantovani & Locati, 2016; Vidyarthi *et al*, 2019). How prominent their role in BrM progression is, must be further elucidated.

An interplay between the innate and adaptive immune system is crucial to achieve a long-term anti-tumor response. Even though microglia are the main immune cell type in the brain, and, as macrophages, naturally can present antigen to e.g. T cells, it is not clear if their antigen presentation capacities are sufficient to unleash a systemic immune response against brain tumors, including BrM (Bowman *et al*, 2016; Sevenich, 2019). Professional antigen presenting cells (APC), such as DC, represent a link between the innate and adaptive immune system, and might be better suited for this purpose. As mentioned before, the presence of DC has been identified in the homeostatic CNS, but not much is known about their role in BrM or other brain tumors (Korin *et al*, 2017; Hove *et al*, 2019). DC are diverse and have a high plasticity. Most are of myeloid origin, but some DC are of lymphoid origin, so called plasmacytoid DC (Dress *et al*, 2019). A detailed study of myeloid cell types in neuroinflammation, demonstrated that DC and monocyte-derived cells are the main APC in physical contact with T cells, in opposition to resident microglia (Jordão *et al*, 2019). Another mouse study of steady state brain demonstrated that in contrast to microglia, meningeal and choroid plexus DC actively present self-antigen and stimulate T cells, also hinting towards increased antigen presentation capacity

(Anandasabapathy *et al*, 2011). Moreover, *in vivo* studies in glioma and BrM mouse models revealed that CNS derived tumor antigens are sufficiently drained to the cervical lymph nodes in the presence of an extracranial tumor or ectopic VEGF-C expression. This drainage enabled the rejection of brain tumors by treatment with checkpoint inhibitors, an effect which was dependent on antigen presentation and T cell priming by DC (Taggart *et al*, 2018; Song *et al*, 2020). All in all, the role of DC in BrM is not yet completely understood. It is not clear how DC are modulated in the BrM microenvironment. However, to harness the full potential of the adaptive immune system against BrM, DC are likely a crucial component in the brain TME.

Lymphocytes

The major lymphatic immune cells, which also have been identified in the homeostatic CNS, are NK cells, B cells and T cells (Korin *et al*, 2017; Hove *et al*, 2019). The first two are poorly investigated in the context of BrM. NK cells have been implicated in playing a role in checkpoint inhibition mediated rejection of experimental BrM (Taggart *et al*, 2018). Nevertheless, they are, like B cells, underrepresented in human BrM and it is not clear which role they play in BrM progression (Klemm *et al*, 2020). More is known about T cells. With the advent of checkpoint inhibitors, which are supposed to reactivate T cell responses, the focus of research has shifted to these tumor infiltrating lymphocytes (TIL). By now, the presence of T cells has been demonstrated for BrM derived from several primary cancers, such as renal cell carcinoma (RCC), small cell lung carcinoma (SCLC) and NSCLC, melanoma and breast cancer. Of these, melanoma and RCC are the most immunogenic with the highest T cell infiltration and the highest CD8/CD3 ratio in BrM. The infiltration patterns of TIL are diverse, ranging from strictly stromal accumulation to a diffuse distribution throughout the lesion (Harter *et al*, 2015). Although the exclusion of T cells from BrM is not as prominent as in case of gliomas, T cells encounter a naturally immune suppressive TME in the brain parenchyma, as it is important for brain homeostasis to avoid detrimental neurodegeneration, induced by misdirected immune responses (Klemm *et al*, 2020; Schulz *et al*, 2019). Additionally, during tumor evolution, described before, cancers develop properties to evade the immune system (Dunn *et al*, 2004). In the case of brain tumors, this can add up to immune suppression and prevent induction of a systemic adaptive immune response. In line with the suppressive milieu, the percentage of TIL is decreased in BrM, compared to the primary tumor, derived e.g. from breast cancer, with 5% and 20%, respectively (Ogiya *et al*, 2017). Nevertheless, several studies demonstrated a correlation between TIL density in BrM and patient survival (Berghoff *et al*, 2013, 2015; Zakaria *et al*, 2018). This indicates, that even though TIL numbers are low in the brain, T cells can influence BrM progression, albeit with impact not strong enough to halt tumor growth. Which factors exactly are responsible for a functional adaptive immune response and dictate number of TIL is not clear. In case of melanoma, a highly immunogenic tumor with high TIL content, it

has been demonstrated that the density of antigen does not explain the presence or absence of TIL (Spranger *et al*, 2016). Additionally, Mansfield et al. applied T cell receptor (TCR) profiling to human BrM samples. The authors were able to show that there was no correlation between T cell richness and tumor mutational burden in lung derived BrM, which was higher in the BrM samples than in the respective primary tumor (Mansfield *et al*, 2018). However, pieces of information from different studies give first insights and allow cautious conclusions.

Hypothetically, to induce a functional T cell response, antigen must be drained from the tumor in the brain parenchyma and reach sentinel lymph nodes, such as the cervical lymph nodes (CLN). Optimally, these antigens are transported to the CLN via APC, such as DC, where they are presented to naïve T cells. These primed T cells than must migrate to the brain tumor, and therefore be able to enter the brain parenchyma. Once in the BrM TME, they must resist the strong immune suppression of the TME to be able to attack the metastatic cancer cells efficiently. It has been demonstrated, that soluble antigen can freely drain from the brain parenchyma and cerebrospinal fluid (CSF) into dural lymphatic vessels, which drain into the CLN (Louveau *et al*, 2015), but it is not clear, if the same route is as easily accessible for DC in the case of brain tumors. Additionally, it is presumed that primed antigen specific, but not naïve T cells can migrate into the brain parenchyma (Galea *et al*, 2007; Prins *et al*, 2008). Recently two preclinical studies demonstrated that melanoma BrM antigen is presented by DC in the CLN, and that the route of drainage includes the abovementioned meningeal lymphatic vessels. However, this drainage was not efficient enough to induce immunity which could reject the tumors in the study by Song et al. (Hu *et al*, 2020; Song *et al*, 2020). In conclusion, drainage of antigen to the CLN can take place in BrM and primed T cells can reach the tumor theoretically, leaving the immune suppressive TME as another critical determinant of T cell number in BrM. This immune suppression can be built up by cancer cells and myeloid cells, however, as mentioned previously, Treg can contribute to it. It has been demonstrated in a number of BrM mouse models that FoxP3+ Treg are increased during BrM progression. These results have been recapitulated in patient samples of melanoma and NSCLC BrM (Sugihara *et al*, 2009). Furthermore, not only the tumors themselves were infiltrated with Tregs, but also the blood of patients was enriched with Treg, compared to healthy donors (Jacobs *et al*, 2009). These inhibitory T cells can hypothetically contribute to the inactivation of effector T cells in the brain TME.

To conclude, there is still a lot more knowledge to be gained in order to understand the complex and evidently numerous interactions of T cells with different cell types in the TME, which define the strength of an adaptive anti-tumor immune response. The exploration of T cell routes and interactions in the BrM TME presents great potential for the treatment of BrM patients by utilizing the adaptive immune system in the future.

1.4. Targeting the tumor microenvironment of brain metastases

Although some progress has been made in the treatment of BrM patients, the diagnosis is still remaining a death sentence and live expectancy incredibly low. Local treatments, such as surgery and radiotherapy, are the standard of care, as systemic targeted therapies often do not reach the brain parenchyma in therapeutic doses. Even though these local treatments initially show good response rates, e.g. WBRT with 60%, tumors regrow fast, and median survival still only comprises 3 to 6 month (McTyre *et al*, 2013; Sevenich, 2019). The mutational load of BrM is often higher than in the primary tumor, increasing the probability of quick development of resistance, making treatment of patients even more complicated and demanding the use of multimodality intervention approaches. As described before, the TME of BrM is strongly immune suppressive, with high content of tumor-supporting myeloid cells and few effector lymphocytes. Therefore, novel approaches will need to be rational combination strategies, which take into account the influence of the TME, especially the immune compartment. With this in mind, this thesis project focused on strategies which modulate the immune microenvironment as adjuvant therapy to standard of care radiotherapy. The goal was to convert the highly immune suppressive, so called 'cold' BrM TME, towards a rather pro-inflammatory, 'hot' TME. Combinatorial immune modulatory approaches have the potential to achieve this goal, and lead to long lasting systemic anti-tumor responses in other cancer entities, as described in the following sections. Harnessing the immune system harbors great potential for patients with BrM, as well, and should be explored in detail.

1.4.1. Radiotherapy – a potential tool to boost anti-cancer immunity

Traditionally, radiotherapy has mostly been applied to induce direct genotoxic effects in tumor cells. Tumorigenic cells regularly have a defective DNA repair machinery, and aberrantly fast proliferation (Hanahan & Weinberg, 2011). This consequently leads to radiation induced DNA damage, which cannot be repaired by tumor cells effectively, leading to tumor cell death, while sparing surrounding healthy cells. Therefore, historically, treatment regimens were designed to most effectively target tumor cells, while keeping toxicity low. Possible immune modulatory effects of radiotherapy have mostly been neglected (Sevenich, 2019). The routine regimen was fractionated WBRT, applying 30 Gy in 10 doses, 37.5 in 15 doses, or for patients with poor prognosis, 20 Gy in 5 fractions. Nowadays, for a limited number of BrM lesions, WBRT is replaced by SRS, a targeted high radiation dose, to minimize the radiation field in the brain and, therefore, reduce acute and late neurotoxicity (Shinde *et al*, 2019). To which extend this change in regimens affects the immune system remains unclear. However, with the advent of immunotherapies, it is increasingly recognized, that radiotherapy also has the potential to substantially modulate the TME (Fig. 1.4).

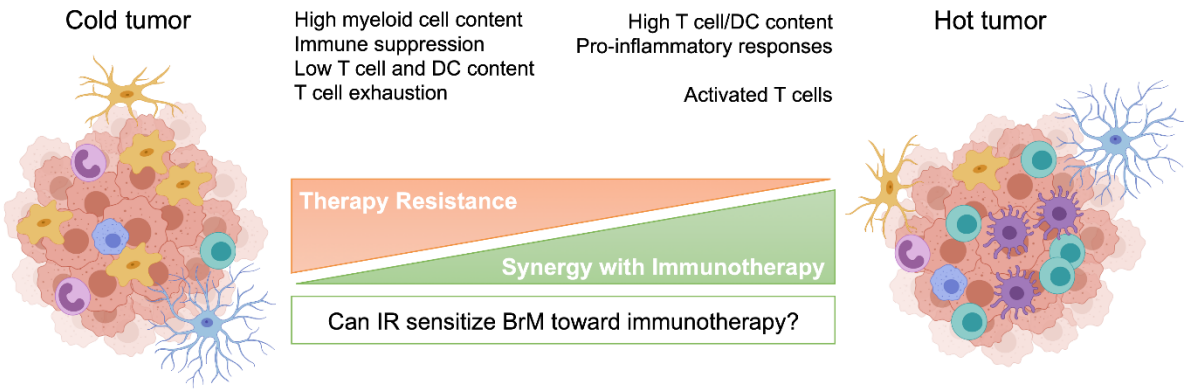

Fig. 1.4: Turning 'cold' tumors into 'hot' tumors via ionizing radiation. In this thesis it was investigated if the low immunogenic, 'cold' TME of breast cancer BrM can be modulated to a 'hot' TME via radiotherapy. 'Cold' tumors are thought to be highly immune suppressive, with high myeloid cell content and low numbers of DC and T cells. 'Hot' tumors are thought to have a high content of DC and T cells and rather demonstrate pro-inflammatory responses. These are properties which can be harnessed for immunotherapies such as immune checkpoint inhibition (Sevenich, 2019).

Radiation can induce several routes of cell death, of which not all are as immunologically inert as apoptosis, but can in fact induce pro-inflammatory responses, such as necrosis or immunogenic cell death. These forms of cell death can lead to the secretion of damage associated molecular patterns (DAMP), such as cytosolic double-stranded DNA (dsDNA), and pro-inflammatory cytokines (Sevenich, 2019). dsDNA can be detected by the cGAS-STING signaling pathway, which induces the expression of type I interferons (IFN-I), important for maturation of DC (Ramakrishna & Formenti, 2019). Moreover, radiotherapy can induce the modulation of surviving cells. Examples are the generation of neoantigens through increased mutational load and upregulation of MHCI expression on tumor cells, which increases antigen presentation and renders them more prone to recognition by the immune system (Corso *et al*, 2011; Reits *et al*, 2006). Additionally, surrounding TME cells can be affected by radiotherapy, e.g. radiotherapy can reverse the immune suppressive and tumor promoting capacity of MDM or induce the recruitment of immune cells essential for an adaptive immune response, such as DC (Teresa Pinto *et al*, 2016; Schulz *et al*, 2020; Vanpouille-Box *et al*, 2017). In the brain, radiotherapy can disturb the BBB and thereby, potentially, facilitates the infiltration of brain tumors with additional peripheral immune cells (Qin *et al*, 1990; Rubin *et al*, 1994; Schulz *et al*, 2020). The discovery of the abscopal effect of radiotherapy further underlines its potential to induce pro-inflammatory responses and to sensitize cancers to immunotherapy. This effect describes the observation that after local radiotherapy of lesions, other untreated lesions can respond or are even rejected, indicating a radiotherapy induced systemic anti-tumor immune response (Mole, 1953). Therefore, radiotherapy, already the mainstay of BrM treatment, is perfectly equipped to boost cancer immunity and potentially synergizes with novel immune modulatory drugs. Retrospective analyses and initial prospective clinical trials of immuno-

radiotherapies for BrM, demonstrate first promising results (Lauko *et al*, 2018), but more detailed research, as well as increased number of clinical trials which include BrM patients, are necessary to efficiently exploit the immunogenic effects of radiotherapy. Dose and scheduling can have tremendous effects on the induction of inflammatory responses. Overly high doses could lead to the ablation of essential radiosensitive immune cells, such as T cells, or induce the three prime repair exonuclease 1 (Trex1), a dsDNA digesting exonuclease, leading to decreased cGAS-STING activation (Vanpouille-Box *et al*, 2017). Too low doses might not be sufficient to induce pro-inflammatory responses. Moreover, fractionated, but not single dose radiotherapy, showed the potential to induce an abscopal effect against experimental tumors in a breast cancer mouse model, when combining with immune checkpoint blockade (Dewan *et al*, 2009). Therefore, comprehensive animal studies of radio-immunotherapy are necessary to increase the understanding of underlying mechanisms and increase response rates to novel combinatorial approaches.

1.4.2. Checkpoint Inhibition

Checkpoints are proteins, mostly receptors expressed on T cells, with immune inhibitory functions. They are supposed to keep the immune system balanced. Specifically, checkpoint pathways are responsible for fine tuning of immune responses and maintaining self-tolerance in a healthy organism, to prevent tissue damage and auto-immunity. During tumor evolution and development, cancer cells can upregulate components of checkpoint pathways to inhibit T effector cells and evade the immune system (Pardoll, 2012). In 2018, the Nobel Prize in Medicine was awarded to James Allison and Tasuku Honjo for unveiling the significance of the checkpoint proteins Programmed cell death 1 (PD-1) and cytotoxic T-lymphocyte-associated Protein 4 (CTLA-4) and paving the way for checkpoint blockade as cancer treatment (Ishida *et al*, 1992; Leach *et al*, 1996). The insights they gained started a new era in cancer research and set a new focus on the immune components of the TME, thereby facilitating research in the field of immuno-oncology. Nowadays, the checkpoint proteins PD-1, or PD-1 ligand 1 (PD-L1), and CTLA-4, are the most extensively studied and most relevant checkpoints in the clinics. For the successful activation of naïve T cells, antigen needs to be presented by APC, and co-stimulatory ligands CD80 and CD86 on APC need to bind to CD28, expressed by T effector cells. CTLA-4 is an inhibitory receptor, expressed on T cells, which competes with CD28 by binding the co-stimulatory ligands, therefore negatively regulating T cell activation. CTLA-4 is also expressed by regulatory T cells to inhibit the excessive accumulation of activated T effector cells (Jain *et al*, 2010). Cancer cells can express CTLA-4 to evade the immune system. The inhibition of CTLA-4 via monoclonal antibodies, such as ipilimumab, has shown promising results for cancer treatment, especially for advanced metastatic melanoma, which is why ipilimumab was FDA-approved in 2011 for the first time for this highly immunogenic

cancer type (Hodi *et al*, 2010; Pardoll, 2012). A 5 year follow up study of advanced melanoma demonstrated a dose dependent overall survival prolonging effect, with 25% of patients still alive after 5 years with a high dose. However, the percentage of patients suffering from grade 3 and 4 treatment-related adverse events was 36%. As it is the case for many studies, patients with symptomatic BrM, or BrM which needed treatment, were excluded from the trial (Ascierto *et al*, 2020) (NCT01515189).

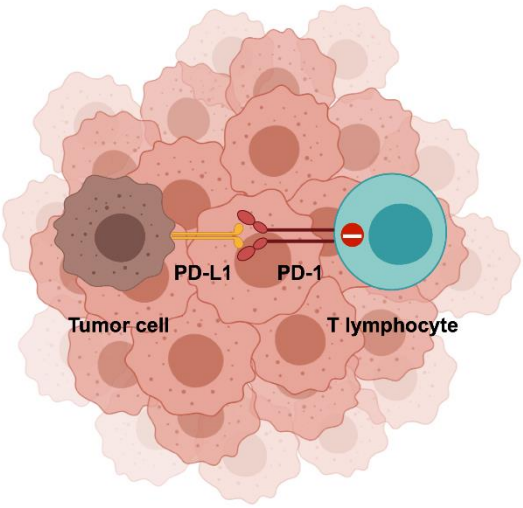

Fig. 1.5: Regulation of T cell activity by immune checkpoints. This figure demonstrates the inhibition of tumor associated T cells by immune checkpoint signaling. Depicted is the PD-1/PD-L1 checkpoint axis, which is a major focus of this PhD thesis. Activated T cells upregulate Programmed cell death 1 (PD-1) receptor. PD-1 ligand 1 (PD-L1) can be expressed by tumors and theoretically, upon binding PD-1 can inhibit T cell activity. This immune resistance can be innate, meaning tumor cells constitutively express PD-L1 or adaptive, meaning PD-L1 can be upregulated upon binding of T cells.

Checkpoint inhibition via PD-1 blockade has shown efficacy in several cancer types, while eliciting less serious adverse events (Brahmer *et al*, 2010). Therefore, CTLA-4 inhibition is often replaced by PD-1 inhibition in the treatment of cancer patients nowadays (Ascierto *et al*, 2020). In 2014 the PD-1 inhibitors nivolumab and pembrolizumab were approved by the FDA for the treatment of advanced melanoma, and, in 2015, for NSCLC. Like CTLA-4, PD-1 is an inhibitory receptor, expressed on T cells after activation. In the event of binding to its ligands PD-L1 or PD-L2, T cells are inactivated and stop proliferating, a state called ‘exhausted’. PD-1 blockade is thought to act primarily on exhausted tissue infiltrating T cells, unlike CTLA-4 blockade, which is thought to allow the activation of naïve T cells in lymphoid organs and lymph nodes. This means that both signaling pathways do not have redundant functions in cancer, which was proven via detailed mass spectrometry analysis in 2017 (Wei *et al*, 2017). Therefore, nowadays both immune checkpoint inhibitors are often combined, despite high toxicities. In 2015 combining ipilimumab with the PD-1 inhibitors nivolumab or pembrolizumab was FDA-approved for the treatment of advanced NSCLC. Even though, PD-1 and CTLA-4 blockade have shown intracranial activity in brain tumors, response rates are low and only a

subset of patients profits (Lorger *et al*, 2019). It has been demonstrated, that in order to elicit a systemic immune response against experimental BrM via checkpoint inhibition, drainage of tumor antigen to lymph nodes must be increased. In preclinical mouse models this could be achieved by introducing extracranial tumors to the system or via ectopic VEGF-C expression in the meninges, which leads to increased lymph angiogenesis and increased antigen drainage (Taggart *et al*, 2018; Song *et al*, 2020). In this thesis project it has been investigated, if radiotherapy also harbors the potential to sensitize BrM to checkpoint inhibition, due to the immunogenic effects on the TME described before.

While checkpoint inhibition of NSCLC and melanoma patients with BrM, also in combination with radiotherapy is extensively studied to date, not many clinical trials investigate these novel therapies in BrM of less immunogenic cancer types, including breast cancer. Nevertheless, it has been shown, that TIL are positively correlated with survival in TNBC, the breast cancer type most often metastasizing to the brain (25-46% of all TNBC patients) (Sylvia Adams et al. 2014; Chamberlain et al. 2017). Moreover, PD-L1 and PD-L2 expression is common in BrM derived from breast cancer, and PD-1 expression on TIL has a favorable prognostic impact for these patients (Duchnowska et al. 2016). In 2019, the treatment of unresectable or metastatic PD-L1 positive TNBC with Atezolizumab (PD-L1 inhibitor), in combination with chemotherapy, was approved. Glioma is another brain tumor type with low immunogenicity and highly immune suppressive TME. Nevertheless, inhibition of PD-L1 increased a radiotherapy induced abscopal effect in a glioma mouse model, leading to prolonged survival in the combination group compared to RT alone (Ene *et al*, 2020). Therefore, it is important to investigate the potential of radiotherapy to sensitize less immunogenic brain tumors, such as breast cancer derived BrM, to immunotherapy. A successful treatment with this approach could lead to systemic long-term immunity and long-term effects on survival.

1.4.3. Macrophage targeting strategies

Macrophages represent the major immune cell type in brain tumors, including BrM (Berghoff *et al*, 2013; Bowman *et al*, 2016; Schulz *et al*, 2020). In cancers they have been associated to a variety of tumor promoting functions such as supplying growth factors, facilitating angiogenesis, establishing an immune suppressive TME, and supporting tumor cell migration, intravasation and extravasation. Furthermore they have been associated to therapy resistance (Cassetta & Pollard, 2018). Therefore, different macrophage targeting strategies are being explored in preclinical trials, some of which show good responses (Ruffell & Coussens, 2015). It is assumed, that macrophages contribute to the strong immune suppression in the BrM TME, while the infiltration of lymphocytes is relatively low (Berghoff *et al*, 2013; Harter *et al*, 2015; Schulz *et al*, 2020). Hence, macrophage targeting strategies harbor the potential to increase the response to checkpoint inhibition by lifting this myeloid mediated immune suppression

which counteracts anti-tumor immunity. However, radiotherapy holds the risk to not only increase the recruitment of immune cells essential for checkpoint inhibition, but also of bone marrow derived myeloid cells, which can be tumor-promoting (Schulz *et al*, 2020; Ahn *et al*, 2010; Kioi *et al*, 2010; Liu *et al*, 2014). Therefore, inhibiting macrophages potentially synergizes with radiotherapy, in addition to increasing the efficacy of checkpoint blockade. Another benefit of targeting macrophages is their genetic stability in comparison to tumor cells, which have high mutation rates and, therefore, quickly develop resistances against tumor cell targeted therapies (Cassetta & Pollard, 2018). In this section the focus will be on two macrophage-targeting strategies, namely the inhibition of colony stimulating factor 1 receptor (CSF1R), which will lead to depletion, or reeducation of macrophages, and the inhibition of C-X-C chemokine receptor type 4 (CXCR4), which is supposed to block the recruitment of peripheral macrophages.

CSF1 is an essential survival factor for macrophages and is highly expressed by all macrophages. In the brain, however, the alternative ligand to CSF1R, namely IL34, is highly expressed. Therefore, microglia are not dependent on CSF1, but rather on IL34 (Rietkötter *et al*, 2015). By inhibiting CSF1R, the receptor to both ligands, all macrophages, including microglia, are affected. In this PhD project, CSF1R was inhibited via a brain penetrant CSF1R inhibitor (confidentiality agreement). In xenograft glioma mouse models, CSF1R inhibition via the tyrosine kinase inhibitor PLX3397 led to depletion of macrophages and to a blockade of M2-differentiation of radiotherapy-recruited monocytes, leading to synergistically increased survival, when combined with radiotherapy (Stafford *et al*, 2016). In experimental glioma mouse models, CSF1R inhibition did not lead to the depletion of macrophages in lesions, but rather to their reeducation, meaning loss of M2 markers and decrease of pro-tumor functions. The survival of macrophages in this scenario was enabled via tumor supplied factors, such as Granulocyte-macrophage colony-stimulating factor (GM-CSF) and IFNγ (Pyonteck *et al*, 2013). Achieving the reeducation of macrophages away from tumor-promoting phenotypes, rather than depleting all macrophages, is an optimal scenario and might be most promising. MDM as well as microglia can elicit immune-suppressive properties. It has been demonstrated in a melanoma mouse model, that BrM are more tolerogenic than extracranial tumors due to T cell dysfunction, induced by microglia-derived TGFβ (Jackson *et al*, 2016). It remains to be investigated, if microglia contribute to immune suppression in breast cancer derived BrM, or if recruited MDM are the major immune-suppressive macrophages.

To additionally target specifically myeloid cells recruited from the periphery, such as MDM, in this project, CXCR4 was inhibited via the small molecule inhibitor AMD3100. CXCR4 is a chemokine receptor, responsible for immune cell migration and homing in the bone marrow and is highly expressed by macrophages. Expression of stromal cell-derived factor 1 (CXCL12/SDF-1), the ligand to CXCR4, can be induced by hypoxia inducible factor-1 (HIF-1),

which is expressed in hypoxic areas of tumors (Kioi *et al*, 2010). Preclinical studies in glioma rat and mouse models demonstrated that the inhibition of the CXCR4/CXCL12 axis decreased infiltration of brain tumors by myeloid cells from the periphery. This diminished infiltration led to impaired restoration of tumor vasculature after radiotherapy and synergistically attenuated tumor regrowth and increased survival in combination with radiotherapy (Kioi *et al*, 2010; Liu *et al*, 2014).

These results indicate that macrophages, especially recruited MDM, can support the recurrence of brain tumors after radiotherapy and that modulating the immune suppressive myeloid compartment bears great chances to improve BrM standard and novel immune checkpoint therapies.

2. Aims of the thesis

Radiotherapy is standard of care for BrM patients. However, it can only prolong the survival of patients for a short duration. With the advent of immune checkpoint inhibitors and the acknowledgment that the immune system of the brain is highly complex and connected to systemic immune responses, checkpoint inhibitors have also gained interest for the treatment of BrM. Nowadays, investigations in this context focus mostly on BrM derived from highly immunogenic cancers, such as melanoma or lung cancer BrM. BrM derived from cancers with low immunogenicity, such as breast cancer BrM, are rarely investigated and are thought to be resistant to checkpoint inhibition.

Therefore, the main aim of this project was to investigate if radiotherapy can be exploited to boost anti-cancer immunity and to sensitize breast cancer BrM to immune checkpoint inhibition. The murine breast cancer BrM model 99LN-BrM served as model system for the majority of experiments performed herein. In the scope of this thesis, several specific aims were pursued:

Analysis of:

1. The composition of the TME of breast cancer BrM

2. The influence of radio-immunotherapy on the TME of BrM

3. T cell mediated anti-tumor immunity in breast cancer BrM

4. The efficacy of radio-immunotherapy against breast cancer BrM

5. The influence of radio-immunotherapy on the TME of breast cancer BrM

6. The influence of macrophages and pharmacological targeting of macrophages on T cells and efficacy of radio-immunotherapy

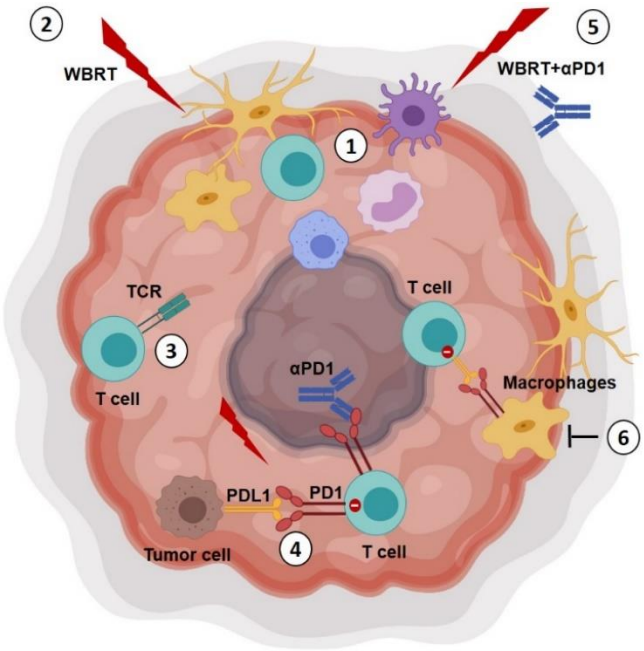

3. Materials

3.1. Equipment

Equipment used for the experiments in this thesis is listed in Tab. 3.1.

Tab. 3.1: List of equipment.

Equipment	Company
Pipette Research Plus 0.1-2.5 µl	Eppendorf
Pipette Research Plus 0.5-10 µl	Eppendorf
Pipette Research Plus 2-20 µl	Eppendorf
Pipette Research Plus 10-100 µl	Eppendorf
Pipette Research Plus 20-200 µl	Eppendorf
Pipette Research Plus 100-1000 µl	Eppendorf
Pipette controller Accu-jet pro	Brand
BVC pump	Vacuubrand
CO_2-Incubator Heracell 240i	Thermo Fisher Scientific
Heraeus HeraSafe HS12/2	Thermo Fisher Scientific
Microcentrifuge Mini Star	VWR International
Heraeus Fresco 21 Centrifuge	Thermo Fisher Scientific
Heraeus Megafuge 40R	Thermo Fisher Scientific
Thermomixer compact	Eppendorf
Dri-Block DB-3D	Thermo-DUX
Magnetic stirrer Ikamag RCT	Ika
Platform shaker Unimax 2000	Heidolph Instruments
Roller mixer RM5	Cat
Vortex-Genie 2 (G-560E)	Scientific Industries
NanoDrop 1000	Thermo Fisher Scientific
PCR Cycler ProFlex Base	Thermo Fisher Scientific
ViiA7 Real-Time PCR System	Thermo Fisher Scientific
Biobeam 2000	Gamma-Service Medical
Microscope Axiovert 100	Zeiss
CQ1 confocal laser microscope	Yokogawa
Leica Bond-Max	Leica Biosystems
Leica Autostainer XL	Leica Biosystems
Aperio ScanScope	Leica Biosystems
Small Animal MR Scanner, PharmaScan	Bruker
Isoflurane vaporizer Sigma Delta	UNO BV
Mouse surgical kit	Kent Scientific
Curved feeding needle G18 (50mm)	Fine Science Tools
Small Animal Radiation Research Platform	X-Strahl Ltd
QuadroMACS Separator	Miltenyi Biotec
gentleMACS Octo Dissociator with Heaters	Miltenyi Biotec
LSR Fortessa flow cytometer with HTS unit	BD Biosciences

3.2. Consumables

Consumables applied for experiments in this thesis are listed in Tab. 3.2.

Tab. 3.2: List of consumables.

Consumable	Company	Catalog number
Cell culture flasks (T25, T75, T175)	Greiner	690175, 658175, 660175
Cell culture plates (24-, 96-well)	Corning Incorporated	3526, 3596
Cell culture dishes (10 cm)	Greiner	664160
Cell culture teflon bags (30 ml)	OriGen Biomedical	PL30-2G
Cell scraper	Sarstedt	83.3951
Cryo vials (1 ml)	Greiner	123263
Kova Glasstic slides with counting grids	Thermo Fisher Scientific	10298483
Fluoroblok inserts (24-well, 8 µm)	Corning Life Sciences	351152
Pipettes (5, 10, 25 ml)	Greiner	606180, 607-180, 760-180
SureOne pipette tips (0.1-10, 20-100 µl)	Thermo Fisher Scientific	02-707-442, 02-707-430
Filtered pipette tips (1250 µl)	Biotix	M-1250-9FC96
Dispenser Tips (0.5, 5 ml)	Ratiolab	2910101, 2910104
Reaction tubes (15, 50 ml)	Greiner	188271, 227261
SafeSeal tubes (1.5, 2 ml)	Sarstedt	72.706, 72.691
PCR Strip tubes (0.2 ml)	VWR	732-0545
PCR plates (96-well)	VWR	PEQL82-0600-A
PCR plates (384-well)	Biozym	710885
Adhesive PCR film	VWR	PEQL82-0558-A
Parafilm	Merck	P7793-1EA
U-bottom plate (96-well)	Corning	353910
FACS tubes	Sarstedt	551.579
EASYstrainer (70 µm)	Greiner	542070
Syringe filter (0.2 µm)	Sarstedt	83.1826.001
Vacuum filter (0.2 µm)	VWR	514-0332
Cutfix stainless scalpel	BD	324825
Omnifix Luer syringe (20 ml)	B.Braun	4616200V
Micro-fine syringe (0.5 ml)	BD	324824
Syringe Microlance 3	BD	300800
Venofix infusion devices	B.Braun	4056353
PlastiPak Syringe 26G (1ml)	BD	303172, 303176
PAP Pen	Sigma-Aldrich	Z672548-EA
Tissue-Tek Cryomold	Thermo Fisher Scientific	4557
SuperFrost microscopy slides	Karl Hecht	42409110
Cover Slips (1x24x60 mm)	Duran group	23 550 36
gentleMACS C Tubes	Miltenyi Biotec	130-096-334
LS Columns	Miltenyi Biotec	130-042-401
Microvette 200 K3E tubes	Sarstedt	20.1288

3.3. Chemicals and solutions

Tab. 3.3. lists chemicals and solutions used in experiments in this thesis.

Tab. 3.3: List of chemicals and solutions.

Compound	Company	Catalog number
TRIzol	Thermo Fisher Scientific	15596-018
10x DPBS	Thermo Fisher Scientific	14200-067
Chloroform	Sigma-Aldrich	288306-100ML
2-Propanol	Sigma-Aldrich	I9516-500ML
RNase free water	VWR	E476-500ML
Ethanol	Thermo Fisher Scientific	10041814
ROTI Histofix (4%)	Roth	P087.3
D(+)-Saccharose	Roth	9097.1
CellTracker Red CMTPX Dye	Thermo Fisher Scientific	C34552
Fluorescence mounting medium	Agilent	S302380-2
Tissue-Tek O.C.T. compound	Sakura Finetek	4583
Triton-X100	Sigma-Aldrich	9002-93-1
RBC Pharma lyse buffer	BD	558-899

3.4. Media and supplements

Tab. 3.4. contains media and cell culture supplements used in the thesis.

Tab. 3.4: List of media and supplements for cell culture.

Compound	Company	Catalog number
DMEM	Gibco	21969-035
RPMI	Gibco	31870-025
L-Glutamine (200 mM)	Gibco	25030-024
Penicillin-Streptomycin (10000 U/ml)	Gibco	15140-122
DPBS (1x)	Gibco	14190-094
HBSS (1x)	Gibco	14175-053
β-Mercaptoethanol	Thermo Fisher Scientific	21985023
rm IL34	Biotechne	5195-ML-010
rm TGFβ1	Biotechne	7666-MB-005
rm M-CSF1	Biotechne	416-ML-050
FBS	PAN-Biotech	3302-p1005
Trypsin-EDTA (0.05%)	Gibco	25300-054
DMSO	Sigma-Aldrich	D2438-5X10ML
αCD3	Thermo Fisher Scientific	16-0031-82
αCD28	Thermo Fisher Scientific	16-0281-82
BSA	Jackson Immuno Research	001-000-162

3.5. Kits

Kits used in the scope of the thesis are listed in Tab. 3.5.

Tab. 3.5: List of Kits and Assays.

Compound	Company	Catalog number
High-Capacity cDNA Reverse Transcription Kit	Thermo Fisher Scientific	4368814
TaqMan Gene Expression Master Mix	Thermo Fisher Scientific	4369016
TaqMan Gene Expression Assay GAPDH	Thermo Fisher Scientific	Mm99999915_g1
TaqMan Gene Expression Assay UBC	Thermo Fisher Scientific	Mm02525934_g1
TaqMan Gene Expression Assay TNFα	Thermo Fisher Scientific	Mm00443258_m1
TaqMan Gene Expression Assay IL6	Thermo Fisher Scientific	Mm00446190_m1
TaqMan Gene Expression Assay IL1β	Thermo Fisher Scientific	Mm00434228_m1
TaqMan Gene Expression Assay PD-1	Thermo Fisher Scientific	Mm01285676_m1
TaqMan Gene Expression Assay PD-L1	Thermo Fisher Scientific	Mm03048248_m1
TaqMan Gene Expression Assay CSF1R	Thermo Fisher Scientific	Mm01266652_m1
TaqMan Gene Expression Assay CSF1	Thermo Fisher Scientific	Mm00432686_m1
TaqMan Gene Expression Assay IL34	Thermo Fisher Scientific	Mm01243248_m1
TaqMan Gene Expression Assay CXCR4	Thermo Fisher Scientific	Mm01996749_s1
TaqMan Gene Expression Assay CXCL12	Thermo Fisher Scientific	Mm00445553_m1
DNeasy Blood & Tissue Kit	Qiagen	69504
Brain tumor dissociation Kit (P)	Miltenyi	130-095-942
Myelin-Removal Beads II	Miltenyi	130-096-433
AbC Total Antibody Compensation Bead Kit	Thermo Fisher Scientific	A10497
ArC Amine Reactive Compensation Bead Kit	Thermo Fisher Scientific	A10346

3.6. Antibodies and staining supplies for immunological methods

Tab. 3.6 lists all antibodies used for flow cytometry analyses. The respective gating strategies are depicted in section 4.2.10.

Tab. 3.6: List of fluorescently labeled antibodies and compounds used for flow cytometry.

Marker	Conjugate	Host/ Species	Clone	Dilution	Company	Catalog no.
Mouse FC-block	-	Rat	2.4G2	1:1000	BD Biosciences	553142
			Myeloid Panel - BrM			
Live/Dead	Fixable Blue	-	-	1:500	Thermo Fisher	L34962
CD45	Alexa Fluor (AF) 700	Rat	30-F11	1:500	BioLegend	103128
CD11b	BV605	Rat	M1/70	1:1000	BD Biosciences	563015
Ly6C	PerCP-Cy5.5	Rat	HK1.4	1:250	BioLegend	128011
Ly6G	FITC	Rat	1A8	1:500	BioLegend	127605
CD49d	PE-Cy7	Rat	R1-2	1:400	BioLegend	103618
PD-1	PE	Rat	29F.1A12	1:100	BioLegend	135205
PD-L1	APC	Rat	MIH5	1:100	BD Biosciences	564715

Dendritic cell/tumor cell panel - BrM						
Live/Dead	Fixable Blue	-	-	1:500	Thermo Fisher	L34962
CD45	AF 700	Rat	30-F11	1:500	BioLegend	103128
CD326	FITC	Rat	G8.8	1:1000	Thermo Fisher	11579180
CD83	PE-Vio770	Human	REA304	1:500	Miltenyi Biotec	130104476
CD11c	BV605	Hamster	N418	1:250	BioLegend	117333
PD-1	PE	Rat	29F.1A12	1:100	BioLegend	135205
PD-L1	APC	Rat	MIH5	1:100	BD Biosciences	564715
cDC1/cDC2 panel -BrM						
Live/Dead	Fixable Blue	-	-	1:500	Thermo Fisher	L34962
CD45	AF 700	Rat	30-F11	1:500	BioLegend	103128
CD11b	FITC	Rat	M1/70	1:1000	BD Biosciences	553310
CD11c	BV605	Hamster	N418	1:250	BioLegend	117333
MHCII	PE-Cy7	Rat	M5/114.15.2	1:500	BioLegend	107629
CD24	PE	Rat	30-F1	1:250	BioLegend	138503
T cell panel – BrM and blood						
Live/Dead	Fixable Blue	-	-	1:500	Thermo Fisher	L34962
CD45	FITC	Rat	30-F11	1:500	BD Biosciences	553080
CD3ε	BV711	Hamster	1452C11	1:500	BD Biosciences	563123
CD4	PE-Vio770	Rat	GK1.5	1:500	Miltenyi Biotec	130102784
CD8α	PerCP-Cy5.5	Rat	53-6.7	1:250	BD Biosciences	561109
PD-1	PE	Rat	29F.1A12	1:100	BioLegend	135205
PD-L1	APC	Rat	MIH5	1:100	BD Biosciences	564715
γδ-/NK T cell panel - BrM						
Live/Dead	Fixable Blue	-	-	1:500	Thermo Fisher	L34962
CD45	AF 700	Rat	30-F11	1:500	BioLegend	103128
CD3ε	BV711	Hamster	1452C11	1:500	BD Biosciences	563123
CD4	PE-Vio770	Rat	GK1.5	1:100	Miltenyi Biotec	130102784
CD8α	PerCP-Cy5.5	Rat	53-6.7	1:100	BD Biosciences	561109
γδ-TCR	PE	Hamster	GL3	1:200	BioLegend	118108
DX5	APC	Rat	DX5	1:100	BioLegend	108910
PD-1/PD-L1 overview panel - BrM						
Viability Dye	eFluor 780	-	-	1:100	Thermo Fisher	65086514
CD3	PE	Human	REA641	1:500	Miltenyi Biotec	130109879
CD45	PerCP	Rat	30-F11	1:200	Thermo Fisher	45045-80
CD11b	BV605	Rat	M1/70	1:1000	BD Biosciences	563015
PD-1	BV421	Hamster	J43	1:500	BD Biosciences	562584
PD-L1	APC	Rat	MIH5	1:200	BD Biosciences	564715
T cell activation panel I – *in vitro*						
Live/Dead	Fixable Blue	-	-	1:500	Thermo Fisher	L34962
CD45	AF 700	Rat	30-F11	1:500	BioLegend	103128
CD11b	FITC	Rat	M1/70	1:1000	BD Biosciences	553310
CD69	BV605	Hamster	H1.2F3	1:500	BioLegend	104529
T cell activation panel II – *in vitro*						
Live/Dead	Fixable Blue	-	-	1:500	Thermo Fisher	L34962
CD45	AF 700	Rat	30-F11	1:500	BioLegend	103128
CD4	PE-Vio770	Rat	GK1.5	1:100	Miltenyi Biotec	130102784
CD8α	PerCP-Cy5.5	Rat	53-6.7	1:100	BD Biosciences	561109
CD69	BV605	Hamster	H1.2F3	1:500	BioLegend	104529

Antibodies and compounds used for immunofluorescent and immunohistochemical analyses are listed in Tab. 3.7.

Tab. 3.7: List of antibodies and markers for histological analyses.

Antigen/compound	Species	Clone	Dilution	Company	Catalog no.
Bond Polymer Refine Detection Kit	-	-	-	Leica Biosystems	DS9800
CD3	Rabbit	EPR20752	1:2800	Abcam	ab215212
CD8a	Rabbit	D4W2Z	1:500	Cell Signaling	98941S
DCIR2	Rat	33D1	1:500	eBioscience	14588482
EpCAM	Rabbit	polyclonal	1:500	Abcam	ab71916
Iba1	Rabbit	polyclonal	1:1000	Novus Biologicals	NBP2-19019
FoxP3	Rabbit	polyclonal	1:500	Abcam	ab54501
PD-1	Goat	polyclonal	1:100	R&D Systems	AF1021
PD-L1	Rabbit	E1L3N	1:200	Cell Signaling	13684S
TMEM119	Guinea pig	polyclonal	1:1000	SYSY	400004
Rabbit IgG Alexa Fluor 594	Donkey	polyclonal	1:500	Jackson ImmunoResearch	711-586-152
Guinea pig IgG Alexa Fluor 647	Donkey	polyclonal	1:500	Jackson ImmunoResearch	706-605-148
Rabbit IgG Alexa Fluor 488	Donkey	polyclonal	1:500	Jackson ImmunoResearch	711-546-152
Rat IgG Alexa Fluor 594	Donkey	polyclonal	1:500	Jackson ImmunoResearch	712-586-150
DAPI (5mg/ml)	-	-	1:2500	Sigma	D9542-5MG
Höchst (10 mg/ml)	-	-	1:10000	Sigma	23491-45-4

3.7. Compounds for *in vivo* application

Inhibitors, anesthetics and other compounds for the *in vivo* application are listed in Tab. 3.8.

Tab. 3.8: List of compounds for *in vivo* application.

Compound	Company	Catalog number
Rompun (2%)	Bayer	-
Ketavet (10%)	Medistar	-
Isoflurane (1000 mg/g)	Virbac	-
Gadobutrol (1 mmol/ml)	Bayer	-
Captisol	CyDex Pharmaceuticals	-
Anti-mouse PD-1 (RMP1-14)	Bio X Cell	BP0146
Rat IgG2a (2A3)	Bio X Cell	BP0089
Anti-mouse CD4 (GK1.5)	Bio X Cell	BP0003-1
Anti-CD8a (YTS 169.4)	Bio X Cell	BP0117
Rat IgG2b, κ (LTF-2)	Bio X Cell	BP0090
Dilution Buffer pH 7.0	Bio X Cell	IP0070
Dilution Buffer pH 6.5	Bio X Cell	IP0065
AMD3100	Selleckchem	S8030
D(+)-Glucose	Roth	X997.1
Propylene glycol	Sigma-Aldrich	W294004-1KG-K
Tween 80	Sigma-Aldrich	P4780-500ML

3.8. Software

Software used for the generation, analysis or presentation of data is listed in Tab. 3.9.

Tab. 3.9: List of applied software.

Software	Version	Company/developer
Muriplan	2.2.1	X-Strahl
Paravision	6.0.1	Bruker
BD FACSDiva	1.4	BD Biosciences
Flow jo	10.6.2	FlowJo LLC/Becton Dickinson
R studio	3.6.2	RStudio
ImmunoSeq Analyzer	3.0	Adaptive Biotechnologies
GraphPad Prism 8	8.4.0	GraphPad Software
ITK-Snap	3.6.0	Paul Yushkevich and Guido Gerig
CQ1 Software	1.04.04.02	Yokogawa
Image J	1.52c	Wayne Rasband
Aperio ImageScope	12.4.0.5043	Leica Biosystems
Excel	14.7.7	Microsoft Corporation
Word	14.7.7	Microsoft Corporation

4. Methods

4.1 Molecular biological methods

4.1.1. RNA isolation and cDNA synthesis

$5x10^5$ tumor cells or $1x10^6$ bone marrow derived macrophages (BMDM) were seeded in T25 flasks for gene expression analysis. To test the influence of ionizing radiation on expression of genes of interest, cells were irradiated 24h later as described in section 4.2.5. RNA was isolated 48h after irradiation via guanidinium thiocyanate-phenol-chloroform extraction. Adherent cells were washed with DPBS and immediately covered with 1 ml of TRIzol (Guanidinium thiocyanate acid phenol solution) per T25 flask. After homogenizing the lysate, it was transferred to 2 ml reaction tubes and incubated for 5 min at RT. Afterwards, 200 µl of chloroform were added. Lysate was shaken and incubated for 2-3 min at RT, followed by centrifugation at 12000xg for 15 min at 4°C. The aqueous phase was transferred to a new 1.5 ml reaction tube and mixed with 500 µl isopropanol by inverting. After 10 min incubation at RT, the samples were centrifuged at 12000xg for 10 min at 4°C. Supernatant was discarded and RNA pellet washed with 75% RNase free ethanol (7500xg, 5 min, 4°C). Supernatant was removed again, and samples air dried for 10-15 min. The RNA pellet was dissolved in 20-50 µl (depending on cell density before harvest) of RNase free water and heated at 55 °C for 10 min. RNA concentration was measured photometrically with the NanoDrop1000. RNA solutions were stored at -80°C or immediately transcribed to cDNA. cDNA synthesis was performed with the Applied Biosystems High Capacity cDNA Reverse Transcription Kit according to the manufacturer's instructions (Thermo Fisher Scientific). After transcription, cDNA was stored at -20°C for analysis by qRT-PCR.

4.1.2. Quantitative Real-time PCR

To quantify gene expression via qRT-PCR, TaqMan Gene Expression Assays and the ViiA 7 Real-Time PCR System were used. cDNA synthesized from 0.5 to 1 µg RNA was analyzed. Samples were run in triplicate and expression of genes of interest was normalized to Glyceraldehyde 3-phosphate dehydrogenase (GAPDH) and Ubiquitin C (UBC).

Tab. 4.1: Composition of the qRT-PCR reaction for triplicates.

Component	Volume per triplicate [µl]
DEPC water	14
TaqMan Gene Expression Assay	2
TaqMan Fast Advanced Mastermix	20
cDNA sample	4

The components of the reaction mix are listed in Tab. 4.1. The settings of the applied standard qRT-PCR program (Comparative CT/ΔΔCT) are depicted in Tab. 4.2.

Tab. 4.2: Standard qRT-PCR program.

Phase	Temperature	Duration [sec]	Number of cycles
Hold Stage - Step 1	50 °C	120	1
Hold Stage - Step 2	95 °C	600	
PCR Stage - Step 1	95 °C	15	40
PCR Stage - Step 2	60 °C	60	

4.1.3. DNA isolation

For TCRβ profiling DNA was isolated from macrodissected BrM and CLN. Tissue was mechanically broken up with the rubber part of a luer syringe, filtered through 70 µm cell strainers and washed with DPBS (5 min, 2000 rpm). DNA was isolated from the generated cell suspension with the DNeasy Blood & Tissue Kit (Qiagen) according to the manufacturer's instructions and suspended in 55 µl DNAse free water. DNA concentration was measured photometrically with the NanoDrop1000. DNA was stored at 4 °C short term. Before sending samples to Adaptive Biotechnologies for sequencing, 50 µl per sample were transferred to a 96-well plate and frozen once at -20 °C.

4.1.4. TCRβ profiling

Purified DNA from BrM and CLN samples was send to Adaptive Biotechnologies (Seattle, WA) for TCRβ sequencing at survey resolution (immunoSEQ Assay). The company applied a two-step, amplification bias-controlled multiplex PCR approach (Robins *et al*, 2009; Carlson *et al*, 2013). In the first step, the hypervariable complementarity-determining region 3 (CDR3) of the TCRβ receptor was amplified. In the second step proprietary barcodes as well as Illumina adapter sequences were added to the amplicons. To quantify the number of total nucleated cells and evaluate the number of T cells per sample, reference gene primers were included in the PCR reaction. Pre-analysis of raw data was also performed by Adaptive Biotechnologies (Removal of adapter and primer sequences, contaminating sequences and primer dimers, correction of technical errors, annotation of V(N)D(N)J genes). For further analysis, the ImmunoSeq Analyzer 3.0 was applied. Analysis of clone size distribution and the generation of Lorenz curves and Venn diagrams was performed with R packages in R studio (R studio version 3.6.2, immunarch version 0.5.5, ineq version 0.2.13, VennDiagram 1.6.20).

4.2. Cell biological and immunological methods

4.2.1. Source, cultivation and storage of cell lines

The murine parental cell line 99LN was derived from a metastatic lymph node of the triple negative MMTV-PyMT breast cancer model (C57Bl6/J background) and selected *in vivo* for brain homing capacity as previously described (Bowman *et al*, 2016). This selection resulted in the 99LN-BrM2 variant used in this PhD project. The murine parental TS1 cell line was derived from primary tumors of the MMTV-PyMT breast cancer model (FVB/n background) as previously described (Shree *et al*, 2011), and also selected *in vivo* for brain homing capacity (Sevenich *et al*, 2014). The human 831RS cell line was derived from the MDA-MB-231 cell line, which was provided by Dr. Joan Massague (Memorial Sloan Kettering Cancer Center), and labeled with a triple imaging vector (TK-GFP-Luc; TGL) (Ponomarev *et al*, 2004).
Handling of cells has been performed in a laminar flow under sterile working conditions. Cells were tested for mycoplasma contamination regularly. The 99LN-BrM, TS1-BrM and 831RS cell lines were maintained in *complete DMEM* (Tab. 4.3).

Tab. 4.3: Composition of *complete DMEM* for cultivation of tumor cell lines.

Component	Volume [ml]
DMEM	450
FBS	50
Glutamine (200 mM)	5
Penicillin-Streptomycin (10000 U/ml)	5

The adherent cell lines (99LN-BrM, TS1-BrM, 831RS) were passaged with Trypsin-EDTA (0.05%, 2 ml per T75 flask) when confluent and media was exchanged regularly (dependent on pH-indicator in the media).
The EOC2 microglia cell line has been acquired from ATCC. The cells were maintained in *microglia media* supplemented with 20 ng/ml rm-IL34 and 5 ng/ml rm-TGF-β. The media was exchanged every third day to guarantee stable cytokine levels (Tab. 4.4).

Tab. 4.4: Composition of media for cultivation of EOC2 microglia cells.

Component	Volume [ml]
DMEM	450
FBS	50
Glutamine (200 mM)	10
Penicillin-Streptomycin (10000 U/ml)	5

For freezing, cells were detached with Trypsin-EDTA (99LN-BrM, TS1-BrM, 831RS) or cell scraper (EOC2), centrifuged (5 min, 1500 rpm), resuspended in 10 ml of the respective media supplemented with 10% DMSO and transferred to freezing vials (1ml/vial). After cooling down to -80 °C, cells were stored in liquid nitrogen. When taking cells into culture, the respective vial was quickly defrosted at 37 °C and cells transferred into preheated DMSO free media.

4.2.2. Differentiation and cultivation of primary BMDM

BMDM were differentiated from monocytes isolated from femurs of female 6-8 week-old mice (CX3CR1-GFP background for migration assays, C57Bl6/J for the remaining experiments). To extract bone marrow, femurs were dissected and rinsed with 15 ml DMEM (16G syringe) through a 70 µm cell strainer. After centrifugation at 1500 rpm for 5 min, media was discarded, and cells resuspended in 30 ml *complete DMEM* (section 4.2.1, Tab. 4.3) supplemented with 10 ng/ml rm-CSF-1. For differentiation, cells were cultured 7 days in Teflon bags, to prevent adhesion. Every other day media with cytokine was exchanged. After one week of differentiation BMDM were used for experiments.

4.2.3. Differentiation and activation of T cells

T cells for the *in vitro* activation assay were differentiated from splenocytes isolated from 6-8 week-old female C57Bl6/J mice. The protocol was obtained and modified from BestProtocols® (Thermo Fisher). Spleens were grinded with the rubber end of a luer syringe and filtered through 70 µm cell strainers to get a single cell suspension. After washing once with DPBS (400xg, 5 min), erythrocytes were removed by red blood cell lysis (RBC lysis buffer, 5 min at RT). After washing with 20 ml PBS (400xg, 5 min), $2x10^5$ splenocytes per well were seeded in αCD3-coated 96-well plates (evening before, 0.5 µg/ml αCD3 in 50 µl DPBS/well) in 100 µl *T cell media* (Tab. 4.5) supplemented with 2 µg/ml αCD28. Cells were used for the T cell activation assay (section 4.2.6) 24 h later.

Tab. 4.5: Composition of *T cell media* for differentiation and activation of splenocytes.

Component	Volume [ml]
RPMI	450
FBS	50
Glutamine (200 mM)	5
Penicillin-Streptomycin (10000 U/ml)	5
β-mercaptoethanol	0.5

4.2.4. Generation of tumor conditioned media

For T cell activation assays, BMDM or EOC2 cells were incubated 24h with tumor conditioned media (TuCM). To generate TuCM, $5x10^6$ 99LN-BrM cells were seeded in 8 ml of the respective media (*complete DMEM* or *microglia media*) in 10 cm petri dishes. After 24h, media was collected, sterile filtered and applied on $2x10^6$ BMDM or EOC2 cells for another 24h. These conditioned cells were then added to the T cell activation assay (section 4.2.6).

4.2.5. Irradiation of cell lines

To analyze the influence of ionizing radiation on brain homing breast cancer cell lines, cells were irradiated *in vitro* with the Biobeam GM. For *in vitro* irradiation, $1x10^6$ tumor cells were seeded one day prior, in T25 culture flasks to allow adhesion. 24h later, cells were irradiated once with 10 Gy. 48h after *in vitro* irradiation, cells were harvested for transcription analysis (section 4.1.2) or migration assays (section 4.2.7).

4.2.6. T cell activation assay

T cells were differentiated and activated from spleens of C57BL6/J mice. Before organ extraction mice were perfused with cold DPBS. RBC lysis and splenocyte activation were performed as described before (section 4.2.3.). 24h after differentiation/activation, $5x10^4$ 99LN-BrM, EOC2 or BMDM cells/well were added to the culture in the same media used for T cell activation (section 4.2.3, Tab. 4.5). To ensure BMDM and EOC2 survival 10 ng/ml CSF1 was added to each well. Another 24h later, splenocytes were transferred to a round bottom 96-well plate, washed with DPBS (400xg, 5 min) and incubated with antibodies against CD69 for analysis by flow cytometry (section 4.2.10, Fig. 4.3 A). To test the influence of preconditioned BMDM and EOC2 on T cells, these cells were cultured in TuCM 24h before starting the T cell assay. TuCM was generated as described in section 4.2.4.

4.2.7. Migration assay

To test the capacity of 99LN-BrM cells to attract BMDM, migration assays were performed. BMDM were seeded on top of the membrane in a transwell system and migration through the 8 µm pores of the membrane towards tumor cells in the bottom chamber was quantified by immunofluorescence. One day prior to the assay, 99LN-BrM cells were irradiated as described in section 4.2.5, or left untreated. Moreover, the tumor cells were labeled with CellTracker Red CMTPX (15 min, RT, according to the manufacturer's protocol), to distinguish them from the GFP-positive BMDM derived from CX3CR1-GFP Bl6 mice. After staining, the tumor cells were washed with DPBS (1500 rpm, 5 min) and $5x10^5$ cells were seeded in 24-well plates. This was performed one night prior to the assay to allow attachment to the bottom of the chamber. BMDM were isolated and differentiated 1 week before the assay as described in section 4.2.2.

On the day of the assay, media in the 24 well plates was exchanged for *complete DMEM*, supplemented with 10 ng/ml CSF1. $2x10^4$ GFP+ BMDM were seeded into the transwell inserts on top of the tumor cells, in *serum free DMEM* (Tab. 4.6), also supplemented with 10 ng/ml CSF1.

Tab. 4.6: Composition of *serum free DMEM* for migration assays.

Component	Volume [ml]
DMEM	450
L-Glutamin (200 mM)	5
Penicillin-Streptomycin (10000 U/ml)	5

Optionally, 10 µM AMD3100 was added to both compartments, to investigate the influence of CXCR4 signaling on BMDM migration. The assay was stopped after 48h at 37°C, via adding 4% ROTI Histofix to the wells. After rinsing with DPBS, membranes were stained with DAPI (1:2500 in DPBS, 5 min, RT). Then, DAPI was rinsed off with DPBS, membranes were extracted with a scalpel, transferred to microscopy slides and covered with mounting media for analysis with the CQ1 confocal laser microscope. After recording of images, BMDM were counted using the Multi-point tool of Image J (Version 1.52c).

4.2.8. Immunofluorescent analysis of frozen tissue

For immunofluorescent analysis of frozen tissue sections, mice were perfused with 20 ml DPBS and 20 ml 4% ROTI Histofix, prior to organ harvest (section 4.3.3). Tissue was dissected and fixed in 4% ROTI Histofix overnight, followed by incubation in 15 ml 30% sucrose (at 4°C), until the tissue was fully equilibrated. Afterwards, tissues were embedded in OCT-compound and cut to 10 µm cryostat tissue sections (Petra Dinse, Histology Core Facility, Georg Speyer Haus) for subsequent analyses. For immunofluorescent staining, frozen sections were thawed and dried for 1h. Afterwards, sections were rehydrated by washing with DPBS on a shaker (3x10 min). For standard staining protocols, tissues on the sections were edged with hydrophobic marker and blocked and permeabilized by addition of 150 µl 3% BSA + 0.1% Triton-X100 in DPBS, on top of the tissue. After incubation for 1h at RT, slides were rinsed with DPBS. Afterwards, 150 µl of primary antibody solutions was added (in 1.5% BSA in DPBS) and incubated overnight at 4°C in a humidified chamber. Antibodies and dilutions are listed in Tab. 3.7 (section 3.6). The following day, slides were washed 3 times for 5 min in DPBS, followed by incubation with fluorophore-conjugated secondary antibodies (1:500 in 1.5% BSA, Tab. 3.7, section 3.6) for 45 min at RT. Afterwards, sections were washed 3 times with DPBS and stained with DAPI (1:2500) or Höchst (1:10000), for 5 min. Then, slides were washed again with DPBS (3x5 min), covered with mounting media and glass slides and dried overnight

at RT. Stained sections were stored at 4°C. Analysis was performed with the confocal laser microscope CQ1 (Yokogawa).

4.2.9. Immunohistochemistry

Mice were perfused with 20 ml DPBS and 4% ROTI Histofix before organ harvest for immunohistochemistry (IHC). Tissue was isolated and incubated in 4% ROTI Histofix at 4°C for at least four weeks. Paraffin-embedded sections were processed for IHC using a Leica Bond Max automated staining device and the Bond Polymer Refine Detection Kit according to the manufacturer's protocol (Petra Dinse, Histology Core Facility, Georg Speyer Haus). After automated deparaffinization and rehydration as well as citrate/EDTA buffer-based antigen retrieval, and blocking of unspecific binding, incubation with primary antibodies, followed. Antibodies and dilutions are listed in Tab. 3.7 (section 3.6). Secondary antibodies were HRP labeled and visualized by 3,3-Diaminobenzidine conversion (Refine Detection Detection Kit, Leica). Hematoxylin and eosin (HE) staining was performed on an automated staining device (Leica Autostainer XL). Tissue sections were visualized using the Aperio ScanScope. The quantification of Iba1+ macrophages was performed with Aperio ImageScope using a pixel counting algorithm, due to the complexity of cell morphology. CD3+, FoxP3+ and CD8+ T cells were quantified via a nuclear counting algorithm. Analysis was performed blinded to the group allocation.

4.2.10. Flow cytometry

For flow cytometric analysis of BrM, mice were perfused with 20 ml DPBS and BrM were macrodissected with a scalpel, based on MRI imaging. BrM tissue was immediately transferred to ice cold DPBS followed by the generation of single cell suspension. For separation of cells, cell-cell-connections were digested with the Brain-tumor-dissociation Kit (Miltenyi) in the gentleMACS Octo Dissociator, according to the manufacturer's protocol. Afterwards, cell suspensions were filtered through 70 µm cell strainers and washed with 10 ml HBSS. Cells were centrifuged (400xg, 10 min) and supernatant discarded. Then, myelin was removed via addition of 2 ml Myelin Removal Beads II mixture (1.8 ml DPBS+0.2 ml beads) and incubation for 15 min at RT. After washing with 20 ml DPBS (400xg, 10 min), pellet was diluted in 2 ml DPBS and filtering through LS-columns (Miltenyi). Myelin bound to the magnetic beads was retained in the columns by the QuadroMACS Separator. Columns were washed with a second addition of 2 ml DPBS. Cell suspensions were centrifuged (400xg, 10 min) and supernatant discarded. In case of blood residues in the cell pellet, red blood cell (RBC) lysis was performed. Cells were resuspended in 1x RBC lysis buffer and incubated for 5 min at RT in the dark. Reaction was stopped by addition of 20 ml DPBS, followed by centrifugation (400xg, 10 min). Cells were resuspended in DPBS and transferred to 96-well plates for subsequent staining.

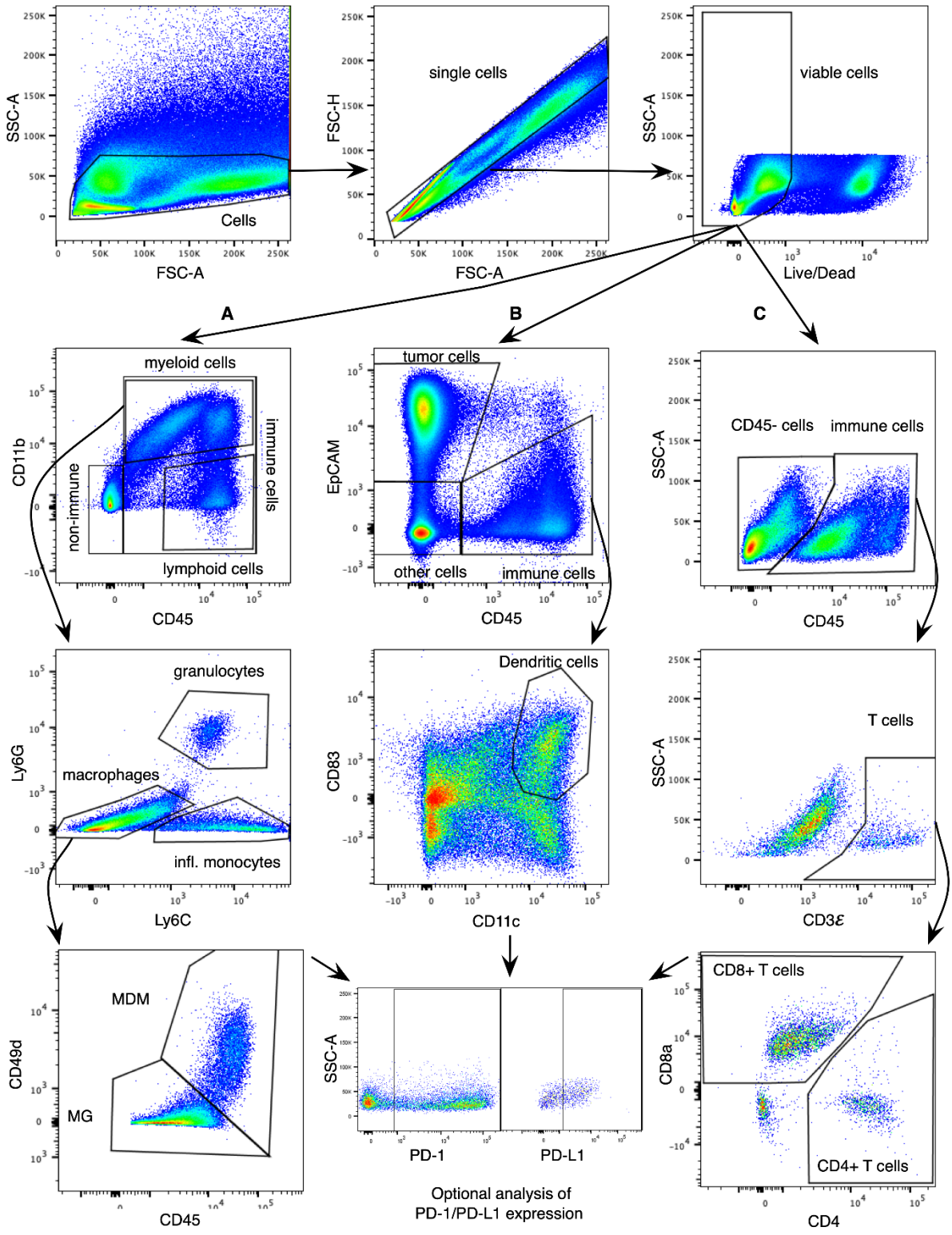

Fig. 4.1: Gating schemes for flow cytometric analysis of BrM and blood. Analysis of (A) myeloid cells, such as microglia (CD45+ CD11b+ Ly6Clow, Ly6G-, CD49d-), granulocytes (CD45+ CD11b+ Ly6Cmed, Ly6G+), inflammatory monocytes (CD45+ CD11b+ Ly6Chigh, Ly6G-) and MDM (CD45+ CD11b+ Ly6Clow, Ly6G-, CD49d+), (B) tumor cells (EpCAM+) and dendritic cells (CD45+ CD11c+ CD83+), and (C) CD4+ T cells (CD45+ CD3+ CD4+) and CD8+ T cells (CD45+ CD3+ CD8+) in 99LN-BrM or blood. Optionally, surface expression of PD-1 and PD-L1 was analyzed in combination with the three panels.

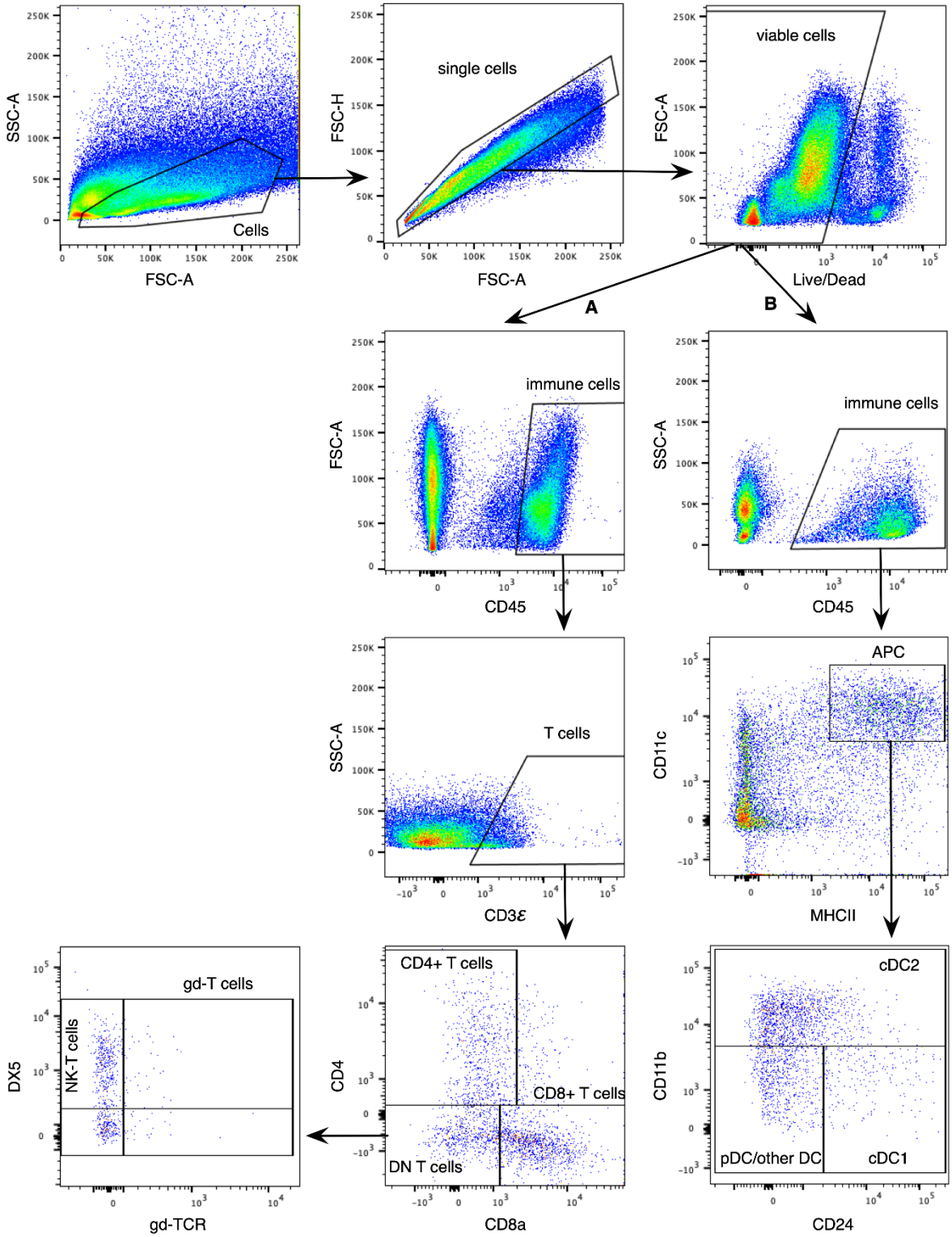

Fig. 4.2: Gating schemes for flow cytometric analysis of 99LN-BrM. Analysis of (A) double negative NKT cells (CD45+ CD3+ CD4- CD8- γδ-TCR- DX5+) and γδ-T cells (CD45+ CD3+ CD4- CD8- γδ-TCR+) and (B) dendritic cells such as cDC1 (CD45+ CD11c+ MHCII+ CD11b- CD24+), cDC2 (CD45+ CD11c+ MHCII+ CD11b+) and pDC/other DC (CD45+ CD11c+ MHCII+ CD11b- CD24-).

Supernatant was removed from the wells by centrifugation (400xg, 5 min). To prevent unspecific binding, samples were incubated with 100 µl Fc-block diluted in DPBS (1:1000), for

15 min at 4°C. Afterwards, cells were incubated for 30 min at 4° C with viability dye and fluorochrome-labeled antibodies (diluted in DPBS), as listed in Tab. 3.6 (section 3.6). Before analysis at the flow cytometer, cells were washed three times with 200 µl DPBS (400xg, 5min). Analysis of the fluorescently labeled cells was performed at a BD LSR Fortessa, using the high throughput sampler (HTS) unit. For laser compensation, ArC and AbC compensation bead kits (Thermo Fisher) were used according to the manufacturer's protocol. Data was recorded via BD FACS Diva. Gating strategies for the analysis of BrM tissue are depicted in Fig. 4.1 and Fig. 4.2. The detailed analysis and calculation of compensation were performed with Flow Jo (BD).

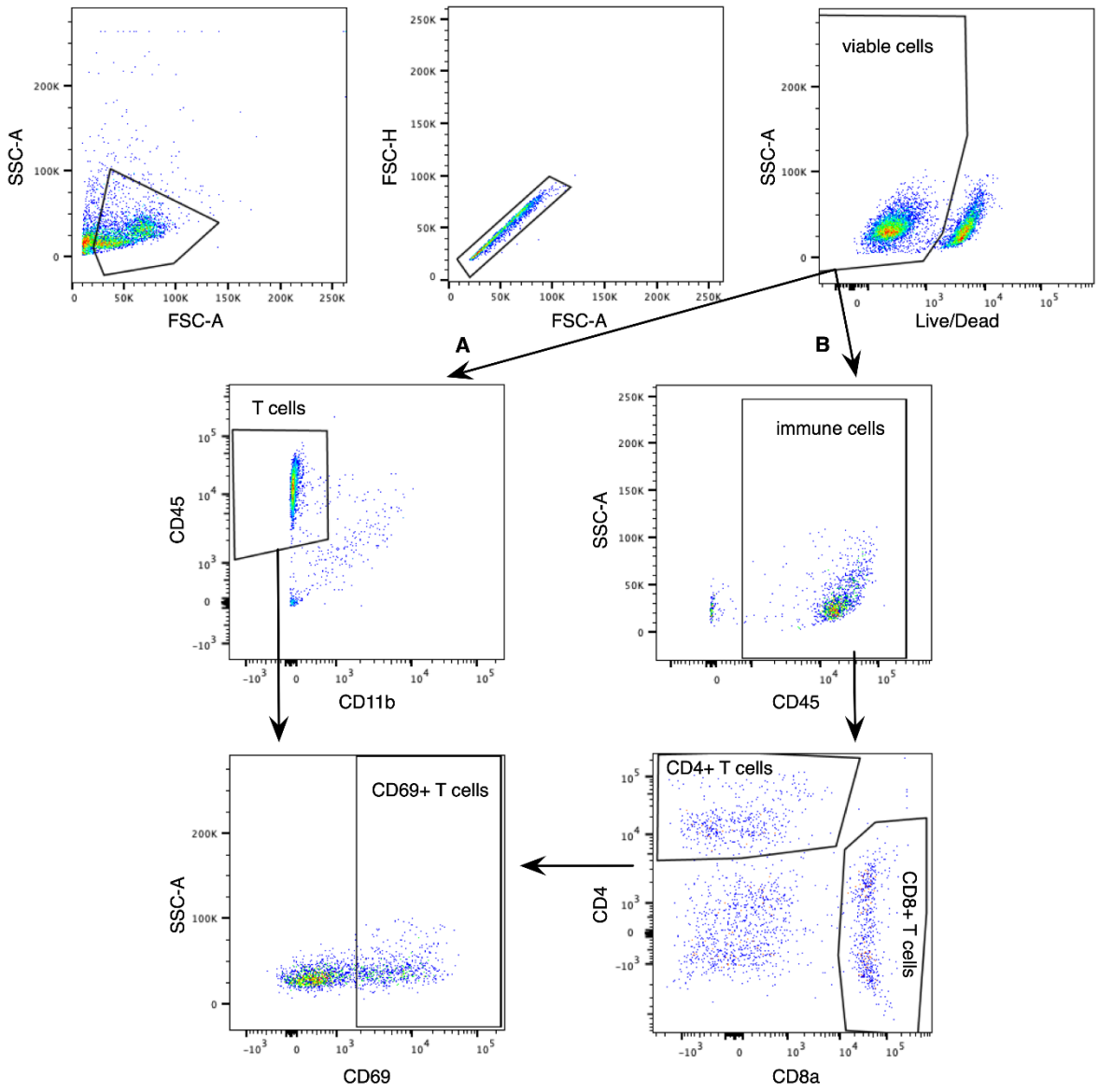

Fig. 4.3: Gating schemes for flow cytometric quantification of splenocytes. (A) Total activated T cells (CD45+ CD11b- CD69+) and (B) CD4+ (CD45+ CD4+ CD69+) and CD8+ (CD45+ CD8+ CD69+) activated T cells. T cells in the assay were activated by αCD3 antibodies which can interfere with antibodies binding to the same antigen. Therefore, T cells were not labeled with αCD3 for flow cytometry.

For the analysis of blood, mice were bled via submandibular routes. Two drops of blood per mouse were collected in EDTA-coated tubes to prevent coagulation. Blood was resuspended in 5 ml RBC-lysis buffer and filtered through 70 µm cell strainers. Samples were incubated for 5 min at RT. RBC-lysis buffer was removed by centrifugation (400xg, 5 min). Optionally, RBC-lysis was repeated. After washing with DPBS (400xg, 5 min), cells were incubated for 15 min with Fc-block and 30 min with antibody solutions at 4°C, as described for BrM tissue. For the quantification of T cells in the blood, the same gating strategy was applied as depicted for BrM tissue in Fig. 4.1 C.

For analysis of the *in vitro* T cell assays, T cells were transferred into round bottom 96-well plates, directly blocked, stained and analyzed at the BD LSR Fortessa, as described for BrM and blood. The gating scheme for the analysis of T cell assays is depicted in Fig. 4.3.

4.3. Animal experiments

4.3.1. Mice

All animal studies were approved by the government committee (Regierungspräsidium Darmstadt, Germany; protocol numbers F123/1016 and F123/1068) and were conducted in accordance with the requirements of the German Animal Welfare Act. Female C57Bl6/J (for the 99LN-BrM model) and FVB/n (for the TS1-BrM model) mice were purchased from Charles River Laboratories. CX3CR1-GFP/wt mice were generated as described previously (Jung *et al*, 2000), purchased from Jax Laboratories and bred in the Georg Speyer Haus animal facility. Mice included in experiments were monitored daily for symptoms. For the harvest of tissue, mice were anesthetized by Ketamine-Xylazine injection followed by perfusion with DPBS (section 4.3.3).

4.3.2. Generation of experimental brain metastasis

For *in vivo* experiments with 99LN-BrM, 10-12 week old C57Bl6/J mice were used. BrM were generated by intracardiac injection (ICI) of $6x10^4$ or $1x10^5$ 99LN-BrM cells in 200 µl DPBS, into the left ventricle of mice, as previously described (Bowman *et al*, 2016; Sevenich *et al*, 2014). ICI was always performed under anesthesia, which was induced by injection of 200 µl Ketamine-Xylazine solution (Tab. 4.7).

Tab. 4.7: Composition of Ketamine-Xylazine solution for anesthesia of mice.

Component	Volume [ml]
Ketavet (10%)	1
Rompun (2%)	0.1
ddH_2O	8.9

For the generation of TS1-BrM, 10-12 week old FVB/n mice were used and $3x10^4$ cells were injected, as described for the 99LN-BrM model.

4.3.3. Perfusion of mice for analyses of tissues

For immunological or molecular analysis of tissues, such as BrM tissue, mice were perfused to avoid contamination by intravascular cells. Prior to perfusion, mice were anesthetized with Ketamine-Xylazine solution. Afterwards the chest cavity was opened surgically, an incision was made at the right auricle of the heart and the needle of the infusion device was placed into the left ventricle of the heart. Then, mice were perfused with 20 ml DPBS for flow cytometric or TCR analysis. For histological analyses, mice were additionally perfused with 10 ml of 4% ROTI Histofix for immediate fixation of tissues.

4.3.4. Magnetic resonance imaging of brain metastasis

Tumor progression was monitored weekly by magnetic resonance imaging (MRI), starting at week 4-5 after tumor injection, until trial end point. MRI measurements were performed with a 7 Tesla Small Animal MR Scanner. A volume coil was used as transmitter and a head surface coil for signal reception, as previously described (Chae *et al*, 2019). Approximately 5 min before the measurement, mice were injected i.p. with 100 µl Gadobutrol (Gadovist, 1 mmol/ml). During the whole procedure, mice were anesthetized via isoflurane application. Data acquisition was performed using the Paravision 6.0.1 software. Images were generated in coronal planes (13-15 planes). For T2-weighted images, localized T2-multislice Turbo rapid acquisition with relaxation enhancement (T2 TurboRARE; TE/TR = 33 ms /2500 ms) was used. For T1-weighted images a RARE sequence (T1 RARE; TE/TR = 6.5 ms /1500ms) was applied. Till first detection of BrM lesions, tumor progression was monitored only with T1-weighted sequences. After first BrM detection, measurements were continued with T1- and T2-weighted sequences. Volumetric analysis of brain metastases was performed based on the T1-weighted images, using the segmentation tool of the ITK-Snap software (Yushkevich *et al*, 2006).

4.3.5. Preclinical trials: Whole brain radiotherapy

To investigate the influence of classical fractionated radiotherapy (mono- or combination-therapy) on BrM, whole brain radiotherapy was applied as doses of 2 Gy, on 5 consecutive days. Radiotherapy was executed with the Small Animal Radiation Research Platform (SARRP), as previously described (Chae *et al*, 2019). The SARRP was operated by Prof. Franz Rödel, PD Dr. Stephanie Hehlgans, Jeannie Peifer and Julius Oppermann (Radiotherapy and Oncology, Goethe University Frankfurt). Mice were anesthetized with isoflurane (2.5 %) during the procedure. Before the radiation of BrM, whole body CT images were recorded with the on-board Cone Beam CT system (CBCT) of the SARRP. The CBCT

was operating at 60 kV and 0.8 mA. The treatment planning was performed, based on these CT images, with the integrated Muriplan software (Fig.4.4). This software allows image-guided treatment design, dose calculation and application of highly focused radiation fields. For each mouse, CT and treatment planning of WBRT in Muriplan were performed daily. Individual isocenter were set for each mouse. Dose delivery was performed using a 10x10 mm collimator, moving in 1 arc and operated at 220 kV and 13 mA with 5.2 cGy/sec.

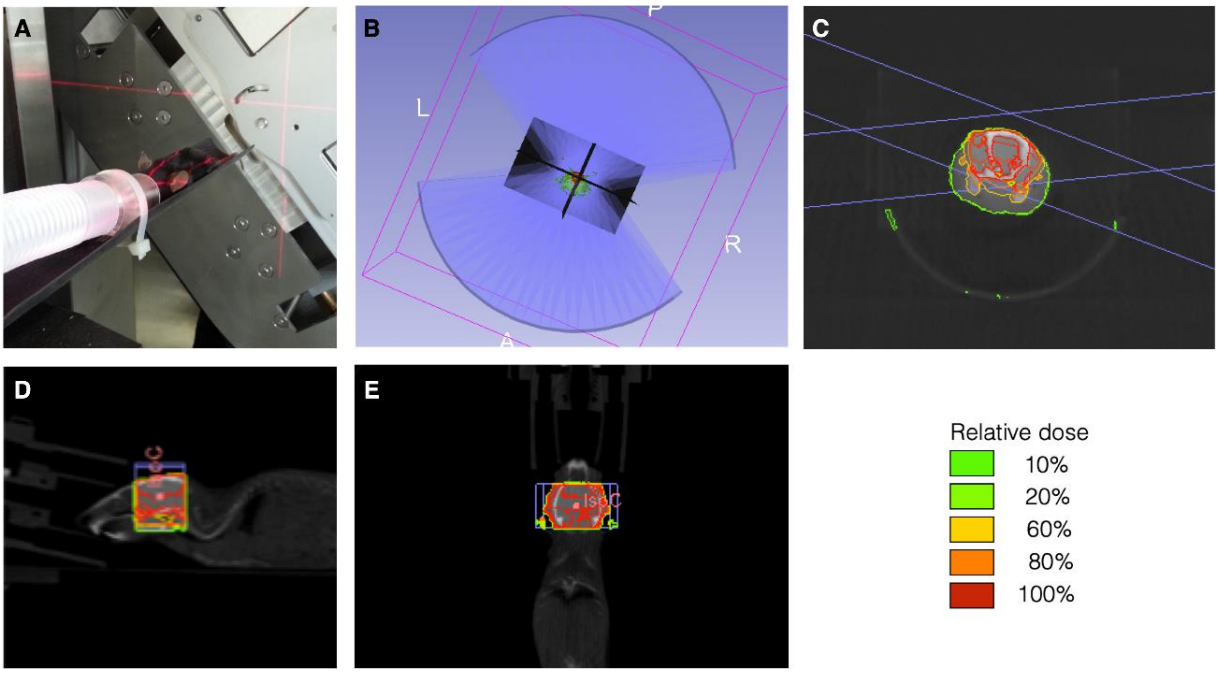

Fig. 4.4: Radiotherapy of mice with the Small animal radiation research platform (SARRP). (A) Picture of a 99LN-BrM mouse being treated with WBRT in the SARRP. (B-E) Representative images of treatment planning and dose calculation for WBRT with the Muriplan software, based on CT images. (B) Representation of the arc position set for dose delivery. (C) Treatment planning and dose distribution in the transverse plane, (D) sagittal plane and (E) coronal plane.

4.3.6. Preclinical trials: Checkpoint combination trial

For the checkpoint combination trial, the 99LN-BrM model was used. $6x10^4$ 99LN-BrM cells were injected per ICI, as described previously (section 4.3.2). In this model, the probability that BrM can be detected before week 5, is very low, which is why MRI monitoring was started 5 weeks after ICI. Approximately 7 weeks after ICI, when most mice developed BrM, mice were stratified into four groups with comparable tumor load, based on volumetric MRI quantification on d -1 (see section 4.3.4). Then, the groups were assigned to the four treatments (Isotype IgG2a, WBRT+IgG2a, anti-PD-1 (αPD-1) and WBRT+αPD-1) randomly. The treatment schedule was started one day later (d0). This schedule included WBRT, with a dose of 2 Gy/per day for five days, as well as immune checkpoint blockade (ICB) (anti-PD-1) or isotype (IgG2a), every third day, also starting at d0. WBRT was applied as described in section 4.3.5. Depending on the group, 250 µg of αPD-1 (clone: RMP1-14) or IgG2a (clone: 2A3) were

injected i.p., in a volume of 100 µl. For the survival trials, mice were treated with ICB or isotype until they developed symptoms (e.g. disequilibrium, leg paralysis, weight loss, piloerection) or BrM lesions reached a maximum volume of >100 mm^3, based on weekly volumetric MRI quantification. For the short-term trials (e.g. for flow cytometry analysis or TCR profiling), mice were sacrificed on d14 after treatment start.

4.3.7. Preclinical trials: AMD3100 combination trial

Mice in the AMD3100 combination trial were treated with WBRT and αPD-1 or IgG2a as described in the previous section. Additionally, the animals received daily doses of 5 mg/kg AMD3100 (1 mg/ml diluted in carrier solution) or carrier solution i.p. (100 µl per 20 g mouse). The composition of the carrier solution is depicted in Tab. 4.8, and was sterile filtered before treatment of animals or addition to AMD3100.

Tab. 4.8: Composition of carrier solution for AMD3100.

Component	Volume [ml]
Glucose (5% in ddH_2O)	65
Tween 80	5
Propylene glycol	30

Mice in the survival trials were sacrificed when they developed symptoms or BrM with a volume of >100 mm^3, as described in the previous section. Mice for flow cytometric analysis were only treated with AMD3100 or carrier solution and sacrificed 14 days after treatment initiation.

4.3.8. Preclinical trials: CSF1R inhibitor combination trial

Mice in the CSF1R inhibitor combination trial were treated with WBRT and αPD-1 as described in the previous sections. Additionally, the mice received a CSF1R inhibitor (confidentiality agreement). This inhibitor was delivered daily per oral gavage. Mice in the long-term survival trial only included the group receiving WBRT, αPD-1 and CSF1R inhibitor, since this trial was a preliminary experiment, run in parallel to the AMD3100 combination trial. As control served the WBRT+αPD-1 group, included in the AMD3100 combination trial (section 4.3.7). Termination criteria were the development of symptoms or BrM lesions of >100 mm^3 as described in the sections before.

4.3.9. T cell depletion

One week after ICI of $1x10^5$ 99LN-BrM cells, mice were stratified into two groups (isotype and depletion group). This timepoint was chosen to allow extravasation of tumor cells, before starting T cell depletion. The depletion group received 150 µg anti-CD4 (clone: GK1.5) and

150 µg anti-CD8a (clone: YTS 169.4) i.p. The isotype group received 300 µg of isotype IgG2b (clone: LTF-2). The first three injections were applied on consecutive days, followed by weekly injections till trial endpoint at d60, or occurrence of symptoms. T cell depletion was confirmed by flow cytometry of blood from 2-3 mice of the depletion group, weekly (section 4.2.10, Fig. 4.1 C). Every week, other mice of the cohort were selected to prevent distress induced by repeated blood collections. BrM onset and progression were monitored by weekly MRI measurements. Volumetric quantification was performed with ITK snap, as described before. At d60 the trial was terminated, and all mice were sacrificed by perfusion (section 4.3.3). Brains were isolated and transferred to 4% ROTI Histofix for subsequent histological analysis. The depletion of T cells in the BrM lesions was confirmed by IHC analysis.

4.3.10. TCRβ profiling trial

For TCRβ profiling, $1x10^5$ 99LN-BrM cells were injected per ICI (section 4.3.2). After first detection of established BrM (8 weeks after ICI), mice were stratified into two groups with comparable metastasis load. One group was treated with 2 Gy WBRT for 5 consecutive days (section 4.3.5). The other group was left untreated. 14 days after treatment start, mice were perfused with DPBS, and BrM and CLN were macrodissected for DNA-isolation (sections 4.1.3), followed by TCRβ-profiling (see and 4.1.4).

4.4. Statistical analysis, data presentation and generation of figures

Data are represented as mean ± SD or mean ± 95% CI as indicated in the figure legend. For the collection, statistical analysis and generation of graphs Excel Office and GraphPad Prism 8 were applied. Statistical tests used for numerical data are mostly paired and unpaired two-tailed students t-test, as indicated in the respective legend. To calculate significance of survival differences, the Log-rank Mantel-Cox test was performed. All figures were generated with OmniGraffle. For the generation of figures in the introduction BioRender and PowerPoint were additionally applied.

5. Results

5.1. The cellular composition of the immune compartment in brain metastasis

To obtain an overview of the cellular composition in the tumor microenvironment (TME) of the syngeneic breast to brain model 99LN (99LN-BrM), flow cytometry analysis of macrodissected BrM was performed 9 weeks after intracardiac injection (ICI) of tumor cells. Weekly MRI was performed to detect and monitor the growth of BrM before sacrificing the mice. The average tumor volume at this stage was approximately 100 mm^3. Two antibody panels, depicted in section 4.2.10, have been applied to identify different cell types in the TME (section 4.2.10, Fig. 4.1 A, B). These analyses were important to elucidate the abundance of lymphoid cells, which can be exploited for immune checkpoint inhibition, versus tumor and myeloid cells, potentially contributing to immune suppression.

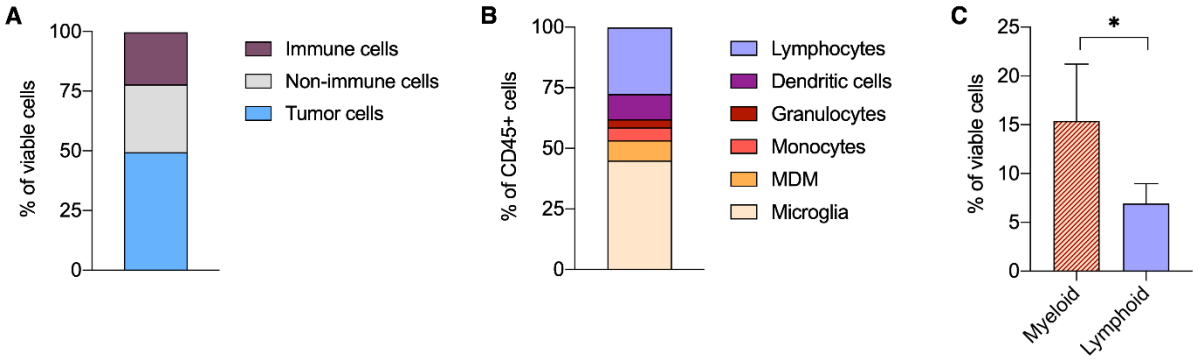

Fig. 5.1: Cellular composition in murine breast cancer derived 99LN-BrM. (A) Overview of proportions of cell types in the TME of 99LN-BrM. Tumors were macrodissected from brains and analyzed by flow cytometry (n=4). (B) Overview of proportions of immune cell populations analyzed by flow cytometry (n=4 for DC, n=5 for the remaining cell types). (C) Quantification of the percentage of total myeloid and lymphoid cells in 99LN-BrM, analyzed by flow cytometry (n=5). Data is represented as mean ± SD. P-values were obtained by unpaired t test with *P<0.05.

Interestingly, only half of the viable cells within the BrM lesions were tumor cells (CD45- EpCAM+), whereas the other half comprised stromal cells. Leukocytes (CD45+ EpCAM-) represented 22% of all viable cells in the TME (Fig. 5.1 A). To gain more detailed insight into the myeloid compartment in BrM, and to distinguish brain resident microglia from blood borne MDM, a recently described gating strategy was applied. The strategy included staining for CD49d, which is expressed by MDM but not by microglia in the brain (Bowman *et al*, 2016). This approach revealed that the immune cell compartment of 99LN-BrM is clearly dominated by myeloid cells, with the brain-resident microglia (CD45+ CD11b+ Ly6Clow Ly6G- CD49d-) accounting for 45% of total immune cells. Furthermore, the analyzed TME was constituted by blood borne myeloid cells, such as inflammatory monocytes (CD45+ CD11b+ Ly6Chigh Ly6G-: 5.4% of all CD45+ cells), MDM (CD45+ CD11b+ Ly6Clow Ly6G- CD49d+:

8.3% of all CD45+ cells) and granulocytes (CD45+ CD11b+ Ly6Cmed Ly6G+: 3.3% of all CD45+ cells), recruited to BrM lesions. Dendritic cells (CD45+ CD11c+ CD83+) accounted for approximately 10.4% (Fig. 5.1 B). Together, myeloid cells accounted for 15.4% of all viable cells in the TME. Immune cells of lymphoid origin accounted for 7% of viable and 27.5% of immune cells (Fig. 5.1 C).

In summary, these data indicate that a relatively high proportion of immune cells is recruited to 99LN-BrM lesions. These are constituted by brain resident microglia, as well as peripheral myeloid and, most importantly, lymphoid cells which can be exploited for T cell targeted therapies, such as immune checkpoint inhibition. This immune cell composition closely mimics the composition of human BrM, therefore confirming the utilization of the murine 99LN-BrM model to investigate breast cancer derived BrM.

5.2. The influence of radiotherapy on breast cancer brain metastasis

Radiotherapy, the standard of care for BrM patients, has been reported to potentially sensitize tumors to immune checkpoint inhibition, and first clinical trials of melanoma BrM seem to confirm this hypothesis (Ahmed *et al*, 2016). The question remains, to which extend radiotherapy can modulate the immune compartment of BrM of less immunogenic cancers, such as breast cancer, and sensitize it to checkpoint inhibition. Therefore, the next step was to investigate effects of ionizing radiation (IR) on breast cancer BrM cells *in vitro* and radiotherapy on 99LN-BrM *in vivo*.

To reveal direct effects of IR on BrM cells, breast cancer cell lines with brain tropism were irradiated *in vitro* with 10 Gy and analyzed via qRT-PCR for changes in expression of inflammatory cytokines at different time points (Fig. 5.2 A). Two cell lines tested were 99LN-BrM and TS1-BrM, both murine cell lines used to generate syngeneic BrM mouse models. The 831RS cell line, also included in this experiment, is derived from metastatic human breast cancer and can be employed for the generation of xenograft BrM models.

In vivo, IR was applied as classically fractionated WBRT (5x2 Gy) to elucidate radiation induced changes in the composition of the BrM TME. For these experiments C57Bl6/J mice were injected with $6x10^4$ 99LN-BrM cells intracardially. Starting from week five, tumor growth was monitored weekly till the day of sample harvest (Fig. 5.2 B, C). The first dose of WBRT was applied seven weeks after injection. Mice were sacrificed 14 days later (nine weeks after initial WBRT dose), and BrM macrodissected for flow cytometry (Fig. 5.2 C). Additionally, mice were sacrificed at endpoints (time of symptom development) to analyze the immune infiltration via histology.

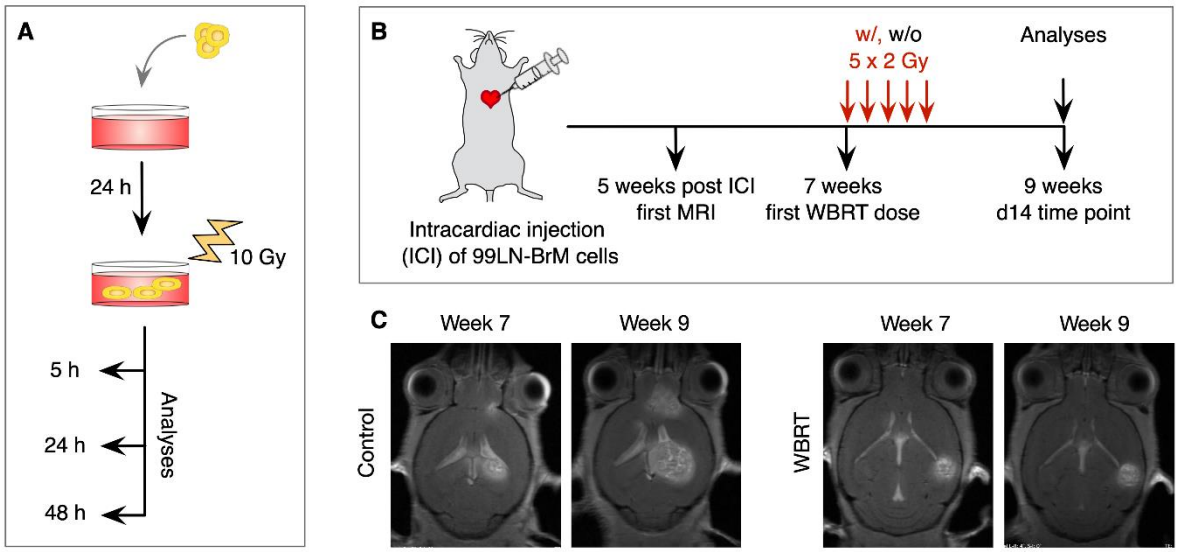

Fig. 5.2: Analyzing the impact of radiotherapy on cellular composition in breast cancer BrM. (A) Schematic of experimental design to reveal ionizing radiation (IR) induced changes of inflammatory markers *in vitro*. (B) Schematic of experimental design of tumor initiation and monitoring, as well as application of WBRT. Samples were taken 9 weeks after injection (d14 after first WBRT dose) and immediately analyzed via flow cytometry. (C) Representative MRI pictures (T1-weighted) of untreated and WBRT treated mice, seven and nine weeks after intracardiac injection of $6x10^4$ 99LN-BrM cells.

5.2.1. Effects of ionizing radiation on expression of inflammatory markers *in vitro*

Radiotherapy can potentially increase the recruitment of inflammatory cells via different mechanisms, described in section 1.4.1. One potential mechanism is the increased expression and secretion of inflammatory cytokines by irradiated tumor cells. To check if breast cancer BrM cells are directly affected by IR in this way, expression changes of inflammatory markers such as tumor necrosis factor α (TNFα), IL1β and IL6, in response to 10Gy *in vitro*, were analyzed via qRT-PCR after 5, 24 and 48 hours.

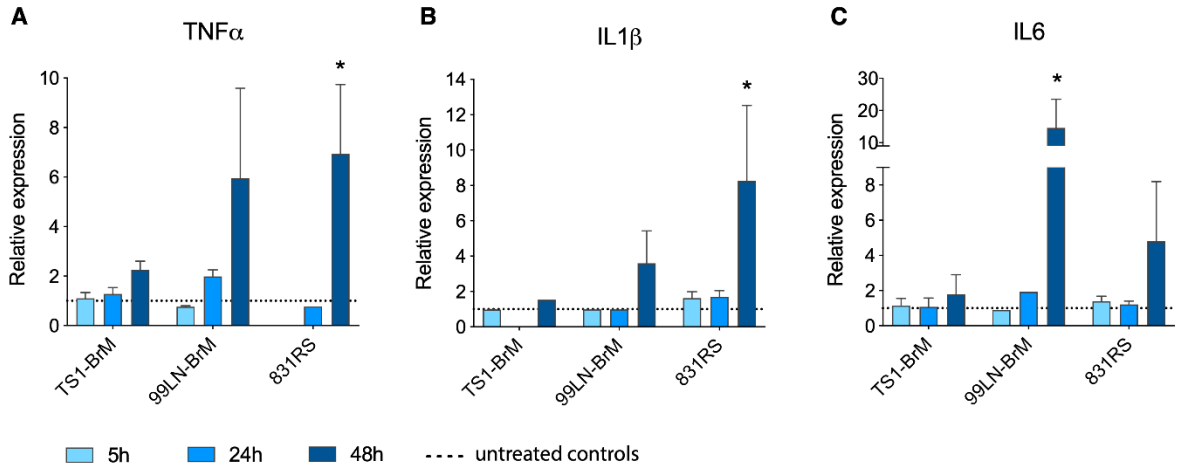

Fig. 5.3: Effects of ionizing radiation on expression of inflammatory markers by breast cancer BrM cell lines. Cells were irradiated with 10 Gy 24h after seeding and harvested for RNA isolation at different time points afterwards to perform qRT-PCR (control n=3, IR 5, 24 and 48h n=3). Results were normalized on untreated controls. Values below a CT threshold of 34 were not included in the analysis and graphs. (A) Relative expression of TNFα after 5, 24 and 48h by TS1-BrM, 99LN-BrM and 831RS cells. (B) Relative expression of IL6. (C) Relative expression of IL1β. P-values were obtained by paired t test with *P<0.05.

These data revealed that the expression of the analyzed inflammatory markers is relatively increased in all breast cancer BrM cell lines over time, albeit to varying degrees. The strongest increase of expression for all markers could be detected after 48h (Fig. 5.3 A-C). These results demonstrate direct effects of IR on cytokine expression, potentially leading to a more inflammatory TME and increased recruitment of inflammatory immune cells in the *in vivo* situation.

5.2.2. Effects of radiotherapy on innate myeloid cells *in vivo*

Given reports of radiotherapy induced recruitment of immune suppressive myeloid cells to the brain (Kioi *et al*, 2010), untreated and WBRT treated 99LN-BrM lesions were analyzed for differences in myeloid cell composition by flow cytometry and histology as described above.

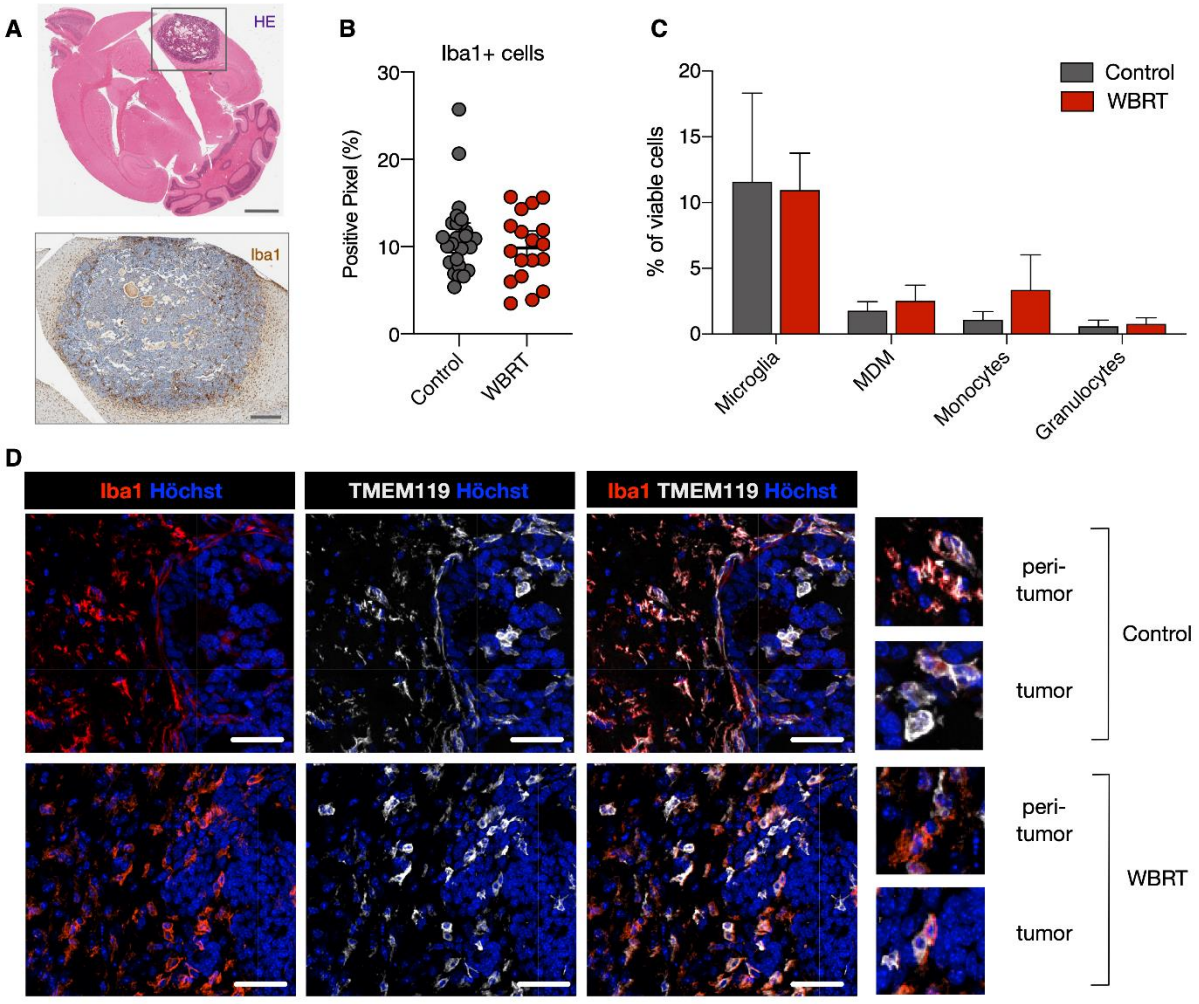

Fig. 5.4: Myeloid cells in the untreated or irradiated TME of breast cancer BrM. (A) Representative images of HE-stained 99LN-BrM sections and IHC, to visualize Iba1+ cells. Scale bars: 2 mm, 500 µm. (B) Quantification of Iba1+ macrophages in the IHC sections, with Aperio ImageScope (control n=26, WBRT n=18). Data is represented as mean ± 95% CI. (C) Flow cytometric quantification of myeloid populations in 99LN-BrM with and without WBRT, at d14 after the first radiation dose (control n=5, WBRT n=4). Data is represented as mean ± SD. (D) Representative immunofluorescence images of 99LN-BrM stained for Iba1 (red) and the microglia marker Transmembrane Protein 119 (TMEM119) (white) to distinguish brain resident microglia (Iba1+ TMEM119high) from MDM (Iba1+ TMEM119low). Höchst was used as nuclear counterstain (blue). Scale bars: 50 µm.

Quantification of immunohistological staining against Iba1, a pan-macrophage marker, revealed no change in total tumor infiltrating macrophages after WBRT (Fig. 5.4 A, B). To gain more detailed insight into WBRT induced changes on myeloid subpopulations, on d14 after first WBRT dose, flow cytometry of BrM tissue was performed with the abovementioned gating strategy (Section 5.1.). This experiment revealed, that neither microglia, nor blood borne myeloid cells, such as MDM, inflammatory monocytes or granulocytes, proportionally changed in response to WBRT (Fig. 5.4 C).

To confirm these results, immunofluorescent staining against Transmembrane Protein 119 (TMEM119), another marker described to distinguish microglia from MDM, and staining against Iba1 was carried out on sections of 99LN-BrM from untreated and irradiated mice. Indeed, no change in the proportion of infiltrating microglia (Iba1+ TMEM119high) and MDM (Iba1+ TMEM119low) in BrM lesions has been observed (Fig. 5.4 D).

In conclusion, WBRT did not lead to increased infiltration of potentially immune suppressive myeloid cells into 99LN-BrM lesions.

5.2.3. Effects of radiotherapy on dendritic cells *in vivo*

To harness the full potential of T cell targeted therapies, such as checkpoint inhibition, DC are thought to be essential. They represent a link between the innate and adaptive immune system. While microglia are known to be radioresistant, other immune cells, including DC, are more sensitive to IR. Therefore, it was essential to verify that DC are not depleted by conventional fractionated WBRT in 99LN-BrM. To identify DC in the lesions and quantify WBRT induced changes, another flow cytometry gating strategy was applied on the same set of samples as described in section 5.2.2. This strategy included CD11c and CD83 as markers for DC (gating strategy: section 4.2.10, Fig. 4.1 B).

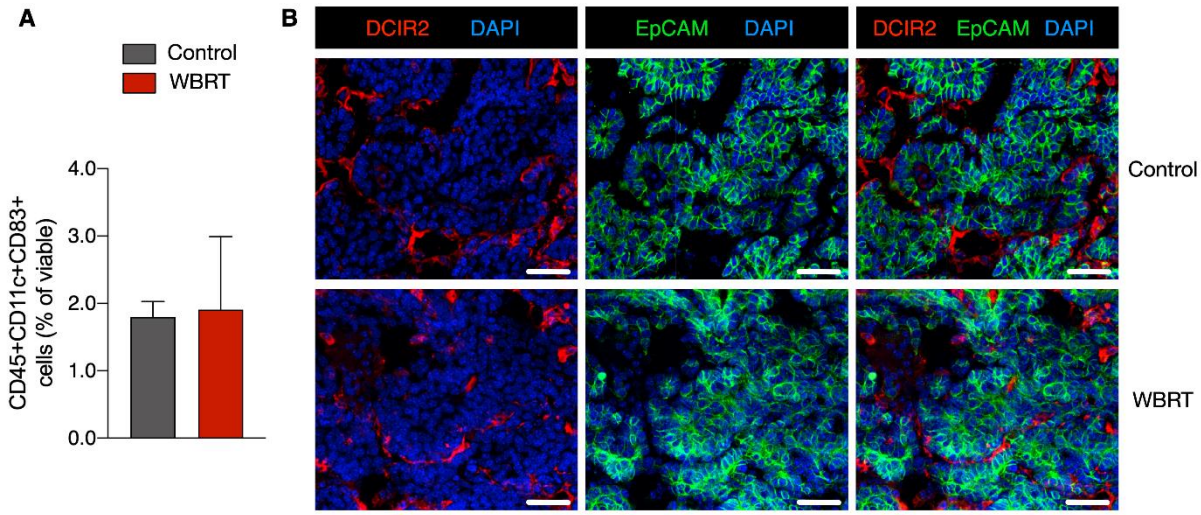

Fig. 5.5: Dendritic cells in the untreated or irradiated TME of breast cancer BrM. (A) Quantification of DC (CD45+ CD11c+ CD83+) in macrodissected untreated or irradiated 99LN-BrM by flow cytometry, 14 days after the first dose (control n=4, WBRT n=3). Data is represented as mean ± SD. (B) Representative immunofluorescence images of 99LN-BrM untreated or treated with WBRT and stained against DCIR2 (red) and EpCAM (green). DAPI (blue) was used as nuclear counterstain. Scale bars: 50 µm.

DC identified via flow cytometry (CD45+ CD11c+ CD83+), accounted for approximately 2% of all viable cells in the BrM lesions. The proportion of DC did not change 14d after WBRT (Fig. 5.5 A). The presence of DC in both untreated and WBRT treated BrM was confirmed via immunofluorescent staining against DC immunoreceptor 2 (DCIR2), another DC marker, which identified these cells within the lesions in close contact to tumor cells (EpCAM+) (Fig. 5.5 B).

To unravel if WBRT influences the proportions of DC subtypes such as conventional DC type 1 (cDC1) and conventional DC type 2 (cDC2), a more detailed flow cytometry panel was applied on a second cohort of mice (section 4.2.10, Fig. 4.2 B). The gating strategy was based on a strategy published by Mrdjen et al. (Mrdjen *et al*, 2018).

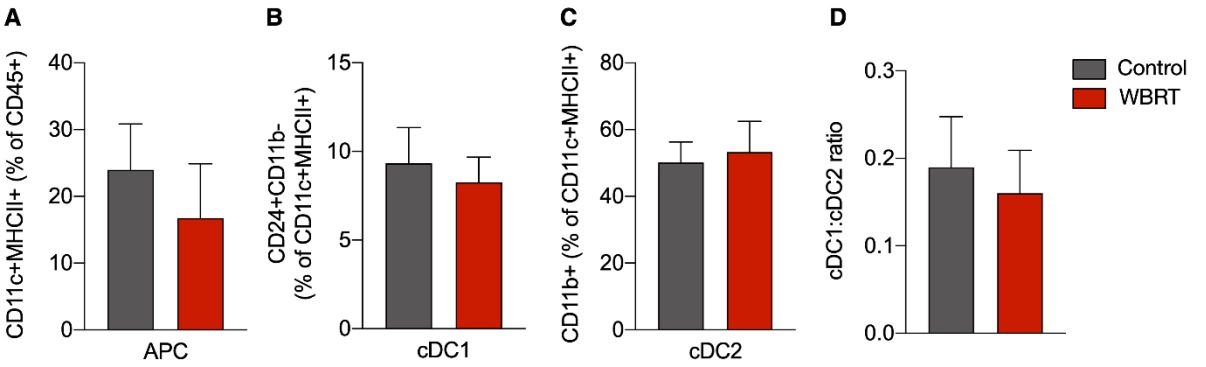

Fig. 5.6: Dendritic subpopulations in the untreated or irradiated TME of breast cancer BrM. Quantification of dendritic cell types by flow cytometry, in macrodissected untreated or irradiated 99LN-BrM, 14 days after the first dose (control n=6, WBRT n=7). Data is represented as mean ± SD. (A) Proportion of antigen presenting cells (APC: CD45+ CD11c+ MHCII+) of CD45+ immune cells. (B) Frequency of cDC1 (CD45+ CD11c+ MHCII+ CD11b- CD24+) of APC. (C) Frequency of cDC2 (CD45+ CD11c+ MHCII+ CD11b+ CD24-) of APC. (D) cDC1:cDC2 ratio.

The results from this analysis demonstrated that the prominent DC population in 99LN-BrM was cDC2 (CD45+ CD11c+ MHCII+ CD11b+), which accounted for 50% of all APC (Fig. 5.6 C). cDC1 (CD45+ CD11c+MHCII+ CD11b- CD24+) represented a smaller proportion, accounting for 9.2% (Fig. 5.6 B). WBRT did not lead to changes in the frequency of these DC subtypes, nor did it induce a shift in the cDC1:cDC2 ratio (Fig.5.6 A-C).

In conclusion, these results demonstrated that conventional fractionated WBRT does not lead to the ablation of DC in the TME of 99LN-BrM, or changes the composition of DC subtypes.

5.2.4. Effects of radiotherapy on tumor infiltrating lymphocytes *in vivo*

Given the aim of modulating T cells in BrM via checkpoint inhibition as adjuvant to standard of care WBRT, the T cell compartment had to be analyzed in detail. As before, it was essential to quantify infiltration in general, as well as to exclude long lasting depletion of radiosensitive cells by conventional fractionated WBRT. The experimental design of the *in vivo* trial was the same as described in section 5.2.2 and 5.2.3. Macrodissected BrM samples were stained with a flow cytometry antibody panel to distinguish different subsets of tumor infiltrating lymphocytes (section 4.2.10, Fig. 4.1 C). Again, the results were complemented by histological analysis of BrM from mice at trial endpoints.

Flow cytometry led to the identification of T cells in 99LN-BrM lesions. These infiltrating lymphocytes accounted for approximately 3% of immune cells. Importantly, WBRT did not lead to depletion of T cells at d14 after treatment initiation (Fig. 5.7 A). Intriguingly, while also no significant increase of total T cells or CD4+ T cells (CD45+ CD3+ CD4+) was detected 14 days after WBRT (Fig. 5.7 A, B), the infiltration of the lesions by CD8+ cytotoxic T cells (CD45+ CD3+ CD8+) significantly increased (Fig. 5.7 C). This observation was accompanied by a shift in the CD4:CD8 ratio compared to untreated controls (Fig. 5.7 D).

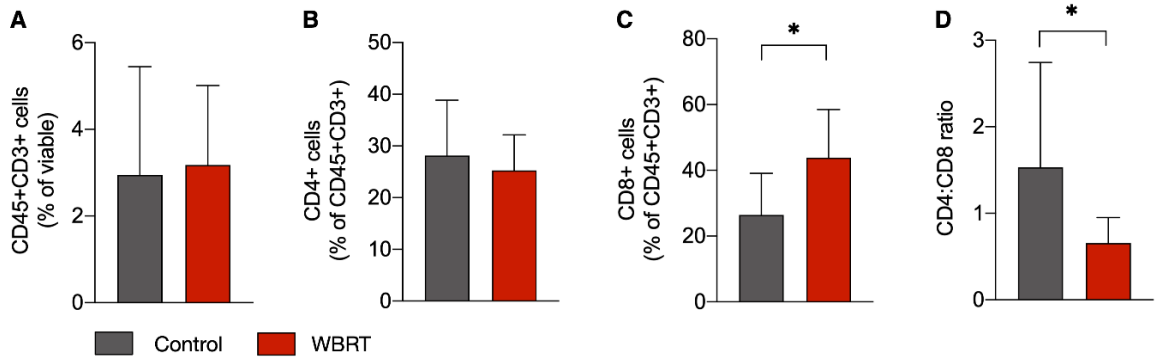

Fig. 5.7: T cells in the untreated or WBRT treated TME of breast cancer BrM analyzed by flow cytometry. T cell composition in macrodissected 99LN-BrM, 14 days after first WBRT dose (control n=10, WBRT n=10). Data is represented as mean ± SD. P values were obtained using unpaired t test with *P<0.05. (A) Percent T cells of viable cells. (B) Percent CD4+ T cells of total T cells. (C) Percent CD8+ T cells of total T cells. (D) Ratio of CD4+ to CD8+ T cells.

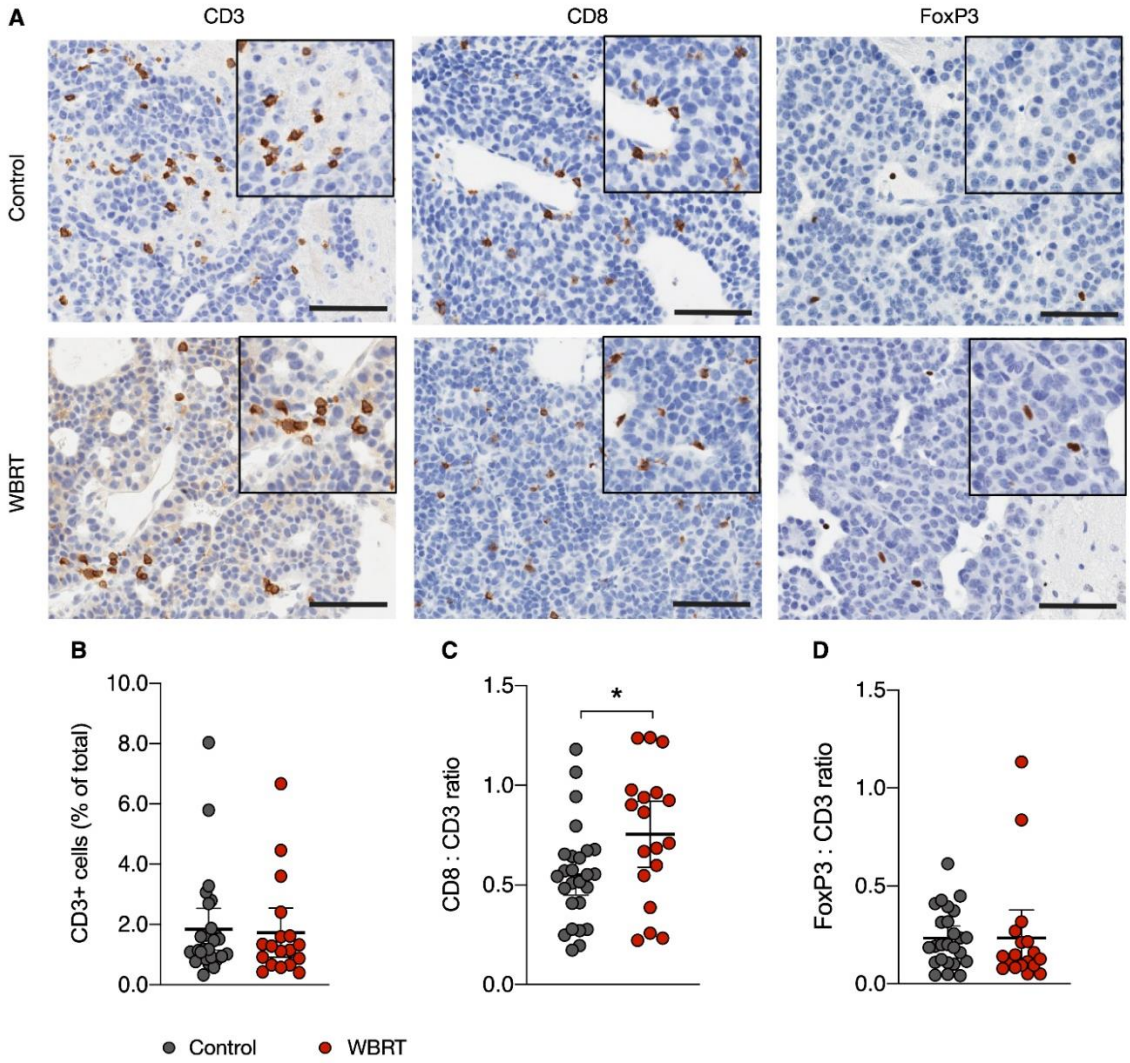

Fig. 5.8: T cells in the untreated or irradiated TME of breast cancer BrM analyzed by IHC. (A) Representative images of CD3+, CD8+ and FoxP3+ T cells in 99LN-BrM with and without WBRT. Scale bar: 100 µm, insert: 1.5x. (B) Percent CD3+ T cells of all cells in the lesions of 99LN-BrM sections, quantified with Aperio ImageScope. (C) Ratio of CD8+ cytotoxic T cells to total CD3+ T cells in the IHC sections of 99LN-BrM. (D) Ratio of FoxP3+ regulatory T cells to total CD3+ T cells. Data is presented as mean ± 95% CI. P values were obtained by unpaired t test with *P<0.05 (Control n=27, WBRT n=18).

Quantitative immunohistochemical analysis of T cells in 99LN-BrM confirmed the flow cytometry results. Again, WBRT did not lead to a change in total T cell infiltration (CD3+ cells) but induced a relative increase of infiltrating CD8+ cytotoxic T cells (Fig. 5.8 A-C). FoxP3+ regulatory T cells, which mediate suppression of adaptive immune responses, were only present in low numbers and were not increasingly recruited after WBRT (Fig. 5.8 A, D).

Flow cytometry analysis also revealed a relatively high proportion of T cells which neither expressed CD4 nor CD8 (Fig. 5.9 A). To characterize these double negative T cells (DN T cells), another flow cytometry panel, identifying NKT cells and γδ-T cells, was applied to BrM of a second cohort of mice (section 4.2.10, Fig. 4.2 A).

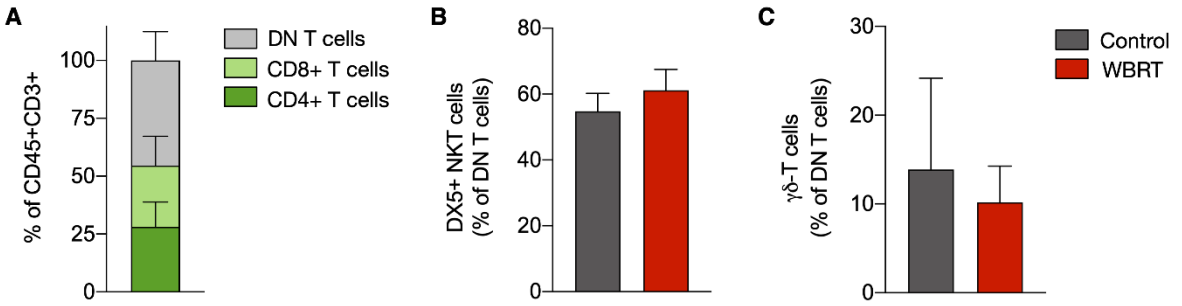

Fig. 5.9: CD4- CD8- double negative (DN) T cells in the untreated or WBRT treated TME of breast cancer BrM. T cell composition in macrodissected 99LN-BrM analyzed by flow cytometry, 14 days after first WBRT dose (control n=6, WBRT n=7). Data is represented as mean ± SD. (A) Percent DN (CD45+ CD3+ CD4- CD8-), CD4+ and CD8+ T cells of total T cells. (B) Percent NKT-T cells (DX5+ γδ-TCR-) of DN T cells. (C) Percent γδ-T cells (γδ-TCR+) of DN T cells. Data is represented as mean ± SD in A-C.

This analysis demonstrated that DN T cells in 99LN-BrM were comprised of NKT cells (CD45+ CD3+ CD4- CD8- γδ-TCR- DX5+: 54.8%), γδ-T cells (CD45+ CD3+ CD4- CD8- γδ-TCR+: 13.9%) and other DN T cells which could not be further characterized with the applied flow cytometry panels. The proportions of the different DN T cells did not change significantly in BrM, isolated from mice 14 days after WBRT, compared to untreated mice (Fig. 5.9 B, C).

In conclusion, these results demonstrate that even though the brain is a strictly controlled microenvironment, the BrM TME harbors critical cell types to execute an adaptive immune response directed against cancer cells. Despite the radio-sensitivity of most immune cells, it has been demonstrated that conventional WBRT does not deplete T cells in the 99LN-BrM TME, but rather increases the relative amount of CD8+ cytotoxic T cells, which can be harnessed for immunotherapy. In contrast, immune cells often associated with pro-tumor functions and immune suppression, such as MDM or FoxP3+ regulatory T cells, were not increasingly recruited after WBRT.

5.3. Clonal expansion and TCR repertoire of T cells infiltrating brain metastases

By this point it has been revealed that T cells and professional APC are present in breast cancer BrM and are not depleted by WBRT. In order to unravel whether T cells identified in the BrM TME migrated to the lesion because they are targeted against tumor antigens, or whether these cells are just passive bystanders, clonality of the T cell pool in 99LN-BrM was analyzed in detail. Once naïve T cells are primed by presentation of antigen, they clonally expand, meaning that descending T cells share the same DNA sequence coding for the T cell receptor (TCR). These T cell clones can be identified via TCRβ profiling, the sequencing of the DNA section, encoding for the highly variable CDR3 region of the β-chain of TCRs. The CDR3 region is unique for each T cell clone, allowing quantification of expanded T cells. In addition to BrM tissue, CLN were analyzed, as antigen derived from BrM lesions potentially is drained to these peripheral lymphoid organs.

5.3.1. Quantification of systemic and BrM infiltrating T cells

For TCRβ profiling BrM tissue and CLN from untreated or WBRT treated mice was collected 14 days after the first radiation dose. DNA was isolated and purified from the samples and subjected to TCR sequencing and pre-analysis (AdaptiveBiotech, ImmunoSeq) (Fig. 5.10 A). In addition to sequencing, the absorbance at 260 nm was measured for each sample by AdaptiveBiotech, to estimate the number of nucleated cells per sample. This allowed the quantification and comparison of T cell proportions in different samples with distinct numbers of total cells.

Data obtained from the ImmunoSeq Analyzer (AdaptiveBiotech) demonstrated, that 14 days after WBRT the percentage of T cells in the BrM lesions did not change, confirming the results of flow cytometry and histological analyses. Furthermore, there was no change in the proportion of T cells in CLN after WBRT, compared to untreated controls (Fig. 5.10 B). Additionally, irrespective of treatment, BrM did not lead to systemic lymphopenia, indicated by a high percentage of T cells in CLN. This was confirmed by flow cytometric analysis of peripheral blood collected from mice with and without BrM. Mice bearing 99LN-BrM did not have reduced proportions of T cells in the blood compared to healthy control mice (Fig. 5.10 C). Interestingly, the percentage of T cells in BrM, derived from TCRβ profiling, negatively correlated with BrM volume, indicating a progressive suppression of adaptive immunity within growing lesions (Fig. 5.10 D).

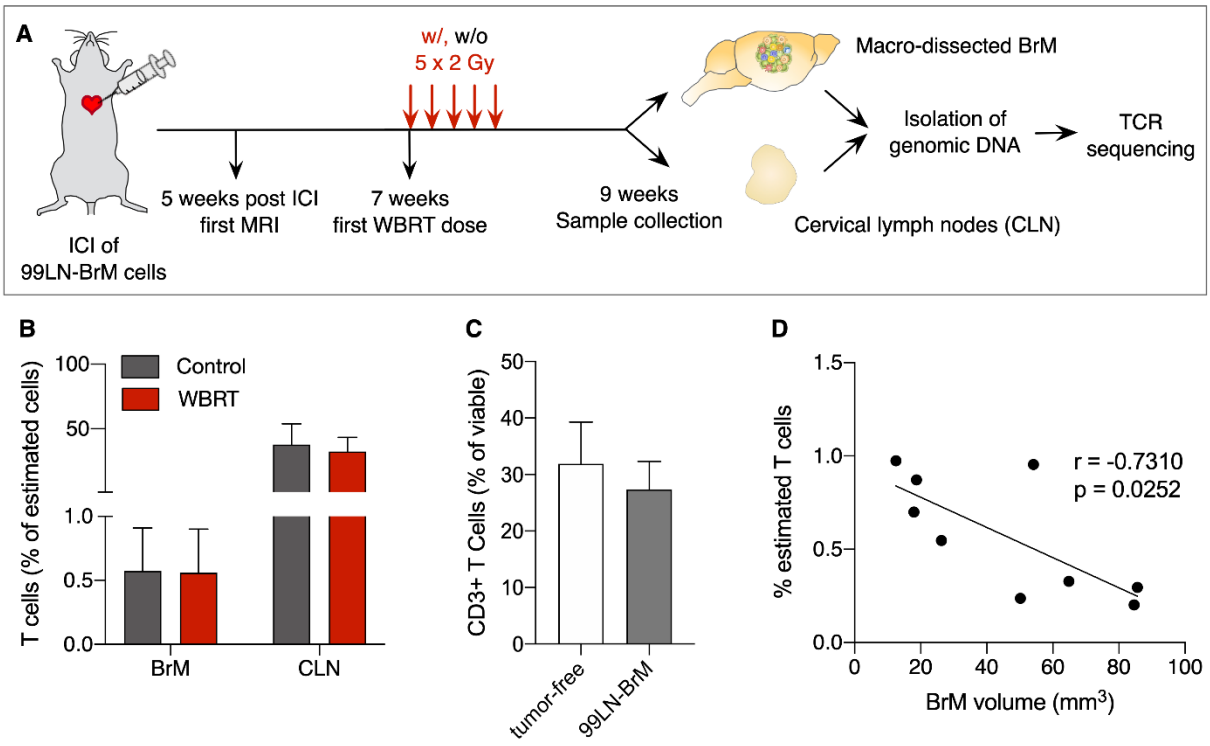

Fig. 5.10: Proportion of T cells in untreated or irradiated breast cancer BrM analyzed by TCRβ profiling. Schematic of experimental design to identify clonal expansion of T cells in BrM and CLN. Mice with 99LN-BrM were left untreated (n=5 for BrM and CLN) or treated with WBRT (n=4 for BrM and n=5 for CLN). Tissue was sampled 14 days after treatment initiation and DNA was isolated from tissue and subjected to TCR sequencing. (B) Percent T cells of estimated cells in 99LN-BrM and CLN samples with and without WBRT (Control BrM n=5, WBRT BrM n=4, control CLN n=5, WBRT CLN n=5). (C) Percent CD3+ T cells in the blood of 99LN-BrM bearing mice quantified via flow cytometry. (D) Percent estimated T cells negatively correlate with BrM volume (n=9, Pearson correlation coefficient r=-0.7319, p=0.0252). Data is represented as mean ± SD in B and C.

5.3.2. Proportion of top clones in BrM

To evaluate the extent of clonal expansion in untreated or irradiated BrM, the maximal productive frequency, as well as productive clonality, was analyzed with the ImmunoSeq Analyzer. The maximal productive frequency is the percentage of the TCR clone which comprises the highest number of T cells (top clone) from the whole T cell pool in the sample. Productive clonality is a measure of the extent to which a T cell pool is dominated by one or few T cell clones and, therefore, an indicator for clonal expansion. A value of 1 implies that a T cell pool is comprised of a single clone (oligoclonal), meaning all T cells share the same TCR sequence. A value of 0 indicates that every T cell clone is comprised of one T cell with no dominant clone in the pool. Polyclonal pools with a high variety of T cell clones, therefore, show a clonality closer to 0.

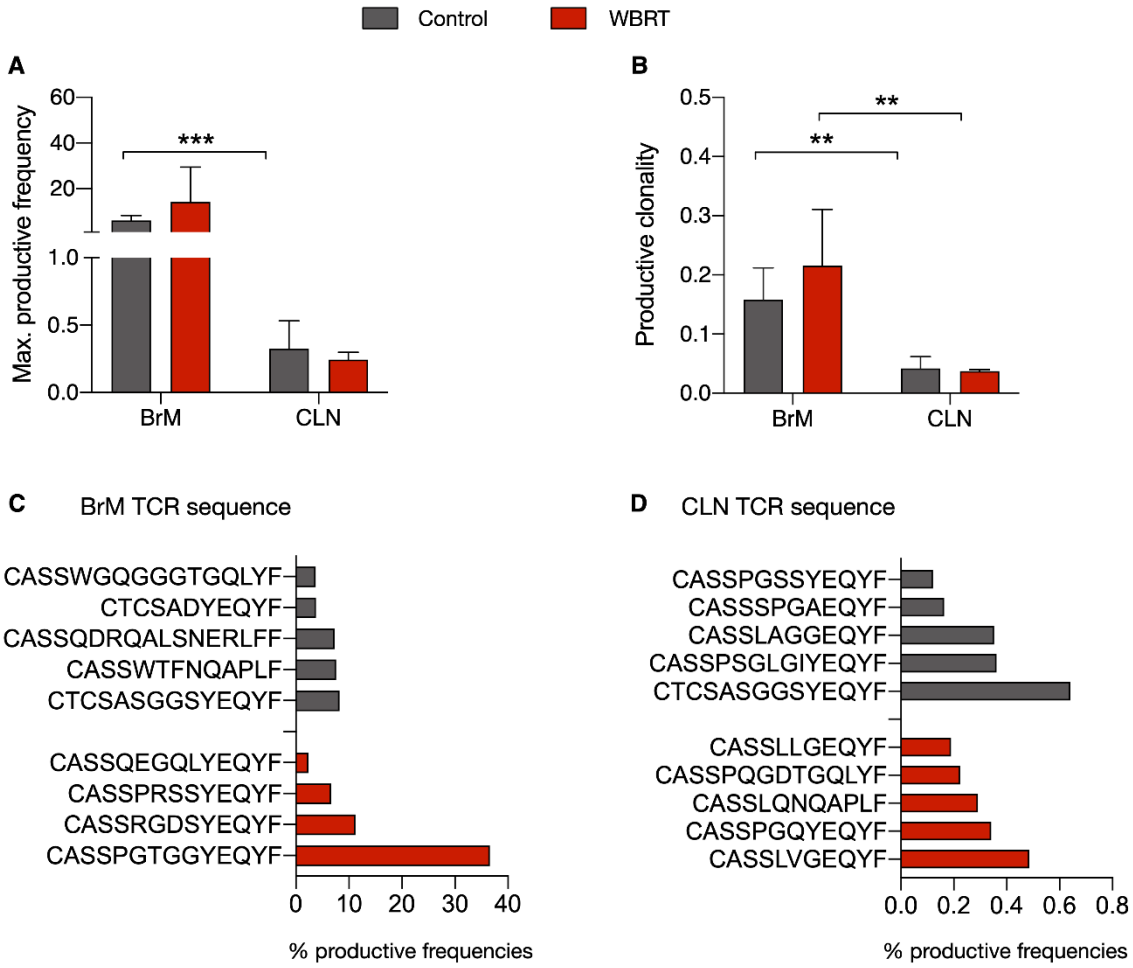

Fig. 5.11: T cells in the untreated or irradiated TME of breast cancer BrM analyzed by TCRβ profiling. Analysis of productive frequency and clonality of TCRs in 99LN-BrM and CLN of untreated and WBRT treated mice (Control BrM n=5, WBRT BrM n=4, control CLN n=5, WBRT CLN n=5). Data is represented as mean ± SD in A and B. (A) Maximal productive frequency of clones in BrM and CLN samples of control or WBRT group (unpaired t test, ***P<0.001). (B) Productive clonality of TCRs in BrM and CLN samples (unpaired t test, **P<0.01). (C) TCR sequence and productive frequency of the top clone of each sample from untreated or WBRT treated BrM. (D) TCR sequence and productive frequency of the top clone of each sample from untreated or WBRT treated CLN.

Interestingly, all BrM samples had a high maximal productive frequency. The results imply that the most expanded T cell clone of each BrM sample accounted for approximately 10% of the whole T cell pool (Fig. 5.11 A, C). This led to a high productive clonality (>0.1), which indicates clonal expansion (Fig. 5.11 B). Maximal productive frequency and productive clonality in the BrM samples were not changed by WBRT (Fig. 5.11 A, B). However, productive clonality was significantly lower in CLN, compared to BrM irrespective of treatment (Fig. 5.11 A, B, D). This is most likely caused by the nature of CLN. As peripheral lymphoid organs, they contain a vast amount of T cell clones, leading to a high variability of the sequenced pool and a lower clonality. Therefore, productive clonality must be considered with caution, as it is dependent on number of T cells in the sample. More advanced analyses of the degree of clonal expansion in BrM will be described in the next section.

5.3.3. Detailed analysis of clonal expansion in BrM

To get detailed insight into the expansion of T cell clones in 99LN-BrM, the immune arch package for 'R' was used. First, the clonal space homeostasis of each sample was plotted. It visualizes the relative abundance of clones with a specific frequency.

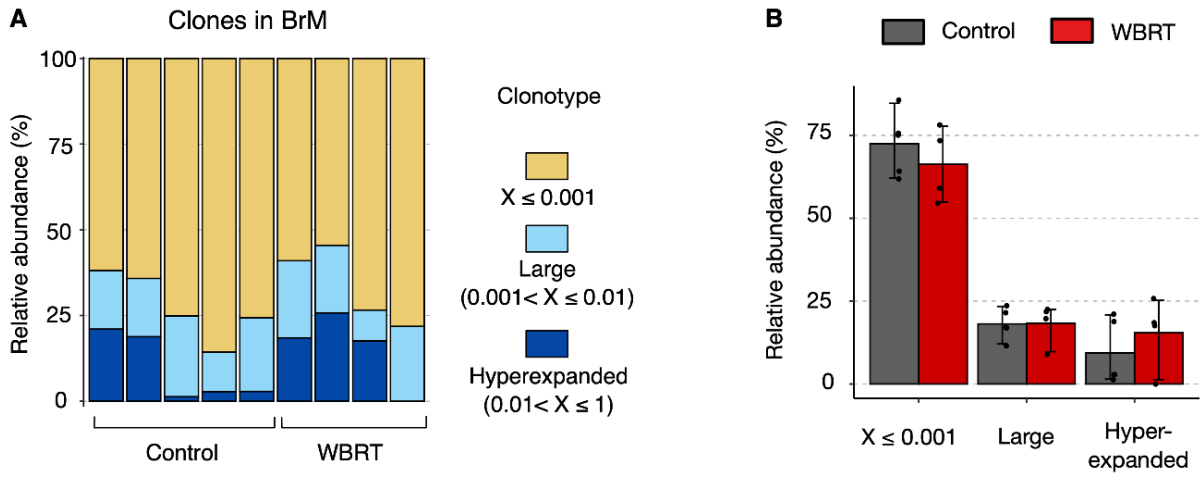

Fig. 5.12: Analysis of clonal expansion in untreated and irradiated BrM by TCRβ profiling. (A) Clonal space homeostasis of BrM samples, indicating the relative abundance of clones with a specific frequency. (B) Relative abundance of clones with a specific frequency in samples from control compared to WBRT group. Analysis was performed with R package 'immunarch' (Control BrM n=5, WBRT BrM n=4, control CLN n=5, WBRT CLN n=5). Data is represented as mean ± 95% CI in B and C.

Indeed, hyperexpanded clones were identified in 8 of 9 samples. In some samples these clones accounted for nearly 25% of the entire T cell pool. Large clones were identified in every BrM sample with varying proportions, up to approximately 40% of the T cell pool (Fig. 5.12 A). These proportions were not significantly different between control and WBRT samples (Fig. 5.12 B).

To analyze the different samples independently of changes in number of sequenced TCR, Lorenz curves were generated (ineq version 0.2.13). These curves allow to visualize the degree of deviation for a certain characteristic (in this case clone size) from perfect equality (line in Fig. 5.13 A, B). To quantify the deviation of the generated curves from the line of perfect equality, Gini indices of each sample were calculated. The Gini index is the ratio of the area between the line of equality and the generated Lorenz curve, over the total area under the line of equality. It ranges from 0 to 1, with 0 representing a perfectly equal distribution (no clonal expansion) and values above 0 indicating skewing of the TCR repertoire and, therefore, clonal expansion.

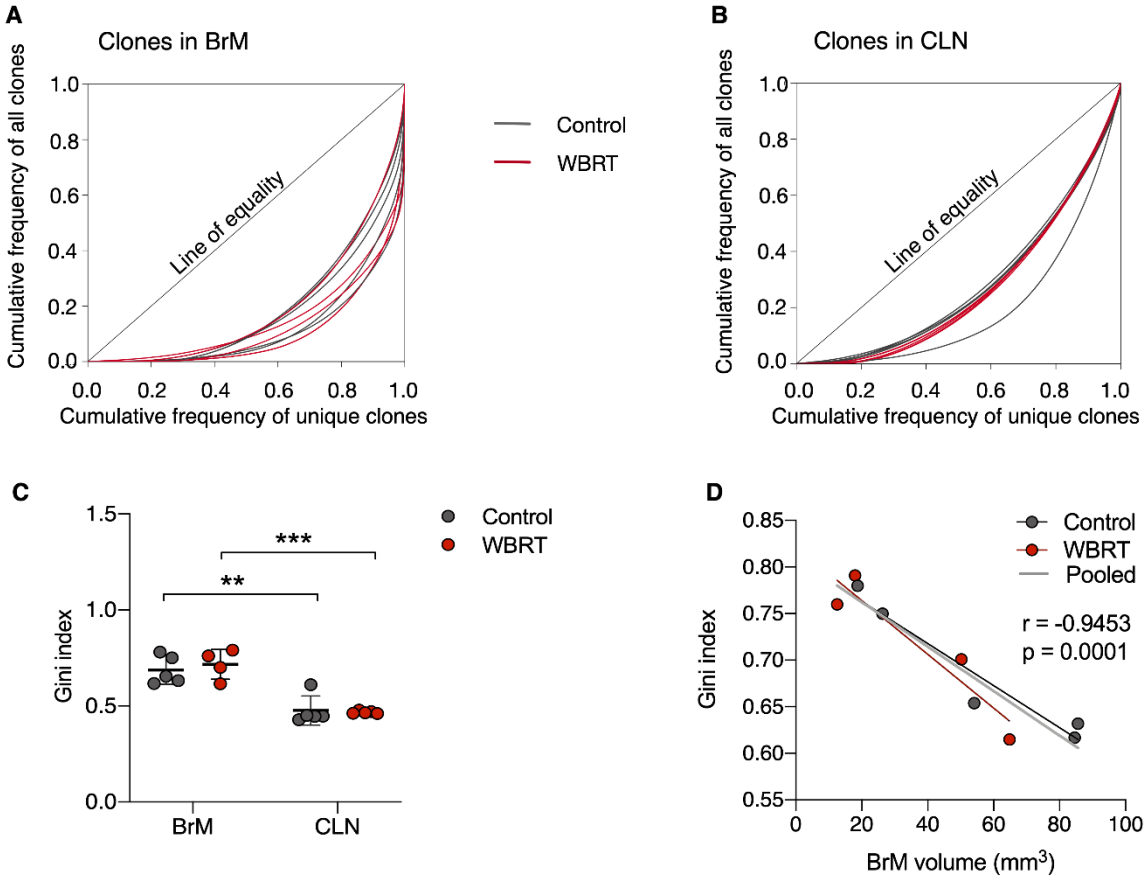

Fig. 5.13: Analysis of clonal expansion in untreated and irradiated BrM by generation of Lorenz curves. (A) Lorenz curves generated with the reads of all clones per BrM sample to visualize deviation from perfect equality. (B) Lorenz curves generated with the reads of all clones per CLN. (C) Lorenz curves were used to determine the Gini index of each sample, which is a measure of inequality reflecting clonal expansion. **P<0.01, ***P<0.001. Data is represented as mean ± SD (D) Gini indices of BrM samples correlated to BrM volume (Pearson correlation coefficient r=-0.9453, p=0.0001).

These analyses confirmed a strong skewing of the TCR repertoire, suggesting a strong clonal expansion in the BrM samples (Fig. 5.13 A, C) Intriguingly, the curves generated of sequences from the CLN samples considerably deviated from the line of equality, indicating that clonal expansion took place in the sentinel lymph nodes of the brain, as well (Fig. 5.13 B, C). This expansion was not as profound, as was the case for the BrM samples, indicated by the smaller Gini index. Again, there was no difference between control and WBRT group (Fig. 5.13 C). Moreover, a significantly negative correlation of the Gini indices from BrM samples with BrM volume was observed, implying a negative correlation of T cell expansion in the TME with tumor volume (Fig. 5.13 D).

The next question after confirming that T cells expanded in the TME of BrM, was to which extend expanded T cell clones were shared between individual mice, and if the number of shared clones changed in response to WBRT. Therefore, the top 100 most expanded clones were compared and visualized via Venn-diagrams, between the mice of each group. Interestingly, neither in the control group nor in the WBRT group a substantial overlap of TCR

clones was observed (Fig. 5.14 A, B). This leads to the conclusion that each mouse has an individual TCR repertoire directed against 99LN-BrM.

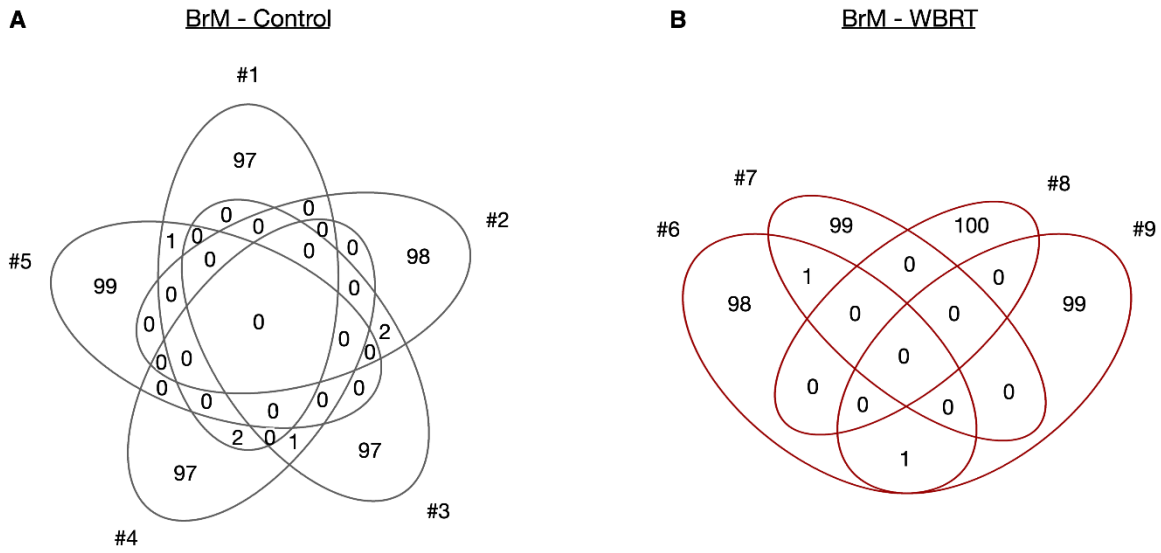

Fig. 5.14: Overlap of the Top 100 clones in BrM of untreated and WBRT treated mice. (A) Venn diagram representing shared TCR clones of BrM from untreated mice based on amino acid sequence. (B) Venn diagram representing shared TCR clones of BrM from WBRT treated mice. Analysis was performed with R Studio (Control n=5, WBRT n=4).

In conclusion, T cells in the TME of breast cancer BrM were identified and clonally expanded, indicating a preceding T cell activation. This implies that T cells are not coincidental bystanders in the TME but expanded in response to tumor antigens. Importantly, WBRT did not lead to diminished expansion of T cell clones in BrM or CLN. Furthermore, a negative correlation of T cell expansion with BrM volume has been revealed, indicating the continuous suppression of T cells and therefore adaptive immunity during BrM progression. This suppression of T cell activation and expansion might be reversed via inhibiting PD-1 and, consequently, may lead to a more effective adaptive immune response against the BrM cells.

5.4. Experimental depletion of T cells in murine BrM

After confirming the presence and expansion of T cells in the TME of 99LN-BrM, the functional impact of T cells on tumor onset and progression was analyzed. T cells were depleted in the 99LN-BrM model via neutralizing αCD4 and αCD8 antibodies. These were delivered i.p., initially on 3 consecutive days, 1 week after intracardiac injection of 99LN-BrM cells, followed by injections once a week. As a start of the treatment day 7 was chosen to ensure that tumor cells already extravasated into the brain parenchyma. Tumor growth was monitored via MRI weekly. T cell frequencies in peripheral blood were monitored via flow cytometry at the time points, indicated in the treatment scheme (Fig. 5.15 A).

5.4.1. Confirmation of T cell depletion by neutralizing antibodies

In order to confirm T cell depletion, 1-2 drops of peripheral blood were drawn from mice of the isotype and αCD4+αCD8 group. After sample processing, the frequencies of total T cells (CD45+ CD3+), CD4+ T cells (CD45+ CD3+ CD4+) and CD8+ T cells (CD45+ CD3+ CD8+) were quantified via flow cytometry (gating scheme: section 4.2.10, Fig. 4.1 C).

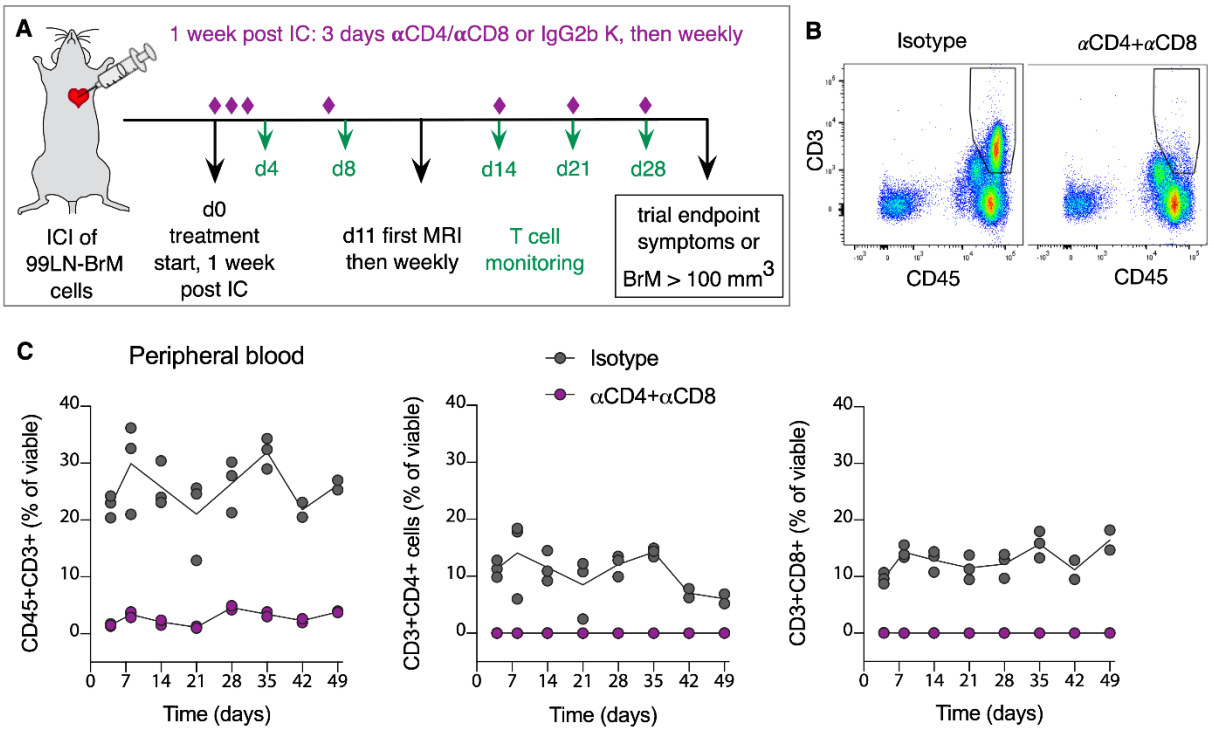

Fig. 5.15: Systemic T cell depletion via neutralizing antibodies in 99LN-BrM. (A) Experimental design of T cell depletion via treatment with neutralizing αCD4 and αCD8a antibodies. $1x10^5$ 99LN-BrM cells were injected intracardially. 7d later antibodies were applied i.p. at three consecutive days, followed by weekly injections (n=19 for isotype and n=19 for αCD4+αCD8). Tumor growth was monitored via MRI weekly, starting on day 25 after treatment initiation. T cell depletion was monitored via flow cytometry at the indicated time points. (B) Representative flow cytometry blots of blood samples from mice of depletion and control group 3 weeks after treatment start, showing successful depletion of CD45+ CD3+ T cells in the αCD4+αCD8 depletion treatment group. (C) Quantification of total CD45+ CD3+ T cells, CD45+ CD3+ CD4+ and CD45+ CD3+ CD8+ T cells in peripheral blood over 7 weeks via flow cytometry.

Representative flow cytometry blots of both groups at week 3, as well as weekly quantifications demonstrate successful systemic depletion of most T cells (Fig. 5.15 B, C) and complete depletion of CD4+ and CD8+ T cells (Fig. 5.15 C). Depletion was apparent already after the initial 3 injections and remained stable in later treatment stages, when neutralizing antibodies were only injected once per week (Fig. 5.15 C).

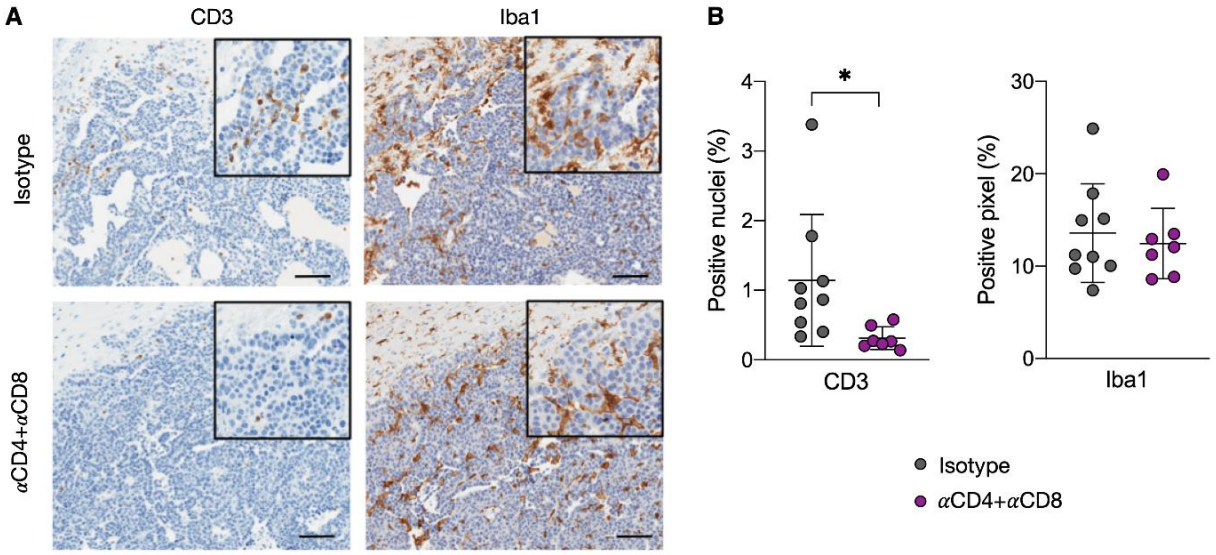

Fig. 5.16: T cell depletion via neutralizing antibodies in 99LN-BrM lesions. (A) Representative images of IHC against CD3+ and Iba1+ cells in 99LN-BrM of the isotype and αCD4+αCD8 groups (Scale bars=100 µm, magnification insert = 1.5x). (B) IHC quantification of CD3+ and Iba1+ cells in paraffin sections of 99LN-BrM at trial endpoint (isotype n=9, αCD4+αCD8 n=7, unpaired t-test, *P<0.05). Data is represented as mean ± SD.

Moreover, the immunohistochemical analysis of the BrM sections at the endpoint of the trial, confirmed T cell depletion (CD3+ cells) in the brain, whereas the number of Iba1+ macrophages (MDM/microglia) remained unaffected (Fig. 5.16. A, B)

5.4.2. Impact of T cell depletion on BrM onset and progression

To evaluate the impact of αCD4/αCD8 mediated T cell depletion on BrM onset and progression, monitoring of the tumor growth started already at d11 and continued weekly. The evaluation of first BrM detection by MRI, revealed no change in time till BrM onset in both groups (Fig. 5.17 A). The weekly analysis of tumor volumes from MRI data via ITK Snap, revealed that tumors grew rapidly in both groups. There was no significant difference in tumor volume over time between the groups (Fig. 5.17 B-D).

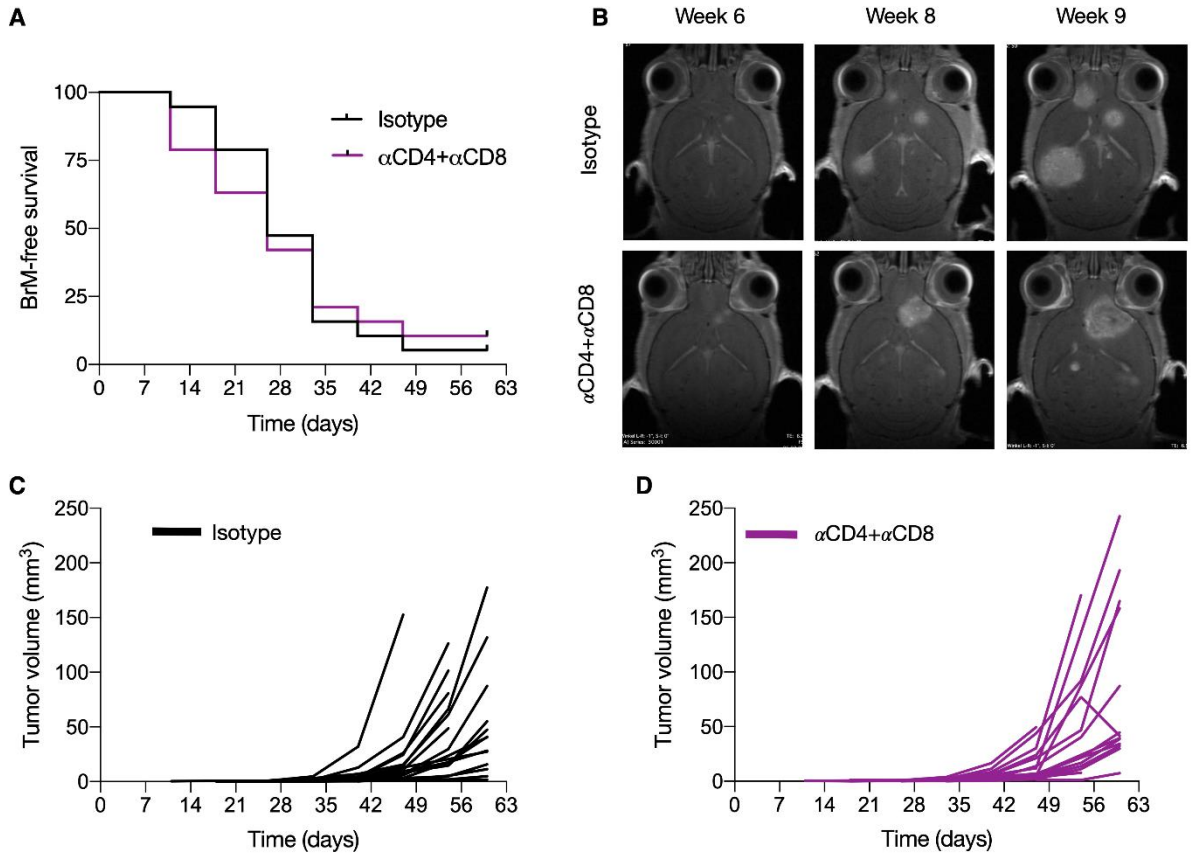

Fig. 5.17: The effect of T cell depletion on tumor growth and onset in 99LN-BrM. (A) Kaplan Meier curves depict BrM free survival of mice in the isotype and αCD4+αCD8 group. (B) Representative MRI pictures of 99LN-BrM at week 6, 8 and 9 after treatment with either isotype or αCD4 and αCD8 antibodies (C) Tumor growth curves depicting the absolute BrM volume for each mouse in the isotype group over time. (D) Tumor growth curves depicting the absolute BrM volume for each mouse in the αCD4+αCD8 group. (n=19 for isotype and n=19 for αCD4+αCD8).

In conclusion, T cells in the TME of 99LN-BrM do not have an impact on BrM onset and progression. This indicates that the immune suppressive TME is strong enough to inhibit adaptive immunity and T cell function. Together with the results of TCRβ profiling, this implies that 99LN directed T cells are activated and expand initially, but are suppressed rapidly in the 99LN-BrM TME, before being able to elicit anti-tumor functions.

5.5. Expression of PD-1 and PD-L1 in TS1-BrM and 99LN-BrM

It has been reported that T cells in the TME of BrM are exhausted, and regularly express components of the T cell inhibitory PD-1/PD-L1 axis (Harter *et al*, 2015). After concluding that T cells are suppressed and unable to elicit anti-tumor functions in the TME of 99LN-BrM, it was important to find out, if and to which extent, as well as by which cell types, PD-1 and PD-L1 are expressed in 99LN-BrM. Therefore, PD-1 and PD-L1 expression was analyzed *in vitro* in different cell lines with brain tropism, as well as *in vivo* in the 99LN-BrM model.

5.5.1. Expression of PD-1 and PD-L1 *in vitro*

For *in vitro* analysis of PD-1 and PD-L1 expression by the brain-homing breast cancer cell lines 99LN-BrM and TS1-BrM, qRT-PCR as well as flow cytometry was performed. qRT-PCR was used to reveal the RNA-expression levels of PD-1 and PD-L1 by the tumor cells. Flow cytometry was performed to reveal the proportion of tumor cells positive for PD-L1 protein. Additionally, the impact of 10 Gy IR on PD-1 and PD-L1 expression by the two BrM cell lines was analyzed *in vitro* by qRT-PCR.

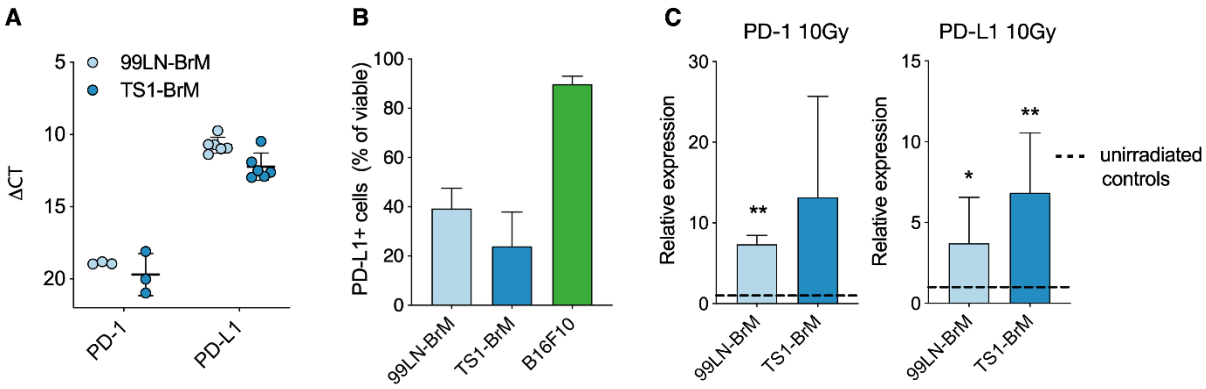

Fig. 5.18: Expression of PD-1 and PD-L1 by breast cancer BrM cells. (A) Expression of PD-1 and PD-L1 by the BrM cell lines 99LN-BrM and TS1-BrM quantified by qRT-PCR. (B) Frequency of 99LN-BrM and TS1-BrM cells positive for PD-L1 measured by flow cytometry. The melanoma cell line B16-F10 was used as positive control (n=3). (C) Expression of PD-1 and PD-L1 by 99LN-BrM and TS1-BrM cells in response to irradiation with 10 Gy, quantified by qRT-PCR and normalized on expression of unirradiated controls (dashed line) (n=3 for PD-1, n=6 for PD-L1, paired t test, *P<0.05, **P<0.01). Data is represented as mean ± SD.

qRT-PCR results showed high PD-L1 expression levels, with delta CT values between 10 and 15 in both breast cancer derived BrM cell lines. In contrast, PD-1 expression levels were low (Fig. 5.18 A). Flow cytometry revealed that approximately 40% of the 99LN-BrM cells and 20% of TS1-BrM cells were positive for PD-L1 *in vitro*. Up to 90% of the B16-F10 melanoma cells, used as positive control, carried PD-L1 on the cell surface (Fig. 5.18 B). Additionally, the influence of IR on the expression levels of PD-1 and PD-L1 was examined. 99LN-BrM and TS1-BrM cells were irradiated *in vitro* with 10 Gy, and expression levels analyzed 48h later via

qRT-PCR. This experiment revealed increased expression of PD-1 and PD-L1 at RNA level by both breast cancer BrM cell lines in response to IR (Fig. 5.18 C).

In summary, the abundance of PD-1 and PD-L1 in 99LN-BrM and TS1-BrM was confirmed on RNA as well as protein level. In response to IR, expression levels of receptor and ligand were even further amplified.

5.5.2. Expression of PD-1 and PD-L1 *in vivo*

In order to confirm the presence of the checkpoint proteins PD-1 and PD-L1 in murine breast cancer derived BrM *in vivo*, paraffin sections of experimental 99LN-BrM and TS1-BrM were stained against PD-1 and PD-L1 via IHC. To elucidate which cell types are positive for PD-1 and PD-L1 a more thorough analysis of the immune microenvironment of 99LN-BrM was performed via flow cytometry.

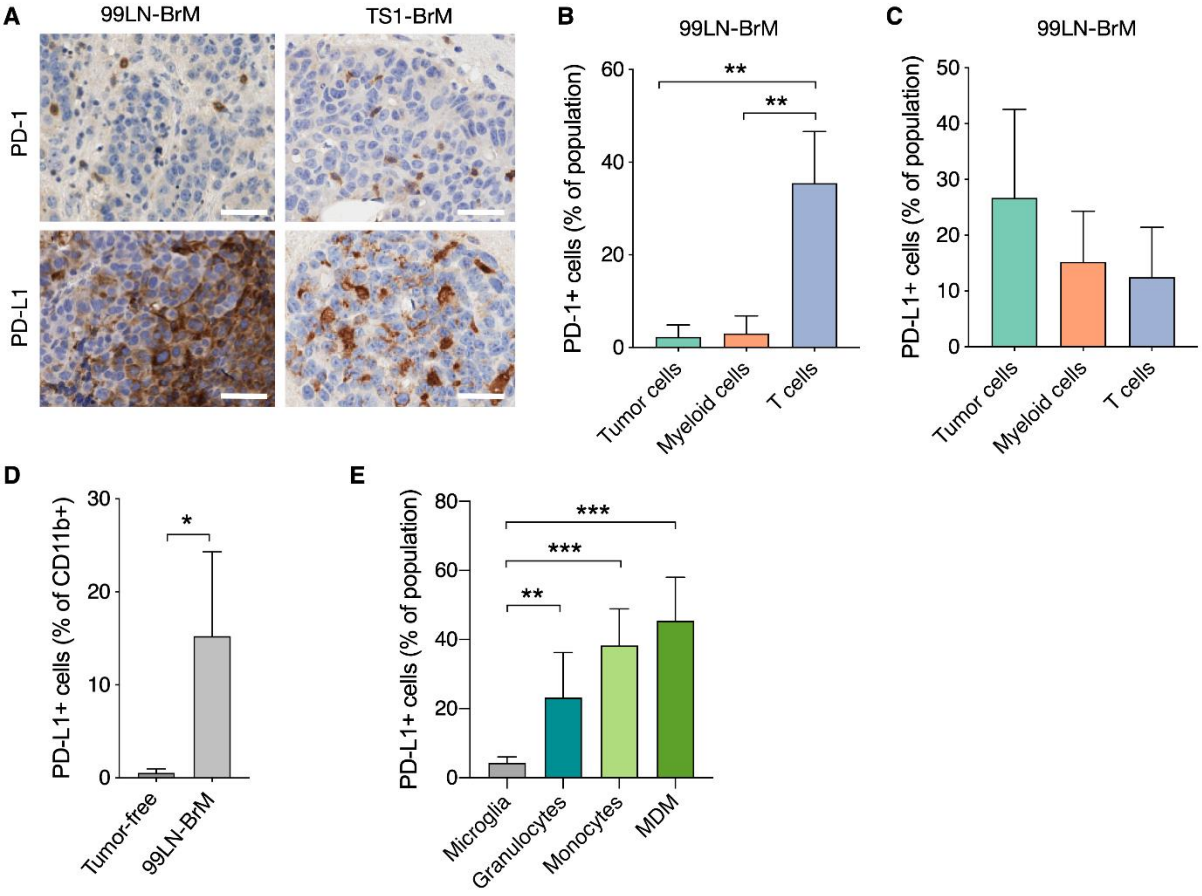

Fig. 5.19: Expression of PD-1 and PD-L1 in experimental 99LN-BrM. (A) Representative IHC images of PD-1 and PD-L1 positive cells in 99LN-BrM and TS1-BrM (Scale bars=50 µm). (B) Proportions of cells in the TME of 99LN-BrM positive for PD-1, quantified by flow cytometry (n=3, unpaired t test, **P<0.01). (C) Proportions of PD-L1 positive cells in 99LN-BrM quantified by flow cytometry (n=3). (D) Flow cytometric analysis of myeloid cells positive for PD-L1 in tumor-free brain and 99LN-BrM (n=3, unpaired t test, *P<0.05). (E) Detailed flow cytometric analysis of frequencies of PD-L1 positive cells in 99LN-BrM associated myeloid cell populations. (n=6, unpaired t test, **P<0.01, ***P<0.001). Data is represented as mean ± SD.

IHC analyses confirmed the presence of PD-1 and PD-L1 in the TME of 99LN-BrM *in vivo*. Cells positive for PD-1 resembled lymphocyte morphology, with small, round cell bodies, and were localized within the tumor stroma. PD-L1 expression was mostly associated with the tumor core (Fig. 5.19 A). Data from flow cytometry analysis confirmed the observation from IHC, that PD-1 was predominantly expressed by T cells. Indeed, up to 40% of T cells were positive for PD-1, indicating a high proportion of exhausted cells. Tumor cells or myeloid cells did not express PD-1 in considerable quantities (Fig. 5.19 B). PD-L1, which can induce T cell exhaustion upon binding to PD-1, was expressed not only by tumor cells, but also by immune cells, such as myeloid and T cells. Approximately 15% of myeloid cells were PD-L1 positive (Fig. 5.19 C). Intriguingly, comparison of PD-L1 expression in the brain of mice bearing 99LN-BrM and of tumor-free mice, revealed that only in the presence of BrM, PD-L1+ myeloid cells can be detected (Fig. 5.19 D). This raised the question, of whether brain resident microglia are educated to express PD-L1 in the BrM TME, or whether PD-L1+ blood borne myeloid cells are recruited to the BrM lesions. To address this, a flow cytometry panel was applied which allows the quantification of PD-L1+ myeloid subpopulations (section 4.2.10, Fig.4.1 A). This approach demonstrated that in the presence of 99LN-BrM, microglia barely expressed PD-L1, whereas a high proportion of blood borne myeloid populations recruited to BrM, such as MDM, inflammatory monocytes and granulocytes was PD-L1 positive (Fig. 5.19 E).

Collectively, it has been shown that PD-1 and PD-L1 are not only expressed *in vitro* by breast cancer BrM cells, but also *in vivo* in the TME of 99LN-BrM. PD-1 is predominantly expressed by T cells, whereas PD-L1 is expressed by tumor cells and immune cells, such as tumor-associated blood borne myeloid cells, which in general do not reside in the brain parenchyma.

5.6. Efficacy of checkpoint inhibition and WBRT in murine breast cancer BrM

It has been demonstrated so far that immune cells, critical for checkpoint inhibition, are present in murine breast cancer BrM. Moreover, T cells in the TME expanded, indicating a preceding T cell activation. With increasing BrM volume T cell expansion was suppressed. Additionally, a high proportion of T cells in 99LN-BrM expressed PD-1, indicating a state of exhaustion which can be targeted via checkpoint blockade with anti-PD-1 (αPD-1), in order to reactivate T cells. Radiotherapy is one of the most important standard of care treatments for BrM patients and bears the potential to sensitize tumors to checkpoint inhibition. It has been shown in this thesis that WBRT indeed increased the relative number of cytotoxic CD8+ T cells critical for checkpoint inhibition.

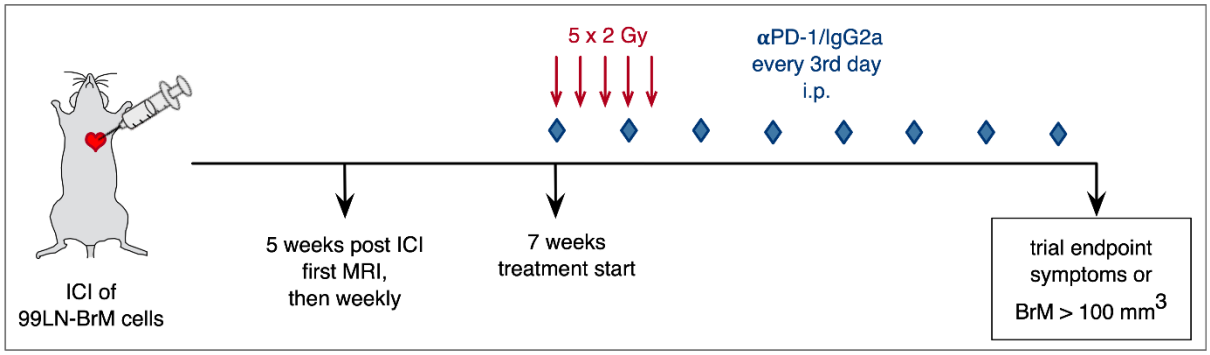

Fig. 5.20: Preclinical trial of combination therapy with WBRT and αPD-1 in 99LN-BrM. Treatment scheme and timeline of the combination trial. $6x10^4$ 99LN-BrM cells were injected intracardially. Starting with 5 weeks post injection, mice were monitored weekly via MRI. 7 weeks post injection, WBRT was applied on 5 consecutive days (5x2 Gy). On the first day of WBRT, 250 µg of αPD-1 or isotype control (IgG2a) were injected i.p.. These injections were continued every third day until trial endpoint. (n=8 for isotype, n=7 for WBRT, n=8 for αPD-1, n=9 for WBRT+αPD-1 group).

To evaluate the potential of checkpoint inhibition, applied as mono- or combination therapy, to reactivate T cells and induce anti-tumor efficacy, a preclinical trial was performed in the 99LN-BrM model (Fig. 5.20). Mice with established BrM (7 weeks post ICI) were treated with fractionated WBRT on 5 consecutive days (5x2 Gy) as described previously (section 5.2). Starting with the first dose of WBRT, αPD-1 or isotype (IgG2a) antibodies were injected i.p. every third day till trial endpoint. BrM progression was monitored weekly via MRI to quantify relative tumor growth in the different groups. Survival curves were generated, and the brains of the respective mice stored for histological assessment.

5.6.1. Effects of radio immunotherapy on BrM growth and survival

To evaluate the efficacy of the different treatment regimens, tumor volumes were measured via ITK snap based on MRI pictures. Percent tumor growth in comparison to treatment start was calculated weekly. To reveal short term effects, d14 and d28 were analyzed in detail. For

the generation of survival curves, days to the development of BrM-related symptoms or reaching a BrM volume >100 mm^3 were plotted. When mice had to be sacrificed due to BrM unrelated events, data points were censored.

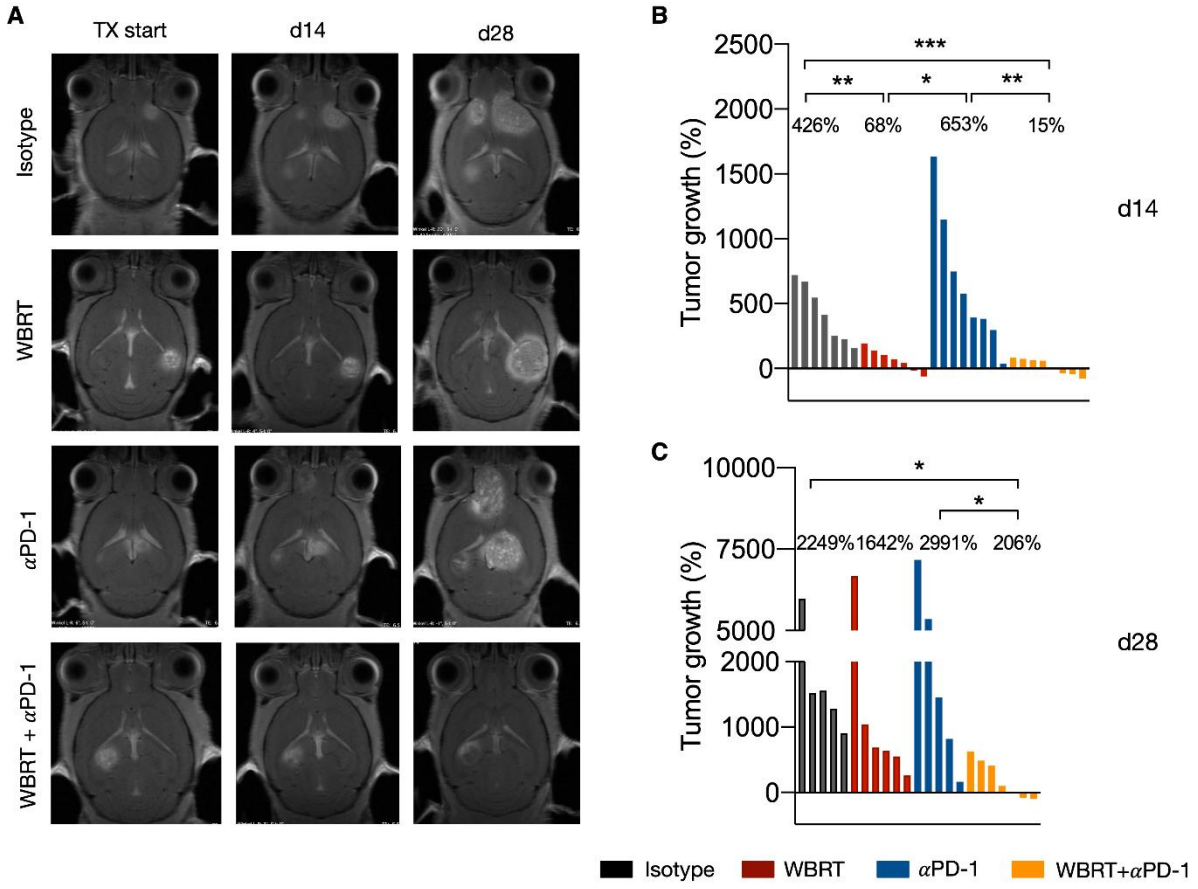

Fig. 5.21: Relative tumor growth on d14 and d28 of WBRT and αPD-1 group in 99LN-BrM. (A) Representative T1-weighted MRI images of 99LN-BrM from mice in all four treatment groups, at treatment start, d14 and d28 after treatment start. (B) Relative tumor growth of the individual mice in each treatment group on d14. (C) Relative tumor growth (%) of the individual mice in each treatment group on d28.

Analysis of tumor growth at d14 and d28 revealed that αPD-1 monotherapy did not lead to reduced BrM growth, compared to the isotype treated group at early time points. Monotherapy with WBRT led to a pronounced reduction of tumor growth at d14 after treatment start. This effect was lost on d28 and WBRT treated BrM grew comparable to control BrM again. The combination of WBRT with αPD-1 on the other hand decreased tumor growth significantly on d14 and d28 (Fig. 5.21 A-C).

To evaluate the influence of radio immunotherapy with WBRT and αPD-1 over a longer time period, the relative tumor growth of each individual mouse was plotted till week 8 after treatment start (Fig. 5.22 A).

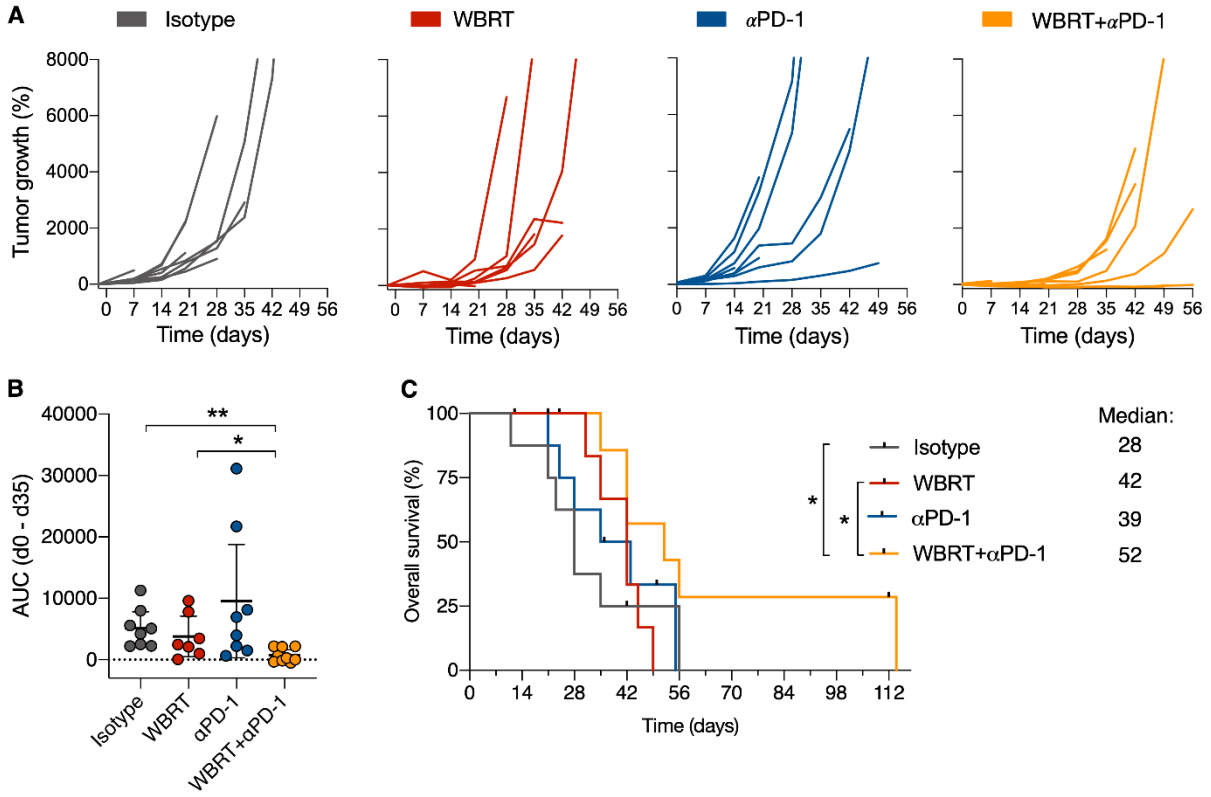

Fig. 5.22: Tumor growth and survival of WBRT and αPD-1 treated 99LN-BrM. (A) Tumor growth curves of individual mice grouped by the four treatments. (B) Quantification of relative tumor growth from d0 to d35. The area under the curve (AUC) for individual mice was plotted and normalized to the survival time in weeks (unpaired t test, *P<0.05, **P<0.01, data is represented as mean ± 95% CI.). (C) Kaplan-Meier curves depict the overall survival in the four treatments group (Log rank test, *P<0.05).

The generated growth curves show that BrM, treated with αPD-1 monotherapy, did not delay tumor outgrowth, compared to isotype treated BrM. WBRT monotherapy put a halt on tumor growth till d14, as described before. Only the combined treatment of WBRT and αPD-1 suppressed BrM growth till approximately d35. After this timepoint, tumors started to grow exponentially in the combination group, as well (Fig. 5.22 A). To quantify the difference in tumor growth until this time point, the area under the curve (AUC) was determined and normalized to the survival time in weeks. This analysis demonstrated a significant suppression of tumor growth in the combination group versus WBRT or isotype group, also over a longer time period (Fig. 5.22. B). The suppression of tumor growth in the combination group also translated into prolonged overall survival of mice. Kaplan-Meier curves show that WBRT and αPD-1 monotherapy did not prolong survival significantly, although the median survival was increased from 28 days in the isotype group to 42 and 39 days in the WBRT and αPD-1 group, respectively. Only the combined treatment significantly prolonged overall survival (median survival of 52 days) compared to isotype as well as WBRT group (Fig. 5.22 C).

In conclusion, WBRT and checkpoint inhibition via αPD-1 demonstrated synergistic efficacy, which led to tumor stasis and significantly increased survival. However, eventually, lesions relapsed, and all mice succumbed to the disease, also in the combination group.

5.6.2. Analysis of responders and non-responders to checkpoint inhibition

It has been reported that checkpoint inhibition can demonstrate impressive anti-tumor activity, however, many patients do not respond to this therapy (Sevenich, 2019). To gain more insight into response rates, BrM were categorized into groups, depending on the extend of response based on relative tumor growth (Fig. 5.23 A) (criteria published by Aslan *et al*, 2020).

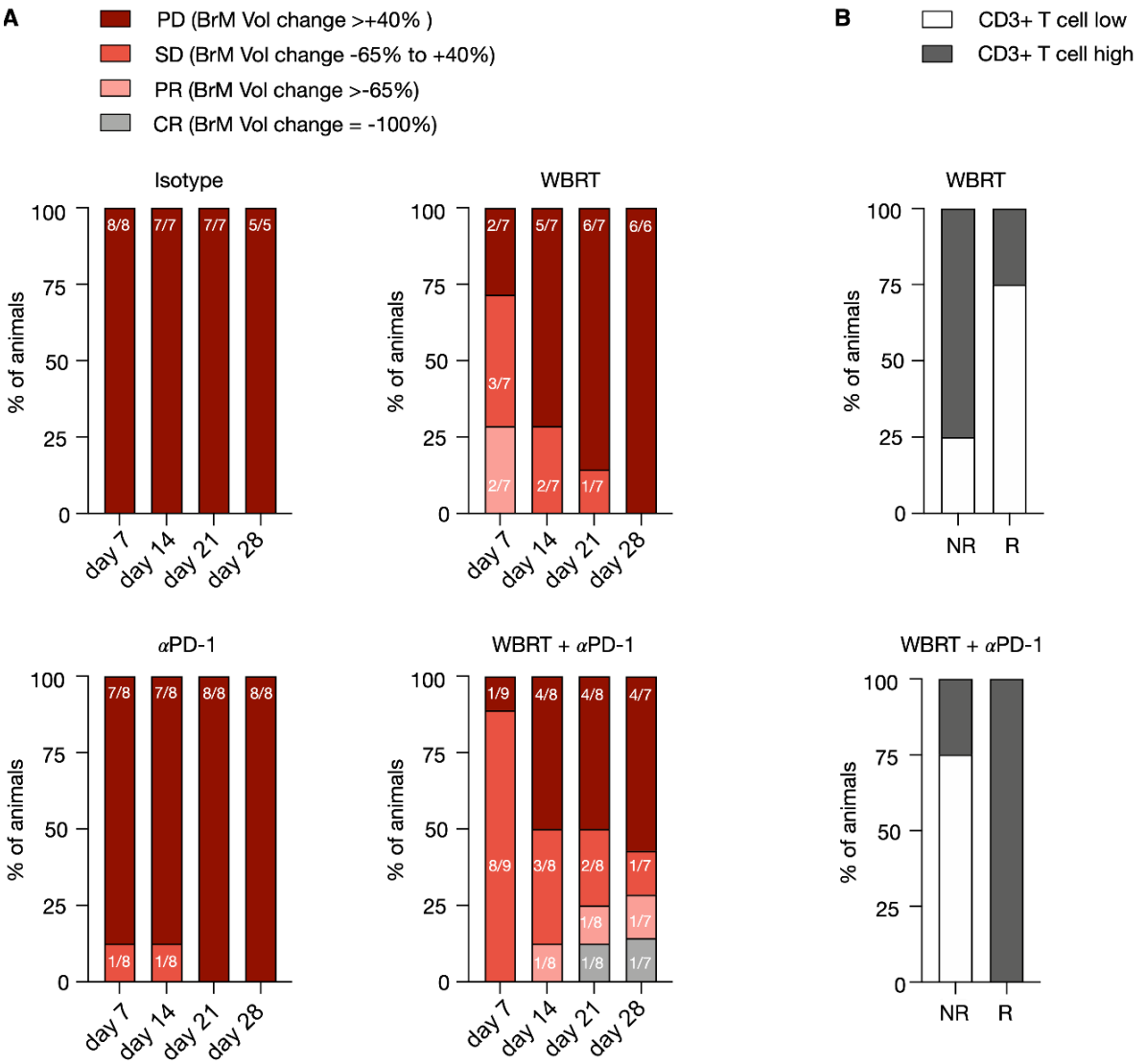

Fig. 5.23: Responders and non-responder to WBRT and αPD-1 treatment of 99LN-BrM. (A) Percentage of mice in the four treatment groups showing progressive disease (PD), stable disease (SD), partial response (PR) and complete response (CR) at different time points in relation to d0. (B) Percentage of responding (SD, PR, CR) or non-responding (PD) mice with high T cell infiltration (>1.6 % of total cells) of 99LN-BrM lesions, plotted for WBRT and WBRT+αPD-1 group. T cell infiltration was determined by quantifying IHC CD3-stainings of BrM sections via Aperio ImageScope.

This stratification revealed that all mice in the isotype group showed PD at the four time points. In the αPD-1 group 12,5% of mice showed SD at d7 and d14. At later time points all mice showed PD, too. In the beginning WBRT demonstrated good responses with only 29% of mice

showing PD at d7 and 42% and 29% showing SD and PR, respectively. However, the percentage of mice with PD in this group increased quickly over time, till on d28 all mice showed PD. The combined treatment of WBRT and αPD-1, on the other hand, showed only 11% of PD on d7 with 89% of mice in this group showing SD. While the percentage of mice with PD increased in the combination group over time as well, it was not as rapid as seen for the WBRT group, so that only 50% of mice showed PD on d28. Moreover, percentage of CR and PR rose steadily from d14 on (Fig. 5.23 A). This indicates the presence of responders and non-responders even in this, rather homogeneous, mouse model.

More detailed analysis of responders and non-responders via IHC revealed high T cell infiltration in BrM of responding mice in the combination group, whereas BrM of non-responders showed low T cell infiltration. This correlation could not be observed in the WBRT group (Fig. 5.23 B).

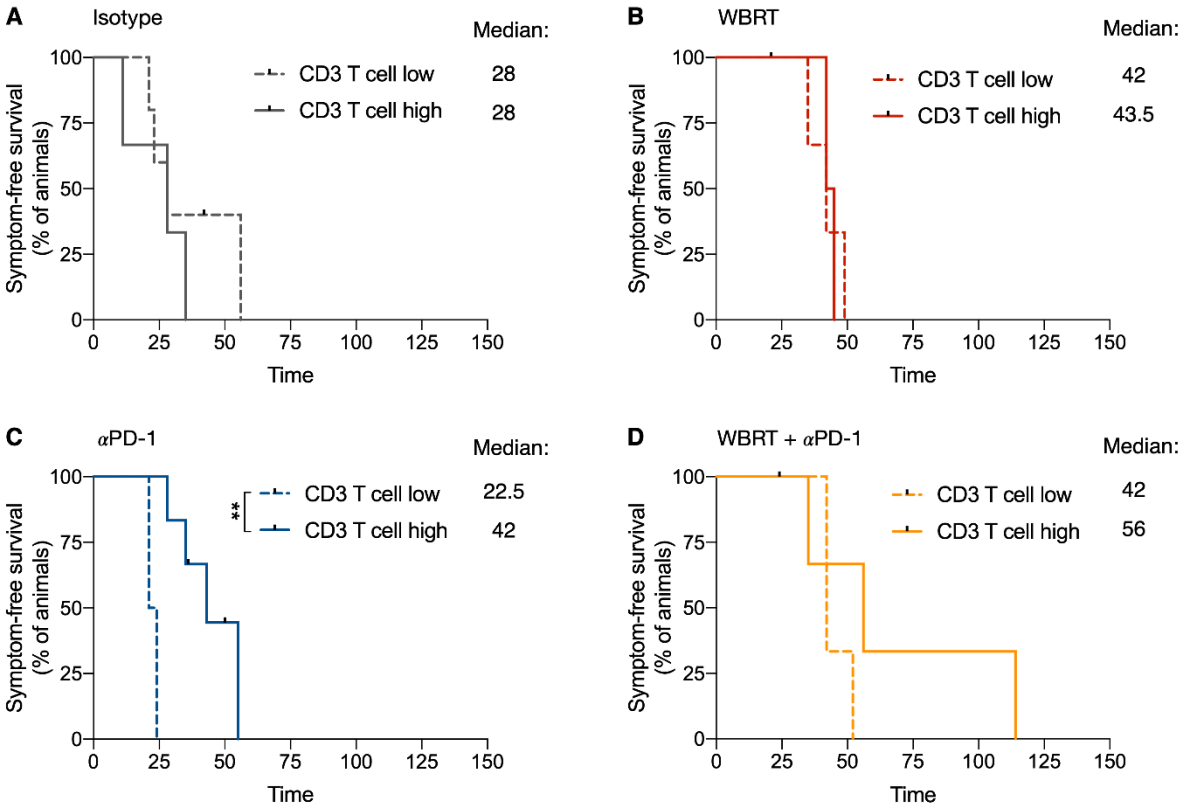

Fig. 5.24: T cell infiltration and survival in WBRT and αPD-1 treated 99LN-BrM. (A) Percentage of symptom-free survival of mice bearing tumors with low or high T cell infiltration in the isotype group. (B) Survival of mice with low and high T cell infiltration after WBRT. (C) Survival of αPD-1 treated mice with low or high T cell infiltration (Log rank test, **P<0.01). (D) Survival of combination treated mice with low or high T cell infiltration. T cell infiltration was determined via IHC staining against CD3. Three BrM lesions (1 in WBRT and 2 in WBRT+αPD-1 group) could not be included in the IHC analysis due to the small lesion size at the endpoint or technical reasons (n=8 for isotype, n=6 for WBRT, n=8 for αPD-1, n=7 for WBRT+αPD-1 group).

The differential infiltration of T cells also affected survival of mice in the αPD-1 monotherapy as well as combination group. In both groups, mice bearing BrM with high T cell content

showed prolonged median survival compared to mice with low T cell infiltration into BrM (Fig. 5.24 C, D). This trend was not apparent in the WBRT monotherapy or in the isotype group (Fig. 5.24 A, B).

In summary, WBRT shows initial tumor activity, but tumors regrow quickly in the 99LN-BrM model. αPD-1 monotherapy is not efficient to increase overall survival, but analysis of T cell content revealed anti-tumor efficacy in BrM with high T cell infiltration also in this group. In the end only the combination of αPD-1 and WBRT was sufficient to halt tumor growth for a longer time period and significantly prolong median survival. Analysis of T cell content indicates that this enhanced efficacy is associated with high T cell infiltration.

5.7. The cellular composition of the TME after radio immunotherapy

Based on the fact that αPD-1 and WBRT showed transient synergistic efficacy, it was crucial to elucidate the underlying mechanisms of the monotherapies versus combination treatment in 99LN-BrM. Moreover, insight into immune cell composition might allow the development of new strategies of immune modulation to further improve response rates and survival. Therefore, flow cytometric analysis of 99LN-BrM was performed 14 days after first dose of isotype, WBRT, αPD-1 or combination therapy. Additionally, BrM sections of mice treated with the abovementioned four regimens (section 5.6), including the sections of the survival trial, were analyzed by IHC.

5.7.1. Analysis of T cells and dendritic cells infiltrating 99LN-BrM

For flow cytometric analysis $6x10^4$ 99LN cells were injected intracardially in Bl6-wiltype mice. After detection of established lesions mice were stratified into four groups and treated as described for the survival trial before (section 5.6). 14 days after treatment start, mice were sacrificed and 99LN-BrM macrodissected. BrM samples were stained with three flow cytometry panels (section 4.2.10, Fig. 4.1) to quantify tumor associated T cell populations, DC and tumor infiltrating myeloid cells. The data obtained by application of the DC and T cell panels will be described in this section. Data obtained from the myeloid panel will be described in section 5.7.2.

Flow cytometry data revealed a mild increase in infiltrating immune cells (CD45+) induced by all treatment regimens, but most prominently after combination therapy. In this group immune cells reached 40% of total viable cells (Fig. 5.25 A). The relative abundance of DC (CD45+ CD11c+ CD83+) remained unchanged (Fig. 5.25 B). T cell infiltration (CD45+ CD3+), on the other hand, was amplified in both groups treated with αPD-1. Interestingly, the stratification into CD8+ T cells (CD45+ CD3+ CD8+) and CD4+ T cells (CD45+ CD3+ CD4+) revealed an increase of CD8+ T cell infiltration induced by WBRT, whereas CD4+ T cell infiltration was

induced by application of αPD-1. Together, WBRT and αPD-1 augmented infiltration of BrM with CD4+ and CD8+ T cells in the combination group (Fig. 5.25 C).

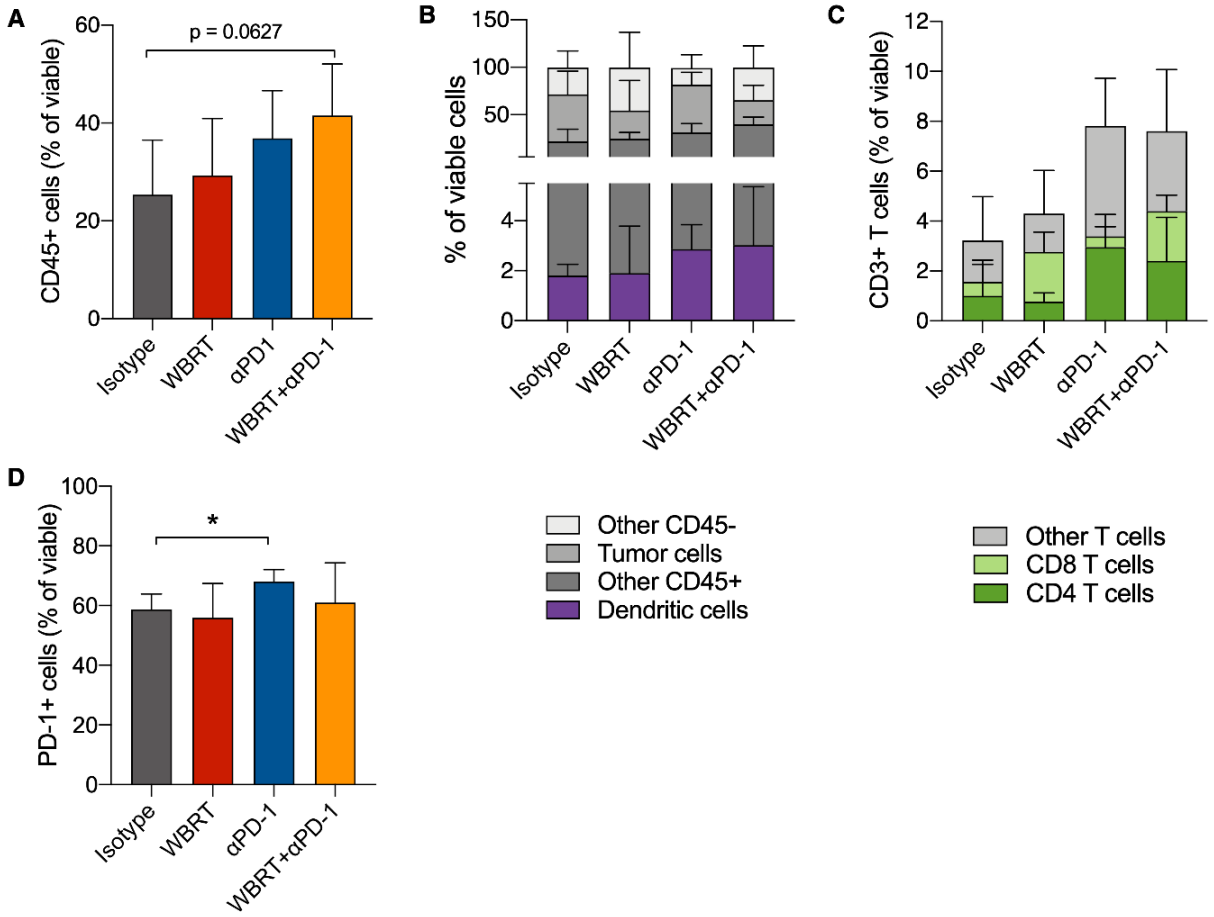

Fig. 5.25: Effects of radio-immunotherapy on T cells and dendritic cells in breast cancer derived BrM. (A) CD45+ immune cells infiltrating 99LN-BrM. The obtained values are averages from the three flow cytometry panels (n=5 for isotype, n=4 for WBRT, αPD-1 and WBRT+αPD-1 group, unpaired t test). (B) Flow cytometric analysis of DC (CD45+ CD11c+ CD83+) infiltrating 99LN-BrM (n=4 for isotype, n=3 for all other groups). (C) Flow cytometric analysis of tumor associated T cell subpopulations (isotype n=4, all other groups n=3). (D) Flow cytometric analysis of changes in PD-1 expression on T cells in response to the treatments (isotype n=4, all other groups n=3, unpaired t-test, *P<0.05). Data is represented as mean ± SD in A-D.

Based on the prior observation of high abundance of PD-1+ T cells in 99LN-BrM (section 5.5.2.), PD-1 expression by T cells was also analyzed in response to the different treatments. Intriguingly, the abundance of PD-1 positive T cells rose significantly after checkpoint inhibition applied as monotherapy. Combination with WBRT, however, prevented this (Fig. 5.25 D).

To confirm the αPD-1 induced infiltration of 99LN-BrM with T cells, paraffin sections of BrM were analyzed by IHC. Additionally, sections were stained for FoxP3, to evaluate the abundance of Treg.

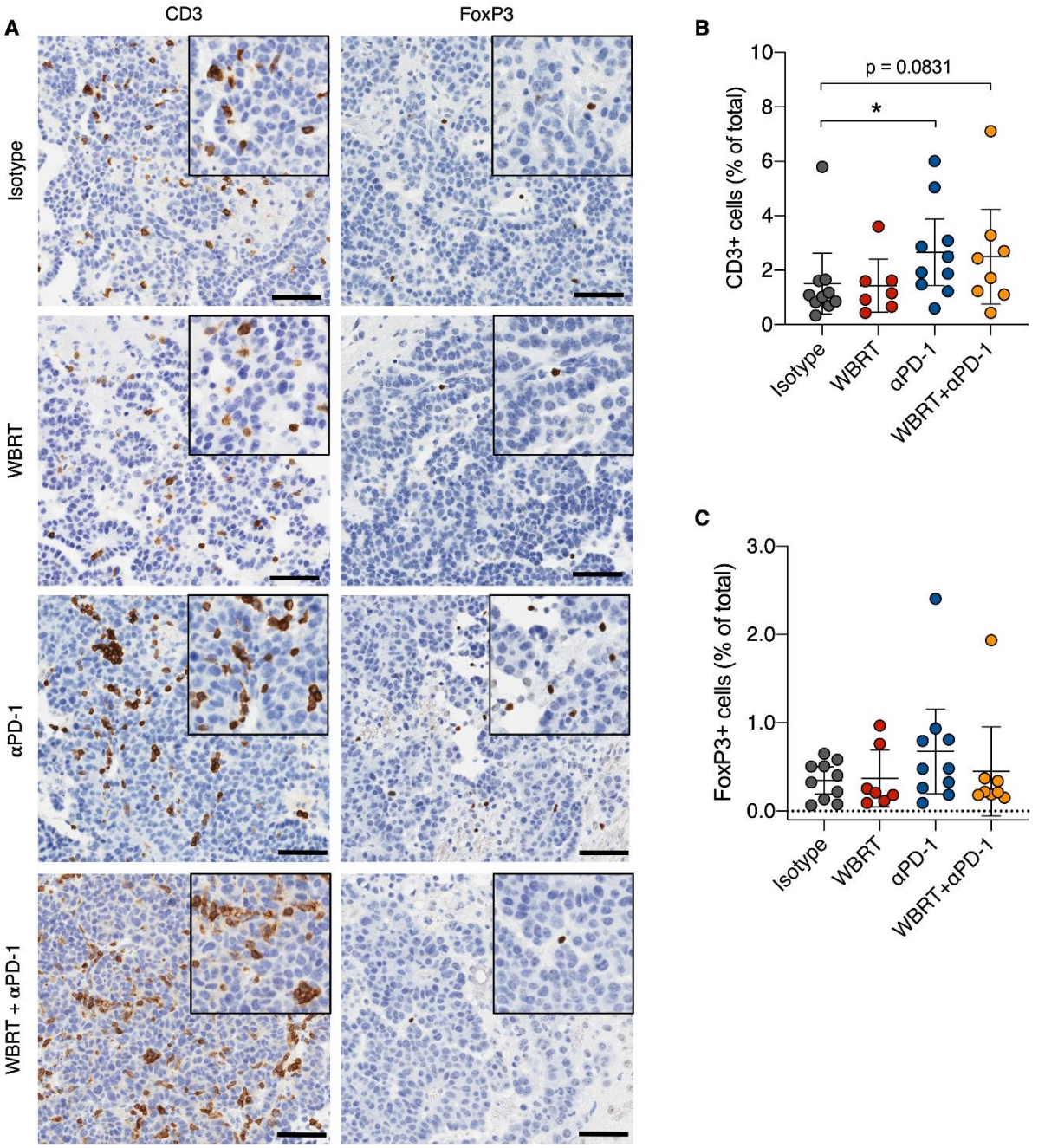

Fig. 5.26: The influence of radio-immunotherapy on T cells in breast cancer derived BrM. (A) Representative images of IHC against CD3+ and FoxP3+ cells in 99LN-BrM of the four treatment groups (Scale bars=100 µm, magnification inserts = 1.5x). (B) IHC quantification of CD3+ cells in paraffin sections of 99LN-BrM at trial endpoint (isotype n=10, WBRT n=7, αPD1 n=10, WBRT+αPD-1 n=8, unpaired t-test, *P<0.05). (C) IHC quantification of FoxP3+ cells in sections of 99LN-BrM (isotype n=10, WBRT n=7, αPD1 n=10, WBRT+αPD-1 n=8). Data is represented as mean ± 95% CI in B and C.

Indeed, the analysis of 99LN-BrM from the survival trial showed that αPD-1 in both checkpoint inhibitor treated groups increased the abundance of BrM associated T cells, up until the trial endpoint (Fig. 5.26 A, B). Quantification of FoxP3 cells revealed a mild increase in the number of Treg in the αPD-1 group. WBRT, on the other hand, resulted in slightly lower proportion of Treg, which might explain the lower Treg infiltration in the combination group (Fig. 5.26 A, C).

In conclusion, treatment with αPD-1 affected the cellular composition of the TME in 99LN-BrM. αPD-1 increased T cell infiltration 14 days after treatment start. This effect was still evident at trial endpoint. Additionally, αPD-1 led to the compensatory upregulation of PD-1 expression on T cells as well as increased recruitment of Treg. These suppressive mechanisms could be prevented by combining αPD-1 with WBRT. Nevertheless, also in the combination group most mice succumbed to BrM after initial tumor stasis.

5.7.2. Analysis of myeloid cell types infiltrating BrM

Myeloid cells can be recruited to tumors, where they elicit pro tumor and immunosuppressive functions (Pyonteck *et al*, 2013; Ahn *et al*, 2010). To elicit mechanisms that might hinder long-term efficacy of radio immunotherapy it has been investigated to which extent αPD-1 or radio-immunotherapy enhances the infiltration of 99LN-BrM with potentially pro tumorigenic myeloid cell types. To this end, flow cytometric analysis of macrodissected 99LN-BrM was performed 14 days after treatment start as described in the previous section. The panel used to define different myeloid subpopulation as well as PD-1 and PD-L1 expression is depicted in section 4.2.10 (Fig.4.1 A).

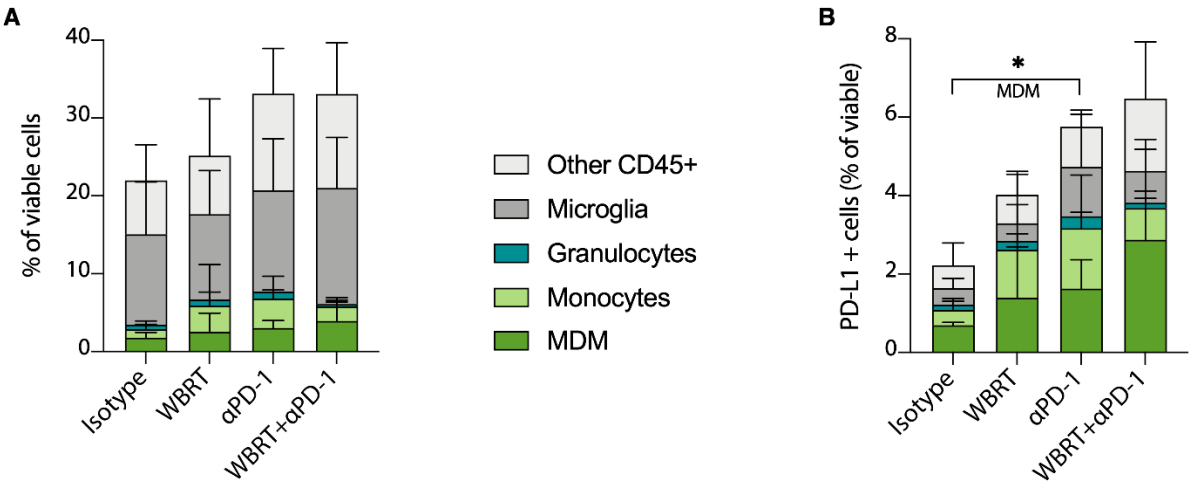

Fig. 5.27: Effects of radio-immunotherapy on T cells in breast cancer derived BrM. (A) Relative abundance of myeloid cell types infiltrating 99LN-BrM in the different treatment groups, measured by flow cytometry at d14 (Isotype n=5, other groups n=4; data is represented as mean ± SD). (B) Relative abundance of PD-L1+ myeloid cell types infiltrating BrM in the four treatment groups, quantified by flow cytometry at d14 (Isotype n=5, other groups n=4; data is represented as mean ± SD, unpaired t-test, *P<0.05 for MDM).

Analysis of the myeloid compartment in 99LN-BrM *in vivo* revealed that MDM, granulocytes and inflammatory monocytes, which are typically not present in the steady state brain parenchyma, were present in BrM of all four treatment groups. Treatment with αPD-1 or αPD-1+WBRT induced a minor increase of total (including microglia), as well as infiltrating myeloid cells (Fig. 5.27 A).

Interestingly, the abundance of total PD-L1+ myeloid cells, as well as infiltrating myeloid cells, was increased by αPD-1 in the monotherapy as well as combination therapy group (Fig. 5.27 B). As described previously (section 5.5.2), in the presence of BrM PD-L1 was mostly expressed by infiltrating myeloid cells, and not by brain resident microglia. This was also apparent in the two checkpoint inhibition groups. While microglia accounted for the highest number of myeloid cells, inflammatory monocytes and MDM represented the major populations of PD-L1+ myeloid cells in 99LN-BrM (Fig. 5.27 A, B). As for PD-L1+ myeloid infiltrating cells, αPD-1 significantly increased the proportion of PD-L1+ MDM compared to isotype (Fig. 5.27 B).

In summary, checkpoint inhibition applied as monotherapy or in combination with WBRT led to a compensatory increase of PD-L1+ myeloid cells and, most prominently, PD-L1+ MDM in 99LN-BrM. The contribution of microglia to PD-L1 expression, on the other hand, was low, in relation to their high abundance.

5.7.3. The potential of macrophages to inhibit T cell activation *in vitro*

As MDM represented the largest proportion of PD-L1+ myeloid cells after checkpoint inhibition, whereas microglia barely expressed PD-L1, the capability of BMDM and the microglia cell line EOC2 to inhibit T cells was tested in an *in vitro* assay. For the assay, T cells derived from splenocytes were artificially differentiated and activated via stimulation with anti-CD3ε and anti-CD28. 24h later, 99LN-BrM cells and unconditioned or tumor media conditioned (TuCM) BMDM or EOC2 were added to the T cells. 24h after starting the coculture, the assay was stopped and T cell activity, represented by the activation marker CD69, was measured via flow cytometry (Fig. 5.28 A) (gating strategy: section 4.2.10, Fig.4.3 A, B).

Intriguingly, this assay revealed that tumor cells, microglia or BMDM alone were not sufficient to significantly inhibit T cell activation (Fig. 5.28 B, dashed line = baseline T cell activation). EOC2 cells alone increased it even further. Only when BMDM were stimulated with TuCM or 99LN-BrM cells were directly added to BMDM and T cells, T cell activation was reduced (Fig. 5.28 B).

In a second assay (performed by Julian Anthes 2020, master student tutored during this project), T cell activation after co-culture with BMDM and 99LN-BrM in the presence or absence of αPD-1 was quantified. This analysis revealed increased activation of CD8+ T cells in the presence of αPD-1, compared to cultures not supplemented with αPD-1 (Fig. 5.28 C).

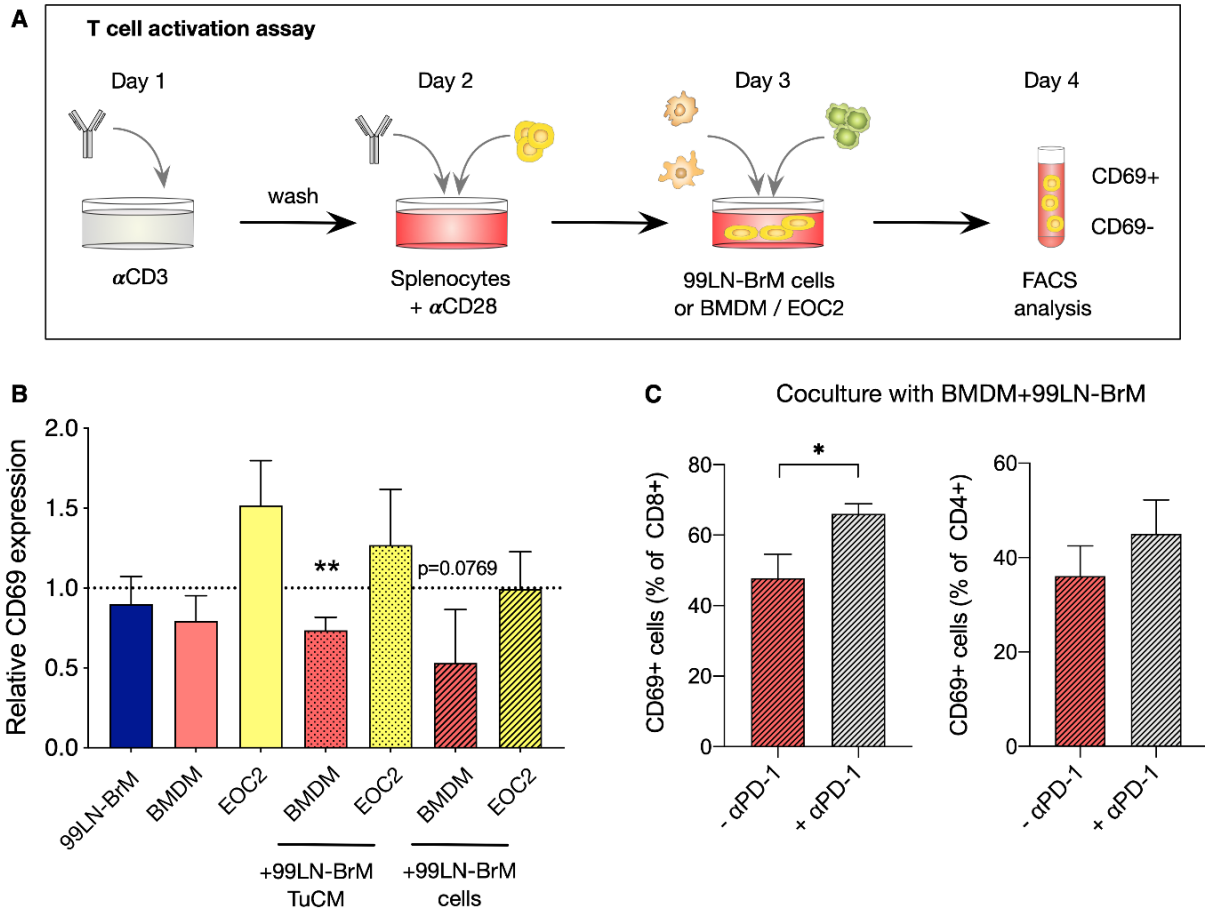

Fig. 5.28: The capacity of tumor cells, microglia and MDM to inhibit T cell activity. (A) Experimental design of the *in vitro* T cell activation assay. Splenocytes were activated and differentiated via αCD3 and αCD8 stimulation. Different cell types were cocultured with T cells to analyze their potential to inhibit T cell activity, which was quantified by flow cytometry analysis of CD69 (B) Relative CD69 expression on T cells cultivated with different cell types, unstimulated or stimulated with tumor conditioned media (TuCM) measured by flow cytometry. CD69 expression of samples to be tested, was normalized on CD69-expression of T cells without the addition of other cell types (n=3, unpaired t test, *P<0.05, data is represented as mean ± SD). (C) Relative expression of CD69 on CD4+ and CD8+ T cells, cocultured with BMDM+99LN-BrM cells in the absence and presence of αPD-1.

In summary, checkpoint inhibition with αPD-1 in breast cancer BrM led to increased recruitment of PD-L1+ myeloid cells from the periphery, especially PD-L1+ MDM *in vivo*. Moreover, in the vicinity of tumor cells or under influence of tumor secreted factors, BMDM showed a higher potential to suppress T cell activity than microglia *in vitro*. The recruitment of PD-L1+ myeloid cells to BrM might represent a compensatory immune suppressive mechanism, counteracting αPD-1 induced T cell reactivation and resulting in tumor regrowth after initial tumor stasis.

5.8. Targeting macrophages as adjuvant to radio-immunotherapy with αPD-1

Up until this point it has been demonstrated that radio immunotherapy with αPD-1 delayed tumor progression and increased survival of 99LN-BrM. The combination treatment counteracted compensatory immune suppressive mechanisms against αPD-1 treatment mediated by T cells. Nevertheless, the induction of myeloid mediated compensatory mechanisms, such as the recruitment of T cell suppressive PD-L1+ macrophages, was not prevented but even enhanced. In the end radio immunotherapy with αPD-1 was not sufficient to overcome the strong myeloid-mediated immune suppression in the TME long-term and most BrM relapsed after initial tumor stasis. To achieve long term efficacy of radio immunotherapy, different strategies to target potentially immune suppressive and tumor promoting macrophages were assessed in addition to the previously tested combination treatment. CXCR4 inhibition via AMD3100 was used to inhibit the recruitment of MDM to 99LN-BrM and a CSF1R inhibitor (confidentiality agreement) to target all macrophage populations, including microglia.

5.8.1. Expression of CXCR4 and CXCL12 *in vitro*

AMD3100 is an antagonist of CXCR4 receptor, theoretically, expressed in high levels by MDM. Tumor cells can express the respective ligand CXCL12, thereby recruiting CXCR4+ MDM to the tumor. Therefore, inhibition of CXCR4 harbors the potential to reduce recruitment of immune suppressive, tumor supportive MDM. qRT-PCRs were performed in order to confirm high CXCR4 expression by macrophages and to evaluate the extend of CXCL12 expression by the breast cancer BrM cell lines TS1-BrM and 99LN-BrM. Moreover, the impact of 10 Gy IR on CXCR4 expression by BMDM and CXCL12 expression by 99LN-BrM cells was analyzed *in vitro* by qRT-PCR.

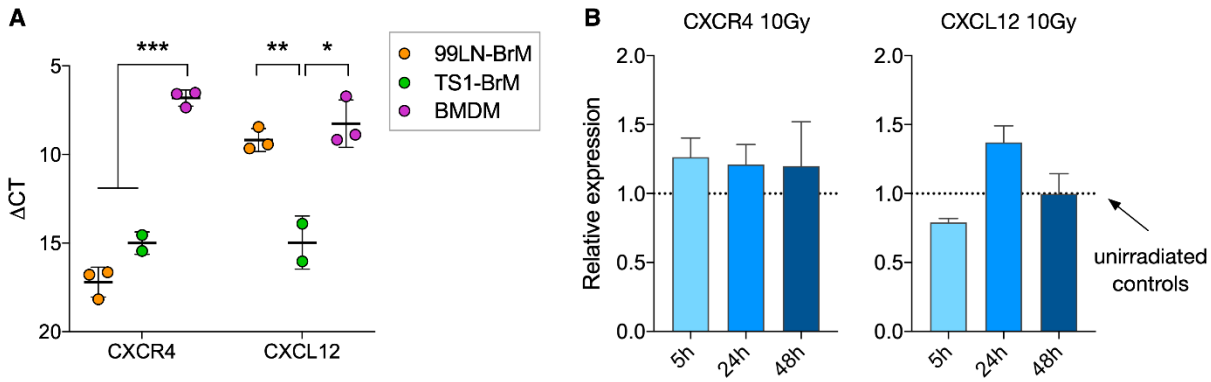

Fig. 5.29: Expression of CXCR4 and CXCL12 by 99LN-BrM, TS1-BrM cells and BMDM *in vitro*. (A) Expression of CXCR4 and CXCL12 in the BrM cell lines 99LN-BrM and TS1-BrM, as well as primary BMDM, quantified by qRT-PCR (unpaired t test, *P<0.05, **P<0.01, ***P<0.001). (B) Relative expression of CXCR4 by BMDM and CXCL12 by 99LN-BrM cells in response to 10 Gy. Different time points were quantified by qRT-PCR and normalized on expression of unirradiated controls (CXCR4 5h, 24h and 48h n=3, CXCL12 5h and 24h n=2, 48h n=3) Data is represented as mean ± SD in A and B.

The data confirmed that CXCR4 is highly expressed by BMDM. Furthermore, BMDM expressed CXCR4 at a much higher level than both BrM cell lines. CXCL12 is expressed at varying levels by the BrM cell lines. Interestingly, BMDM also expressed the ligand at a level comparable to 99LN-BrM (Fig. 5.29 A). *In vitro* irradiation of BMDM with 10 Gy did not have a significant effect on the expression of CXCR4 at different time points. Moreover, while CXCL12 expression by 99LN-BrM cells fluctuated slightly 5 and 24h after IR, the expression level after 48h returned to homeostatic (unirradiated) level (Fig. 5.29 B).

These results demonstrate that the breast cancer BrM cells express the chemokine CXCL12 which potentially leads to the recruitment of BMDM, which were shown to highly express CXCR4. IR with 10 Gy had no major impact on expression of this chemokine axis *in vitro*.

5.8.2. BMDM migration towards 99LN-BrM cells *in vitro*

To test whether the expression of CXCR4 by BMDM and CXCL12 by 99LN-BrM cells enables migration of BMDM towards the cancer cells, migration assays were performed *in vitro* (J. Anthes, 2020, master student).

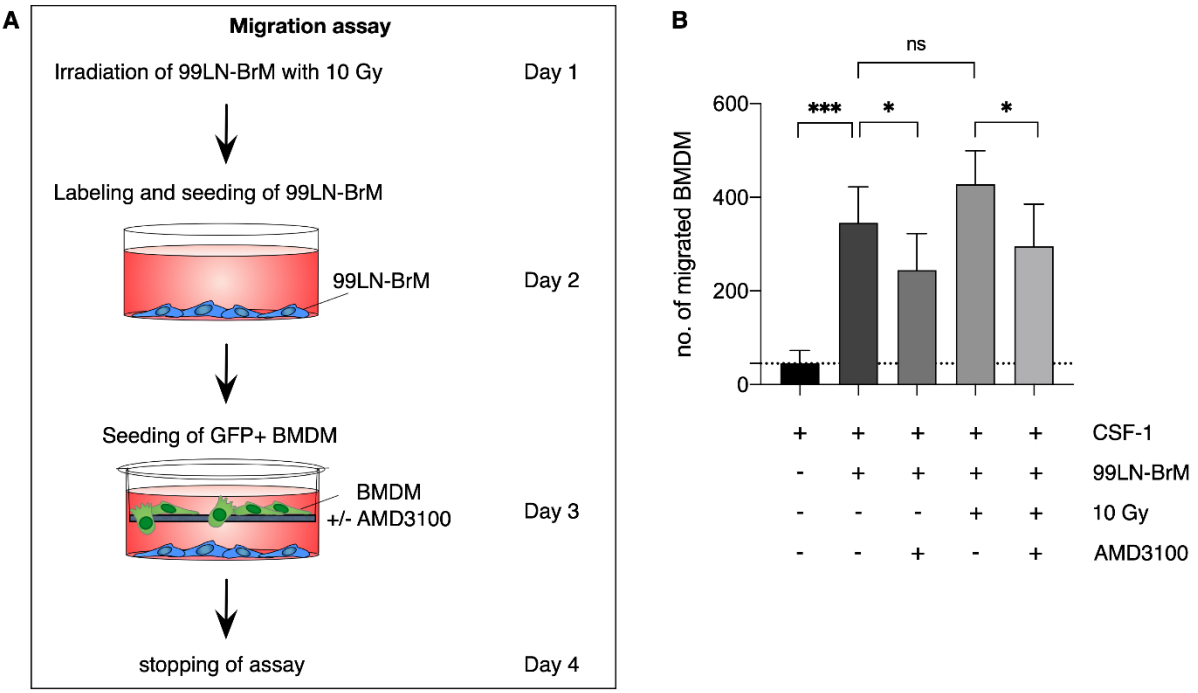

Fig. 5.30: Migration of BMDM to 99LN-BrM cells *in vitro*. (A) Experimental design of the *in vitro* migration assay. Primary BMDM isolated from CX3CR1-GFP/wt mice were seeded in the upper chamber of a transwell system. In the bottom chamber irradiated (10 Gy) or unirradiated 99LN-BrM cells were seeded. AMD3100 was added to the media of both chambers. (B) Number of BMDM that crossed the transwell membrane quantified by analysis of IF images of membranes. Data is represented as mean ± SD (n=8-10, paired t test, *P<0.05, ***P<0.001).

99LN-BrM cells were irradiated with 10 Gy or left untreated. On the next day, they were stained with CellTracker Red and seeded in the bottom chambers of a transwell plate. To allow

attachment of tumor cells, BMDM from CX3CR1-GFP mice were seeded one day later, in the top chambers of the transwell assay (Fig. 5.30 A). CSF1 was added to the media to ensure BMDM viability. Depending on the tested condition AMD3100 was added to the media of both chambers. Migrated BMDM were detected via IF, on the tumor facing side of the membranes. Migration of BMDM increased significantly in the presence of 99LN-BrM in the bottom chamber compared to media supplemented with CSF1 only. Irradiation of tumor cells with 10 Gy 48h before addition of BMDM did not change the number of migrated BMDM significantly. Addition of AMD3100 to the media in both chambers of the transwell system significantly reduced the migration of BMDM towards unirradiated and irradiated 99LN-BrM cells. Nevertheless, AMD3100 did not lower the number of migrated BMDM to control level (Fig. 5.30 B).

In conclusion, 99LN-BrM cells recruited BMDM without direct contact, via secreted factors *in vitro*. Results from the migration assay indicate that this recruitment is at least partially dependent on the CXCR4/CXCL12 axis, as indicated by reduced migration after addition of AMD3100.

5.8.3. Efficacy of pharmacological targeting of CXCR4 *in vivo*

To test the hypothesis that reduced MDM recruitment might prolong the efficacy of combined treatment with WBRT+αPD-1 by lifting immune suppression, 99LN-BrM mice were additionally treated with the CXCR4 inhibitor AMD3100. For this preclinical trial, the number of intracardially injected 99LN-BrM cells was increased from $6x10^4$ to $1x10^5$ to boost the incidence of BrM. The trial also included an unirradiated control group receiving only isotype (IgG2a) and carrier, as well as an AMD3100 monotherapy group, receiving AMD3100 and isotype control, to test the efficacy of AMD3100 alone.

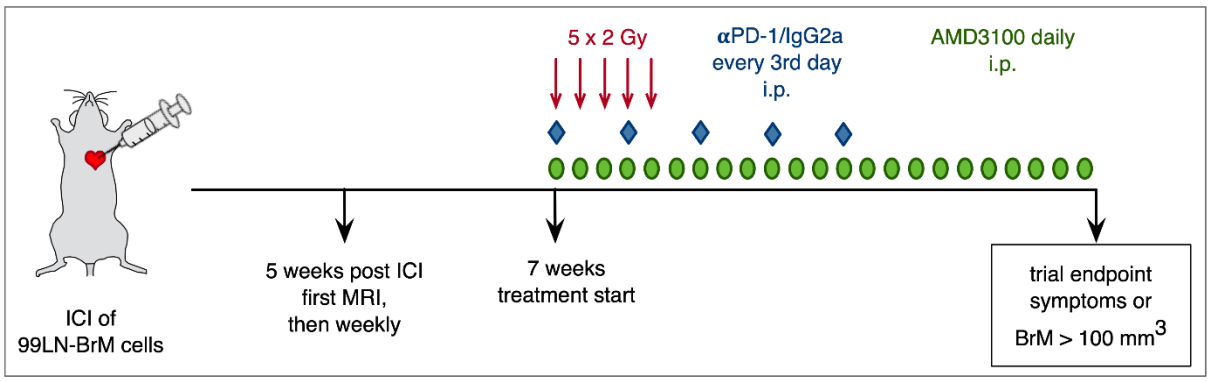

Fig. 5.31: Preclinical trial of combination therapy with WBRT, αPD-1 and AMD3100 in 99LN-BrM. Experimental design of the *in vivo* trial to test AMD3100 as monotherapy and adjuvant to WBRT+αPD-1 in 99LN-BrM. From week 5 on BrM were monitored weekly. At week 7 after intracardiac injection of $1x10^5$ 99LN cells, treatment was commenced and mice irradiated fractionally with 5x2 Gy. 100 µg of AMD3100 and 250 µg of αPD-1 were injected i.p.. αPD-1 was injected every third day, AMD3100 daily till trial endpoint. Mice in the control group received IgG2a and carrier solution instead of αPD-1 and AMD3100.

Starting with week five after ICI, BrM development was monitored via weekly MRI. After 7 weeks mice were stratified into groups and treatment commenced. As before, WBRT was applied as 2 Gy doses at 5 consecutive days. Treatment with αPD-1 (or isotype) and AMD3100 (or carrier) started together with the first radiation dose and continued every third day or every day, respectively. Mice were sacrificed when showing symptoms or a BrM load over 100 mm^3 (Fig. 5.31). Tumor growths was quantified by analyzing weekly MRI images with the ITK Snap Segmentation tool.

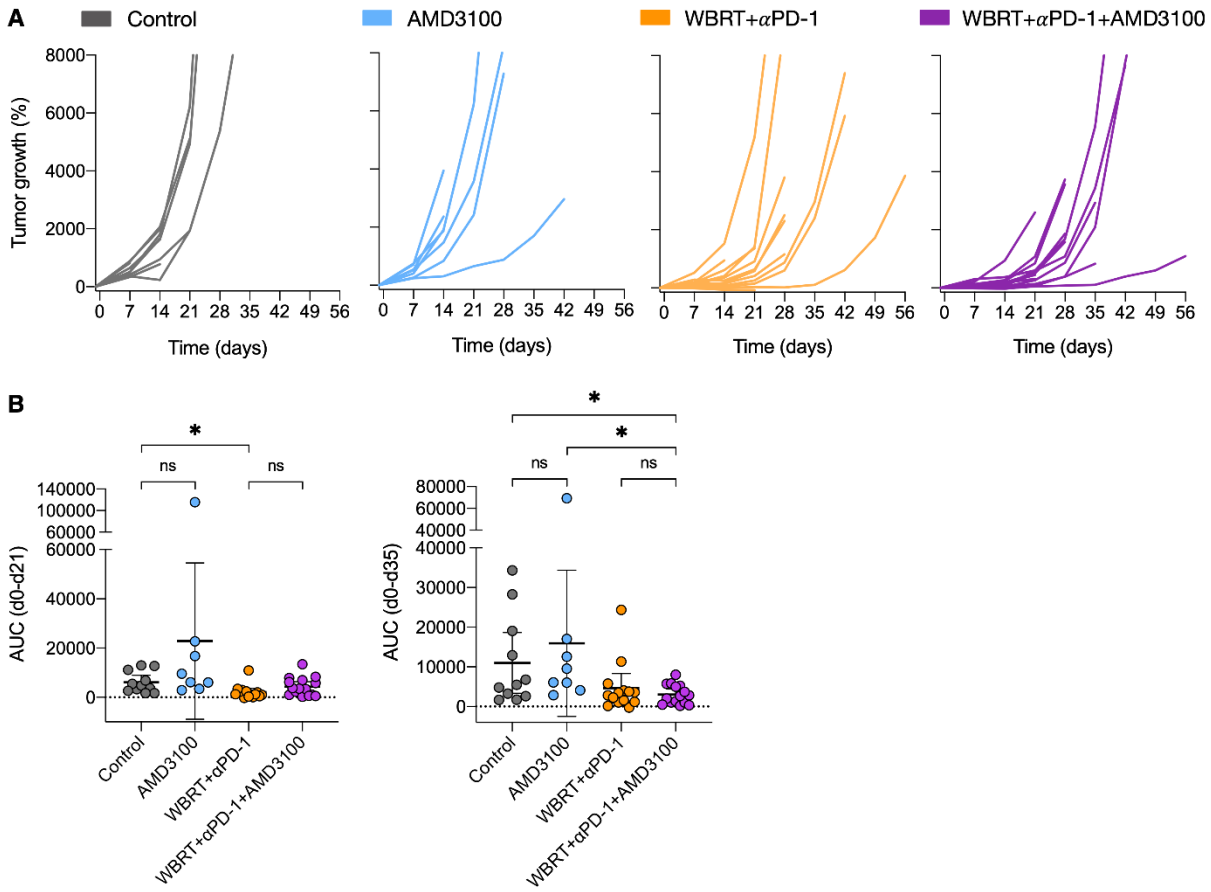

Fig. 5.32: Tumor growth after radio-immunotherapy with WBRT, αPD-1 and AMD3100 in 99LN-BrM. (A) Percentual tumor growth relative to treatment start is depicted for the individual mice of the four treatment groups (control n=11, AMD3100 n=8, WBRT+αPD-1 n=14, WBRT+αPD-1+AMD3100 n=15). (B) Quantification of relative tumor growth from d0 to d21 and d0 to d35 in the four groups. The area under the curve for individual mice was plotted and normalized to the survival time in weeks (unpaired t test, *P<0.05, data is represented as mean ± 95% CI.).

The generation of growth curves for the individual mice per group revealed that AMD3100 as monotherapy did not change relative tumor growth compared to the control group. In both groups, control and AMD3100, BrM growth was evident in the first week after treatment start. In the two combination groups, tumor growth was delayed until approximately d21. After this timepoint most BrM continued growing fast. However, the addition of AMD3100 to WBRT+αPD-1 did not affect relative tumor growth compared to WBRT+αPD-1

alone (Fig. 5.32 A). The calculation of the AUC for d21 and d35 confirmed that AMD3100 applied as monotherapy or in addition to the combination therapy did not affect tumor growth significantly compared to control or WBRT+αPD-1 group, respectively (Fig. 5.32 B).

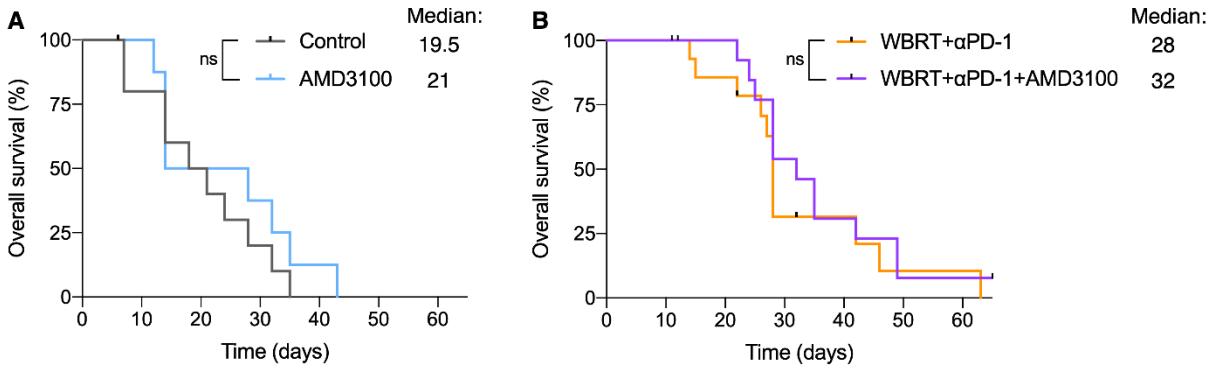

Fig. 5.33: Tumor growth after radio-immunotherapy with WBRT, αPD-1 and AMD3100 in 99LN-BrM. (A) Kaplan-Meier curves depict the overall survival in the control and AMD3100 monotherapy group (control n=11, AMD3100 n=8, Log rank test, *P<0.05). (B) Kaplan-Meier curves depict the overall survival in the WBRT+αPD-1 and WBRT+αPD-1+AMD3100 group (WBRT+αPD-1 n=14, WBRT+αPD-1+AMD3100 n=15, Log rank test, *P<0.05).

The lack of change in tumor growth was mirrored by the generated survival curves. The survival in the AMD3100 monotherapy group was not extended compared to the control group (Fig. 5.33 A). Moreover, AMD3100 in combination with WBRT+αPD-1 did not affect survival significantly in comparison to WBRT+αPD-1 alone, and all mice succumbed to BrM eventually (Fig. 5.33 B).

In conclusion, while migration of CXCR4-expressing BMDM towards CXCL12-expressing 99LN-BrM cells was partially inhibited by AMD3100 *in vitro*, AMD3100 was not sufficient to induce long term efficacy of radio-immunotherapy with WBRT+αPD-1 *in vivo* in 99LN-BrM.

5.8.4. The influence of AMD3100 on the tumor microenvironment of 99LN-BrM

To identify the reason for the lack of efficacy of AMD3100 in 99LN-BrM treatment, brains of mice from the survival trial were analyzed by IHC. An additional cohort of 99LN-BrM bearing mice, treated with AMD3100 or carrier, was sacrificed after 14 days and BrM were macrodissected. Single cell suspensions were generated from the BrM tissue and analyzed by flow cytometry with the myeloid panel described in section 4.2.10 (Fig. 4.1 A).

Histological analysis of 99LN-BrM from the survival trial revealed no obvious differences in infiltration of Iba1+ macrophages between the different treatment groups (Fig. 5.34 A). Quantification of Iba1+ cells from the IHC images with Aperio image scope confirmed that AMD3100 did not reduce the infiltration of Iba1+ macrophages (MDM and microglia) in both AMD3100 treated groups (Fig. 5.34 B).

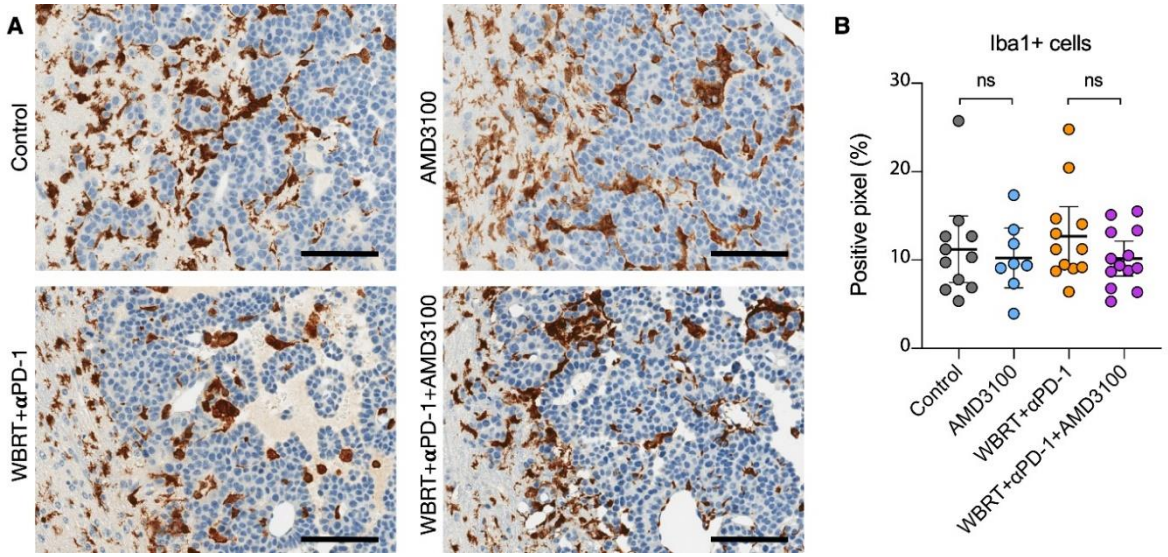

Fig. 5.34: Infiltration of 99LN-BrM with Iba1+ macrophages after treatment with AMD3100. (A) Representative images of IHC staining against Iba1+ cells in 99LN-BrM of the four treatment groups (Scale bars = 100 µm). (B) IHC quantification of Iba1+ cells in paraffin sections of 99LN-BrM at trial endpoint (control n=11, AMD3100 n=8, WBRT+αPD-1 n=12, WBRT+αPD-1+AMD3100 n=13, unpaired t-test).

As described in section 5.7.2., the major PD-L1 expressing myeloid cells after treatment with αPD-1+WBRT were MDM. Hypothetically, CXCR4 inhibition can inhibit recruitment of these MDM. To check if this was the case and distinguish MDM from brain resident microglia in AMD3100 treated BrM, flow cytometry of myeloid subpopulations was performed.

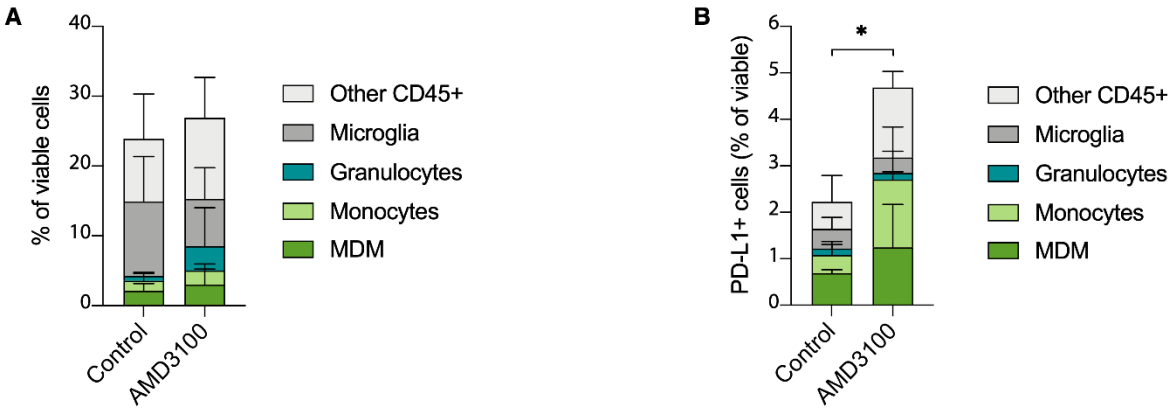

Fig. 5.35: Effects of AMD3100 on myeloid cells in breast cancer derived BrM. (A) Relative abundance of myeloid cell types infiltrating 99LN-BrM in the two treatment groups at d14 after treatment start (Control n=5, AMD3100 n=3). (B) Relative abundance of PD-L1+ myeloid cell types infiltrating BrM in the two treatment groups (Control n=5, AMD3100 n=3, unpaired t-test, *P<0.05 for total PD-L1+ immune cells). Data is represented as mean ± SD in A and B.

This analysis revealed that treatment with AMD3100 did not prevent the recruitment of MDM (CD45+ CD11b+ Ly6Clow Ly6G- CD49d+) or total myeloid cells (CD45+ CD11b+) to 99LN-BrM (Fig. 5.35 A). Furthermore, the infiltration of PD-L1+ myeloid cells from the periphery, including MDM, was not reduced, but further increased by treatment with AMD3100 (Fig. 5.35 B).

To sum up, AMD3100 was able to partially inhibit the migration of BMDM to 99LN-BrM *in vitro*. Nevertheless, AMD3100 could not prevent recruitment of MDM to 99LN-BrM *in vivo* but led to even higher infiltration of suppressive PD-L1+ myeloid cells. Therefore, use of AMD3100 was insufficient to release immune suppression and induce long term efficacy of radio-immunotherapy with WBRT+αPD-1.

5.8.5. Expression of CSF1R and CSF1 *in vitro*

Another strategy to target immune suppressive macrophages is inhibiting CSF1R via a brain penetrant CSF1R inhibitor (confidentiality agreement). CSF1R is highly expressed by all macrophages and binds to its ligands CSF1 and IL34 which are important survival factors for MDM and microglia, respectively. Inhibiting this pathway, therefore, targets all macrophage populations, including microglia. It has been shown that CSF1R inhibition can lead to the depletion as well as reeducation of immune suppressive macrophages towards rather inflammatory phenotypes and prolongs the survival of glioma bearing mice (Stafford *et al*, 2016; Pyonteck *et al*, 2013). In order to evaluate the expression of CSF1R and its ligands by BMDM, 99LN-BrM and TS1-BrM cells, qRT-PCR was used. Additionally, BMDM and 99LN-BrM cells were irradiated with 10 Gy *in vitro* to assess the influence of IR on the axis.

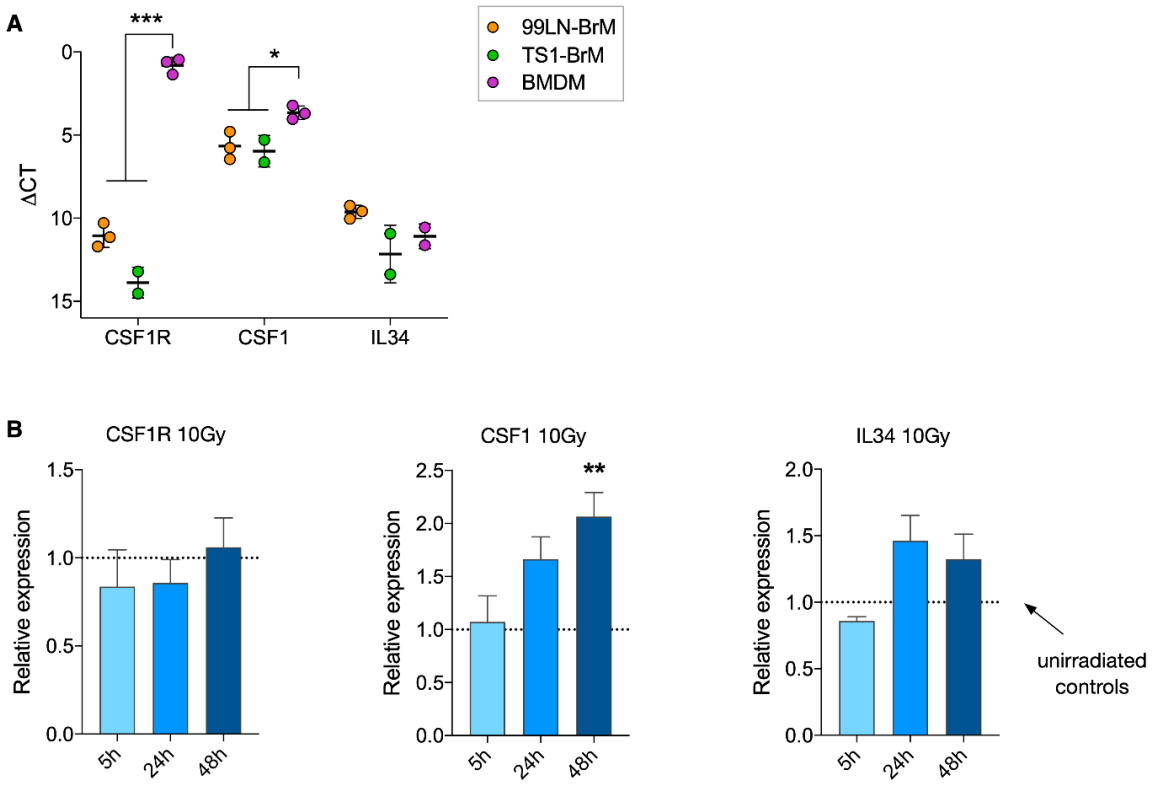

Fig. 5.36: Expression of CSF1R, CSF1 and IL34 by 99LN-BrM, TS1-BrM cells and BMDM *in vitro*. (A) Expression of CSF1R, CSF1 and IL34 in the BrM cell lines 99LN-BrM and TS1-BrM, and primary BMDM, quantified by qRT-PCR (unpaired t test, *P<0.05, ***P<0.001). (B) Expression of CSF1R by BMDM and CSF1 and IL34 by 99LN-BrM cells after irradiation (10 Gy). Different time points were quantified by qRT-PCR and normalized on expression of unirradiated controls (5h and 24h n=3, 48h n=5; paired t test, **P<0.01). Data is represented as mean ± SD in A and B.

Analysis of CSF1R expression revealed that CSF1R is expressed significantly higher by primary BMDM than by both tumor cell lines. The ligand CSF1 is not only expressed at a high level by the tumor cell lines, but also by BMDM. IL34 is expressed at a lower level than CSF1 by the tumor cells and BMDM (Fig. 5.36 A). *In vitro* IR with 10 Gy did not induce significant changes in CSF1R expression by BMDM or IL34 expression by 99LN-BrM cells. Interestingly, CSF1 expression by 99LN-BrM cells was significantly higher 48h after irradiation with 10Gy (Fig. 5.36 B).

In summary, CSF1R is highly expressed by BMDM, as expected. The tumor cell lines express both ligands to the receptor at a high level. Moreover, CSF1 expression by 99LN-BrM cells is further increased by IR.

5.8.5. Efficacy of pharmacological inhibition of CSF1R *in vivo*

To evaluate, if CSF1R inhibition synergizes with WBRT+αPD-1 radio-immunotherapy, mice were treated with either WBRT+αPD-1 or WBRT+αPD-1+CSF1R inhibitor (CSF1R-I) and sacrificed when symptomatic or BrM reached a volume of ≥100 mm^3 (J.Anthes, master student, contributed to the *in vivo* experiment).

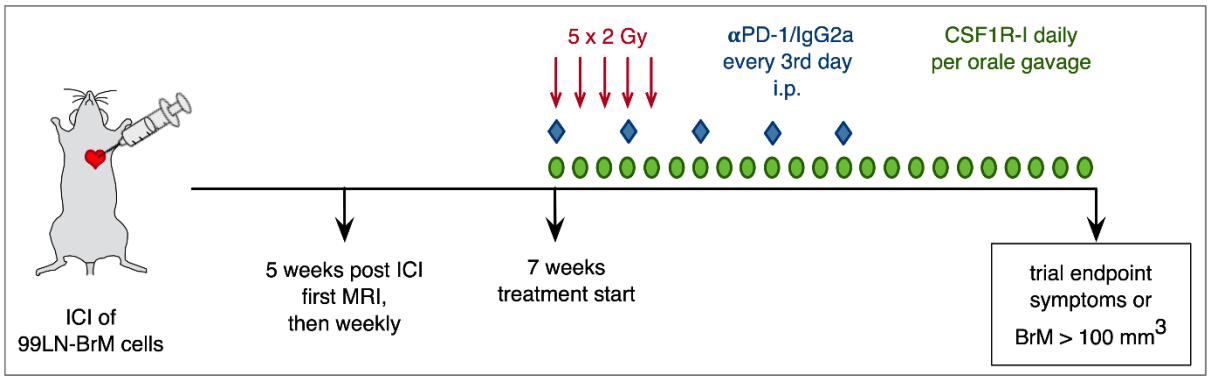

Fig. 5.37: Preclinical trial of combination therapy with WBRT, αPD-1 and CSF1R inhibitor in 99LN-BrM. Experimental design of the *in vivo* trial to test CSF1R-I in combination with WBRT+αPD-1 compared to WBRT+αPD-1 alone, in 99LN-BrM. From week 5 on BrM were monitored weekly via MRI. At week 7 after intracardiac injection of $1x10^5$ 99LN cells treatment was commenced and mice irradiated fractionally with 5x2 Gy. 10 µl/g of CSF1R-I and 250 µg of αPD-1 were injected per oral gavage or i.p., respectively. αPD-1 was injected every third day, CSF1R-I daily till trial endpoint.

WBRT and αPD-1 were applied as described in section 5.8.3. The schematic overview of this trial is depicted in Fig. 5.37. Again, BrM volume was monitored weekly via MRI and brains of mice were analyzed via IHC after completion of the survival trial.

Generated tumor growth curves of the individual mice demonstrated that the initial growth delay, induced by radio-immunotherapy with WBRT+αPD-1, was not extended by the addition of CSF1R-I to the combination (Fig. 5.38 A). The growth curves were used to calculate the AUC for each mouse normalized to weeks of survival. This quantification confirmed that tumor

growth was not significantly affected by addition of CSF1R-I, neither after 21 days nor 35 days (Fig. 5.38 B).

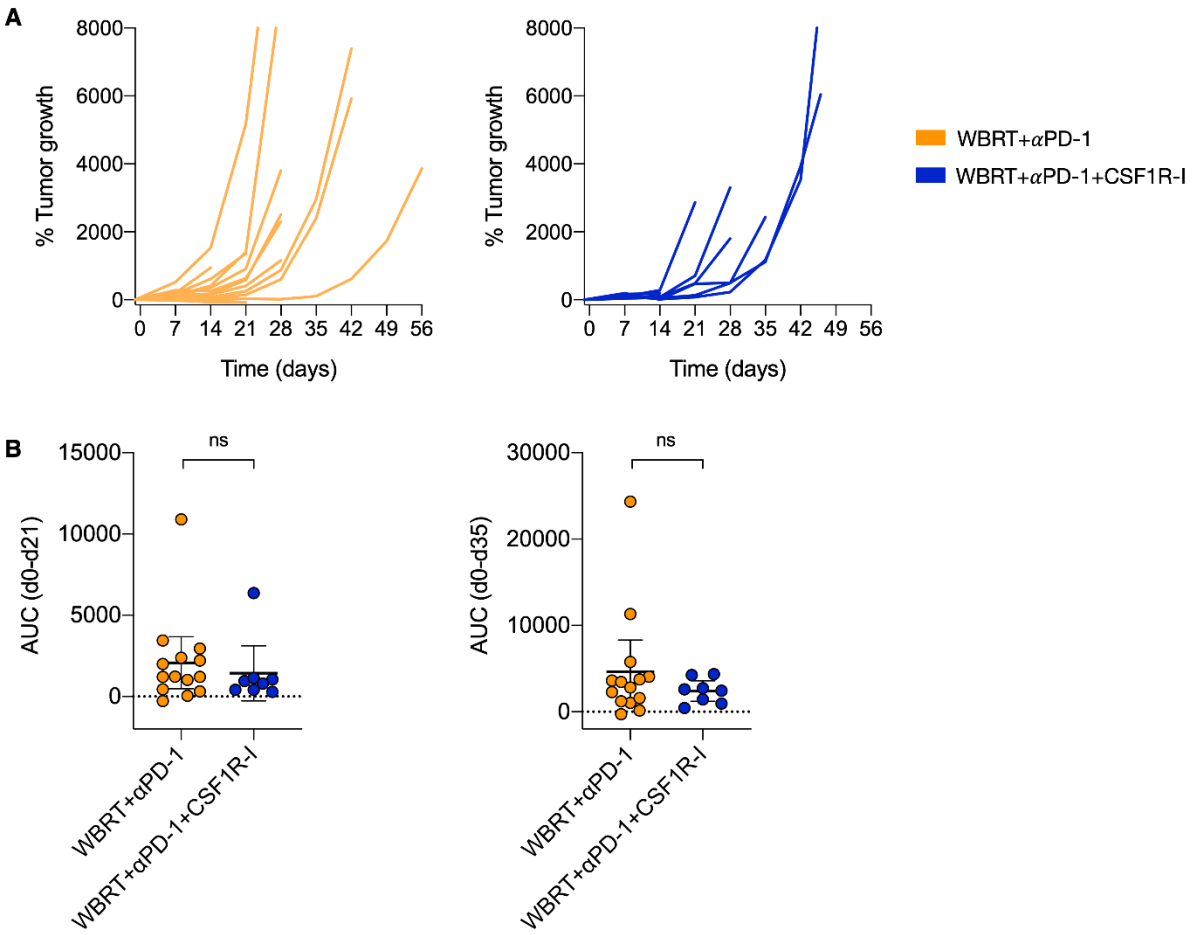

Fig. 5.38: Tumor growth of WBRT and αPD-1 treated 99LN-BrM with concurrent CSF1R inhibition. (A) Percentual tumor growth relative to treatment start is depicted for the individual mice of WBRT+αPD-1 and WBRT+αPD-1+CSF1R-I group (WBRT+αPD-1 n=14, WBRT+αPD-1+CSF1R-I n=8). (B) Quantification of relative tumor growth from d0 to d21 and d0 to d35 in the two groups. The area under the curve for individual mice was plotted and normalized to the survival time in weeks (unpaired t test, *P<0.05, data is represented as mean ± 95% CI.).

In line with these results, survival analysis revealed that addition of CSF1R-I to radio-immunotherapy with WBRT+αPD-1 does not further prolong survival, compared to the latter treatment (Fig. 5.39 A). Interestingly, 1 of 8 mice in the CSF1R-I group had to be sacrificed with tumor volumes <100 mm^3 in comparison to 8/14 in the WBRT+αPD-1 group, indicating possible side effects of the triple therapy with WBRT+αPD-1+CSF1R-I (Fig. 5.39 B).

In conclusion, CSF1R is expressed by BMDM which can potentially be recruited to CSF1 and IL34 expressing 99LN-BrM and TS1-BrM cancer cell lines. Nevertheless, inhibition of CSF1R *in vivo* did not affect tumor growth or survival, demonstrating that this inhibitor is not capable of improving efficacy of radio-immunotherapy with WBRT+αPD-1 in 99LN-BrM.

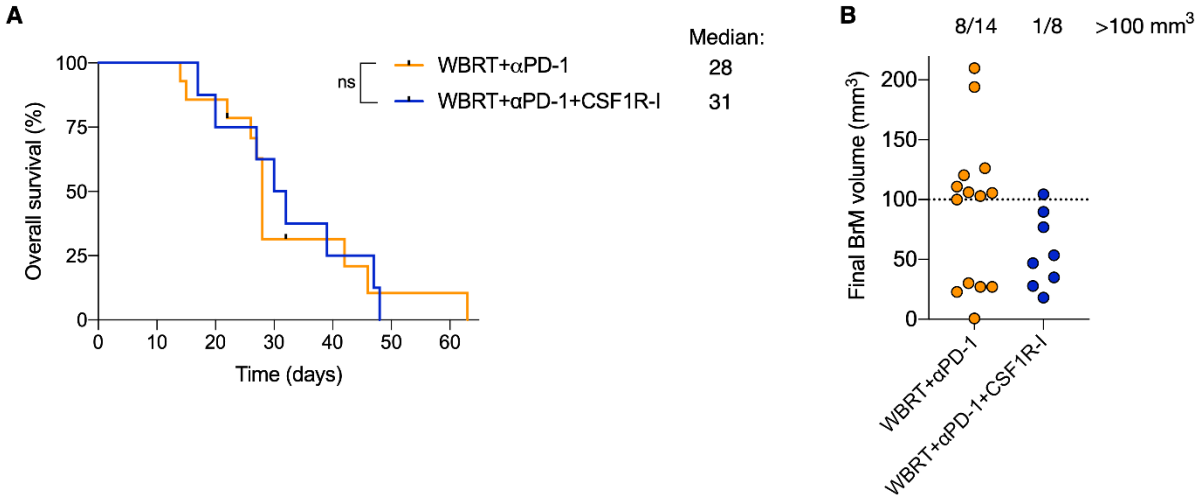

Fig. 5.39: Survival and final BrM volume after treatment of 99LN-BrM with WBRT+αPD-1+CSF1R-I. (A) Kaplan-Meier curves depict the overall survival in the WBRT+αPD-1 and WBRT+αPD-1+CSF1R-I group (WBRT+αPD-1 n=14, WBRT+αPD-1+CSF1R-I n=8, Log rank test). (B) Final BrM volume measured by ITK snap, based on MRI images, for each mouse separated by groups (WBRT+αPD-1 n=14, WBRT+αPD-1+CSF1R-I n=8).

5.8.6. The influence of CSF1R inhibition on immune cell infiltration in 99LN-BrM

To assess, if the lack of CSFR-I efficacy was due to inefficient macrophage depletion or other reasons, BrM from mice of the survival trial were analyzed via IHC. Sections were stained for Iba1 to label all macrophages and for CD3ε to label T cells, which are indispensable for immune checkpoint blockade. Positive cells were quantified via analyzing IHC images with Aperio ImageScope (in collaboration with J.Anthes, master student).

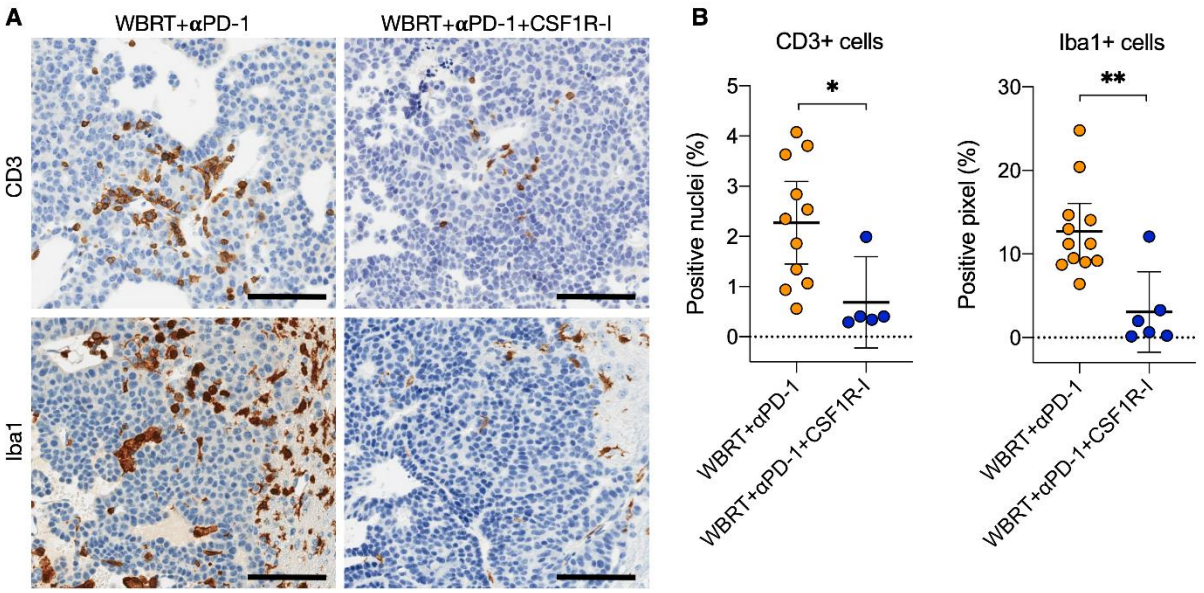

Fig. 5.40: Infiltration of 99LN-BrM with CD3+ and Iba1+ cells after radio immunotherapy with CSF1R inhibitor. (A) Representative images of IHC stainings of CD3+ and Iba1+ cells in 99LN-BrM of the two treatment groups (Scale bars = 100 µm). (B) IHC quantification of CD3+ and Iba1+ cells in paraffin sections of 99LN-BrM at trial endpoint (WBRT+αPD-1: n=11 for CD3ε and n=12 for Iba1, WBRT+αPD-1+CSF1R-I: n=5 for CD3ε and n=6 for Iba1, unpaired t-test, *P<0.05, **P<0.01).

IHC analysis showed a nearly complete depletion of Iba1+ cells in the WBRT+αPD-1+CSF1R-I group, confirming macrophage depletion in the BBB protected brain (Fig. 5.40 A, B). Intriguingly, the analysis of CD3+ cells also revealed a significant reduction of T cells from approximately 2% to 0.5% in the WBRT+αPD-1+CSF1R-I group compared to the WBRT+αPD-1 group (Fig. 5.40 A, B).

To conclude, CSF1R inhibition did not improve the efficacy of radio immunotherapy with WBRT+αPD-1. This was not due to inefficient macrophage depletion caused by improper BBB penetration of the small molecule inhibitor, but rather caused by decreased T cell infiltration, abolishing the efficacy of radio-immunotherapy with αPD-1.

6. Discussion

Novel immunotherapies, especially checkpoint inhibitors, have revolutionized cancer treatment. However, BrM patients are excluded from clinical trials with checkpoint inhibitors regularly and, therefore, cannot profit from promising advances in the field to the same extend as other cancer patients. One reason for the neglect of BrM patients in clinical research of immunotherapies is due to the fact that the brain parenchyma historically has been regarded as a sanctuary side for tumor cells, with microglia, the resident macrophages, being the predominant immune cell type. The BBB had been thought to prevent the entrance of blood borne immune cells, including T cells or DC, that could be harnessed for immunotherapies. This paradigm shifted in the past few years. Now, it is widely accepted that, while the entrance of substances or cells to the CNS is regulated, the CNS is not excluded from the systemic immune system. Indeed, a lymphatic system in the meninges, with classical lymphatic vessels possessing the ability to drain antigen from the brain parenchyma into cervical lymph nodes, has been discovered recently (Aspelund *et al*, 2015; Louveau *et al*, 2015). Moreover, it has been demonstrated that the CNS contains a multitude of various immune cell types under both homeostatic state and pathological conditions, including brain tumors (Mrdjen *et al*, 2018; Klemm *et al*, 2020). Therefore, immunotherapies gained interest for the treatment of BrM patients. To date, the most intensively investigated immunotherapies in cancer treatment are immune checkpoint inhibitors and, among these, antibodies targeting CTLA-4 and PD-1 on T cells. Immune checkpoint blockade can reactivate and increase cancer directed T cell responses, which have been suppressed in the TME before (Pardoll, 2012). The outcomes for highly immunogenic cancer entities, such as melanoma or NSCLC, are promising and even demonstrate activity in the CNS (Kamath & Kumthekar, 2018). For BrM derived from less immunogenic and highly immune suppressive cancers, including breast cancer, it is more complicated, as response rates to monotherapies are expected to be low or even non-existent. However, rational combination therapies might sensitize BrM to checkpoint inhibition and improve response rates. Radiotherapy, the standard of care for BrM patients, has been used predominantly for its direct genotoxic effects on tumor cells for a long time. Nowadays, it is recognized that radiotherapy can lead to immunogenic forms of cell death, leading to immune modulation in the tumor microenvironment. For example, upregulation of MHCI on tumor cells, the generation of neoantigens and the secretion of a variety of proinflammatory cytokines can lead to the recruitment and activation of immune cells (Sevenich, 2019). These immune cells can be harnessed, which is why radiotherapy is combined with different immunotherapies in clinical trials now. The hypothesis is that IR acts as a sensitizer for immunotherapies, such as checkpoint inhibition. Currently, clinical trials investigating BrM, mostly focus on testing this hypothesis for melanoma or NSCLC derived BrM (e.g.: Ahmed *et al*, 2016, NCT03340129,

NCT03955198). Less immunogenic BrM, such as breast cancer BrM, are not well investigated in this perspective, and only very few clinical trials evaluate the combination (NCT03807765, NCT03483012, NCT03449238).

Therefore, the aim of this thesis was to investigate, if classically fractionated radiotherapy can sensitize breast cancer BrM to checkpoint inhibition via monoclonal antibodies against PD-1. To test this hypothesis, it has been studied if radiotherapy modulates the immune microenvironment in the syngeneic breast cancer BrM mouse model 99LN-BrM. Specifically, these analyses should reveal if radiotherapy leads to the recruitment of immune suppressive pro-tumorigenic cells or ablation of radiosensitive effector immune cells, or, alternatively, induction of proinflammatory responses and recruitment of immune cells which can be harnessed for checkpoint inhibition. Furthermore, T cells in 99LN-BrM, which are indispensable for effective checkpoint inhibition, have been investigated in detail. In line with this, clonal expansion of T cells and expression of checkpoint molecules in breast cancer BrM have been analyzed. Finally, the combination of WBRT and αPD-1 has been tested *in vivo* in the 99LN-BrM mouse model. Additionally, it has been investigated if targeting the dominating myeloid immune microenvironment of breast cancer BrM, can prolong the efficacy of radio immunotherapy with WBRT+αPD-1, by lifting myeloid mediated immune suppression. Therefore, two macrophage targeting strategies have been evaluated in the 99LN-BrM model, in combination with WBRT+αPD-1, in a preclinical trial.

6.1. The immune suppressive microenvironment of breast cancer brain metastasis

The first crucial step of this thesis was to analyze the composition of the TME in BrM lesions of the syngeneic 99LN-BrM mouse. These analyses were essential to prove the presence of lymphoid cells which can be harnessed for immune checkpoint inhibition, and to quantify them. The goal of the analysis of the TME composition was also to identify potentially immune suppressive cells, such as myeloid cells, opposing adaptive immunity. Additionally, the comparability of the murine model with human breast cancer BrM needed to be assessed.

First results of this thesis demonstrated, via flow cytometry of macrodissected 99LN-BrM, that the proportion of leukocytes was relatively high, accounting for 22% of all viable cells in the lesions (section 5.1). This reflects the proportion of leukocytes identified recently in human BrM tissue. The authors of this study demonstrated that leukocytes in breast cancer derived BrM accounted for approximately 20% of viable cells. In lung cancer and melanoma derived BrM, the infiltration of immune cells was even higher, and accounted for approximately 30% and 40%, respectively (Klemm *et al*, 2020).

Furthermore, the analysis of 99LN-BrM in this thesis revealed that the TME is highly dominated by myeloid cells, accounting for 68.5% of all leukocytes (section 5.1). Bearing in mind that the main immune cell type of the brain parenchyma are the myeloid microglia, this is not surprising. The investigation of human BrM tissues demonstrated that macrophages/microglia dominate the immune compartment of human BrM (Berghoff *et al*, 2013). However, the detailed analysis of the myeloid compartment in 99LN-BrM in this thesis revealed that myeloid cells, recruited from the periphery (extra-parenchymal), such as MDM, granulocytes and inflammatory monocytes, add to myeloid cells in breast cancer BrM (section 5.1). This confirms results derived from a lung cancer BrM mouse model, demonstrating the infiltration of different myeloid cell types from the periphery in response to growing BrM lesions (Schulz *et al*, 2020). Again, this mirrors the situation in human BrM, were the presence of different myeloid cells such as granulocytes, monocytes and MDM, has been demonstrated (Bowman *et al*, 2016; Klemm *et al*, 2020). The infiltration of human BrM with peripheral myeloid cells is higher than in case of primary brain tumors, such as glioma, where microglia account for nearly 90% of all leukocytes (Klemm *et al*, 2020). It is widely accepted in the field of cancer research that in both extracranial and brain tumors, tumor associated myeloid cells, especially macrophages, often have tumor promoting functions, suppress tumor directed immunity and mediate therapy resistance (Goswami *et al*, 2017; Quail & Joyce, 2017; Vidyarthi *et al*, 2019; Aslan *et al*, 2020).

Therefore, it was important to assess, if lymphoid cells are present in the 99LN-BrM model and can persist in this highly immune suppressive myeloid TME. Lymphocytes have been shown to infiltrate human BrM, albeit to a lesser extend in breast cancer BrM compared to BrM derived from many other entities, or, indeed, primary breast cancer (Harter *et al*, 2015; Ogiya *et al*, 2017). Infiltrating CD3+ lymphocytes were correlated with favorable median survival of BrM patients and can be harnessed to elicit an adaptive anti-tumor immune response (Berghoff *et al*, 2015). In fact, in this thesis it has been demonstrated that up to 27.5% of 99LN-BrM associated leukocytes are of lymphoid origin (section 5.1). Again, this is in line with data derived from human breast cancer BrM, where approximately 35% of immune cells have been shown to be lymphoid. In human lung and melanoma BrM, lymphocytes account for up to 50% and 60% of leukocytes, respectively (Klemm *et al*, 2020). These results support the assumption that breast cancer BrM are less immunogenic than those derived from immune checkpoint inhibition responsive cancers, such as melanoma BrM.

In conclusion, these data confirm that the immune cell composition in the syngeneic breast cancer BrM model 99LN-BrM closely mimics the composition of human breast cancer BrM, with myeloid cells dominating the immune cell pool, and lymphocytes infiltrating to a lower extend, compared to extracranial tumors, as well as lung and melanoma BrM. Therefore, the

99LN-BrM model is a valid model to study the influence of immune modulation in a highly immune suppressive BrM-TME.

6.2. Potential limitations of radiotherapy as immune booster for brain metastasis

To test the hypothesis that radiotherapy can sensitize highly immune suppressive BrM to checkpoint inhibition, it was crucial to exclude the possibility that IR, applied as classically fractionated WBRT, might hamper an adaptive immune response against BrM, instead of stimulating it. Potential scenarios here were: (1) WBRT further increases the infiltration of BrM with immune suppressive cell types, (2) WBRT leads to the decreased infiltration of immune cells essential for an adaptive immune response, e.g. via depletion of radiosensitive immune cells or (3) WBRT has no effect on the immune microenvironment of breast cancer BrM.

It has been shown for a number of cancer models, that IR can lead to the recruitment of tumor promoting myeloid cells (Ahn *et al*, 2010; Krombach *et al*, 2018). As described in section 1.4.1 of this thesis, IR can disturb the integrity of the BBB or lead to the secretion of DAMP and, thereby, facilitate the infiltration of brain tumors with peripheral immune cells, including potentially immune suppressive cells (Qin *et al*, 1990; Rubin *et al*, 1994; Sevenich, 2019; Schulz *et al*, 2020). For example, the recruitment of MDM to BrM lesions of a xenograft lung cancer BrM mouse model, or to brain tumors in different glioblastoma mouse models, has been observed after fractionated WBRT (Schulz *et al*, 2020; Akkari *et al*, 2020). In the latter study the authors demonstrated that these MDM acquire a tumor promoting M2-like phenotype after an initial transient anti-tumor response (Akkari *et al*, 2020). Additionally, tumors are often infiltrated with Treg, which were associated with shorter overall survival for patients suffering from different solid cancers, including breast cancer (Shang *et al*, 2015). Treg have been shown to be less radiosensitive compared to other T cells, which might result in increased proportions of this cells in irradiated tissues (Qu *et al*, 2010). Therefore, the infiltration of 99LN-BrM with potentially immune suppressive myeloid cell types, as well as FoxP3+ Treg, has been studied in untreated or WBRT treated mice in this thesis. It has been demonstrated that, unlike in the before described studies, WBRT did not lead to increased infiltration of 99LN-BrM with total myeloid cells, inflammatory monocytes, MDM or granulocytes. Neither did this radiotherapy regimen change the proportion of infiltrating microglia versus MDM (section 5.2.2). Furthermore, the percentage of infiltrating FoxP3+ Treg, which was low in untreated BrM, was not increased by WBRT (section 5.2.4). These results indicated that classically fractionated WBRT might not hamper the efficacy of checkpoint inhibition by increasing infiltration of immune suppressive cell types in breast cancer BrM.

A further limitation of radiotherapy, in the perspective of immunotherapies, is the ablative effects it can have on radiosensitive immune cells essential for checkpoint inhibition, such as DC, the main APC and essential for a strong adaptive immune response. They are thought to be crucial for efficacy of checkpoint inhibition, also against brain tumors, as they can prime and activate T effector cells by presenting tumor antigens (Song *et al*, 2020). However, they belong to the most radiosensitive cells in the body (Manda *et al*, 2012). Moreover, radiotherapy can induce the expression of Trex1, an exonuclease digesting cytosolic dsDNA. However, the latter is crucial for, the expression of type I IFN via the cGAS-STING pathway, which is important for the maturation of DC (Vanpouille-Box *et al*, 2017; Sevenich, 2019). Another common side effect of radiotherapy is the depletion of T lymphocytes, which would be counterproductive when combining radiotherapy with a T cell targeted approach, such as checkpoint inhibition (Trowell, 1952). To prevent systemic depletion of sensitive immune cells in this thesis, mice were irradiated with a CT-guided beam to target the brain specifically, while sparing the rest of the body, including CLN. These are thought to be the sentinel lymph nodes of the brain, were APC, such as DC, present brain tumor derived antigens to naïve T cells (Louveau *et al*, 2015; Song *et al*, 2020; Hu *et al*, 2020). Even though the CLN were spared by the radiation approach in this thesis, it was necessary to confirm the presence of DC and T cells in both untreated 99LN-BrM and after WBRT. Flow cytometric analysis, as well as histological assessment, confirmed that DC, as well as T cells, are present in the 99LN-BrM model. Moreover, the infiltration of the lesions with these crucial cell types was not reduced by WBRT, providing that they were not depleted by the applied radiation regimen (section 5.2.3 and 5.2.4). The reason for this might be that the fractionation into 5 doses of 2 Gy, instead of a single higher dose, is mild enough to spare DC and T cells. Another explanation might come from previous studies, which reported that antigen experienced and memory T lymphocytes are more radioresistant than their naïve counterparts (Grayson *et al*, 2002; Schaue & McBride, 2012). Additionally, it has been demonstrated on subcutaneous tumor mouse models, that a large proportion of tumor associated T cells, including CD8+ cytotoxic T cells, are radioresistant and are sufficient to mediate anti-tumoral effects of local radiotherapy (Arina *et al*, 2019). This radioresistance was dependent on TGFβ (Arina *et al*, 2019), a cytokine essential for microglia homeostasis and therefore present in the brain microenvironment (Zöller *et al*, 2018). Finally, it is possible that these cells are depleted to some extent, but repopulate BrM quickly after radiotherapy, as the earliest time point analyzed in this thesis was 14 days after initial WBRT dose.

To sum up, it has been demonstrated in this thesis, that classically fractionated WBRT neither led to the accumulation of immune suppressive cell types, nor did it deplete radiosensitive immune cells crucial for checkpoint inhibition. Therefore, WBRT did not diminish prerequisites for an adaptive immune response against breast cancer BrM. It remained to be evaluated, if

WBRT, applied with the chosen treatment regimen, had any effect on the immune microenvironment of 99LN-BrM.

6.3. The potential of radiotherapy to sensitize breast cancer BrM to immunotherapy

As described in section 1.4.1, IR can lead to such ways of cell death which are not immunological inert, but can induce proinflammatory responses and lead to secretion of DAMP and proinflammatory cytokines (Sevenich, 2019; Schaue *et al*, 2012). For example, the inflammatory markers IL1β and TNFα have been shown to be amplified in the lungs of lung cancer mouse models after radiotherapy (Hong *et al*, 1999). Another example is the detection of elevated levels of IL-6 in the serum of breast cancer patients up to 1 year after receiving radiotherapy (Shibayama *et al*, 2014). Inflammatory chemokines and cytokines, such as these, could lead to the recruitment of crucial pro-inflammatory immune cells to 99LN-BrM. Therefore, the expression of the inflammatory markers TNFα, IL1β and IL-6, in response to IR, was analyzed in this thesis. It was confirmed for murine, as well as human breast cancer BrM cell lines, that IR leads to increased expression of inflammatory markers by these cells *in vitro* (section 5.2.1). This allowed the hypothesis that IR has the potential to induce pro-inflammatory responses in breast cancer BrM *in vivo*.

As mentioned previously, antigen presentation by DC is thought to be crucial for efficacy of checkpoint inhibition against brain tumors (Taggart *et al*, 2018; Song *et al*, 2020). In this thesis it has been shown that DC are part of the 99LN-BrM TME, but WBRT did not induce increased infiltration of these cells or a shift in DC subpopulations (section 5.2.3). However, there are other ways for radiotherapy to increase antigen presentation by DC. Krombach et al. demonstrated that irradiating TNBC cells with 20 Gy induced the release of DAMP. These DAMP in turn led to differentiation and maturation of DC, with the consequence of improved T cell priming *in vitro.* This effect was confirmed by injection of supernatant from unirradiated or irradiated TNBC cells into air pouches in mice *in vivo* (Krombach *et al*, 2018). Furthermore, Gupta et al. demonstrated, in several subcutaneous cancer mouse models, that irradiation of tumors with 10 Gy led to activation of tumor associated DC, consequently leading to activation of CD8+ cytotoxic T cells (Gupta *et al*, 2012).

Apart from DC, T cells, especially cytotoxic CD8+ T cells are indispensable for the efficacy of checkpoint inhibitors, such as monoclonal antibodies against PD-1 (Taggart *et al*, 2018). Therefore, in addition to the infiltration of granulocytes, inflammatory monocytes, macrophages and DC, the infiltration of T lymphocytes in response to WBRT was analyzed by flow cytometry as well as histology in this thesis. These experiments revealed no change of total T cell

infiltration after WBRT, meaning WBRT did not increase the absolute number of T cells in breast cancer BrM. However, a more detailed analysis of T cell subsets revealed a relative increase of cytotoxic CD8+ T cells, consistent with a decreased CD4/CD8 ratio after WBRT (section 5.2.4). For patients with TNBC or breast cancer BrM, a high CD4/CD8 ratio was associated with worse overall survival (Wang *et al*, 2017; Griguolo *et al*, 2020). Furthermore, it has been shown that CD8+ T cells are essential for ablative radiation effectiveness, and exclusion of these in tumors might mediate radioresistance (Lee *et al*, 2009; Chen *et al*, 2018a). Recently, it has been demonstrated in an intracranial melanoma BrM mouse model, that increased CD8+ T cell trafficking to BrM lesions is crucial for the efficacy of checkpoint inhibition via αPD-1 and anti-CTLA4 (Taggart *et al*, 2018). In this thesis, WBRT was sufficient to cause an increase in the infiltration of CD8+ cytotoxic T cells, already 14 days after first radiation dose. Furthermore, this increase of CD8+ T cells was detectable in symptomatic mice bearing mostly large end-stage BrM (section 5.2.4). At this stage of established BrM, the TME is most likely highly immune suppressive, and initial proinflammatory responses will be suppressed by the tumor. The fact that WBRT also increased CD8+ T cell infiltration in these tumors speaks for its potential to induce inflammatory responses, which can be harnessed for checkpoint inhibition in the treatment of highly immune suppressive BrM, such as breast cancer BrM.

6.4. T cell mediated anti-tumor responses in breast cancer brain metastasis

As the major focus of this work was to figure out if radio-immunotherapy with checkpoint inhibition can elicit an adaptive immune response against highly immune suppressive BrM, it was important to gain more insight on T cell mediated anti-tumor responses in breast cancer BrM. Therefore, T cell functionality and expression of checkpoint molecules in the TME of 99LN-BrM were analyzed in detail.

Firstly, T cell expansion in 99LN-BrM was analyzed *ex vivo* (section 5.3). It was crucial to clarify if T cells identified in the TME were truly directed against tumor antigens and did not home to lesions by coincidence e.g. through the heterogeneously permeable BTB. If T cells were primed and activated against tumor antigens, one would expect preceding clonal expansion of T cells. This clonal expansion has been investigated via TCR sequencing of BrM tissue from untreated and WBRT treated mice. A publication in 2018 demonstrated, that brain tumors such as GBM, but also BrM, can lead to systemic lymphopenia induced by loss of Sphingosine-1-phosphate receptor 1 (S1P1). This loss led to sequestration of T cells in the bone marrow and, consequently, to contracted T cell deficient lymphoid organs and decreased systemic levels of T cells (Chongsathidkiet *et al*, 2018). An immune evasion mechanism as this would hamper

the efficiency of checkpoint inhibition. Therefore, it was important to exclude systemic reduction in T cell numbers elicited by breast cancer BrM and to obtain insight into the extracranial T cell response. Furthermore, it was important to exclude systemic depletion of T cells by WBRT, as mentioned in section 6.2. To achieve this, clonal expansion was also investigated by TCR profiling of CLN, the CNS draining peripheral lymphoid organs. Indeed, TCR profiling revealed a high abundance of T cells in CLN, which was not reduced by radiotherapy, applied as WBRT 14 days after first dose, proving that the applied radiation scheme, as well as BrM itself, does not lead to systemic lymphopenia. Additionally, flow cytometric analysis of blood samples from healthy, as well as BrM bearing mice, confirmed that T cell numbers were not systemically reduced through BrM induced sequestration of T cells in the bone marrow. The analysis of BrM tissue by TCR profiling confirmed the results obtained by flow cytometry in section 5.2.4, demonstrating that T cell infiltration of breast cancer BrM was not reduced by WBRT, compared to untreated mice (section 5.3.1). These findings, obtained by TCR profiling, show that breast cancer BrM itself, as well as classical fractionated WBRT, do not deplete target cells for checkpoint inhibition in the lesions or systemically. The next logical step was the analysis of primed T cells as output for BrM directed T cell immunity. Priming of T cells should lead to their clonal expansion, and subsequent migration to the target tissue, in this case BrM lesions in the brain parenchyma. Clonal expansion of T cells was therefore analyzed in detail in 99LN-BrM in this thesis. These results revealed a high maximal productive frequency and a high productive clonality of T cells in BrM lesion, indicative of clonal expansion. This was not changed significantly by WBRT after 14 days. Both productive frequency and clonal expansion were much higher in BrM samples, than in CLN samples (section 5.3.2). It was to be expected, as CLN are peripheral lymphoid organs, containing a vast amount of T cells, which are most certainly not exclusively directed against BrM. The high variety of T cells in CLN automatically leads to lower frequency of single clones from the T cell pool. To gain more detailed insight into clonal expansion in breast cancer BrM, the clonal space homeostasis was calculated. This analysis revealed hyperexpanded T cell clones in 8 out of 9 samples and large clones in all BrM samples. Again, radiotherapy did not lead to significant changes of this parameter (section 5.3.3). So far, these results indicated clonal expansion of T cells in BrM irrespective of application of WBRT. Nevertheless, a low overall number of infiltrating T cells in BrM lesions might lead to increased frequency of unique clones from the total T cell pool, independent of clonal expansion. Mansfield et al. demonstrated the contraction of T cell clones and low T cell richness in NSCLC BrM, compared to the primary tumor (Mansfield *et al*, 2018). Moreover, it has been shown, that in breast cancer BrM the infiltration of T cells is lower, compared to the respective primary tumor (Ogiya *et al*, 2017). The generation of Lorenz curves and the calculation of Gini indices in this thesis allowed the evaluation of clonal expansion of T cells, independently of changes in T cell numbers. The

high Gini indices, extracted from the curves of BrM samples, confirmed the clonal expansion of T cell clones in 99LN-BrM, also after radiotherapy, demonstrating preceding T cell priming and activation. This analysis also revealed that T cells in CLN expanded, indicating priming of T cells in these sentinel lymph nodes. Moreover, clonal expansion was negatively correlated with tumor volume, as was the number of total infiltrating T cells, which indicates progressing suppression of T cell immunity in breast cancer BrM (section 5.3.3). These results are in line with the highly immune suppressive BrM-TME, and one would expect mechanisms to evade a direct attack by T cells in BrM (Sampson *et al*, 2020). In accordance with this conclusion, it has been demonstrated in human BrM, derived from several primary entities, including breast cancer, that T cell number decreases with increasing lesion size (Harter *et al*, 2015).

Combined, these results indicate that a T cell response against breast cancer BrM is initially elicited but inhibited with progressing tumor growth by the heavily immune suppressive tumor microenvironment. The initial T cell response seems to be individual for each mouse as indicated by the low overlap of the Top 100 most abundant BrM clones between mice (section 5.3.3). This is in line with a study demonstrating that the most abundant clones in NSCLC BrM are specific to single lesions (Mansfield *et al*, 2018).

To test how efficient the TME of breast cancer BrM suppresses T cell responses, T cells were depleted in mice, injected with brain homing 99LN cells. To evaluate the influence of T cells on BrM progression and not the initial steps of extravasation into the brain parenchyma, T cell depleting antibodies have been administered a week after tumor cell injection. BrM onset and progression has been followed over the course of several weeks. The depletion study performed in this thesis, demonstrated a strong suppression of T cell responses by 99LN-BrM. The depletion of most T cells did not accelerate the outgrowth of BrM in the treated mice. Furthermore, the time till BrM onset was not shortened by depletion of T cells, indicating that anti-tumor T cell responses are suppressed quickly and efficiently in the breast cancer BrM TME (section 5.4.1 and section 5.4.2).

One important mechanism for tumors to evade an adaptive immune response is the suppression of T cells by binding to immune checkpoints, as discussed previously (Pardoll, 2012). To date, a lot of effort went into unveiling treatment strategies that can sensitize tumors to checkpoint inhibition, with the goal of inducing long lasting anti-tumor immunity. One of the most extensively studied checkpoints is PD-1 receptor on the surface of T cells, the investigation of which was also the focus of this thesis. PD-1 is mostly expressed after T cell activation to prevent overshooting of T cell responses in the healthy system and is used, therefore, as activation and exhaustion marker in cancer research (Maleki Vareki *et al*, 2017). By expression of PD-L1 in the TME, PD-1+ T cells can be inhibited, which is why the expression of PD-L1 by the breast cancer BrM cell lines 99LN-BrM and TS1-BrM has been

probed *in vitro* in this thesis. It was confirmed that both breast cancer BrM cell lines express the transcript of PD-L1 and carry the protein on the cell surface. The proportion of tumor cells, positive for PD-L1 *in vitro*, was lower in the two breast cancer cell lines, compared to the more immunogenic melanoma cell line B16F10 (section 5.5.1). However, it has been shown that often high levels of PD-L1 are not constitutively expressed by cancer cell lines, but in the TME upon stimulation by cytokines, mainly IFNγ (Dong *et al*, 2002). Moreover, there is still dispute, whether PD-L1 expression by tumor cells can serve as a prognostic marker for response to checkpoint inhibition (Maleki Vareki *et al*, 2017). A study published in 2019 investigated PD-L1 expression at the primary and metastatic site in melanoma patients. No correlation with response to checkpoint inhibition has been found in this study (Kümpers *et al*, 2019). However, for NSCLC, PD-L1 expression is often used as prerequisite for participation in clinical trials investigating checkpoint inhibition (Hui *et al*, 2017). After confirming the expression of PD-L1 by brain homing breast cancer cell lines in this thesis, the effect of IR on PD-1 and PD-L1 expression was investigated. Interestingly, IR with a dose of 10 Gy led to increased expression of receptor and ligand transcript by the breast cancer BrM cell lines (section 5.5.1). Upregulation of PD-L1 in response to radiotherapy was reported to be a resistance mechanism by tumor cells, which could be overcome by concurrent PD-L1 inhibition in a subcutaneous CT26 mouse model (Dovedi *et al*, 2014). This highlights the potential of synergistic efficacy of radiotherapy, in combination with immune checkpoint inhibition, in the TS1-BrM and 99LN-BrM models. The surface expression of PD-1 and its ligand PD-L1 in breast cancer BrM was also confirmed histologically for both models (99LN-BrM and TS1-BrM) *in vivo*. More detailed flow cytometric analysis of PD-1 and PD-L1 expression in BrM of the 99LN-BrM model, revealed that PD-1, as expected, was mostly expressed by T cells and barely by myeloid or tumor cells (section 5.5.2). As mentioned, the expression of PD-1 on T cells is a marker for prior activation followed by exhaustion, confirming the results obtained by TCR sequencing. The inhibitory ligand PD-L1 was not only expressed by tumor cells, but also by leukocytes, such as myeloid and T cells, highlighting a potential tumor promoting and immune suppressive role of the immune microenvironment in breast cancer BrM. Interestingly, on myeloid cells PD-L1 was only expressed in the presence of BrM in the 99LN-BrM model and not on myeloid cells in the healthy brain parenchyma of tumor-free mice. This can mean one of two things: either microglia in the TME are stimulated by the tumor to express PD-L1, which they do not under healthy conditions, or 99LN-BrM leads to the recruitment of potentially immune suppressive PD-L1+ myeloid cells. The flow cytometric analysis of myeloid subpopulations in 99LN-BrM confirmed the latter hypothesis (section 5.5.2). While microglia in the TME barely expressed PD-L1, a high proportion of infiltrating myeloid cell types from the periphery, such as granulocytes, inflammatory monocytes and especially MDM, expressed this T cell inhibitory ligand. Taking together all the results up to this point, allowed the conclusion that the TME of breast cancer

BrM harbors crucial cell types to elicit an adaptive immune response, such as DC and T cells. Furthermore, classically fractionated WBRT increased the proportion of tumor infiltrating cytotoxic T cells, without further increasing the infiltration of potentially immune suppressive myeloid cells. T cells, infiltrating breast cancer BrM, expanded, also after WBRT, indicating preceding activation. Initial T cell priming and activation against breast cancer BrM was followed by a rapid suppression of T cell function. This suppression of anti-tumor immunity was probably not only mediated by tumor cells, but also by PD-L1+ myeloid cells, recruited from the periphery. The results obtained up to this point, underline the potential of PD-1 inhibition to lift the strong suppression of T cell mediated anti-tumor responses and to synergize with radiotherapy.

6.5. Sensitization of breast cancer brain metastasis to PD-1 blockade by WBRT

Checkpoint inhibitors are not only approved as first line treatment for metastatic melanoma and NSCLC, two cancer types prone to BrM, but also demonstrated clinical efficacy in BrM patients in retrospective trials (Rausch & Hastings, 2017; Peters *et al*, 2019; Kamath & Kumthekar, 2018). Nevertheless, even for highly immunogenic cancers, such as cutaneous melanoma, objective response rates are 11-15% for ipilimumab and 33-40% for αPD-1 antibodies, meaning the majority of these patients do not profit from monotherapies with checkpoint inhibitors (Bol *et al*, 2019). Therefore, a lot of effort is put into finding combination therapies, to sensitize cancers to immune checkpoint inhibition, and improve response rates. The combination of checkpoint inhibition with radiotherapy is one promising option, which is heavily investigated to date. Recently, there has been a meta-analysis of studies investigating the efficacy and safety of hypo-fractionated radiotherapy (HFRT) with and without immune checkpoint inhibition in BrM patients. The authors demonstrated an increased 6-month, 1-year, 2-year and median overall survival of the combination with radiotherapy, compared to immune checkpoint inhibition alone (Yang *et al*, 2020). Sadly, most clinical studies including BrM patients are retrospective, while prospective trials are rare. Furthermore, prospective trials, investigating the combination of radiotherapy with immune checkpoint inhibition, focus mostly on patients with NSCLC and melanoma. Therefore, only a limited number of phase 1 or 2 clinical trials recruit breast cancer BrM patients for testing the efficacy of radio immunotherapy with checkpoint inhibitors (NCT03807765, NCT03483012, NCT03449238, NCT04047602). Hence, the evaluation of this combination in preclinical trials of breast cancer BrM models is of increasing interest and has the potential to initiate new clinical trials for breast cancer BrM patients, therefore pushing forward research in this field.

In this thesis, mice were treated with a combination of classically fractionated WBRT and immune checkpoint inhibitor αPD-1. The efficacy of the combination treatment, as well as monotherapy was evaluated by performing survival trials. Furthermore, BrM of treated mice were analyzed in detail via histology and flow cytometry, to gain deeper understanding of the mechanism of treatment response. Such information is crucial for the design and improvement of future clinical trials, and to overcome potential therapy resistance. The preclinical trial performed in this thesis, demonstrated that monotherapy of breast cancer BrM, a highly immune suppressive TME, with αPD-1, is not sufficient to halt tumor growth or increase overall survival (section 5.6.1). This result was not surprising, as clinical trials of primary TNBC, treated with PD-1 inhibitor pembrolizumab alone, demonstrated response rates of only 5-23% (Wein *et al*, 2018). For TNBC BrM, responses are to be expected rarer, as the infiltration of TIL is significantly lower, compared to the primary tumors (Ogiya *et al*, 2017). Radiotherapy, the mainstay of BrM patient treatment, applied as classically fractionated WBRT in this thesis, slowed down tumor progression for a short period and transiently prolonged survival (section 5.6.1). The percentage of mice responding to radiotherapy after 7d was high, with 75%, but quickly decreased to approximately 25% only one week later (section 5.6.2). This is in line with patient response rates to WBRT, which are initially high, however tumor control is only achieved transiently (McTyre *et al*, 2013; Sevenich, 2019). In the combination group of this preclinical trial, αPD-1 was applied as concurrent therapy to WBRT. The reason behind the strategy was that a number of retrospective clinical trials suggest superior efficacy of concurrent over non-concurrent treatment with checkpoint inhibitors in combination with radiotherapy for the treatment of BrM patients (Chen *et al*, 2018b; Lehrer *et al*, 2018; Jm *et al*, 2020). The preclinical trial, performed as part of this thesis, showed synergistic efficacy of concurrent αPD-1 treatment with WBRT. The combination therapy decreased tumor growth and increased overall survival, compared to the control group and monotherapies (section 5.6.1). The proportion of responders after 7d of treatment was comparable to WBRT monotherapy but in contrary to WBRT alone stayed at a high level for several weeks, indicating prolonged therapeutic efficacy. Nevertheless, the combination group also contained mice, not responding to the treatment. The histological assessment of BrM from mice in this group revealed that BrM from all responders showed high T cell infiltration, whereas most of the non-responders showed low T cell infiltration. This was not the case for the group, treated with WBRT as monotherapy. High T cell infiltration also translated into prolonged survival in the combination group, which again was not the case for the WBRT or control group. Interestingly, even though αPD-1 monotherapy had no effect on the overall survival of all mice in the group taken together, mice with high T cell infiltration survived significantly longer, than mice with low T cell infiltration (section 5.6.2). These results indicate that checkpoint inhibition with αPD-1 leads to the accumulation of active anti-tumor effector T cells in lesions of 99LN-BrM bearing

mice. The heterogeneity of response to αPD-1 could be induced by the presence or absence of extracranial tumors, which was beyond the scope of this thesis. However, Taggart et al. demonstrated in an intracranial melanoma BrM model, that the efficacy of checkpoint inhibition is dependent on the presence of extracranial tumor, which increases the efficacy of T cell priming (Taggart *et al*, 2018). To evaluate if this holds true for breast cancer BrM, it will be crucial to monitor extracranial tumor load in addition to BrM growth in future experiments. Another factor, which potentially influences the response to checkpoint inhibition, is the localization of BrM. Already in 1923 it was recognized that tissue transplanted into the brain parenchyma was only rejected when it touched border regions or the ventricles (Murphy & Sturm, 1923). This indicates that immune surveillance is more effective in certain areas of the brain compared to others. Therefore, evaluating if the response to radio immunotherapy is correlated with the localization of breast cancer BrM lesions might shed light onto factors, determining a strong anti-tumor immune response.

To elucidate potential immune modulatory effects on the TME of breast cancer BrM, induced by radio-immunotherapy with αPD-1, 99LN-BrM lesions were analyzed in detail by flow cytometry and histology. These analyses revealed an increase in leukocyte infiltration, induced by both monotherapies, and to a greater extent by combination treatment. A closer look into defined immune cell populations revealed no significant change in DC infiltration. However, the infiltration of BrM lesions with CD3+ T cells was increased following checkpoint inhibition, demonstrating that αPD-1 carries the potential to reactivate T cell responses and induce greater T cell infiltration also in breast cancer BrM (section 5.7.1). T cell infiltration has been shown to correlate with improved survival of patients with BrM, derived from different entities (Berghoff *et al*, 2015). Moreover, it correlated with improved response to checkpoint inhibition in terms of overall survival in a prospective study of metastatic melanoma (Kümpers *et al*, 2019). In a mouse model of hypermutated glioblastoma, checkpoint inhibition increased T cell infiltration of tumors in responders, compared to non-responders (Aslan *et al*, 2020). A prospective study is about to start soon, which investigates neoadjuvant checkpoint inhibition before surgery and SRS for the treatment of BrM from different entities, including PD-L1+ TNBC. One primary outcome of the study, apart from survival data, will be the proportion of proliferating circulating T cells. First results are expected in 2023 and will hopefully confirm increased systemic proliferation of T cells after checkpoint inhibition in BrM in humans (NCT04434560). A closer look onto BrM infiltrating T cell subsets in this thesis, revealed that checkpoint inhibitor αPD-1 especially increased the infiltration of CD4+ T helper cells in both checkpoint inhibitor treated groups. WBRT, on the other hand, increased the infiltration of CD8+ cytotoxic T cells in the monotherapy, as well as combination group. In the end, only the combination of WBRT and checkpoint inhibition increased infiltration of both, CD4+ and CD8+ T cells (section 5.7.1). As elaborated in section 6.3., the priming and trafficking of CD8+ T cells

to the brain is crucial for the efficacy of checkpoint inhibition against melanoma BrM (Taggart *et al*, 2018; Song *et al*, 2020). However, reports on the necessity of CD4+ T cells for tumor control are controversial. In 2017, a study of human breast cancer samples and a humanized breast cancer mouse model showed a positive correlation of naïve tumor infiltrating CD4+ T cells with Treg infiltration. Both naïve CD4+ T cells and Tregs were associated with poor prognosis for patients. The authors revealed in this study, that naïve CD4+ T cells, recruited to the TME of breast cancers, convert to highly immune suppressive tumor infiltrating Tregs. Blocking the recruitment of naïve CD4+ T cells to the tumors pharmacologically in a humanized TNBC mouse model reversed immunosuppression and inhibited tumor progression (Su *et al*, 2017). Therefore, the increased infiltration of CD4+ T cells, observed after αPD-1 monotherapy in this thesis, might not be advantageous for tumor control. Indeed, αPD-1 induced the compensatory upregulation of PD-1 and increased the infiltration of FoxP3+ Tregs in 99LN-BrM. However, this was prevented when αPD-1 was combined with WBRT (section 5.7.1). On the other hand, it has been demonstrated for glioblastoma, that depletion of CD4+ T cells abrogates the efficacy of checkpoint inhibition, indicating a crucial role of CD4+ T cells in checkpoint inhibitor induced brain tumor regression (Aslan *et al*, 2020). Additionally, it has been described that both, CD4+ and CD8+ T cells, are important for optimal tumor control (Shankaran *et al*, 2001; Ostroumov *et al*, 2018). CD4+ T cells have not only regulatory immune suppressive functions in the tumor context, as the case for Treg, but can also stimulate DC to present antigen to cytotoxic T cells, activate CD8+ T cells directly via secretion of IL-2 and even exhibit direct anti-tumor activity via secretion of tumoricidal cytokines such as IFNγ (Tay *et al*, 2020). Taken together, data obtained from previous publications and from this thesis, lead to the hypothesis that the combination of checkpoint inhibitor αPD-1 with WBRT is superior compared to both monotherapies, as it increases CD4+ and CD8+ T cell infiltration into 99LN-BrM, while at the same time preventing increased infiltration of FoxP3+ T cells and compensatory upregulation of PD-1.

6.6. Myeloid mediated resistance development against PD-1 blockade in breast cancer brain metastasis

So far it has been demonstrated that the combination of αPD-1 with WBRT leads to (re-) activation of CD4+ and CD8+ T cell responses and synergistic efficacy in the treatment of murine breast cancer BrM. Still, long term survival of mice could not be achieved, indicating development of resistances in 99LN-BrM, against this radio-immunotherapy regimen. Often, resistance is mediated by compensatory upregulation of inhibitor targets. As mentioned before, receptor PD-1 was not increasingly expressed on T cells in the combination treated group

compared to the control group, excluding increased target expression as resistance mechanism.

Expression of the ligand PD-L1 has been shown to correlate with response to checkpoint inhibition in some cancers. However, PD-L1 negative tumors can also respond to checkpoint inhibition, as has been demonstrated in two tumor mouse models, generated by subcutaneous injection of PD-L1 knock-out cancer cells. The authors of the study revealed, that stromal cells, especially immune cells, contribute to PD-L1 mediated tumor escape (Kleinovink *et al*, 2017). Reports such as this highlight the crucial role of the immune microenvironment in mediating suppression of T cell responses and potentially contributing to resistance development against checkpoint inhibition. Herein it has been demonstrated that the infiltration of immune suppressive FoxP3+ T cells was generally low and was not increased by the combined treatment of αPD-1 and WBRT (section 5.7.1). Therefore, resistance most probably is not mediated by these lymphocytes in 99LN-BrM. Myeloid cells, however, have been shown to play crucial roles in mediating resistance to checkpoint inhibition. Aslan et al. investigated myeloid cells in a mouse model of hypermutated glioblastoma. They compared microglia and infiltrating myeloid cells in mice, responding to checkpoint inhibition with mice resistant to checkpoint inhibition. This analysis revealed that in the resistant mice, tumor associated myeloid cells, especially macrophages, increasingly express anti-inflammatory markers involved in T cell suppression. These markers included PD-L1. Furthermore, PD-L1 expression on myeloid cells strongly negatively correlated with response to checkpoint inhibition (Aslan *et al*, 2020). Intravital imaging of a skinfold tumor mouse model (MC38) revealed that tumor associated macrophages can take up therapeutic antibodies against PD-1. By removal of the antibodies from the surface of tumor infiltrating T cells, PD-1 receptor was liberated, and T cells were inactivated rapidly in the TME. Simultaneous inhibition of αPD-1 uptake by macrophages, significantly prolonged the efficacy of checkpoint inhibition (Arlauckas *et al*, 2017). Results such as these highlight the crucial role infiltrating myeloid cells, such as macrophages, can play in inducing resistance to checkpoint inhibition.

To evaluate the influence of myeloid cells on immune suppression and acquired resistance in 99LN-BrM, the infiltration of these cells after radio immunotherapy with αPD-1 was investigated in detail in this thesis. It has been demonstrated that breast cancer BrM in general leads to recruitment of PD-L1+ myeloid cells from the periphery, whereas resident BrM-associated microglia barely express PD-L1. αPD-1, applied as monotherapy or in combination with radiotherapy, did not lead to increased infiltration of total blood borne myeloid cells. However, it led to further increase in infiltration of PD-L1+ myeloid cells compared to the control group. PD-L1+ MDM especially greatly infiltrated 99LN-BrM in both checkpoint inhibitor treated groups. These results allow the conclusion that infiltrating PD-L1+ myeloid cells and,

especially, macrophages, prevent long-term efficacy of checkpoint inhibition. Resident microglia on the other hand do not seem to play a crucial role in the PD-1 mediated inhibition of tumor infiltrating T cells, as they barely express PD-L1, even in the BrM context (section 5.7.2).

To compare the T cell inhibitory capacity of blood borne macrophages and microglia, T cell activation assays were performed. These assays also served to investigate, if tumor education plays a role in the T cell inhibitory capacity of the myeloid cell types. Moreover, it had to be confirmed, that the PD-1/PD-L1 axis is a crucial part of myeloid mediated T cell inhibition. It has been shown that T cells cocultured with the microglia cell line EOC2 express the activation marker CD69 more frequently than when incubated with BMDM or 99LN-BrM cells. However, uneducated BMDM, or 99LN-BrM cells alone, were not sufficient to decrease T cell activity below the baseline. T cell activity was only reduced when BMDM and tumor cells were co-cultured, or when BMDM were pre-stimulated with tumor conditioned media. Furthermore, addition of αPD-1 to the coculture of 99LN-BrM cells, preconditioned BMDM and T cells, increased the activity of cytotoxic T cells significantly (section 5.7.3). These results demonstrate that (1) blood borne macrophages have a greater potential to inhibit T cell activity than resident microglia, (2) education by tumor cells polarizes macrophages towards a phenotype which is more potent to inhibit T cell activation, (3) secreted factors play a role in this polarization and (4) the inhibition of T cells by tumor educated BMDM is partly, but not exclusively, mediated by the PD-1/PD-L1 axis. These results also confirm the data obtained from the *in vivo* combination trial, indicating that contrary to microglia, MDM are a crucial component in preventing long-term efficacy of radio-immunotherapy with αPD-1. The results are in line with recently published transcription data of tumor associated MDM and microglia in a lung cancer BrM mouse model. This study revealed that BrM associated microglia expressed genes connected to housekeeping functions including synaptic pruning, and to host defense mechanisms, whereas MDM displayed expression profiles related to wound healing, antigen presentation and immune suppression. (Schulz *et al*, 2020). Taken together, the results from this thesis and of the study by Schulz et al., lead to the hypothesis that microglia maintain a pro-inflammatory phenotype in the BrM context, whereas infiltrating MDM acquire an immune-suppressive tumor-promoting phenotype. The increased infiltration of immune-suppressive PD-L1+ MDM into BrM after checkpoint inhibition, observed in this thesis, led to acquired resistance and prevented long-term efficacy of radio immunotherapy with αPD-1. To lift myeloid mediated immune suppression and prolong efficacy of the combination therapy (αPD-1+WBRT), different myeloid targeting strategies have been applied in the scope of this thesis and will be discussed in the following section.

6.7. Targeting of myeloid cells to lift immune suppression in breast cancer brain metastasis

In this thesis, two strategies have been applied to target macrophages simultaneously with combination therapy with αPD-1+WBRT. One strategy was aimed at blocking the recruitment of potentially immune suppressive myeloid cells, including MDM, to the BrM lesions. To achieve this, an inhibitor targeting the chemokine receptor CXCR4 was used. Another approach was aimed at targeting all macrophages, including MDM and microglia, via CSF1R-inhibition.

It has been shown in the past that myeloid cells not only play a role in suppressing adaptive immunity, but also foster tumor regrowth after radiotherapy (Ahn *et al*, 2010). In a glioblastoma mouse model, radiotherapy led to increased hypoxia in the brain tumor lesions. Hypoxia in turn led to the upregulation of CXCL12 expression, in part induced by hypoxia-inducible factor 1-alpha (HIF-1α). Interestingly, CXCL12 promoted the recruitment of CXCR4+ myeloid cells, which fostered revascularization of tumors after radiotherapy. The blockade of CXCR4 with the inhibitor, also tested in this project (AMD3100), led to inhibition of myeloid cell recruitment and improved the response to radiotherapy (Kioi *et al*, 2010). Similar results were obtained in a rat brain tumor model. Here, CXCL12 was inhibited by the spiegelmer NOX-A12. The combination of NOX-A12 with radiotherapy significantly decreased tumor burden and improved survival, compared to radiotherapy alone (Liu *et al*, 2014). These data, led to the conclusion that inhibition of the CXCR4/CXCL12 axis bears the potential to increase the efficacy of radiotherapy, in addition to increasing the efficacy of checkpoint inhibitors, by decreasing recruitment of immune suppressive macrophages.

In vitro experiments, performed in the scope of this thesis, confirmed CXCL12 expression by the brain homing breast cancer cell lines TS1-BrM and 99LN-BrM (section 5.8.1). There have been reports, indicating that high CXCR4 expression by tumors can lead to increased proliferation and metastasis of cancer cells (Guo *et al*, 2016). However, analysis of the brain homing breast cancer cells in this thesis revealed only low CXCR4 expression, compared to BMDM, which expressed CXCR4 at a remarkably high level. Furthermore, expression of the ligand CXCL12 by the cancer cells was not enhanced after IR with 10 Gy (section 5.8.1). This, however, is not surprising, as the cells were kept under standard culture conditions with optimal oxygenation and supply of nutrients. HIF-1α induction, followed by upregulation of CXCL12, expression is not to be expected under these conditions. Moreover, the results obtained from *in vitro* migration assays demonstrated, that 99LN-BrM cells are capable of recruiting BMDM. BMDM and 99LN-BrM cells were physically separated by a porous membrane in these assays and had no direct contact when the assay was initiated.

This allows the conclusion that the observed migration of BMDM to 99LN-BrM was mediated by secreted factors. The addition of the CXCR4 inhibitor AMD3100 to the assay, decreased the migration of BMDM to the breast cancer cells significantly (section 5.8.2). This confirms the hypothesis that the CXCR4/CXCL12 axis plays a role in the recruitment of macrophages by 99LN-BrM cells. Again, irradiation with 10 Gy did not induce significant changes. Hypothetically, CXCL12 expression and recruitment of macrophages in the *in vivo* scenario could be much higher, compared to the *in vitro* scenario, due to optimal oxygenation of cells *in vitro*. BrM, however, are expected to contain hypoxic areas. As mentioned before, RT can induce destruction of vessels. The resulting increase of hypoxia can lead to induction of HIF1α expression, followed by increased CXCL12 secretion (Kioi *et al*, 2010). AMD3100, therefore, harbors the potential not only to prolong the efficacy of checkpoint inhibition by reducing myeloid mediated immune suppression, but also to prolong the efficacy of radiotherapy by preventing revascularization of BrM.

To test this hypothesis, AMD3100 was combined with αPD-1 + WBRT *in vivo* in the 99LN-BrM model. To evaluate the effect of the drug on BrM progression without influence of other treatments, monotherapy was tested additionally. In contrary to the results reported for glioblastoma, AMD3100 did not slow down BrM progression and did not improve survival, neither in combination with WBRT+αPD-1 nor as monotherapy (section 5.8.3). These results demonstrate that even though BrM share the same TME with primary brain tumors, there might be crucial differences, which influence therapy responses. Analysis of the BrM lesions of mice in this trial revealed, that the ineffectiveness of AMD3100 was most likely due to the lack of inhibition of macrophage migration to the lesions. This was the case in the monotherapy and combination group. Moreover, treatment with AMD3100 led to increased infiltration of 99LN-BrM with PD-L1+ cells, especially PD-L1+ myeloid cells, instead of preventing it (section 5.8.4). CXCR4 receptor is known to be important for the homing of hematopoietic stem and progenitor cells to the bone marrow, and continued inhibition of CXCR4 was reported to lead to increased mobilization and expansion of these cells (Karpova *et al*, 2017). Therefore, it is conceivable that reduction of macrophage migration to 99LN-BrM by CXCR4 inhibition was compensated by systemic increase of the number of these cells due to massive release from the bone marrow. Moreover, AMD3100 did not lead to a complete blockade of BMDM migration to 99LN-BrM cells in *in vitro* migration assays (section 5.8.2). This indicates that other chemokine signaling pathways are involved in the recruitment of MDM to 99LN-BrM lesions. For example, 99LN-BrM cells secrete CCL2, CCL5, CXCL1 and CSF3 (Data unpublished, Anna Salamero-Boix, AG Sevenich). Indeed, neutralization of CCL2 and CXCL1 in migration assays with 99LN-BrM cells reduced the migration of BMDM and microglia towards the tumor cells *in vitro* (Data unpublished, Jessica Kondol, AG Sevenich).

It is conceivable that these pathways could also compensate the inhibition of CXCR4 receptor. In summary, these results led to the overall conclusion, that CXCR4-inhibitors are not suitable candidates for the treatment of breast cancer BrM, neither applied as monotherapy nor as adjuvant to radio-immunotherapy with αPD-1.

Another approach, chosen to target myeloid mediated immune suppression in 99LN-BrM, is the inhibition of CSF1R. Its ligands, CSF1 and IL34, are essential differentiation and survival factors for macrophages and microglia, respectively. While CSF1 is crucial for the survival of MDM, microglia can survive without CSF1, due to the presence of the alternative ligand IL34 in the brain (Rietkötter *et al*, 2015). Inhibiting the receptor to both ligands, however, affects all macrophages, including microglia, systemically.

The *in vitro* assessment of CSF1R, CSF1 and IL34 expression by BMDM, 99LN-BrM and TS1-BrM cells in the scope of this thesis, confirmed high CSF1R expression by BMDM compared to the tumor cells. CSF1, on the other hand, was highly expressed by both, BrM cells and BMDM (section 5.8.5). This is in line with reports from a glioma mouse model. Expression analysis of the glioma tissue revealed that CSF1R expression was restricted to tumor associated macrophages, whereas CSF1 was expressed by macrophages and tumor cells (Pyonteck *et al*, 2013). The authors did not investigate expression of IL34. However, analysis of IL34 expression in this thesis revealed that the ligand is expressed at a lower level by BMDM and tumor cells than CSF1 (section 5.8.5). This is in accordance with the beforementioned prevalence of IL34 expression in the brain and by microglia (Rietkötter *et al*, 2015). It is also reported in the literature, that IL34 and CSF1 expression is upregulated by glioma cells after IR in culture, as well as in the tumor tissue of glioma mouse models (Stafford *et al*, 2016). Increased expression of both ligands after IR with 10 Gy could be confirmed for the BrM cell line 99LN-BrM *in vitro* in this thesis (section 5.8.5). These results indicate that the CSF1R-CSF1/IL34 axis might play an important role in BrM, too, especially in the context of radiotherapy.

In the tumor microenvironment, CSF1R inhibition can affect macrophages in different ways. Depending on the supply of alternative survival factors in the TME, CSF1R can either lead to reeducation of macrophages, reducing their tumor promoting functions, or to their depletion (Pyonteck *et al*, 2013; Stafford *et al*, 2016). In this thesis, a brain penetrant CSF1R inhibitor was tested for its efficacy to lift myeloid mediated immune suppression from the TME of breast cancer BrM. In a glioma mouse models, CSF1R inhibition has proven exceedingly efficient in restricting tumor growth and improving survival applied as monotherapy. In this study, the CSF1R inhibitor BLZ945 successfully depleted macrophages/microglia in glioma unaffected brain areas. However, tumor associated macrophages were protected from the depletion. This protection was mediated by glioma supplied factors including CSF2, IFNγ and CXCL10.

Detailed analysis of the surviving tumor associated macrophages revealed that they were reeducated by BLZ945 in the glioma microenvironment. They had lost their tumor promoting M2 polarization and instead showed increased phagocytotic activity (Pyonteck *et al*, 2013). To achieve a reeducation of tumor promoting macrophages and harness them to fight cancer, instead of completely depleting total macrophages, sounds like the optimal scenario. Stafford and colleagues investigated the efficacy of CSF1R inhibitor PLX3397 in two different glioma models. In this study, CSF1R inhibition led to reduction of macrophages in untreated and irradiated tumors. In accordance with the theory that reeducation of macrophages is superior to depletion, the monotherapy with PLX3397 did not improve survival significantly. However, the combination with radiotherapy led to synergistic anti-tumor efficacy. Comparison of the irradiated tumors with combination treated tumors, revealed decreased recruitment of macrophages in the latter. In line with the publication of Pyonteck et al., macrophages in CSF1R inhibitor treated tumors showed decreased expression of M2 and increased expression of M1 markers (Stafford *et al*, 2016).

In this thesis, the efficacy of CSF1R inhibition to improve radio-immunotherapy with WBRT+αPD-1 was investigated. At that timepoint, it was not possible to predict, if CSF1R inhibition would lead to depletion of macrophages, when combined with radio-immunotherapy, in the breast cancer BrM model. As mentioned before, one factor secreted by glioma cells, protecting macrophages from CSF1R inhibition is IFNγ (Pyonteck *et al*, 2013). IFNγ was also reported to be secreted after radiotherapy and to be essential for mediating anti-tumor efficacy of radiotherapy in models of melanoma and colon cancer (Lugade *et al*, 2008; Gerber *et al*, 2013). Therefore, hypothetically, it would have been possible that the applied radiotherapy regimen in this thesis might have led to protection of macrophages from CSF1R mediated depletion. Moreover, it was not predictable, how addition of CSF1R-I to radio-immunotherapy with αPD-1 might affect T cell mediated anti-tumor immunity. The preclinical trial, performed in the scope of this thesis, demonstrated that addition of CSF1R-I to radio-immunotherapy with αPD-1, did not improve survival, nor was tumor growth reduced significantly. However, tumor growth was marginally decreased after three weeks. After five weeks, this effect was lost (section 5.8.6). Therefore, it is possible, that CSF1R-I elicited transient, early anti-tumor efficacy. Nevertheless, the targeting of macrophages in the scope of this thesis was aimed at finding a way of achieving long term efficacy of radio-immunotherapy. The addition of CSF1R-I, therefore, did not fulfill this requirement. There are several possible reasons for the lack of long-term efficacy of the triple treatment. Potential side effects might have led to earlier symptom development of mice compared to WBRT+αPD-1 without CSF1R-I, indicated by lower BrM volumes at the endpoints. Most prominently, the addition of CSF1R-I led to the depletion of all macrophages in BrM, including microglia, as well as to a strong reduction of T cell infiltration (section 5.8.6). In this work, it was revealed that microglia barely express

PD-L1 in 99LN-BrM and, therefore, are not expected to play an important role in the T cell inhibitory PD-1/PD-L1 axis (section 5.5.2). Moreover, transcription analysis in glioma models and lung cancer BrM indicated that while MDM are polarized to an immune suppressive pro-tumor phenotype in the brain TME, microglia maintain pro inflammatory functions (Bowman *et al*, 2016; Schulz *et al*, 2020). This is in line with abovementioned publications, which indicate that the reeducation of recruited macrophages, induced by CSF1R inhibition, is superior to the complete depletion of total macrophages (Pyonteck *et al*, 2013; Stafford *et al*, 2016). Finally, the reduction of T cell infiltration excludes CSF1R-I as appropriate candidate to combine with checkpoint inhibition. Future studies should aim at a more specific targeting of infiltrating macrophages, while sparing lymphocytes and brain resident microglia. Moreover, the distinct functions of different macrophage populations in breast cancer BrM must be studied in more detail.

6.8. Outlook

Within this thesis, it was investigated if BrM of low immunogenicity can be sensitized to immune checkpoint inhibition by standard of care radiotherapy. It was revealed that all cell populations, essential for checkpoint inhibition, are present in breast cancer BrM, including exhausted clonally expanded T cells. Indeed, the combination of αPD-1+ WBRT showed anti-tumor efficacy, superior to both monotherapies. Analysis of combination treated BrM showed increased infiltration of T cells, crucial for a potent anti-tumor immune response. In other brain tumor models, the checkpoint inhibitor αPD-1 was combined with CTLA-4 and achieved responses, superior to blocking one axis (Taggart *et al*, 2018). Therefore, it will be crucial to evaluate whether dual checkpoint blockade in combination with radiotherapy might induce long term survival of 99LN-BrM mice by strengthening adaptive immunity and overcoming the strong immune suppression in the brain TME. A deeper understanding of T cell responses in BrM will, hopefully, pave the way to the identification of new adjuvant strategies to achieve long term efficacy of radio-immunotherapy with αPD-1. To gain more knowledge on functions of distinct T cell subsets, depletion of T cell subpopulations can be performed in combination treated mice. The loss of efficacy of radio-immunotherapy after depletion of a certain T cell population would reveal its relevance and give insight on modes of action. Moreover, efferent and afferent routes of antigens and immune cells to and from brain tumors are not fully understood, yet. Current knowledge of the lymphatic system and immune drainage of the central nervous system is based on insight from inflammatory or intracranial models. However, intracranial injections require drilling a hole through the skull and meninges, with unknown consequences on the delicate immune system of the brain. Inflammatory models, unrelated to BrM, represent another system and can differ greatly, as experimental brain tumors have been shown to induce remodeling of meningeal lymphatic vessels (Hu *et al*, 2020). Therefore, to gain more insight on the lymphatic drainage in BrM specifically, it is crucial to use accurate BrM mouse models which have been generated in a non-invasive way. A solution might be the Kaede mouse model, which expresses a photoconvertible fluorescent protein. This protein can change from green to red fluorescence after exposure to a violet laser (Tomura *et al*, 2008). Using this model as intracardial BrM model, would allow labeling of T cells and tracking of T cell routes in the BrM context. This approach would also have the advantage that T cells would be primed against realistic tumor antigens, instead of making use of xenoantigens, such as OVA, which are regularly used in the field (Garzon-Muvdi *et al*, 2018). Another non-invasive method would be the transfer of fluor-labeled T cells and the tracking of these via MRI.

In this thesis it has been demonstrated that, even with the combination treatment, mice succumbed to BrM eventually. Further analysis indicated that this is due to peripheral PD-L1+ myeloid cells. Two macrophage targeting strategies were tested in preclinical trials, however,

failed to further improve efficacy of radio immunotherapy with αPD-1. In the future, it is important to confirm that the efficacy of radio immunotherapy with αPD-1 is dependent on these immune suppressive myeloid cells. This could be achieved by other strategies of recruitment blockade, such as the inhibition of the chemokine receptor CCR2, or by applying genetic depletion models, such as Cx3cr1$^{CreERT/+}$:ROSA26^{iDTR} mice, which allows selective depletion of CNS resident myeloid cells (Guldner *et al*, 2020). Another hypothesis driven approach would be the inhibition of Phosphoinositid-3-Kinase gamma (PI3Kγ), which has been demonstrated to reeducate tumor associated macrophages from immune suppressive pro-tumorigenic to inflammatory phenotypes (De Henau *et al*, 2016). A promising screening approach would be RNA-sequencing of sorted BrM-associated myeloid cell types, such as infiltrating MDM or monocytes, in opposition to resident microglia. Comparing immune suppressive signatures in these cells at different time points of radio-immunotherapy could lead to the identification of resistance mechanisms and cell types responsible for resistance development. This would unveil new targets to dampen immune suppression in breast cancer BrM in an unbiased way. More general aims for the future would be the detailed analysis of responders versus non-responders, and the investigation of other radiation regimens, which could lead to stronger induction of pro inflammatory responses than the applied regimen.

7. Literature

Adams S, Gray RJ, Demaria S, Goldstein L, Perez EA, Shulman LN, Martino S, Wang M, Jones VE, Saphner TJ, *et al* (2014) Prognostic Value of Tumor-Infiltrating Lymphocytes in Triple-Negative Breast Cancers From Two Phase III Randomized Adjuvant Breast Cancer Trials: ECOG 2197 and ECOG 1199. *J Clin Oncol* 32: 2959–2966

Ahmed KA, Stallworth DG, Kim Y, Johnstone P a. S, Harrison LB, Caudell JJ, Yu HHM, Etame AB, Weber JS & Gibney GT (2016) Clinical outcomes of melanoma brain metastases treated with stereotactic radiation and anti-PD-1 therapy. *Ann Oncol* 27: 434–441

Ahn G-O, Tseng D, Liao C-H, Dorie MJ, Czechowicz A & Brown JM (2010) Inhibition of Mac-1 (CD11b/CD18) enhances tumor response to radiation by reducing myeloid cell recruitment. *Proceedings of the National Academy of Sciences* 107: 8363–8368

Akkari L, Bowman RL, Tessier J, Klemm F, Handgraaf SM, Groot M de, Quail DF, Tillard L, Gadiot J, Huse JT, *et al* (2020) Dynamic changes in glioma macrophage populations after radiotherapy reveal CSF-1R inhibition as a strategy to overcome resistance. *Science Translational Medicine* 12

Allen NJ & Eroglu C (2017) Cell Biology of Astrocyte-Synapse Interactions. *Neuron* 96: 697–708

Anandasabapathy N, Victora GD, Meredith M, Feder R, Dong B, Kluger C, Yao K, Dustin ML, Nussenzweig MC, Steinman RM, *et al* (2011) Flt3L controls the development of radiosensitive dendritic cells in the meninges and choroid plexus of the steady-state mouse brain. *J Exp Med* 208: 1695–1705

Anderson MA, Burda JE, Ren Y, Ao Y, O'Shea TM, Kawaguchi R, Coppola G, Khakh BS, Deming TJ & Sofroniew MV (2016) Astrocyte scar formation aids central nervous system axon regeneration. *Nature* 532: 195–200

Anthes J (2020) Effects of macrophage depletion on radio-immunotherapy in breast-to-brain metastasis. *Master thesis, AG Sevenich.*

Aras S & Zaidi MR (2017) TAMeless traitors: macrophages in cancer progression and metastasis. *British Journal of Cancer* 117: 1583–1591

Arina A, Beckett M, Fernandez C, Zheng W, Pitroda S, Chmura SJ, Luke JJ, Forde M, Hou Y, Burnette B, *et al* (2019) Tumor-reprogrammed resident T cells resist radiation to control tumors. *Nat Commun* 10

Arlauckas SP, Garris CS, Kohler RH, Kitaoka M, Cuccarese MF, Yang KS, Miller MA, Carlson JC, Freeman GJ, Anthony RM, *et al* (2017) In vivo imaging reveals a tumor-associated macrophage–mediated resistance pathway in anti–PD-1 therapy. *Science Translational Medicine* 9

Arvanitis CD, Ferraro GB & Jain RK (2020) The blood–brain barrier and blood–tumour barrier in brain tumours and metastases. *Nat Rev Cancer* 20: 26–41

Ascierto PA, Del Vecchio M, Mackiewicz A, Robert C, Chiarion-Sileni V, Arance A, Lebbé C, Svane IM, McNeil C, Rutkowski P, *et al* (2020) Overall survival at 5 years of follow-up in a phase III trial comparing ipilimumab 10 mg/kg with 3 mg/kg in patients with advanced melanoma. *J Immunother Cancer* 8

Aslan K, Turco V, Blobner J, Sonner JK, Liuzzi AR, Núñez NG, De Feo D, Kickingereder P, Fischer M, Green E, *et al* (2020) Heterogeneity of response to immune checkpoint blockade in hypermutated experimental gliomas. *Nature Communications* 11: 931

Aspelund A, Antila S, Proulx ST, Karlsen TV, Karaman S, Detmar M, Wiig H & Alitalo K (2015) A dural lymphatic vascular system that drains brain interstitial fluid and macromolecules. *Journal of Experimental Medicine* 212: 991–999

Balkwill F, Charles KA & Mantovani A (2005) Smoldering and polarized inflammation in the initiation and promotion of malignant disease. *Cancer Cell* 7: 211–217

Balkwill F & Mantovani A (2001) Inflammation and cancer: back to Virchow? *Lancet* 357: 539–545

Bechmann I, Steiner B, Gimsa U, Mor G, Wolf S, Beyer M, Nitsch R & Zipp F (2002) Astrocyte-induced T cell elimination is CD95 ligand dependent. *J Neuroimmunol* 132: 60–65

Berghoff AS, Fuchs E, Ricken G, Mlecnik B, Bindea G, Spanberger T, Hackl M, Widhalm G, Dieckmann K, Prayer D, *et al* (2015) Density of tumor-infiltrating lymphocytes correlates with extent of brain edema and overall survival time in patients with brain metastases. *Oncoimmunology* 5

Berghoff AS, Lassmann H, Preusser M & Höftberger R (2013) Characterization of the inflammatory response to solid cancer metastases in the human brain. *Clin Exp Metastasis* 30: 69–81

Bingle L, Brown NJ & Lewis CE (2002) The role of tumour-associated macrophages in tumour progression: implications for new anticancer therapies. *J Pathol* 196: 254–265

Bol KF, Ellebaek E, Hoejberg L, Bagger MM, Larsen MS, Klausen TW, Køhler UH, Schmidt H, Bastholt L, Kiilgaard JF, *et al* (2019) Real-World Impact of Immune Checkpoint Inhibitors in Metastatic Uveal Melanoma. *Cancers* 11

Bos PD, Zhang XH-F, Nadal C, Shu W, Gomis RR, Nguyen DX, Minn AJ, Vijver MJ van de, Gerald WL, Foekens JA, *et al* (2009) Genes that mediate breast cancer metastasis to the brain. *Nature* 459: 1005–1009

Bowman RL, Klemm F, Akkari L, Pyonteck SM, Sevenich L, Quail DF, Dhara S, Simpson K, Gardner EE, Iacobuzio-Donahue CA, *et al* (2016) Macrophage ontogeny underlies differences in tumor-specific education in brain malignancies. *Cell Rep* 17: 2445–2459

Brahmer JR, Drake CG, Wollner I, Powderly JD, Picus J, Sharfman WH, Stankevich E, Pons A, Salay TM, McMiller TL, *et al* (2010) Phase I study of single-agent anti-programmed death-1 (MDX-1106) in refractory solid tumors: safety, clinical activity, pharmacodynamics, and immunologic correlates. *J Clin Oncol* 28: 3167–3175

Brown JM, Recht L & Strober S (2017) The Promise of Targeting Macrophages in Cancer Therapy. *Clin Cancer Res* 23: 3241–3250

Bruttger J, Karram K, Wörtge S, Regen T, Marini F, Hoppmann N, Klein M, Blank T, Yona S, Wolf Y, *et al* (2015) Genetic Cell Ablation Reveals Clusters of Local Self-Renewing Microglia in the Mammalian Central Nervous System. *Immunity* 43: 92–106

Burnet FM (1971) Immunological surveillance in neoplasia. *Transplant Rev* 7: 3–25

Burnet M (1964) Immunological factors in the process of carcinogenesis. *Br Med Bull* 20: 154–158

Cagney DN, Martin AM, Catalano PJ, Redig AJ, Lin NU, Lee EQ, Wen PY, Dunn IF, Bi WL, Weiss SE, *et al* (2017) Incidence and prognosis of patients with brain metastases at diagnosis of systemic malignancy: a population-based study. *Neuro-oncology* 19: 1511–1521

Carlson CS, Emerson RO, Sherwood AM, Desmarais C, Chung M-W, Parsons JM, Steen MS, LaMadrid-Herrmannsfeldt MA, Williamson DW, Livingston RJ, *et al* (2013) Using synthetic templates to design an unbiased multiplex PCR assay. *Nat Commun* 4: 2680

Cassetta L & Pollard JW (2018) Targeting macrophages: therapeutic approaches in cancer. *Nature Reviews Drug Discovery* 17: 887–904

Cavallaro U & Christofori G (2004) Cell adhesion and signalling by cadherins and Ig-CAMs in cancer. *Nat Rev Cancer* 4: 118–132

Chae WH, Niesel K, Schulz M, Klemm F, Joyce JA, Prümmer M, Brill B, Bergs J, Rödel F, Pilatus U, *et al* (2019) Evaluating Magnetic Resonance Spectroscopy as a Tool for Monitoring Therapeutic Response of Whole Brain Radiotherapy in a Mouse Model for Breast-to-Brain Metastasis. *Front Oncol* 9: 1324

Chamberlain MC, Baik CS, Gadi VK, Bhatia S & Chow LQM (2017) Systemic therapy of brain metastases: non–small cell lung cancer, breast cancer, and melanoma. *Neuro Oncol* 19: i1–i24

Chen H, Xu L, Li L, Liu X, Gao J & Bai Y (2018a) Inhibiting the CD8 + T cell infiltration in the tumor microenvironment after radiotherapy is an important mechanism of radioresistance. *Scientific Reports* 8: 11934

Chen L, Douglass J, Kleinberg L, Ye X, Marciscano AE, Forde PM, Brahmer J, Lipson E, Sharfman W, Hammers H, *et al* (2018b) Concurrent Immune Checkpoint Inhibitors and Stereotactic Radiosurgery for Brain Metastases in Non-Small Cell Lung Cancer, Melanoma, and Renal Cell Carcinoma. *International Journal of Radiation Oncology • Biology • Physics* 100: 916–925

Chongsathidkiet P, Jackson C, Koyama S, Loebel F, Cui X, Farber SH, Woroniecka K, Elsamadicy AA, Dechant CA, Kemeny HR, *et al* (2018) Sequestration of T cells in bone marrow in the setting of glioblastoma and other intracranial tumors. *Nature Medicine* 24: 1459

Chowdhary M, Switchenko JM, Press RH, Jhaveri J, Buchwald ZS, Blumenfeld PA, Marwaha G, Diaz A, Wang D, Abrams RA, *et al* (2018) Post-treatment neutrophil-to-lymphocyte ratio predicts for overall survival in brain metastases treated with stereotactic radiosurgery. *J Neurooncol* 139: 689–697

Corso CD, Ali AN & Diaz R (2011) Radiation-induced tumor neoantigens: imaging and therapeutic implications. *Am J Cancer Res* 1: 390–412

D'Agostino PM, Gottfried-Blackmore A, Anandasabapathy N & Bulloch K (2012) Brain dendritic cells: biology and pathology. *Acta Neuropathol* 124: 599–614

De Henau O, Rausch M, Winkler D, Campesato LF, Liu C, Cymerman DH, Budhu S, Ghosh A, Pink M, Tchaicha J, *et al* (2016) Overcoming resistance to checkpoint blockade therapy by targeting PI3Kγ in myeloid cells. *Nature* 539: 443–447

Deczkowska A, Keren-Shaul H, Weiner A, Colonna M, Schwartz M & Amit I (2018) Disease-Associated Microglia: A Universal Immune Sensor of Neurodegeneration. *Cell* 173: 1073–1081

Dewan MZ, Galloway AE, Kawashima N, Dewyngaert JK, Babb JS, Formenti SC & Demaria S (2009) Fractionated but not single-dose radiotherapy induces an immune-mediated abscopal effect when combined with anti-CTLA-4 antibody. *Clin Cancer Res* 15: 5379–5388

Dong H, Strome SE, Salomao DR, Tamura H, Hirano F, Flies DB, Roche PC, Lu J, Zhu G, Tamada K, *et al* (2002) Tumor-associated B7-H1 promotes T-cell apoptosis: A potential mechanism of immune evasion. *Nature Medicine* 8: 793–800

Dovedi SJ, Adlard AL, Lipowska-Bhalla G, McKenna C, Jones S, Cheadle EJ, Stratford IJ, Poon E, Morrow M, Stewart R, *et al* (2014) Acquired resistance to fractionated radiotherapy can be overcome by concurrent PD-L1 blockade. *Cancer Res* 74: 5458–5468

Dress RJ, Dutertre C-A, Giladi A, Schlitzer A, Low I, Shadan NB, Tay A, Lum J, Kairi MFBM, Hwang YY, *et al* (2019) Plasmacytoid dendritic cells develop from Ly6D + lymphoid progenitors distinct from the myeloid lineage. *Nature Immunology* 20: 852–864

Dunn GP, Bruce AT, Ikeda H, Old LJ & Schreiber RD (2002) Cancer immunoediting: from immunosurveillance to tumor escape. *Nat Immunol* 3: 991–998

Dunn GP, Old LJ & Schreiber RD (2004) The Three Es of Cancer Immunoediting. *Annu Rev Immunol* 22: 329–360

Ehrlich P (1909) Üeber den jetzigen Stand der Karzinomforschung. *Ned. Tijdschr. Geneeskd.* 1909; 5:273-290

Ene CI, Kreuser SA, Jung M, Zhang H, Arora S, White Moyes K, Szulzewsky F, Barber J, Cimino PJ, Wirsching H-G, *et al* (2020) Anti-PD-L1 antibody direct activation of macrophages contributes to a radiation-induced abscopal response in glioblastoma. *Neuro-oncology* 22: 639–651

Facciabene A, Motz GT & Coukos G (2012) T Regulatory Cells: Key Players in Tumor Immune Escape and Angiogenesis. *Cancer Res* 72: 2162–2171

Fidler IJ (2015) The Biology of Brain Metastasis: Challenges for Therapy. *Cancer J* 21: 284–293

Flavell RA, Sanjabi S, Wrzesinski SH & Licona-Limón P (2010) The polarization of immune cells in the tumour environment by TGFβ. *Nat Rev Immunol* 10

Galea I, Bernardes-Silva M, Forse PA, van Rooijen N, Liblau RS & Perry VH (2007) An antigen-specific pathway for CD8 T cells across the blood-brain barrier. *J Exp Med* 204: 2023–2030

Garrido F & Algarra I (2001) MHC antigens and tumor escape from immune surveillance. *Adv Cancer Res* 83: 117–158

Garzon-Muvdi T, Theodros D, Luksik AS, Maxwell R, Kim E, Jackson CM, Belcaid Z, Ganguly S, Tyler B, Brem H, *et al* (2018) Dendritic cell activation enhances anti-PD-1 mediated immunotherapy against glioblastoma. *Oncotarget* 9: 20681–20697

Gay LJ & Felding-Habermann B (2011) Contribution of platelets to tumour metastasis. *Nat Rev Cancer* 11: 123–134

Gerber SA, Sedlacek AL, Cron KR, Murphy SP, Frelinger JG & Lord EM (2013) IFN-γ Mediates the Antitumor Effects of Radiation Therapy in a Murine Colon Tumor. *Am J Pathol* 182: 2345–2354

Ginhoux F, Greter M, Leboeuf M, Nandi S, See P, Gokhan S, Mehler MF, Conway SJ, Ng LG, Stanley ER, *et al* (2010) Fate mapping analysis reveals that adult microglia derive from primitive macrophages. *Science* 330: 841–845

Gong X, Hou Z, Endsley MP, Gronseth EI, Rarick KR, Jorns JM, Yang Q, Du Z, Yan K, Bordas ML, *et al* (2019) Interaction of tumor cells and astrocytes promotes breast cancer brain metastases through TGF-β2/ANGPTL4 axes. *npj Precis Onc* 3: 1–9

Goswami KK, Ghosh T, Ghosh S, Sarkar M, Bose A & Baral R (2017) Tumor promoting role of anti-tumor macrophages in tumor microenvironment. *Cell Immunol* 316: 1–10

Grayson JM, Harrington LE, Lanier JG, Wherry EJ & Ahmed R (2002) Differential Sensitivity of Naive and Memory CD8+ T Cells to Apoptosis in Vivo. *The Journal of Immunology* 169: 3760–3770

Griguolo G, Tosi A, Guarneri V, Dieci MV, Fineberg S, Ventura A, Bauchet L, Jacob J, Rigau V, Jacot W, *et al* (2020) Immune microenvironment profiling of breast cancer brain metastases using multiplex immunofluorescence. *JCO* 38: 2526–2526

Gril B, Paranjape AN, Woditschka S, Hua E, Dolan EL, Hanson J, Wu X, Kloc W, Izycka-Swieszewska E, Duchnowska R, *et al* (2018) Reactive astrocytic S1P3 signaling modulates the blood-tumor barrier in brain metastases. *Nat Commun* 9: 2705

Guldner IH, Wang Q, Yang L, Golomb SM, Zhao Z, Lopez JA, Brunory A, Howe EN, Zhang Y, Palakurthi B, *et al* (2020) CNS-Native Myeloid Cells Drive Immune Suppression in the Brain Metastatic Niche through Cxcl10. *Cell* 183: 1234-1248.e25

Guo F, Wang Y, Liu J, Mok SC, Xue F & Zhang W (2016) CXCL12/CXCR4: a symbiotic bridge linking cancer cells and their stromal neighbors in oncogenic communication networks. *Oncogene* 35: 816–826

Gupta A, Probst HC, Vuong V, Landshammer A, Muth S, Yagita H, Schwendener R, Pruschy M, Knuth A & Broek M van den (2012) Radiotherapy Promotes Tumor-Specific Effector CD8+ T Cells via Dendritic Cell Activation. *The Journal of Immunology* 189: 558–566

Hanahan D & Weinberg RA (2000) The hallmarks of cancer. *Cell* 100: 57–70

Hanahan D & Weinberg RA (2011) Hallmarks of Cancer: The Next Generation. *Cell* 144: 646–674

Harris MG, Hulseberg P, Ling C, Karman J, Clarkson BD, Harding JS, Zhang M, Sandor A, Christensen K, Nagy A, *et al* (2014) Immune privilege of the CNS is not the consequence of limited antigen sampling. *Sci Rep* 4: 4422

Harter PN, Bernatz S, Scholz A, Zeiner PS, Zinke J, Kiyose M, Blasel S, Beschorner R, Senft C, Bender B, *et al* (2015) Distribution and prognostic relevance of tumor-infiltrating lymphocytes (TILs) and PD-1/PD-L1 immune checkpoints in human brain metastases. *Oncotarget* 6: 40836–40849

Head JR & Griffin WS (1985) Functional capacity of solid tissue transplants in the brain: evidence for immunological privilege. *Proc R Soc Lond, B, Biol Sci* 224: 375–387

Hodi FS, O'Day SJ, McDermott DF, Weber RW, Sosman JA, Haanen JB, Gonzalez R, Robert C, Schadendorf D, Hassel JC, *et al* (2010) Improved survival with ipilimumab in patients with metastatic melanoma. *N Engl J Med* 363: 711–723

Holmgaard RB, Zamarin D, Li Y, Gasmi B, Munn DH, Allison JP, Merghoub T & Wolchok JD (2015) Tumor-expressed IDO recruits and activates MDSCs in a Treg-dependent manner. *Cell Rep* 13: 412–424

Hong JH, Chiang CS, Tsao CY, Lin PY, McBride WH & Wu CJ (1999) Rapid induction of cytokine gene expression in the lung after single and fractionated doses of radiation. *Int J Radiat Biol* 75: 1421–1427

Houghton J, Stoicov C, Nomura S, Rogers AB, Carlson J, Li H, Cai X, Fox JG, Goldenring JR & Wang TC (2004) Gastric Cancer Originating from Bone Marrow-Derived Cells. *Science* 306: 1568–1571

Hove HV, Martens L, Scheyltjens I, Vlaminck KD, Antunes ARP, Prijck SD, Vandamme N, Schepper SD, Isterdael GV, Scott CL, *et al* (2019) A single-cell atlas of mouse brain macrophages reveals unique transcriptional identities shaped by ontogeny and tissue environment. *Nat Neurosci* 22: 1021–1035

Hu X, Deng Q, Ma L, Li Q, Chen Y, Liao Y, Zhou F, Zhang C, Shao L, Feng J, *et al* (2020) Meningeal lymphatic vessels regulate brain tumor drainage and immunity. *Cell Res* 30: 229–243

Hui R, Garon EB, Goldman JW, Leighl NB, Hellmann MD, Patnaik A, Gandhi L, Eder JP, Ahn M-J, Horn L, *et al* (2017) Pembrolizumab as first-line therapy for patients with PD-L1-positive advanced non-small cell lung cancer: a phase 1 trial. *Annals of Oncology* 28: 874–881

Ishida Y, Agata Y, Shibahara K & Honjo T (1992) Induced expression of PD-1, a novel member of the immunoglobulin gene superfamily, upon programmed cell death. *EMBO J* 11: 3887–3895

Jackson CM, Kochel CM, Nirschl CJ, Durham NM, Ruzevick J, Alme A, Francica BJ, Elias J, Daniels A, Dubensky TW, *et al* (2016) Systemic Tolerance Mediated by Melanoma Brain Tumors Is Reversible by Radiotherapy and Vaccination. *Clin Cancer Res* 22: 1161–1172

Jacobs JFM, Idema AJ, Bol KF, Nierkens S, Grauer OM, Wesseling P, Grotenhuis JA, Hoogerbrugge PM, de Vries IJM & Adema GJ (2009) Regulatory T cells and the PD-L1/PD-1 pathway mediate immune suppression in malignant human brain tumors. *Neuro Oncol* 11: 394–402

Jain N, Nguyen H, Chambers C & Kang J (2010) Dual function of CTLA-4 in regulatory T cells and conventional T cells to prevent multiorgan autoimmunity. *Proc Natl Acad Sci U S A* 107: 1524–1528

Jiang WG, Sanders AJ, Katoh M, Ungefroren H, Gieseler F, Prince M, Thompson SK, Zollo M, Spano D, Dhawan P, *et al* (2015) Tissue invasion and metastasis: Molecular, biological and clinical perspectives. *Seminars in Cancer Biology* 35: 244–275

Qian JM, Martin AM, Martin K, Hammoudeh L, Catalano P, Hodi FS, Cagney DN, Haas-Kogan DA, Schoenfeld JD & Aizer AA (2020) Response rate and local recurrence after concurrent immune checkpoint therapy and radiotherapy for non-small cell lung cancer and melanoma brain metastases. *Cancer* 126: 5274-5282

Jordão MJC, Sankowski R, Brendecke SM, Sagar, Locatelli G, Tai Y-H, Tay TL, Schramm E, Armbruster S, Hagemeyer N, *et al* (2019) Single-cell profiling identifies myeloid cell subsets with distinct fates during neuroinflammation. *Science* 363

Jung S, Aliberti J, Graemmel P, Sunshine MJ, Kreutzberg GW, Sher A & Littman DR (2000) Analysis of Fractalkine Receptor CX3CR1 Function by Targeted Deletion and Green Fluorescent Protein Reporter Gene Insertion. *Mol Cell Biol* 20: 4106–4114

Kaler P, Galea V, Augenlicht L & Klampfer L (2010) Tumor associated macrophages protect colon cancer cells from TRAIL-induced apoptosis through IL-1beta-dependent stabilization of Snail in tumor cells. *PLoS ONE* 5: e11700

Kamath SD & Kumthekar PU (2018) Immune Checkpoint Inhibitors for the Treatment of Central Nervous System (CNS) Metastatic Disease. *Front Oncol* 8: 414

Karpova D, Ritchey JK, Holt MS, Abou-Ezzi G, Monlish D, Batoon L, Millard S, Spohn G, Wiercinska E, Chendamarai E, *et al* (2017) Continuous blockade of CXCR4 results in dramatic mobilization and expansion of hematopoietic stem and progenitor cells. *Blood* 129: 2939–2949

Keren-Shaul H, Spinrad A, Weiner A, Matcovitch-Natan O, Dvir-Szternfeld R, Ulland TK, David E, Baruch K, Lara-Astaiso D, Toth B, *et al* (2017) A Unique Microglia Type Associated with Restricting Development of Alzheimer's Disease. *Cell* 169: 1276-1290.e17

Kessenbrock K, Plaks V & Werb Z (2010) Matrix metalloproteinases: regulators of the tumor microenvironment. *Cell* 141: 52–67

Kienast Y, Baumgarten L von, Fuhrmann M, Klinkert WEF, Goldbrunner R, Herms J & Winkler F (2010) Real-time imaging reveals the single steps of brain metastasis formation. *Nat Med* 16: 116–122

Kioi M, Vogel H, Schultz G, Hoffman RM, Harsh GR & Brown JM (2010) Inhibition of vasculogenesis, but not angiogenesis, prevents the recurrence of glioblastoma after irradiation in mice. *J Clin Invest* 120: 694–705

Klein CA (2008) The Metastasis Cascade. *Science* 321: 1785–1787

Kleinovink JW, Marijt KA, Schoonderwoerd MJA, van Hall T, Ossendorp F & Fransen MF (2017) PD-L1 expression on malignant cells is no prerequisite for checkpoint therapy. *Oncoimmunology* 6: e1294299

Klemm F, Maas RR, Bowman RL, Kornete M, Soukup K, Nassiri S, Brouland J-P, Iacobuzio-Donahue CA, Brennan C, Tabar V, *et al* (2020) Interrogation of the Microenvironmental Landscape in Brain Tumors Reveals Disease-Specific Alterations of Immune Cells. *Cell* 181: 1643-1660

Klemm F, Möckl A, Salamero-Boix A, Alekseeva T, Schäffer A, Schulz M, Niesel K, Maas RR, Groth M, Elie BT, *et al*. Compensatory CSF2-driven macrophage activation promotes adaptive resistance to CSF1R inhibition in breast-to-brain metastasis. *Manuscript in revision.*

Koh YW, Choi J-H, Ahn MS, Choi YW & Lee HW (2016) Baseline neutrophil–lymphocyte ratio is associated with baseline and subsequent presence of brain metastases in advanced non-small-cell lung cancer. *Sci Rep* 6: 38585

Korin B, Ben-Shaanan TL, Schiller M, Dubovik T, Azulay-Debby H, Boshnak NT, Koren T & Rolls A (2017) High-dimensional, single-cell characterization of the brain's immune compartment. *Nature Neuroscience* 20: 1300–1309

Korn T & Kallies A (2017) T cell responses in the central nervous system. *Nature Reviews Immunology* 17: 179–194

Kroemer G, Senovilla L, Galluzzi L, André F & Zitvogel L (2015) Natural and therapy-induced immunosurveillance in breast cancer. *Nat Med* 21: 1128–1138

Krombach J, Hennel R, Brix N, Orth M, Schoetz U, Ernst A, Schuster J, Zuchtriegel G, Reichel CA, Bierschenk S, *et al* (2018) Priming anti-tumor immunity by radiotherapy: Dying tumor cell-derived DAMPs trigger endothelial cell activation and recruitment of myeloid cells. *Oncoimmunology* 8: e1523097

Kümpers C, Jokic M, Haase O, Offermann A, Vogel W, Grätz V, Langan EA, Perner S & Terheyden P (2019) Immune Cell Infiltration of the Primary Tumor, Not PD-L1 Status, Is Associated With Improved Response to Checkpoint Inhibition in Metastatic Melanoma. *Front Med* 6: 27

Lauko A, Thapa B, Venur VA & Ahluwalia MS (2018) Management of Brain Metastases in the New Era of Checkpoint Inhibition. *Curr Neurol Neurosci Rep* 18: 70

Leach DR, Krummel MF & Allison JP (1996) Enhancement of antitumor immunity by CTLA-4 blockade. *Science* 271: 1734–1736

Lee KY, Kim Y-J, Yoo H, Lee SH, Park JB & Kim HJ (2011) Human brain endothelial cell-derived COX-2 facilitates extravasation of breast cancer cells across the blood-brain barrier. *Anticancer Res* 31: 4307–4313

Lee Y, Auh SL, Wang Y, Burnette B, Wang Y, Meng Y, Beckett M, Sharma R, Chin R, Tu T, *et al* (2009) Therapeutic effects of ablative radiation on local tumor require CD8+ T cells: changing strategies for cancer treatment. *Blood* 114: 589–595

Lehrer EJ, McGee HM, Peterson JL, Vallow L, Ruiz-Garcia H, Zaorsky NG, Sharma S & Trifiletti DM (2018) Stereotactic Radiosurgery and Immune Checkpoint Inhibitors in the Management of Brain Metastases. *Int J Mol Sci* 19: 3054

Leibold AT, Monaco GN & Dey M (2019) The role of the immune system in brain metastasis. *Curr Neurobiol* 10: 33–48

Liu S-C, Alomran R, Chernikova SB, Lartey F, Stafford J, Jang T, Merchant M, Zboralski D, Zöllner S, Kruschinski A, *et al* (2014) Blockade of SDF-1 after irradiation inhibits tumor recurrences of autochthonous brain tumors in rats. *Neuro-oncology* 16: 21–28

Liu Y, Kosaka A, Ikeura M, Kohanbash G, Fellows-Mayle W, Snyder LA & Okada H (2013) Premetastatic soil and prevention of breast cancer brain metastasis. *Neuro-oncology* 15: 891–903

Lorger M, Andreou T, Fife C & James F (2019) Immune Checkpoint Blockade – How Does It Work in Brain Metastases? *Front Mol Neurosci* 12: 282

Louveau A, Smirnov I, Keyes TJ, Eccles JD, Rouhani SJ, Peske JD, Derecki NC, Castle D, Mandell JW, Lee KS, *et al* (2015) Structural and functional features of central nervous system lymphatic vessels. *Nature* 523: 337–341

Low D & Ginhoux F (2018) Recent advances in the understanding of microglial development and homeostasis. *Cellular Immunology* 330: 68–78

Lugade AA, Sorensen EW, Gerber SA, Moran JP, Frelinger JG & Lord EM (2008) Radiation-Induced IFN-γ Production within the Tumor Microenvironment Influences Antitumor Immunity. *The Journal of Immunology* 180: 3132–3139

Mahmoud SMA, Lee AHS, Paish EC, Macmillan RD, Ellis IO & Green AR (2012) Tumour-infiltrating macrophages and clinical outcome in breast cancer. *J Clin Pathol* 65: 159–163

Maleki Vareki S, Garrigós C & Duran I (2017) Biomarkers of response to PD-1/PD-L1 inhibition. *Crit Rev Oncol Hematol* 116: 116–124

Manda K, Glasow A, Paape D & Hildebrandt G (2012) Effects of ionizing radiation on the immune system with special emphasis on the interaction of dendritic and T cells. *Front Oncol* 2: 102

Mansfield AS, Ren H, Sutor S, Sarangi V, Nair A, Davila J, Elsbernd LR, Udell JB, Dronca RS, Park S, *et al* (2018) Contraction of T cell richness in lung cancer brain metastases. *Scientific Reports* 8: 2171

Mantovani A & Locati M (2016) Macrophage Metabolism Shapes Angiogenesis in Tumors. *Cell Metabolism* 24: 653–654

Mantovani A, Sica A, Sozzani S, Allavena P, Vecchi A & Locati M (2004) The chemokine system in diverse forms of macrophage activation and polarization. *Trends in Immunology* 25: 677–686

Marina N, Turovsky E, Christie IN, Hosford PS, Hadjihambi A, Korsak A, Ang R, Mastitskaya S, Sheikhbahaei S, Theparambil SM, *et al* (2018) Brain metabolic sensing and metabolic signaling at the level of an astrocyte. *Glia* 66: 1185–1199

McTyre E, Scott J & Chinnaiyan P (2013) Whole brain radiotherapy for brain metastasis. *Surg Neurol Int* 4: 236-244

Mitsuya K, Nakasu Y, Kurakane T, Hayashi N, Harada H & Nozaki K (2017) Elevated preoperative neutrophil-to-lymphocyte ratio as a predictor of worse survival after resection in patients with brain metastasis. *Journal of Neurosurgery* 127: 433–437

Mole RH (1953) Whole body irradiation; radiobiology or medicine? *Br J Radiol* 26: 234–241

Mollica Poeta V, Massara M, Capucetti A & Bonecchi R (2019) Chemokines and Chemokine Receptors: New Targets for Cancer Immunotherapy. *Front Immunol* 10

Mrdjen D, Pavlovic A, Hartmann FJ, Schreiner B, Utz SG, Leung BP, Lelios I, Heppner FL, Kipnis J, Merkler D, *et al* (2018) High-Dimensional Single-Cell Mapping of Central Nervous System Immune Cells Reveals Distinct Myeloid Subsets in Health, Aging, and Disease. *Immunity* 48: 380-395.e6

Murphy JB & Sturm E (1923) Conditions determining the transplantability of tissues in the brain. *J Exp Med* 38: 183–197

Neman J, Termini J, Wilczynski S, Vaidehi N, Choy C, Kowolik CM, Li H, Hambrecht AC, Roberts E & Jandial R (2014) Human breast cancer metastases to the brain display GABAergic properties in the neural niche. *Proc Natl Acad Sci U S A* 111: 984–989

Butovsky O, Jedrychowski MP, Moore CS, Cialic R, Lanser AJ, Gabriely G, Koegelsperger T, Dake B, Wu PM, Doykan CE, *et al* (2014) Identification of a Unique TGF-β-dependent Molecular and Functional Signature in Microglia. *Nature neuroscience* 17: 131-143

Ogiya R, Niikura N, Kumaki N, Yasojima H, Iwasa T, Kanbayashi C, Oshitanai R, Tsuneizumi M, Watanabe K, Matsui A, *et al* (2017) Comparison of immune microenvironments between primary tumors and brain metastases in patients with breast cancer. *Oncotarget* 8: 103671–103681

Onder TT, Gupta PB, Mani SA, Yang J, Lander ES & Weinberg RA (2008) Loss of E-Cadherin Promotes Metastasis via Multiple Downstream Transcriptional Pathways. *Cancer Res* 68: 3645–3654

Ostroumov D, Fekete-Drimusz N, Saborowski M, Kühnel F & Woller N (2018) CD4 and CD8 T lymphocyte interplay in controlling tumor growth. *Cell Mol Life Sci* 75: 689–713

Paget S (1889) The distribution of secondary growths in cancer of the breast. *The Lancet* 133: 571–573

Pardoll DM (2012) The blockade of immune checkpoints in cancer immunotherapy. *Nature Reviews Cancer* 12: 252–264

Peters S, Reck M, Smit EF, Mok T & Hellmann MD (2019) How to make the best use of immunotherapy as first-line treatment of advanced/metastatic non-small-cell lung cancer. *Annals of Oncology* 30: 884–896

Ponomarev V, Doubrovin M, Serganova I, Vider J, Shavrin A, Beresten T, Ivanova A, Ageyeva L, Tourkova V, Balatoni J, *et al* (2004) A novel triple-modality reporter gene for whole-body fluorescent, bioluminescent, and nuclear noninvasive imaging. *Eur J Nucl Med Mol Imaging* 31: 740–751

Prins RM, Shu CJ, Radu CG, Vo DD, Khan-Farooqi H, Soto H, Yang M-Y, Lin M-S, Shelly S, Witte ON, *et al* (2008) Anti-tumor activity and trafficking of self, tumor-specific T cells against tumors located in the brain,. *Cancer Immunol Immunother* 57: 1279–1289

Pukrop T, Dehghani F, Chuang H-N, Lohaus R, Bayanga K, Heermann S, Regen T, Rossum DV, Klemm F, Schulz M, *et al* (2010) Microglia promote colonization of brain tissue by breast cancer cells in a Wnt-dependent way. *Glia* 58: 1477–1489

Pyonteck SM, Akkari L, Schuhmacher AJ, Bowman RL, Sevenich L, Quail DF, Olson OC, Quick ML, Huse JT, Teijeiro V, *et al* (2013) CSF-1R inhibition alters macrophage polarization and blocks glioma progression. *Nat Med* 19: 1264–1272

Qin DX, Zheng R, Tang J, Li JX & Hu YH (1990) Influence of radiation on the blood-brain barrier and optimum time of chemotherapy. *Int J Radiat Oncol Biol Phys* 19: 1507–1510

Qu Y, Jin S, Zhang A, Zhang B, Shi X, Wang J & Zhao Y (2010) Gamma-ray resistance of regulatory CD4+CD25+Foxp3+ T cells in mice. *Radiat Res* 173: 148–157

Quail DF & Joyce JA (2017) The microenvironmental landscape of brain tumors. *Cancer Cell* 31: 326–341

Ramakrishna R & Formenti S (2019) Radiosurgery and Immunotherapy in the Treatment of Brain Metastases. *World Neurosurg* 130: 615–622

Raper D, Louveau A & Kipnis J (2016) How Do Meningeal Lymphatic Vessels Drain the CNS? *Trends in Neurosciences* 39: 581–586

Rausch MP & Hastings KT (2017) Immune Checkpoint Inhibitors in the Treatment of Melanoma: From Basic Science to Clinical Application. In *Cutaneous Melanoma: Etiology and Therapy*, Ward WH & Farma JM (eds) Brisbane (AU): Codon Publications

Reits EA, Hodge JW, Herberts CA, Groothuis TA, Chakraborty M, Wansley EK, Camphausen K, Luiten RM, de Ru AH, Neijssen J, *et al* (2006) Radiation modulates the peptide repertoire, enhances MHC class I expression, and induces successful antitumor immunotherapy. *J Exp Med* 203: 1259–1271

Rietkötter E, Bleckmann A, Bayerlová M, Menck K, Chuang H-N, Wenske B, Schwartz H, Erez N, Binder C, Hanisch U-K, *et al* (2015) Anti-CSF-1 treatment is effective to prevent carcinoma invasion induced by monocyte-derived cells but scarcely by microglia. *Oncotarget* 6: 15482–15493

Robins HS, Campregher PV, Srivastava SK, Wacher A, Turtle CJ, Kahsai O, Riddell SR, Warren EH & Carlson CS (2009) Comprehensive assessment of T-cell receptor beta-chain diversity in alphabeta T cells. *Blood* 114: 4099–4107

Rubin P, Gash DM, Hansen JT, Nelson DF & Williams JP (1994) Disruption of the blood-brain barrier as the primary effect of CNS irradiation. *Radiother Oncol* 31: 51–60

Ruffell B & Coussens LM (2015) Macrophages and therapeutic resistance in cancer. *Cancer Cell* 27: 462–472

Russo MV & McGavern DB (2015) Immune Surveillance of the CNS following Infection and Injury. *Trends in Immunology* 36: 637–650

Sakaguchi S, Miyara M, Costantino CM & Hafler DA (2010) FOXP3+ regulatory T cells in the human immune system. *Nat Rev Immunol* 10: 490–500

Sampson JH, Gunn MD, Fecci PE & Ashley DM (2020) Brain immunology and immunotherapy in brain tumours. *Nature Reviews Cancer* 20: 12–25

Schaue D, Kachikwu EL & McBride WH (2012) Cytokines in radiobiological responses: a review. *Radiat Res* 178: 505–523

Schaue D & McBride WH (2012) T lymphocytes and normal tissue responses to radiation. *Front Oncol* 2: 119

Schulz M, Michels B, Niesel K, Stein S, Farin H, Rödel F & Sevenich L (2020) Cellular and molecular changes of brain metastases-associated myeloid cells during disease progression and therapeutic response. *iScience* 23: 101178

Schulz M, Salamero-Boix A, Niesel K, Alekseeva T & Sevenich L (2019) Microenvironmental Regulation of Tumor Progression and Therapeutic Response in Brain Metastasis. *Front Immunol* 10: 1713

Seano G, Nia HT, Emblem KE, Datta M, Ren J, Krishnan S, Kloepper J, Pinho MC, Ho WW, Ghosh M, *et al* (2019) Solid stress in brain tumours causes neuronal loss and neurological dysfunction and can be reversed by lithium. *Nat Biomed Eng* 3: 230–245

Sevenich L (2019) Turning 'Cold' Into 'Hot' Tumors-Opportunities and Challenges for Radio-Immunotherapy Against Primary and Metastatic Brain Cancers. *Front Oncol* 9: 163

Sevenich L, Bowman RL, Mason SD, Quail DF, Rapaport F, Elie BT, Brogi E, Brastianos PK, Hahn WC, Holsinger LJ, *et al* (2014) Analysis of tumour- and stroma-supplied proteolytic networks reveals a brain-metastasis-promoting role for cathepsin S. *Nat Cell Biol* 16: 876–888

Shang B, Liu Y, Jiang S & Liu Y (2015) Prognostic value of tumor-infiltrating FoxP3 + regulatory T cells in cancers: a systematic review and meta-analysis. *Sci Rep* 5: 1–9

Shankaran V, Ikeda H, Bruce AT, White JM, Swanson PE, Old LJ & Schreiber RD (2001) IFNgamma and lymphocytes prevent primary tumour development and shape tumour immunogenicity. *Nature* 410: 1107–1111

Shibayama O, Yoshiuchi K, Inagaki M, Matsuoka Y, Yoshikawa E, Sugawara Y, Akechi T, Wada N, Imoto S, Murakami K, *et al* (2014) Association between adjuvant regional radiotherapy and cognitive function in breast cancer patients treated with conservation therapy. *Cancer Med* 3: 702–709

Shinde A, Akhavan D, Sedrak M, Glaser S & Amini A (2019) Shifting paradigms: whole brain radiation therapy versus stereotactic radiosurgery for brain metastases. *CNS Oncology* 8: CNS27

Shree T, Olson OC, Elie BT, Kester JC, Garfall AL, Simpson K, Bell-McGuinn KM, Zabor EC, Brogi E & Joyce JA (2011) Macrophages and cathepsin proteases blunt chemotherapeutic response in breast cancer. *Genes Dev* 25: 2465–2479

Smyth MJ, Crowe NY & Godfrey DI (2001) NK cells and NKT cells collaborate in host protection from methylcholanthrene-induced fibrosarcoma. *International Immunology* 13: 459–463

Song E, Mao T, Dong H, Boisserand LSB, Antila S, Bosenberg M, Alitalo K, Thomas J-L & Iwasaki A (2020) VEGF-C-driven lymphatic drainage enables immunosurveillance of brain tumours. *Nature* 577: 689–694

Spranger S, Luke JJ, Bao R, Zha Y, Hernandez KM, Li Y, Gajewski AP, Andrade J & Gajewski TF (2016) Density of immunogenic antigens does not explain the presence or absence of the T-cell-inflamed tumor microenvironment in melanoma. *Proc Natl Acad Sci USA* 113: E7759–E7768

Stafford JH, Hirai T, Deng L, Chernikova SB, Urata K, West BL & Brown JM (2016) Colony stimulating factor 1 receptor inhibition delays recurrence of glioblastoma after radiation by altering myeloid cell recruitment and polarization. *Neuro Oncol* 18: 797–806

Stelzer KJ (2013) Epidemiology and prognosis of brain metastases. *Surg Neurol Int* 4: 192-202

Strilic B & Offermanns S (2017) Intravascular Survival and Extravasation of Tumor Cells. *Cancer Cell* 32: 282–293

Su S, Liao J, Liu J, Huang D, He C, Chen F, Yang L, Wu W, Chen J, Lin L, *et al* (2017) Blocking the recruitment of naive CD4 + T cells reverses immunosuppression in breast cancer. *Cell Research* 27: 461–482

Sugihara AQ, Rolle CE & Lesniak MS (2009) Regulatory T cells actively infiltrate metastatic brain tumors. *International Journal of Oncology* 34: 1533–1540

Suh JH, Kotecha R, Chao ST, Ahluwalia MS, Sahgal A & Chang EL (2020) Current approaches to the management of brain metastases. *Nat Rev Clin Oncol* 17: 279–299

Tabouret E, Chinot O, Metellus P, Tallet A, Viens P & Gonçalves A (2012) Recent trends in epidemiology of brain metastases: an overview. *Anticancer Res* 32: 4655–4662

Taggart D, Andreou T, Scott KJ, Williams J, Rippaus N, Brownlie RJ, Ilett EJ, Salmond RJ, Melcher A & Lorger M (2018) Anti–PD-1/anti–CTLA-4 efficacy in melanoma brain metastases depends on extracranial disease and augmentation of CD8+ T cell trafficking. *PNAS* 115: 1540–1549

Tay RE, Richardson EK & Toh HC (2020) Revisiting the role of CD4 + T cells in cancer immunotherapy—new insights into old paradigms. *Cancer Gene Therapy 28*: 5–17

Teresa Pinto A, Laranjeiro Pinto M, Patrícia Cardoso A, Monteiro C, Teixeira Pinto M, Filipe Maia A, Castro P, Figueira R, Monteiro A, Marques M, *et al* (2016) Ionizing radiation modulates human macrophages towards a pro-inflammatory phenotype preserving their pro-invasive and pro-angiogenic capacities. *Sci Rep* 6: 18765

Thomas L (1961) Cellular and humoral aspects of the hypersensitive states. *Acta Medica Scandinavica* 170: 128–128

Tomura M, Yoshida N, Tanaka J, Karasawa S, Miwa Y, Miyawaki A & Kanagawa O (2008) Monitoring cellular movement in vivo with photoconvertible fluorescence protein “Kaede” transgenic mice. *Proc Natl Acad Sci U S A* 105: 10871–10876

Trowell OA (1952) The sensitivity of lymphocytes to ionising radiation. *The Journal of Pathology and Bacteriology* 64: 687–704

Valiente M, Obenauf AC, Jin X, Chen Q, Zhang XH-F, Lee DJ, Chaft JE, Kris MG, Huse JT, Brogi E, *et al* (2014) Serpins promote cancer cell survival and vascular co-option in brain metastasis. *Cell* 156: 1002–1016

Vanpouille-Box C, Alard A, Aryankalayil MJ, Sarfraz Y, Diamond JM, Schneider RJ, Inghirami G, Coleman CN, Formenti SC & Demaria S (2017) DNA exonuclease Trex1 regulates radiotherapy-induced tumour immunogenicity. *Nat Commun* 8: 15618

Venkataramani V, Tanev DI, Strahle C, Studier-Fischer A, Fankhauser L, Kessler T, Körber C, Kardorff M, Ratliff M, Xie R, *et al* (2019) Glutamatergic synaptic input to glioma cells drives brain tumour progression. *Nature* 573: 532–538

Venkatesh HS, Morishita W, Geraghty AC, Silverbush D, Gillespie SM, Arzt M, Tam LT, Espenel C, Ponnuswami A, Ni L, *et al* (2019) Electrical and synaptic integration of glioma into neural circuits. *Nature* 573: 539–545

Vidyarthi A, Agnihotri T, Khan N, Singh S, Tewari MK, Radotra BD, Chatterjee D & Agrewala JN (2019) Predominance of M2 macrophages in gliomas leads to the suppression of local and systemic immunity. *Cancer Immunol Immunother* 68: 1995–2004

Wang K, Shen T, Siegal GP & Wei S (2017) The CD4/CD8 ratio of tumor-infiltrating lymphocytes at the tumor-host interface has prognostic value in triple-negative breast cancer. *Human Pathology* 69: 110–117

Wei SC, Levine JH, Cogdill AP, Zhao Y, Anang N-AAS, Andrews MC, Sharma P, Wang J, Wargo JA, Pe'er D, *et al* (2017) Distinct cellular mechanisms underlie anti-CTLA-4 and anti-PD-1 checkpoint blockade. *Cell* 170: 1120-1133.e17

Wein L, Luen SJ, Savas P, Salgado R & Loi S (2018) Checkpoint blockade in the treatment of breast cancer: current status and future directions. *British Journal of Cancer* 119: 4–11

Weinberg F, Ramnath N & Nagrath D (2019) Reactive Oxygen Species in the Tumor Microenvironment: An Overview. *Cancers* 11: 1191

Weiss L (1992) Biomechanical interactions of cancer cells with the microvasculature during hematogenous metastasis. *Cancer Metastasis Rev* 11: 227–235

Wischhusen J, Jung G, Radovanovic I, Beier C, Steinbach JP, Rimner A, Huang H, Schulz JB, Ohgaki H, Aguzzi A, *et al* (2002) Identification of CD70-mediated Apoptosis of Immune Effector Cells as a Novel Immune Escape Pathway of Human Glioblastoma. *Cancer Res* 62: 2592–2599

Wong CW, Lee A, Shientag L, Yu J, Dong Y, Kao G, Al-Mehdi AB, Bernhard EJ & Muschel RJ (2001) Apoptosis: An Early Event in Metastatic Inefficiency. *Cancer Res* 61: 333–338

Wyckoff J, Wang W, Lin EY, Wang Y, Pixley F, Stanley ER, Graf T, Pollard JW, Segall J & Condeelis J (2004) A paracrine loop between tumor cells and macrophages is required for tumor cell migration in mammary tumors. *Cancer Res* 64: 7022–7029

Wyckoff JB, Wang Y, Lin EY, Li J, Goswami S, Stanley ER, Segall JE, Pollard JW & Condeelis J (2007) Direct visualization of macrophage-assisted tumor cell intravasation in mammary tumors. *Cancer Res* 67: 2649–2656

Yang L, Liu L, Wu X, Guo X, Yang Y & Wang T (2020) Hypofractionated radiation therapy with versus without immune checkpoint inhibitors in patients with brain metastases: A meta-analysis. *International Immunopharmacology* 80: 106148

Yushkevich PA, Piven J, Hazlett HC, Smith RG, Ho S, Gee JC & Gerig G (2006) User-guided 3D active contour segmentation of anatomical structures: significantly improved efficiency and reliability. *Neuroimage* 31: 1116–1128

Zakaria R, Platt-Higgins A, Rathi N, Radon M, Das S, Das K, Bhojak M, Brodbelt A, Chavredakis E, Jenkinson MD, *et al* (2018) T-Cell Densities in Brain Metastases Are Associated with Patient Survival Times and Diffusion Tensor MRI Changes. *Cancer Res* 78: 610–616

Zeng Q, Michael IP, Zhang P, Saghafinia S, Knott G, Jiao W, McCabe BD, Galván JA, Robinson HPC, Zlobec I, *et al* (2019) Synaptic proximity enables NMDAR signalling to promote brain metastasis. *Nature* 573: 526–531

Zhang L, Yao J, Wei Y, Zhou Z, Li P, Qu J, Badu-Nkansah A, Yuan X, Huang Y-W, Fukumura K, *et al* (2020) Blocking immunosuppressive neutrophils deters pY696-EZH2–driven brain metastases. *Science Translational Medicine* 12: 545

Zöller T, Schneider A, Kleimeyer C, Masuda T, Potru PS, Pfeifer D, Blank T, Prinz M & Spittau B (2018) Silencing of TGFβ signalling in microglia results in impaired homeostasis. *Nature Communications* 9: 4011

Zou Y, Watters A, Cheng N, Perry CE, Xu K, Alicea GM, Parris JLD, Baraban E, Ray P, Nayak A, *et al* (2019) Polyunsaturated Fatty Acids from Astrocytes Activate PPARγ Signaling in Cancer Cells to Promote Brain Metastasis. *Cancer Discov* 9: 1720–1735

8. Abbreviations

α-	Anti-
AF	Alexa Fluor
AMP	Adenosine monophosphate
Ang-2	Angiopoietin 2
Arg1	Arginase 1
ANGPTL4	Angiopoietin-like 4
APC	Antigen presenting cells
ATCC	American Type Culture Collection
AUC	Area under the curve
BBB	Blood brain barrier
BMDM	Bone marrow derived macrophages
BrM	Brain metastasis
BSA	Bovine serum albumin
BTB	Blood tumor barrier
BV	Brilliant Violet
CBCT	Cone Beam computed tomography system
CCL	C-C chemokine ligand
CCR2	C-C chemokine receptor type 2
CD	Cluster of differentiation
CDR3	Complementarity-determining region 3
cGAS	Cyclic GMP-AMP
CI	Confidence interval
CLN	Cervical lymph nodes
CNS	Central nervous system
COX2	Cyclooxygenase 2
CR	Complete response
CSF	Cerebrospinal fluid
CSF1/2/3	Colony stimulating factor 1/2/3
CSF1R	CSF1 receptor
CSF1R-I	CSF1R inhibitor
CT	Cycle threshold
CTLA-4	Cytotoxic T-lymphocyte-associated protein 4
Ctrl	Control
CX3CR1	C-X3-C Motif Chemokine Receptor 1
CXCL	C-X-C Motif Chemokine
CXCL12 (SDF1)	Stromal cell-derived factor 1
CXCR4	C-X-C Motif Chemokine Receptor 4
d	day
DAM	Disease associated microglia
DAMP	Damage associated molecular patterns
DAPI	4′,6-Diamidin-2-phenylindol
DC	Dendritic cells
cDC1/2	Conventional DC 1/2
DCIR2	DC immunoreceptor 2
ddH_2O	Double distilled water
DMEM	Dulbecco's Modified Eagle's Medium
DMSO	Dimethyl sulfoxide
DN T cells	CD4- CD8- double negative T cells
DNA	Desoxyribonucleic acid
cDNA	Complementary DNA
dsDNA	Double-stranded cytosolic DNA
DPBS	Dulbecco's phosphate buffered saline
EAE	Experimental autoimmune encephalomyelitis
ECM	Extracellular matrix
EDTA	Ethylenediaminetetraacetic acid
e.g.	Exempli gratia/for example
EGF	Epidermal growth factor
EGFR	EGF receptor
EMT	Epithelial-mesenchymal transition
EpCAM	Epithelial cell adhesion molecule
FACS	Fluorescence-activated cell sorting
FasL	Fas ligand
FBS	Fetal bovine serum
FDA	U.S. Food and Drug Administration
Fig.	Figure
FITC	Fluorescein isothiocyanate
FoxP3	Forkhead-Box-Protein P3
g	Gravitational acceleration
GABA	Gamma-aminobutyric acid
GAPDH	Glyceraldehyde 3-phosphate dehydrogenase
GFP	Green fluorescent protein
GM-CSF	Granulocyte-macrophage colony-stimulating factor
GMP	Guanosine monophosphate
h	hours
HBSS	Hank's balanced salt solution
HE	Hematoxylin eosin
HFRT	Hypo-fractionated radiotherapy
HIF1	Hypoxia inducible factor-1

HTS	High throughput sampler
Iba1	Ionized calcium-binding adapter molecule 1
ICB	Immune checkpoint blockade
ICI	Intracardiac injection
IF	Immunofluorescence
IFN	Interferon
IHC	Immunohistochemistry
IL	Interleukin
i.p.	intraperitoneally
IR	Ionizing radiation
JAM-B	Junctional adhesion molecule B
Ly6G	Lymphocyte antigen 6 complex locus G6D
MDM	Monocyte derived macrophages
MG	Microglia
MHC	Major histocompatibility complex
MMP-2	Matrix metalloproteinase 2
MRI	Magnetic resonance imaging
NK cells	Natural killer cells
NKT cells	Natural killer T cells
NLR	Neutrophil lymphocyte ratio
no.	Number
ns	Not significant
NSCLC	Non-small-cell lung carcinoma
NVU	Neurovascular unit
PBS	Phosphate buffered saline
PCR	Polymerase chain reaction
PD	Progressive disease
PD-1	Programmed cell death protein 1
PD-L1/2	PD-1 ligand 1/2
PE	Phycoerythrin
PI3Kγ	Phosphoinositid-3 kinase
PPARγ	Peroxisome proliferator-activated receptor γ
PR	Partial response
qRT-PCR	Quantitative Real-time PCR
RBC	Red blood cell
RCC	Renal cell carcinoma
rm-	Recombinant murine -
RNA	Ribonucleic acid
rpm	Rounds per minute
RPMI	RPMI-1640 media
RT	Room temperature
ROS	Reactive oxygen species
S1P3	Sphingosin-1-phosphat-Rezeptor 3
SARRP	Small animal radiation research platform
SCLC	Small cell lung carcinoma
SD	Standard deviation
SD	Stable disease
SRS	Stereotactic radiosurgery
STING	cGAS receptor stimulator of interferon genes
Tab.	Table
TAM	Tumor associated macrophages
TCR	T cell receptor
TGFβ	Transforming growth factor
TIL	Tumor infiltrating lymphocytes
TME	Tumor microenvironment
TMEM119	Transmembrane Protein 119
TNBC	Triple negative breast cancer
TNFα	Tumor necrosis factor α
Treg	Regulatory T cells
Trex1	Three prime repair exonuclease 1
TuCM	Tumor conditioned media
UBC	Ubiquitin C
VEGF-C	Vascular endothelial growth factor C
WBRT	Whole brain radiotherapy
w/	With
w/o	Without

Publications

Articles

Niesel K, Schulz M, Anthes J, Alekseeva T, Macas J, Salamero-Boix A, Möckl A, Oberwahrenbrock T, Lolies M, Stein S, Plate KH, Reiss Y, Rödel F & Sevenich L (2021) The immune suppressive microenvironment affects efficacy of radio-immunotherapy in brain metastasis. *EMBO Mol Med* 13: e13412

Klemm F, Möckl A, Salamero-Boix A, Alekseeva T, Schäffer A, Schulz M, Niesel K, Maas R, Groth M, Elie BT, Bowman RL, Hegi ME, Daniel RT, Zeiner PS, Zinke J, Harter PN, Plate KH, Joyce JA & Sevenich L (2021) Compensatory CSF2-driven macrophage activation promotes adaptive resistance to CSF1R inhibition in breast-to-brain metastasis.
Manuscript in revision.

Schulz M, Michels B, Niesel K, Stein S, Farin H, Rödel F & Sevenich L (2020) Cellular and molecular changes of brain metastases-associated myeloid cells during disease progression and therapeutic response*. iScience* 23: 101178

Chae WH, Niesel K, Schulz M, Klemm F, Joyce JA, Prümmer M, Brill B, Bergs J, Rödel F, Pilatus U & Sevenich L (2019) Evaluating Magnetic Resonance Spectroscopy as a Tool for Monitoring Therapeutic Response of Whole Brain Radiotherapy in a Mouse Model for Breast-to-Brain Metastasis. *Front Oncol* 9: 1324

Schulz M, Salamero-Boix A, Niesel K, Alekseeva T & Sevenich L (2019) Microenvironmental Regulation of Tumor Progression and Therapeutic Response in Brain Metastasis. *Front Immunol* 10: 1713

Oral presentations

Niesel K, Schulz M, Salamero-Boix A, Chae WH, Alekseeva T, Michels B, Schäffer A, Strecker M, Rödel F, Harter PN, Plate K & Sevenich L (2018) Effects of Ionizing Irradiation on Brain Metastasis-Associated Inflammation and its Implication for Immuno-Therapy.
21st Annual Meeting of the Society for Biological Radiation Research, Frankfurt, Germany

Selected posters and conference papers

Möckl A, Salamero-Boix A, Schulz M, Niesel K, Anthes J, Alekseeva T & Sevenich L (2019) Inflammation in spontaneous brain metastasis models.
1st Rhein Main Cancer Retreat, Königstein, Germany

Schulz M, Niesel K, Salamero-Boix A, Chae WH, Michels B, Schaeffer A, Strecker M, Alekseeva T, Stein S, Farin H, Rödel F, Harter PN, Plate KH & Sevenich L (2019) Effects of ionizing radiation on brain metastasis-associated inflammation and its implication for immunotherapy.
CRI-CIMT-EATI-AACR International Cancer Immunotherapy Conference, New York, USA

Niesel K, Rödel F & Sevenich L (2018) The influence of immune modulatory drugs as adjuvant therapy on the tumor microenvironment in brain metastasis.
Mechanisms of Metastasis IRB Conference, Barcelona, Spain

Schulz M, Niesel K, Salamero Boix A, Chae WH, Alekseeva T Michels B, Schäffer A, Strecker M, Rödel M, Harter PN, Plate KH & Sevenich L (2018) Effects of Ionizing Irradiation on Brain Metastasis-Associated Inflammation and its Implication for Immuno-Therapy.
Frankfurt Cancer Conference, Frankfurt, Germany

Niesel K, Harter PN, Rödel F & Sevenich L (2017) The influence of immune modulatory drugs as adjuvant therapy on the tumor microenvironment in brain metastasis.
UCT Science Day, Frankfurt, Germany

Danksagung

Hiermit möchte ich mich für die großzügige Unterstützung und Hilfsbereitschaft, die ich während meiner Doktorarbeit erfahren habe, bedanken. An erster Stelle bedanke ich mich bei Dr. Lisa Sevenich, für die Möglichkeit in ihrer, damals brandneuen, Gruppe die Doktorarbeit zu beginnen. Da ich zuvor keine Erfahrung in der translationalen Forschung sammeln konnte, war dies für mich eine ganz besondere Chance, die ich sehr zu schätzen weiß. Ihre Betreuung, Kreativität, Hilfsbereitschaft und ihr Optimismus haben diese Arbeit maßgeblich mitgeformt. Des Weiteren bedanke ich mich bei Prof. Beatrix Süß und Prof. Ralf Galuske für die Begutachtung meiner Arbeit.

Bei unserem Kooperationspartner Prof. Franz Rödel von der Strahlenbiologie bedanke ich mich für die Möglichkeit Mäuse in präklinischen Studien zu bestrahlen. Vielen Dank auch Julius Oppermann, PD Dr. Stephanie Hehlgans und Jeannie Peifer für die Bedienung des SARRP. Mein Dank gilt außerdem Petra Dinse aus der Histologie für die Anfertigung histologischer Präparate, Dr. Stefan Stein und Anette Trzmiel für die kompetente Beratung und Hilfe bei der Bedienung der Durchflusszytometer und Dr. Tijna Alekseeva und Marco Lolies für die Hilfe und vielen Stunden am MRT.

Ganz herzlich möchte ich mich bei allen aktuellen und ehemaligen Mitgliedern der AG Sevenich für die Unterstützung und angenehme Arbeitsatmosphäre bedanken: Dr. Tijna Alekseeva, Julian Anthes, Woon Hyung Chae, Abdallah El Sheikha, Sebastian Friemel, Melanie Jatta, Jessica Kondol, Dominic Menger, Aylin Möckl, Maria Nolte, Anna Salamero-Boix, Alexander Schäffer, Michael Schulz und Maja Strecker. Besonders hervorheben möchte ich hier Julian für die enge Zusammenarbeit und Tijna für die Freundschaft und tatkräftige Hilfe über mehrere Jahre und das Korrekturlesen dieser Arbeit. Danke auch nochmal an Anna, Aylin, Dominic, Jessica, Alex, Sebi, Maja N. und Maja S. für die lustigen und schönen Kaffee- und Mittagspausen, aber auch den wissenschaftlichen Austausch und die gegenseitige Unterstützung.

Zum Schluss möchte ich mich bei meiner Familie, besonders bei meinen Eltern und meiner Schwester, meinen Freunden und meinem Partner Timm für den stetigen Rückhalt, die Unterstützung und Aufmunterungen von Herzen bedanken.

Ehrenwörtliche Erklärung

Ich erkläre hiermit ehrenwörtlich, dass ich die vorliegende Arbeit entsprechend den Regeln guter wissenschaftlicher Praxis selbstständig und ohne unzulässige Hilfe Dritter angefertigt habe.

Sämtliche aus fremden Quellen direkt oder indirekt übernommenen Gedanken sowie sämtliche von Anderen direkt oder indirekt übernommenen Daten, Techniken und Materialien sind als solche kenntlich gemacht. Die Arbeit wurde bisher bei keiner anderen Hochschule zu Prüfungszwecken eingereicht.

Frankfurt, den ……..... ….....

(Unterschrift)